DOCTOR OF PHILOSOPHY

Massive MIMO for communication and radar coexistence

Elfiatoure, Mohamed

Award date:
2024

Awarding institution:
Queen's University Belfast

Massive MIMO for Communication and Radar Coexistence

Mohamed Elfiatoure

School of Electronics, Electrical Engineering and Computer Science
Queen's University Belfast

This dissertation is submitted for the degree of
Doctor of Philosophy

April 2024

I would like to dedicate this thesis to my loving parents ...

Declaration

Mohamed Elfiatoure
April 2024

Acknowledgements

As I reflect on the journey of my academic endeavor, it becomes imperative to express my profound gratitude to those who have been the bedrock of my scholarly pursuits. At the forefront of this esteemed group are my main supervisors, **Professor Michalis Matthaiou** and **Dr. Hien Quoc Ngo**, whose contributions have not only shaped my academic trajectory but have also endowed me with a wealth of knowledge and opportunities unparalleled in my field.

Professor Michalis Matthaiou, your support transcends the conventional mentor-student relationship. It is your belief in my potential and your unwavering mentorship that have inspired me throughout this journey. The dedication you have shown towards my success, coupled with your patience and encouragement, has been a beacon of guidance. The opportunities you have provided me with are treasures I hold dear, fostering a confidence in me that I carry forward. For this, my gratitude knows no bounds.

Dr. Hien Quoc Ngo, your constant support and technical acumen have been instrumental in my development as a researcher. Working alongside you has been one of the highlights of my academic career, offering me a source of inspiration and learning that is rare and invaluable. Your willingness to share your expertise and engage in profound discussions has greatly enriched my comprehension and passion for our field. The dedication you have shown towards my growth is something I am eternally grateful for.

The privilege to collaborate closely with both Professor Michalis Matthaiou and Dr. Hien Quoc Ngo is an honor I cherish deeply. The impact of your guidance is immeasurable, and I consider myself truly fortunate for this opportunity.

In addition to my supervisors, I extend my sincere appreciation to **Dr. Mohammadali Mohammadi** for his valuable contributions and steadfast support throughout my academic journey. Your assistance has been a cornerstone of my development, and for that, I am thankful.

Lastly, my journey would have been significantly more challenging without the unwavering support and encouragement from my family back in Libya. Your presence, albeit from afar,

has been a constant source of strength and motivation. The realization of this thesis, and the milestones reached along the way, are as much yours as they are mine.

To my dearest mother, Your love and sacrifices have laid the foundation upon which I have built my aspirations. From my earliest days, you instilled in me the values of hard work, perseverance, and humility. Your wisdom and guidance have been my guiding light, illuminating the path through the most challenging times. You have always believed in me, even when I doubted myself, and your encouragement has been the wind beneath my wings. Your prayers and blessings have been my shield, protecting and comforting me across distances and through times. I owe every achievement, not least this thesis, to your unwavering support and boundless love. Thank you for everything, for without you, none of this would have been possible.

To my beloved wife, Words fall short when I attempt to express my gratitude for your unwavering support, love, and patience throughout this challenging yet rewarding journey. Your strength and encouragement have been my anchor in times of doubt and my beacon during moments of darkness. The sacrifices you have made, often silently, have not gone unnoticed. Your belief in my dreams, even when they seemed distant, has been a source of endless motivation. You have been my steadfast partner, not just in life but in every step of this academic endeavor. For all the late nights, the endless discussions, and the unwavering faith, I am eternally grateful. Thank you for being my companion, my confidant, and my inspiration.

Abstract

In the evolving landscape of wireless communications, spectrum sharing, integrated sensing and communication (ISAC), and massive multiple-input multiple-output (mMIMO) technologies emerge as pivotal enablers for the 5G and forthcoming 6G networks. This thesis delves into the increasingly pertinent topic of frequency spectrum sharing between radar and communication systems, with a specific focus on the coexistence of mMIMO systems and MIMO radar. The research encompasses four comprehensive studies, each offering unique insights and innovative solutions to this challenging domain.

The first study investigates the coexistence between a multiuser mMIMO downlink system and MIMO radar. It reveals that increasing the number of antennas at the base station (BS) enhances the mMIMO performance while maintaining the interference levels to the radar system. A significant contribution of this study is the derivation of closed-form expressions for the probability of detection of the radar system and the downlink spectral efficiency of the mMIMO system. Furthermore, the study introduces an innovative power allocation scheme that enables optimal transmit power selection in closed-form. This scheme maximizes the radar detection probability without compromising the performance of the mMIMO system.

Building on the foundational insights established in the first study, the second chapter expands the scope to include a nuanced analysis of linear precoding designs and their impact under channel estimation errors. This chapter explores the coexistence of a downlink multiuser mMIMO communication system and MIMO radar, with a focus on power control. The study characterizes the performance of the mMIMO system and the probability of detection with maximum ratio (MR), zero-forcing (ZF), and protective ZF (PZF) precoding designs. The PZF precoding design is highlighted for its ability to protect radar operations by projecting the communication signals onto the null space of the radar channel. The study derives closed-form expressions for the detection probability under these precoding designs and explores the detection probability in multiple target scenarios and correlated fading environments. A power control problem is efficiently solved using a linear programming approach and the bisection method, aiming to maximize the radar detection probability while satisfying the per-user SE

requirements. The analysis shows that the PZF design achieves the highest radar detection probability among all designs, with an intermediate SE performance that improves significantly with optimized power control.

Transitioning from the detailed exploration in the second chapter, the third study extends the discussion to the broader domain of cell-free massive MIMO (CF-mMIMO) systems within the ISAC framework. It addresses the problem of access point (AP) operation mode selection, where some APs are dedicated to downlink communication and others to sensing. The research derives closed-form expressions for the individual SE and mainlobe-to-average-sidelobe ratio (MASR), assessing communication and sensing performances. A max–min fairness problem is formulated and solved, optimizing the minimum SE of users while adhering to per-AP power constraints and sensing MASR requirements. The numerical results demonstrate that the proposed AP operation mode selection with power control improves significantly the communication performance while meeting the specified sensing requirements. This approach not only enhances the overall network performance but also paves the way for future wireless networks where integrated communication and precise sensing are paramount. The findings and methodologies presented offer valuable insights for the development of advanced ISAC systems. Building upon the sophisticated analysis presented in the third study, the fourth chapter advances the discourse into the more intricate realm of CF-mMIMO systems within the ISAC framework, with a special emphasis on the innovative concept of multi-zone sensing. This chapter not only builds upon the foundational insights from the third study but also explores the effectiveness of advanced precoding strategies—MR, ZF, and PZF—in downlink communication for CF-mMIMO ISAC systems. It provides a comprehensive comparative analysis of each strategy, evaluating their unique advantages and potential limitations to identify the most beneficial approach. PZF is spotlighted as a transformative strategy that skillfully integrates the strengths of both ZF and MR precoding. The strategic essence of PZF is its refined interference management technique, which focuses on minimizing interference for users with the highest channel gains, effectively prioritizing the network's most robust users while tolerating some interference for its weakest users. This approach marks a significant leap in optimizing network efficiency and enhancing user experience. Moreover, the study embarks on a thorough examination of system scalability and efficiency as the number of APs designated for both sensing and communication approaches infinity, while each AP's antenna count remains fixed. The analysis of the dynamics when the antenna count per AP increases to infinity, while the total number of APs remains constant. This detailed analysis is crucial for comprehending the scalability and adaptability of CF-mMIMO ISAC systems in complex wireless scenarios. Additionally, this chapter addresses the complex challenge of AP mode selection optimization. It ambitiously seeks to refine the operation mode selection and power

control coefficients, aiming to maximize the minimum per-user SE within the boundaries set by specified MASR levels for target detection and transmit power constraints at the APs. Together, these studies provide comprehensive theoretical and practical insights into the coexistence of mMIMO communication systems and MIMO radar. They make significant contributions to the field of ISAC, paving the way for more efficient spectrum sharing in the future.

Table of Contents

List of Figures

List of Tables

List of Notations

Lower-case boldface symbols and upper-case boldface symbols denote vectors and matrices respectively, while non-bold letters denote scalars.

$(\cdot)^*$	Conjugate of complex number
$(\cdot)^T$	Transpose of matrix
$(\cdot)^H$	Conjugate transpose of matrix
$\lvert.\rvert$	Absolute value
$\lVert\cdot\rVert$	Norm value
$\mathbb{E}\{\cdot\}$	Expectation operator of a random variable
$\mathbb{P}\{\cdot\}$	Probability of a random variable
$\mathbb{C}\{\cdot\}$	Covariance operator of a random variable
$\mathtt{Var}\{\cdot\}$	Variance operator
$\mathrm{diag}\{a_1,\ldots,a_N\}$	Diagonal matrix with diagonal entries $a_1,\ldots,a_N$
$\mathrm{tr}\{\cdot\}$	Trace operation
$\Gamma(\cdot)$	Gamma function
$\mathbf{a}\cdot\mathbf{b}$	Inner product of vectors $\mathbf{a}$ and $\mathbf{b}$
$\mathbf{I}_M$	$M\times M$ identity matrix
$\mathscr{CN}(\cdot,\cdot)$	Circularly symmetric complex Gaussian distribution
$X\sim\mathscr{CN}(0,\sigma^2)$	Circularly symmetric complex Gaussian random variable (RV) X with zero mean and variance σ^2
$X\sim\mathscr{N}(0,1)$	Real valued Gaussian RV with zero mean and unit variance
$I_{(n)}(x)$	Bessel function of the second kind and n-th order
$Q_n(\cdot,\cdot)$	Marcum Q-function of order n

List of Abbreviations

AO	Alternating Optimization
AP	Access Point
BS	Base Station
CDF	Cumulative Distribution Function
CF	Cell Free
CSI	Channel State Information
CPU	Central Processing Unit
D2D	Device to Device
DoF	Degrees Of Freedom
DL	Deep Learning
DRL	Deep Reinforcement Learning
EE	Energy Efficiency
GLQR	Gaussian-Legendre Quadrature Rule
IoE	Internet of Everything
IoT	Internet of Things
LMMSE	Linear Minimum Mean Square Error
LoS	Line of Sight
LTE	Long Term Evolution
MIMO	Multiple-Input Multiple-Output
ML	Machine Learning
MISO	Multiple-Input Single-Output
mMIMO	Massive Multiple-Input Multiple-Output
MRT	Maximum Ratio Transmission
NLOS	Non Line of Sight
NOMA	Non Orthogonal Multiple Access
OP	Outage Probability
PA	Power Amplifier
QoS	Quality of Service
RF	Radio Frequency
RRU	Remote Radio Unit
SE	Spectral Efficiency
SINR	Signal to Interference plus Noise Ratio
SISO	Single-Input-Single-Output

SNR	Signal to Noise Ratio
SWIPT	Simultaneous Wireless Information and Power Transfer
TDD	Time Division Duplex
THz	Terahertz
UAV	Unmanned Aerial Vehicle
UE	User Equipment
UPA	Uniform Planar Array

Chapter 1

Introduction

1.1 5G, 6G Innovations: Exploring Spectrum Sharing and MIMO Technologies

Wireless communication technology, a fundamental pillar of our digital society, is experiencing transformative shifts. The transition from the fourth generation (4G) long-term evolution (LTE) to fifth-generation (5G) mobile systems marks a revolutionary change in digital interactions, driven by the demand for increased data speeds, lower latency, improved energy efficiency, and more reliable, widespread connectivity. Originating as a means for data transmission without physical connectors, wireless communication has rapidly evolved, leading to a proliferation of advanced applications and services.

However, the growth of wireless communication is not without challenges. Network congestion, primarily fueled by the ever-increasing demands for additional bandwidth and data services, poses a significant issue. This congestion often leads to reduced data speeds and degraded service quality, adversely affecting the user experience. This problem, a consequence of the exponential growth in the number of connected devices and services, remains a pressing concern in the network infrastructure [1].

In response to network congestion, spectrum sharing emerges as a promising solution. By enabling the shared use of spectrum among multiple networks or users, this approach optimizes the utilization of this limited and expensive resource, thus alleviating congestion. Spectrum sharing not only enhances the network efficiency but also underpins more innovative, adaptive wireless communication systems, particularly in the beyond-5G era, where it facilitates the

coexistence of communication and radar systems within the same frequency bands [2–4]. The radar bands, in particular, present an excellent opportunity for shared use with cellular communication systems due to the extensive spectrum available for both commercial and governmental uses. These bands encompass a wide frequency range, including airborne navigation radars around 3.4 GHz, shipborne radars as well as vessel traffic service radars (VTS) at 5.6 GHz [5, 6]. The broad availability and diverse applications of radar bands make them ideal for integration into advanced wireless networks, leading to more efficient spectrum utilization to significantly enhance the network capabilities and functionalities. Addressing the challenges in network infrastructure, massive multiple-input multiple-output (mMIMO) technology has emerged as a significant advancement, significantly enhancing the network capacity and energy efficiency by employing a large number of antennas at the base stations (BSs). This technology enables the simultaneous transmission and processing of multiple data streams, increasing throughput and efficiency, and playing a pivotal role in the evolution of 5G and subsequent wireless technologies [7]. It offers solutions for interference mitigation and enhances spectrum sharing [8]. By leveraging recent advancements in mMIMO communications, this thesis explores the benefits of using a large number of antennas in scenarios where mMIMO coexists with MIMO radar, focusing on mitigating the mutual interference between communication and radar operations to enhance the overall system performance and spectral efficiency (SE).

Building on the foundation of mMIMO, the concept of cell-free massive MIMO (CF-mMIMO) extends these benefits further. CF-mMIMO decentralizes the antenna deployment, leading to improved coverage and reduced latency. Characterized by numerous distributed access points (APs), each linked to a central processing unit (CPU), CF-mMIMO serves a relatively small number of users over the same time-frequency resources, thereby significantly enhancing the network performance. This technology effectively addresses challenges, such as increased SE, fairness, and reduced latency. The integration of CF-mMIMO with emerging technologies for 5G and beyond ensures substantial enhancements in network performance, particularly in urban and densely populated areas, by maintaining consistent service quality [9–11]. The benefits of CF-mMIMO are particularly pronounced in the context of integrated sensing and communication (ISAC) and spectrum sharing. The distributed nature of APs in CF-mMIMO facilitates the detection of multiple targets, thereby expanding the range and accuracy of sensing capabilities. This is crucial for applications like vehicular networks and remote sensing, where detecting and communicating with multiple targets simultaneously is critical. This distributed architecture, combined with advanced power control and pilot assignment strategies, makes CF-mMIMO an ideal solution for next-generation wireless networks, where uniform SE and comprehensive coverage are paramount [12]. As we advance into the era of

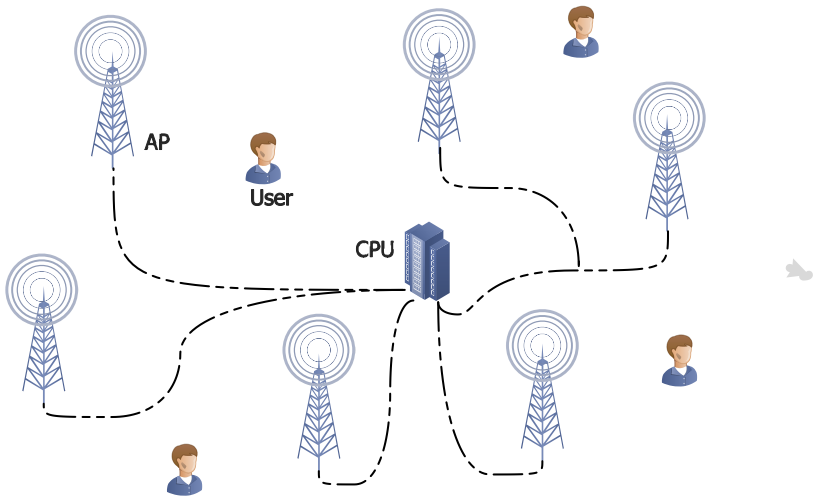

Fig. 1.1 A typical CF-mMIMO architecture.

ubiquitous wireless communication, the exploration of spectrum sharing and ISAC becomes essential. This includes addressing the demands for efficient spectrum utilization in densely populated wireless networks and delivering enhanced performance in both communication and sensing. The development of innovative applications in fields like vehicular networks, remote sensing, and the Internet of Things (IoT), is also anticipated.

This thesis is dedicated to delving into the intricacies of spectrum sharing, interference management, and massive MIMO innovations. These elements are pivotal in shaping the future of wireless communication. Through a comprehensive analysis and exploration, it aims to identify potential strategies for overcoming challenges and leveraging the opportunities presented by these groundbreaking technologies. As technology continues to evolve, the boundaries between communication and sensing are increasingly relaxed, presenting a dynamic and rapidly developing field of study.

1.2 Challenges of Spectrum Sharing between Communication and Sensing

Spectrum sharing between communication and sensing systems is a critical aspect of contemporary wireless technology, presenting several complex challenges crucial for the effective utilization of the wireless spectrum. These challenges pertain to harmonizing the operational requirements of communication systems, such as mobile networks, with those of sensing systems, like radar. Addressing these challenges effectively is important to fully leveraging the potential of spectrum sharing. The primary challenges, presented concisely, include:

- **Interference Management**: The primary challenge in spectrum sharing lies in managing mutual interference between the communication and sensing systems operating within the same frequency bands. This interference risk can lead to reduced data rates and higher error rates in communication systems, and will eventually compromise the data accuracy in sensing systems. Developing advanced mitigation techniques, which include the precise adjustment of transmission power, frequency selections, and modulation schemes, is crucial.
- **Dynamic Spectrum Allocation**: The dynamic nature of spectrum demand calls for intelligent and adaptive allocation strategies. These strategies must balance the efficient and fair spectrum usage, accommodating the fluctuating requirements of various systems across different temporal and spatial conditions.
- **Hardware Requirements**: Effective spectrum sharing requires advanced hardware capable of supporting both communication and sensing functions. This encompasses wideband operations, high linearity, and swift reconfigurability, potentially escalating system complexity and cost.
- **Quality of Service (QoS) and Quality of Experience (QoE)**: A major challenge is maintaining a high-quality service for both communication and sensing systems. In terms of communication, this means ensuring high data rates and low latency. For sensing systems, accuracy and reliability are paramount. Additionally, the energy efficiency is vital, particularly in scenarios involving battery-powered or remote devices, calling for optimized hardware and algorithmic solutions.

This thesis delves into these challenges in depth, exploring a range of strategies and solutions for managing and potentially resolving them. The focus will be on developing an in-

depth understanding of the complexities involved in spectrum sharing between communication and sensing systems. This encompasses a thorough examination of interference management techniques, principles of dynamic spectrum allocation, specifications for sophisticated hardware requirements, and strategies to deliver high quality of service (QoS) and quality of experience (QoE).

Through this exploration, the thesis aims to offer valuable insights and propose novel solutions that can substantially enhance the efficiency and effectiveness of spectrum sharing in modern wireless communication systems. The ultimate objective is to navigate these challenges and present practical methods applicable in real-world settings. This thesis not only seeks to advance the field of wireless communication but also to pave the way for future technological innovations in this rapidly evolving domain.

1.3 Motivation

The motivation for this thesis is deeply rooted in the technological advancement and pressing needs of modern wireless communication. As we transition into the 6G incubation era, a significant leap from previous generations, there is a compelling need to understand and harness these advanced technologies, especially given their profound implications for global connectivity. A central aspect of this exploration is addressing the spectrum congestion problem, an increasingly critical issue as the number of connected devices and demand for wireless services surge. Spectrum sharing emerges as a promising solution to this challenge, warranting an in-depth study and analysis. Additionally, the reliance of 5G networks on mMIMO technology for improved efficiency and performance further fuels the motivation for this research. Understanding the capabilities, challenges, and future potential of mMIMO is crucial for advancing the field. It aims to provide both theoretical and practical contributions to the field, enhancing academic understanding while proposing realistic applications. Moreover, the broader societal and economic impacts of 5G technology, from enabling new services to driving economic growth, present a compelling area of study. This thesis, therefore, seeks to address these multifaceted challenges and opportunities, aiming to contribute significantly to the advancement of wireless communication technology in the 5G era and beyond.

1.4 Thesis Contributions

This thesis represents a comprehensive exploration into the intricate realm of coexistence strategies between mMIMO systems and radar communications. Encompassing four research papers, the thesis navigates through the challenges and solutions pertinent to this coexistence, particularly in the context of performance analysis, precoding design, power control, and operational mode selection in CF-mMIMO systems. Each chapter, corresponding to a published paper, delves into unique aspects of this coexistence, offering theoretical analyses, algorithmic solutions, and practical insights that contribute significantly to the field of ISAC. The contributions, segregated by the chapters they appear in, are as follows:

Chapter 3 sets the foundation by analyzing the system performance in the asymptotic regime and exploring the impact of increasing BS antennas on both mMIMO and radar systems.

- **Asymptotic Performance Analysis**

  Explores the system performance in the asymptotic regime with an infinite number of BS antennas (M). Demonstrates that increasing M enhances the mMIMO performance while maintaining the radar system interference to tolerable levels.

- **Spectral Efficiency and Detection Probability Analysis**

  Derives closed-form expressions for the radar system's average probability of detection and the mMIMO system's downlink SE using the use-and-then-forget technique. These findings are validated through numerical results, offering insights into the coexistence of mMIMO communications and radar operations.

- **Optimal Power Allocation Scheme**

  Introduces a power allocation scheme to optimize the transmit powers for maximizing the MIMO radar's detection probability within the communication systems' QoS constraints. This leads to significant improvements in detection probability.

- **Impact of Antenna Numbers**

  Shows how increasing the number of antennas at both the BS and radar enhances the target detection performance and SE, especially in low signal-to-noise ratio (SNR) conditions. The chapter also discusses the trade-off between the radar and communication system performance.

Building upon the insights gained in **Chapter 3**, and by looking into the interplay between mMIMO and radar systems, **Chapter 4** delves deeper into the practical aspects of this coexistence, particularly focusing on the challenges of imperfect CSI, precoding design and power control to enhance the coexistence efficiency. Moreover, this chapter extends the analysis to include multiple target scenarios and correlated fading environments, offering a more comprehensive understanding of the dynamics in varied and realistic operational conditions.

- **Performance Characterization with Imperfect CSI**

  This paper characterizes the performance of mMIMO and MIMO radar systems under the influence of imperfect channel state information (CSI). It provides analytical results for different beamforming techniques at the BS, including MR and ZF. Importantly, it introduces a protective ZF (PZF) precoding approach at the BS to manage the inter-system interference, ensuring minimal impact on radar functionality.

- **Power Allocation Strategy.**

  A power allocation problem is formulated and solved, focusing on maximizing the detection probability for MIMO radar while adhering to power budget constraints at the radar and minimum spectral efficiency requirements at the cellular users. This strategy is shown to significantly enhance the detection probabilities for all considered precoding designs.

- **Influence of Antenna Numbers and Power Control**

  The paper provides insights into how increasing the number of BS antennas affects the performance of different precoding schemes. Additionally, it highlights that power control at both the BS and radar can significantly improve detection probabilities.

These contributions in **Chapter 4** not only advance the theoretical understanding of mMIMO and MIMO radar system coexistence but also provide practical solutions for optimizing their performance in real-world scenarios with imperfect CSI. Following the advanced analyses in **Chapter 4**, **Chapter 5** is focused on the intricacies of CF-mMIMO systems within the ISAC framework. This chapter not only builds upon the earlier discussions but also introduces novel methodologies for optimizing the functionality of CF-mMIMO networks. Key contributions in **Chapter 5** include:

- **Performance Evaluation**

  By leveraging the use-and-then-forget strategy, closed-form expressions for the downlink SE and mainlobe-to-average-sidelobe ratio (MASR) are derived to assess the communication and sensing performances.

- **Dynamic AP Operation Mode Selection**

  Presents a novel approach for dynamic operation mode selection in CF-mMIMO ISAC networks, focusing on maximizing the downlink users' SE while meeting the sensing requirements.

- **Algorithmic Solutions for AP Mode Selection**

  Proposes a greedy algorithm for AP operation mode selection and an alternating optimization (AO) algorithm for power control coefficient design. This combination addresses the complex interaction between the communication APs (C-APs) and radar APs (R-APs), ensuring efficient operation.

- **Numerical Results and Comparison**

  Numerical results show that the proposed greedy AP operation mode selection with optimal power control (GAP-OPC) significantly improves the SE performance of downlink users for a given MASR, compared to the greedy/random operation mode selection scheme without power control (GAP/RAP-NPC).

Building upon the sophisticated analysis presented in **Chapter 5**, **Chapter 6** advances the discourse into the more intricate realm of CF-mMIMO systems within the ISAC framework, with a special emphasis on the innovative concept of multi-zone sensing. This chapter not only builds upon the foundational insights from **Chapter 5** but also explores the effectiveness of advanced precoding strategie PZF in downlink communication for CF-mMIMO ISAC systems. It provides a comprehensive comparative analysis of each strategy, evaluating their unique advantages and potential limitations to identify the most beneficial approach. PZF is spotlighted as a transformative strategy that skillfully integrates the strengths of both ZF and MR precoding. The strategic essence of PZF is its refined interference management technique, which focuses on minimizing the interference for users with the highest channel gains, effectively prioritizing the network's most robust users while tolerating some interference for its weakest users. This approach marks a significant leap in optimizing the network efficiency and enhancing the user experience. The examination of the system's behavior as the number of APs designated for both sensing and communication approaches infinity, with each AP's antenna count remaining

fixed. The analysis of the dynamics when the antenna count per AP increases to infinity, while the total number of APs remains constant. This detailed analysis is crucial for comprehending the scalability and adaptability of CF-mMIMO ISAC systems in complex wireless scenarios. Moreover, **Chapter 6** delves into the asymptotic analysis underscores the potential for transmit power reduction at both Communication and Sensing APs. Additionally, this chapter addresses the complex challenge of AP mode selection optimization. It ambitiously seeks to refine the operation mode selection and power control coefficients, aiming to maximize the minimum per-user SE within the boundaries set by specified MASR levels for target detection and transmit power constraints at the APs.

In summary, **Chapter 6** makes a significant contribution towards enhancing the theoretical and practical frameworks for CF-mMIMO ISAC systems. It paves the way for improved communication performance and robust sensing capabilities across multi-zone environments, marking a noteworthy advancement in the field of wireless communication technologies.

1.5 Thesis Organization

This thesis is organized into several chapters, each dedicated to exploring different aspects of wireless communication technologies, with a particular focus on mMIMO, radar communications, and ISAC. The structure is outlined as follows:

1. **Chapter 1: Introduction** This chapter sets the foundational context for the thesis, introducing key concepts in wireless communication, the evolution of technologies such as mMIMO, and the challenges associated with spectrum sharing. It establishes the base for understanding the complexities and advancements in modern wireless communications systems.

2. **Chapter 2: Literature Review** The second chapter offers a thorough review of existing literature. It discusses the development and current state of wireless communication technologies, mMIMO and ISAC. This review critically evaluates previous research and identifies gaps.

3. **Chapter 3: Published Paper - "Coexistence Between Massive MIMO and Radar Communications: Performance Analysis" (Special Issue on ISAC)** In this chapter, the focus is on the published paper "Coexistence Between Massive MIMO and Radar Communications: Performance Analysis," featured in one of the first Special Issues on

ISAC. It examines the performance and coexistence strategies for mMIMO systems in radar communications.

4. **Chapter 4: Published Paper - "Protecting Massive MIMO-Radar Coexistence: Precoding Design and Power Control"** Chapter 4 presents the published paper "Protecting Massive MIMO-Radar Coexistence: Precoding Design and Power Control." This paper delves into the design of precoding strategies and power control to safeguard the coexistence of mMIMO and radar systems, which are both critical components of modern wireless communication.

5. **Chapter 5: Published Paper - "Cell-Free Massive MIMO for ISAC: Access Point Operation Mode Selection and Power Control"** The fifth chapter explores the paper "Cell-Free Massive MIMO for ISAC: Access Point Operation Mode Selection and Power Control." It discusses CF-mMIMO in the context of ISAC, focusing on the selection of operation modes for APs and power control strategies.

6. **Chapter 6: (Paper under review) "Multiple-Target Detection in Cell-Free Massive MIMO-Assisted ISAC"** Chapter 6 marks a pivotal extension of the study initiated in Chapter 5, advancing the exploration of CF-mMIMO systems within ISAC frameworks. This segment notably shifts the spotlight to multi-zone sensing areas, providing a nuanced understanding of the complex landscape that CF-mMIMO ISAC systems navigate across.

1.6 Thesis Publications

During the thesis, the author has produced the following publications:

- **M. Elfiatoure**, H. Q. Ngo, and M. Matthaiou, "Coexistence between massive MIMO and radar communications: Performance analysis," *Journal of Communications and Information Networks*, vol. 8, no. 1, pp. 37-47, March 2023.

- **M. Elfiatoure**, M. Mohammadi, H. Q. Ngo, P. J. Smith, and M. Matthaiou, "Protecting massive MIMO-radar coexistence: Precoding design and power control systems," *IEEE Open Journal of the Communications Society*, vol. 5, no. 1, pp. 276-293, January 2024.

- **M. Elfiatoure**, M. Mohammadi, H. Q. Ngo, and M. Matthaiou, "Cell-free massive MIMO for ISAC: Access point operation mode selection and power control," in *Proc. IEEE GLOBECOM*, December 2023.

- **M. Elfiatoure**, M. Mohammadi, H. Q. Ngo, and M. Matthaiou, "Multiple-target detection in cell-free massive MIMO-assisted ISAC," submitted to *IEEE Transactions on Wireless Communications*, April 2024.

Chapter 2

Literature Review and Background

In this chapter, we first present a literature review focusing on mMIMO and CF-mMIMO technologies, followed by an exploration of spectrum sharing between communication and sensing systems. This review sets the stage for understanding the evolution and integration of these advanced technologies in modern wireless communication networks.

2.1 The Evolution from Massive to Cell-Free MIMO

A pivotal multi-user MIMO technology, is at the forefront of the 5G era. Defined by its capability to provide consistently high-quality service in high-mobility environments, mMIMO equips BSs with a significantly large number of antennas. This setup allows for simultaneous service to users in the same time-frequency resource, making it a revolutionary wireless access technology in both sub-6 GHz and mmWave bands, as established in [13]. Marzetta's work in [13] also reveals that the impact of fast fading diminishes with the deployment of large antenna arrays at the BS, enhancing the user service. These attributes underscore massive MIMO's potential in 5G wireless communication systems [14]. However, this increase in the number of antennas introduces new technical challenges in comparison to conventional MIMO topologies [15].

Massive MIMO, also known as large-scale antenna systems or hyper MIMO, marks a significant departure from current practices by utilizing an abundance of service antennas over active terminals, coupled with time-division duplex operation (TDD). This technology focuses energy into smaller spatial regions, thereby significantly boosting the throughput and energy efficiency. Additional benefits of massive MIMO include the use of cost-effective low-power

components, reduced latency, MAC layer simplification, and resilience against intentional jamming [14, 16].

To meet the rising demands of wireless data traffic, 5G networks integrating massive MIMO systems are envisioned to support the capacity demands with increased SE. These systems utilize spatial multiplexing with high-resolution degrees of freedom (DoF) in both elevation and azimuth angles [17]. Additionally, massive MIMO systems can direct more energy towards user equipments (UEs), enhancing the energy efficiency and reducing interference. Note that the deployment of 5G networks is expected to be dense, especially in urban environments, ensuring UEs are within the range of multiple BSs [18, 19].

One notable advantage of mMIMO is its potential for improved energy efficiency compared to single-antenna systems. As shown by Ngo *et al.* [20], in a mMIMO setup, single-antenna users can significantly reduce their transmit power in proportion to the number of BS antennas with perfect CSI, or to the square root of the antenna count with imperfect CSI. This reduction in power is crucial for future wireless networks, where managing high energy consumption is a growing concern [21]. Additionally, with adequate transmit power, massive MIMO can surpass the operational range of single antenna systems, although these findings do not take into account the power consumption of the radio front-ends [20].

Beyond energy efficiency, mMIMO excels in interference management. Linear combining and precoding schemes within mMIMO are capable of completely nullifying interference as the number of antennas increases, even in scenarios with imperfect channel knowledge. This core property represents a significant shift in the modeling, operation, theory, and implementation of MIMO systems, paving the way for novel research opportunities, such as applications in radar systems [22].

The evolution of wireless networks, particularly with 5G and beyond, has been significantly marked by the introduction of CF-mMIMO systems. As Ngo *et al.* [9] proposed, this technology utilizes numerous distributed APs linked to a CPU, enhancing the network capabilities by outperforming traditional MIMO and small-cell systems in terms of efficiency and reliability [10]. Additionally, CF mMIMO's adaptability with emerging technologies offers substantial improvements in network performance. Its deployment strategy, involving APs spread across a large area connected to a CPU, addresses challenges like SE and latency variations in dense urban settings [11].

In the 6G era, CF-mMIMO stands out as a vital solution, merging distributed communication with mMIMO to overcome challenges like inter-cell interference in ultra-dense networks. Its

unique architecture of multiple APs connected to central units boosts macro-diversity and reduces inter-user interference, adding a new dimension to network performance [12, 23]. Furthermore, the integration of CF-mMIMO with emerging technologies, especially in the context of ISAC systems, represents a significant development in next-generation wireless networks. This integration allows distributed APs to perform dual roles: communication and target sensing. Techniques, such as power control [24], beamforming design [25], or a combination of both [26] are utilized to optimize these functions, similar to how in network-assisted full-duplex (NAFD) CF-mMIMO networks [27], specific APs are designated for sensing tasks, while others focus on communication, thereby enhancing the overall network functionality [12].

In conclusion, the shift from mMIMO to CF marks a significant milestone in the evolution of wireless networks. This transition not only addresses the limitations of previous generations but also lays the groundwork for future advancements in the field of wireless communications.

2.2 Radar

Radar, an acronym for RAdio Detection And Ranging, is a system that uses electromagnetic signals to detect and measure characteristics, such as position and velocity of reflective objectives, known as "targets" [28]. The fundamental mechanism involves a radar station emitting electromagnetic waves and collecting the echoes returned from targets. This process is pivotal in differentiating between actual targets and noise, which is heavily influenced by the SNR. The standard radar setup, known as monostatic radar, involves co-located transmitters and receivers. This differs from bistatic or multistatic systems, where these components are significantly separated or involve multiple radars [29, 30]. Technological advancements in radar have led to the development of specialized functions like radar imaging, enabling high-resolution mapping in two or three dimensions [31]. The application dictates the configuration of antennas, transmitters, and receivers in radar systems, whether for air traffic control, maritime navigation, weather forecasting, military surveillance, space exploration, or automotive safety. Based on the type of probing signals, radar systems are mainly divided into continuous waveform radars and pulse radars, with the latter being more prevalent in modern applications [31].

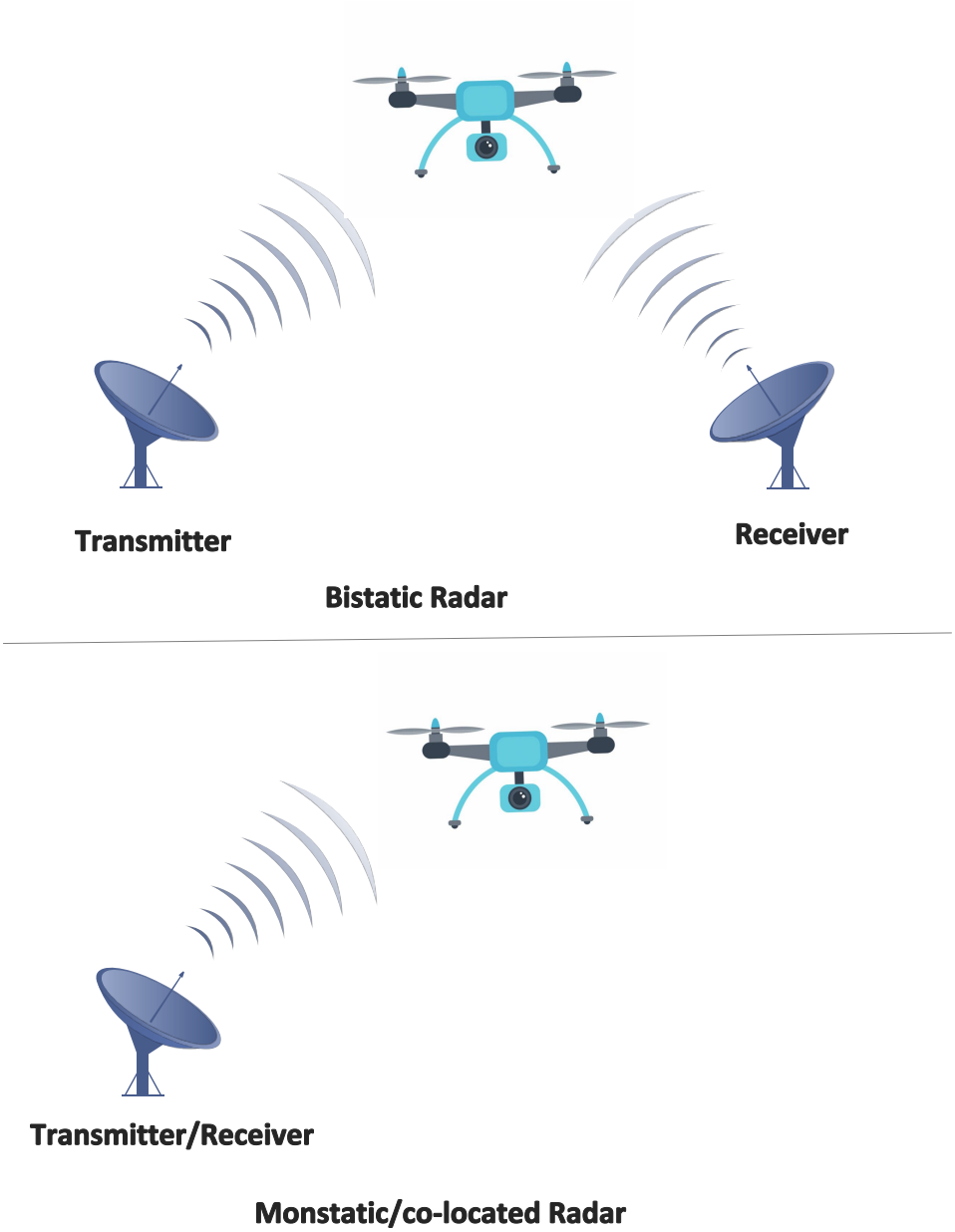

Fig. 2.1 Radar systems.

2.3 MIMO Radar

Over the past decade, the MIMO technology, initially prominent in wireless communications, has become a key area of research in radar signal processing. MIMO radar is characterized by

its use of multiple antennas to transmit diverse orthogonal waveforms and receive the echoes reflected by targets [32–35]. This approach has garnered increasing attention from commercial and military sectors for its enhanced capabilities in target detection, tracking, and localization [30, 36–39]. The diverse waveform emission from multiple antennas in MIMO radar systems is a key feature that enhances its operational capabilities. Unlike traditional phased-array systems, MIMO radars can transmit correlated or uncorrelated probing signals, facilitating more adaptive techniques in localization and detection [30, 40]. The design of MIMO radar systems has focused on leveraging waveform diversity and spatial separation, leading to significant improvements in target detection and parameter estimation. However, they also introduce challenges, such as increased signal dimensionality and receiver complexity [6, 22]. MIMO radar systems are generally classified into two categories: co-located MIMO radar and MIMO radar with extensively separated antennas. Co-located MIMO radar, akin to phased array systems, uses closely positioned antennas to transmit independent signals, maximizing waveform diversity. In contrast, MIMO radar with separated antennas aims to achieve spatial diversity by capturing targets from various spatial angles, which is especially beneficial in applications requiring precise location data [41]. While the co-located type can offer within-aperture diversity, the separated antenna type provides spatial diversity by observing targets from different angles. Both types offer improvements over conventional radar systems, especially in precision and accuracy in challenging environments [42–44]. MIMO radar technology has seen significant advancements, particularly in the areas of signal processing and antenna design. One notable advancement is the development of adaptive beamforming techniques, which allow MIMO radars to dynamically adjust the directionality of their beams for optimized target detection and interference suppression. Furthermore, the integration of advanced signal processing algorithms has enabled these systems to handle complex environments with high clutter and interference [45]. Despite these advancements, MIMO radar systems face several challenges. One of the primary challenges is the increased signal dimensionality, which results from using multiple transmit and receive antennas. This increase in dimensionality can exacerbate the computational complexity and requires more sophisticated signal processing techniques [22]. Another challenge is the design and implementation of the antenna arrays themselves. The need for multiple antennas to be integrated into a single system can lead to practical difficulties in terms of size, weight, and power consumption. Additionally, ensuring that the transmitted waveforms are orthogonal and do not interfere with each other is a complex task, particularly in dynamic environments [6]. Looking forward, there are several exciting areas of research in MIMO radar technology. One area is the development of cognitive radar systems, which can adapt their operating parameters in real-time based on the environment and target behavior.

This could involve dynamically changing waveform characteristics, beam patterns, or even the radar's operating frequency to optimize the system performance [46]. Another promising area is the integration of machine learning and artificial intelligence (AI) techniques into MIMO radar systems. AI could be used to improve target classification, automate complex signal processing tasks, and enhance decision-making processes in real-time [47]. Lastly, the exploration of new materials and technologies for antenna design could lead to more compact, efficient, and powerful MIMO radar systems [22].

To summarize, MIMO radar technology, with its roots in wireless communications, has revolutionized the radar capabilities, offering significant improvements in target detection and tracking. However, it also entails new challenges, primarily in signal processing and antenna design. The future of MIMO radar is likely to see further integration of advanced computational techniques and materials, driving its evolution and expanding its application scope.

2.4 Communication and Radar Spectrum Sharing

In the rapidly evolving landscape of wireless communications, the pressing challenge of limited spectrum availability stands as a formidable barrier against the burgeoning demands for enhanced capacity and QoS. This scarcity not only hampers the operators' ability to meet the user expectations but also exacerbates the capital and operating expenditures, invariably reflected in the service prices charged to customers. Amidst this backdrop, the surge in connected devices and services further intensifies the strain, propelling the industry towards a critical point of spectrum congestion. In this fast-evolving arena, the aforementioned surge has led to considerable spectrum congestion, impacting the auction prices of available frequency spectrum significantly [6]. In the UK, mobile network operators have been facing substantial annual fees since 2015 for the 900 MHz and 1800 MHz bands, a scenario echoed in Germany, where Bundesnetzagentur's auction of frequency bands garnered over €5 billion, reflecting the high market value of these spectral resources [48]. Similarly, in the US, the FCC's 5G auction for 28 GHz spectrum licenses raised $702 million, indicating the strong demand for advanced communication technologies [49]. This economic perspective underscores the tangible implications of spectrum scarcity, further compounding the urgency for innovative solutions. To address these challenges, network providers are increasingly venturing into the innovative realm of spectrum sharing, particularly eyeing the spectra currently earmarked for radar systems. This strategy stems from the broad bandwidths radar technologies occupy, coupled with their pivotal global applications ranging from air traffic control to weather monitoring and security. Such systems,

especially within the 1 to 10 GHz range, present lucrative opportunities for coexistence with emerging communication technologies, like 5G New Radio (5G NR), LTE, and Wi-Fi, thereby heralding a new era of synergy between radar and communication systems [6, 50]. The adaptability of many radar systems for spectrum sharing with communication technologies further underscores the potential for innovative coexistence approaches [51–54]. However, the path to spectrum optimization is fraught with hurdles. The advent of advanced radar technologies demanding higher frequency bands, alongside the exponential rise in civilian digital activities, particularly on social media, exerts unprecedented pressure on bandwidth allocation. This scenario underscores the critical need for identifying suitable frequency bands that can sustain the enhanced performance of integrated radar and communication systems, a task that is becoming increasingly complex as the International Telecommunication Union (ITU) and World Radio Communication Conference (WRC) regularly review frequency spectrum allocations [5]. Studies indicating overlaps between the global system for mobile communications (GSM) in the L band with ultra-high frequency (UHF) radars, and LTE and WiMax with air traffic control (ATC) radars in the S band, highlight the urgency of this endeavor [55–57]. Compounding the issue is the pervasive problem of network congestion, primarily driven by the insatiable demand for bandwidth and data services. This congestion not only diminishes the data speeds but also degrades the service quality, adversely affecting the user experience. In response, the concept of spectrum sharing has emerged as a beacon of hope. By promoting the shared use of spectrum among multiple networks or users, we could optimize the scarce resource's utilization, mitigate congestion, and pave the way for more adaptive and innovative wireless communication systems. This approach is particularly promising in beyond-5G systems, facilitating the coexistence of communication and radar systems within the same frequency bands [2–4]. The broad availability and diverse applications of radar bands, including airborne navigation radars around 3.4 GHz and shipborne radars as well as vessel traffic service radars (VTS) at 5.6 GHz, make them ideal for integration into advanced wireless networks, leading to more efficient spectrum utilization and significantly enhancing the network capabilities [5, 6]. The study of spectrum sharing between communication and radar applications can be delineated into two main categories:

- Radar-Communication Coexistence (RCC).
- Dual Functional Radar-Communication (DFRC) system design.

Regarding RCC, the primary goal is to ensure that both the radar and communication systems operate concurrently with minimal interference to each other. This objective is pursued

by devising effective strategies to handle and minimize the interference between the systems. Conversely, the focus of DFRC system design lies in the development of integrated systems capable of performing both communication and remote sensing simultaneously. The benefit of such systems is their dual functionality, which not only alleviates congestion in the RF spectrum but also provides a singular hardware solution that supports both sensing and communication capabilities [6]. Advancing beyond DFRC, the ISAC paradigm marks a significant leap towards a cohesive fusion of radar and communication operations. Distinct from RCC and DFRC, which prioritize mutual operation and dual-functionality, ISAC proposes a holistic model where sensing and communication processes are not merely adjunct but intricately unified, sharing both the spectral and computational resources. This profound integration facilitates a more strategic utilization of the spectrum, boosts the system efficacy, and heralds novel opportunities for applications necessitating both precise sensing and dependable communication [58–61]. With the escalating demand for spectrum resources, ISAC emerges as an innovative strategy to maximize the shared spectrum's capacity, promising to accommodate the complex requirements of future wireless infrastructures [62–64]. This advanced integration not only seeks to mitigate interference and optimize spectrum usage but also enhances the capabilities of both systems by leveraging their mutual benefits. To sum up, the pivotal role of ISAC in the development of future wireless systems underscores its importance in ensuring efficient spectrum use and enhanced functionalities, meeting the complex demands of modern wireless applications.

2.4.1 Radar and Communications System Coexistence

Delving into the first category of spectrum sharing between communication and the radar applications, RCC emerges as a critical area of focus. The primary objective in RCC is to ensure that both radar and communication systems can operate concurrently with minimal interference, a goal that is vital for the efficient functioning of both systems. This pursuit involves the development of various strategies aimed at effectively managing and minimizing the cross-interference between these systems. Historically, research in RCC has primarily concentrated on scenarios involving a limited number of antennas at both the BS and the radar such as [40, 65–71]. The main challenge in these studies has been the interference from the BS to the receiving radar. From the cellular system's perspective, these investigations involved the BS estimating the radar-cellular interference by assessing whether the radar was in search or tracking mode. This process was often complemented by CSI estimation at the BS to obtain precise channel parameters [72–74]. The study in [66] delved into a sophisticated technique aimed at mitigating the interference between the radar and telecommunication

systems by utilizing a projection method for radar waveforms. This method involves projecting the radar signals onto the null space of the channel matrix that exists between the radar and communication systems. As the field progressed, the coexistence of MIMO communication systems and MIMO radar came to the forefront. This new phase of research focused on the development of mutual interference management techniques to enable a harmonious operation of both systems without compromising their individual performances. Key developments in this area included the integration of orthogonal frequency division multiplexing (OFDM) communications with MIMO radar, and the adoption of transmit beamforming as a method to reduce interference between radar and communications [40]. Additionally, cognitive MIMO radar prototypes, using technologies such as software-defined radio (SDR) and Universal Software Radio Peripheral (USRP), have been explored for compatibility with LTE links [75]. Further advancements in RCC have seen the introduction of various techniques like null space projection, optimum beamforming design, and waveform design to effectively manage the interference between MIMO radar systems and MIMO cellular networks. These methods are aimed at reducing interference and optimizing the detection capabilities of MIMO radar systems while meeting specific operational constraints [40, 76–79]. Recent studies have further diversified RCC research, particularly in the context of complex environments and joint system designs. For instance, [80] emphasized the operational dynamics in cluttered scenarios, focusing on signal management without stringent synchronization between systems. This approach contrasts with [72] which adopted a holistic methodology. The latter paper delved into the intricate balance of optimizing waveforms and filters for both radar and communication systems, reflecting a comprehensive approach to spectrum sharing. These studies exemplify the evolving nature of RCC research, moving towards more integrated and environmentally adaptive solutions. The introduction of reconfigurable intelligent surfaces (RISs) has further opened up new possibilities for enhancing the coexistence and reducing mutual interference between these systems [81, 82]. The integration of mMIMO technologies into RCC is a recent development that has begun to receive attention in the literature. Studies like [8, 83–86] started to explore the implications of incorporating massive MIMO into coexisting communication and radar systems. These studies have characterized important metrics, such as the rate region of joint radar and communication systems and derived expressions for the radar detection probability and downlink SE in the presence of mMIMO. However, this area of research is still burgeoning, and many aspects, particularly those related to joint precoding design and power allocation in the coexistence of mMIMO communications and radar systems, remain to be thoroughly investigated. In radar and communication system coexistence, precoder configuration can be established on either the radar or the communication side. This setup mirrors the ZF precoding

utilized in conventional MIMO communication systems. A fundamental approach in this regard is null-space projection (NSP) [67], predicated on the radar's access to the interference channel state information (ICSI). The NSP method involves the radar first determining the right singular vectors of the interference channel matrix through a singular value decomposition (SVD). Subsequently, it constructs an NSP precoder based on these vectors, which correspond to the channel's null space. This approach ensures that the radar signal, when precoded, is projected onto the channel's null space, effectively canceling interference at the BS. Nonetheless, this strategy may result in considerable degradation of the MIMO radar performance, such as reducing the spatial orthogonality of its search waveforms. To address this, a modified NSP approach was proposed in [87], involving a meticulously set threshold for the channel matrix's singular values. This threshold-based NSP precoder utilizes right singular vectors associated with values below this threshold, enhancing the radar performance while slightly increasing the interference at the BS. Despite these advancements, NSP methods have inherent drawbacks. For instance, they do not allow for precise control over the interference power, which is correlated with the singular values of the stochastic channel. Moreover, there is a risk that the radar might miss the target's response if it aligns with the row space of the communication channel matrix, due to its suppression by the NSP precoder [6]. These challenges, however, can be addressed through convex optimization techniques [70, 88], which aim to optimize the performance of both systems within manageable constraints.

In [89], an innovative precoding design methodology was introduced, aiming at optimizing the DoF within environments where communication and radar systems coexist. This design is pivotal in navigating the complex interference that arises in such scenarios. Concurrently, the research outlined in [90] tackled the intricacies of enhancing the SINR for radar systems, particularly in circumstances characterized by non-uniform interference, and highlights the strategic importance of spectral coexistence management through novel approaches. Additionally, [91] unveiled a cutting-edge optimization method that employs the Alternating Direction Method of Multipliers (ADMM) for the resolution of non-convex problems, primarily aimed at minimizing the Cramér-Rao Bound (CRB) for the precise estimation of radar targets amidst the disturbances from a MU-MIMO communication setup. Extending this framework, [79] proposed a beamforming design, that capitalizes on constructive interference by utilizing the well-understood downlink (DL) multi-user interference (MUI) to amplify the signal strength in mixed-use scenarios.

In conclusion, while significant strides have been made in RCC, the journey is far from complete. The ongoing advancements in massive MIMO technologies present both new

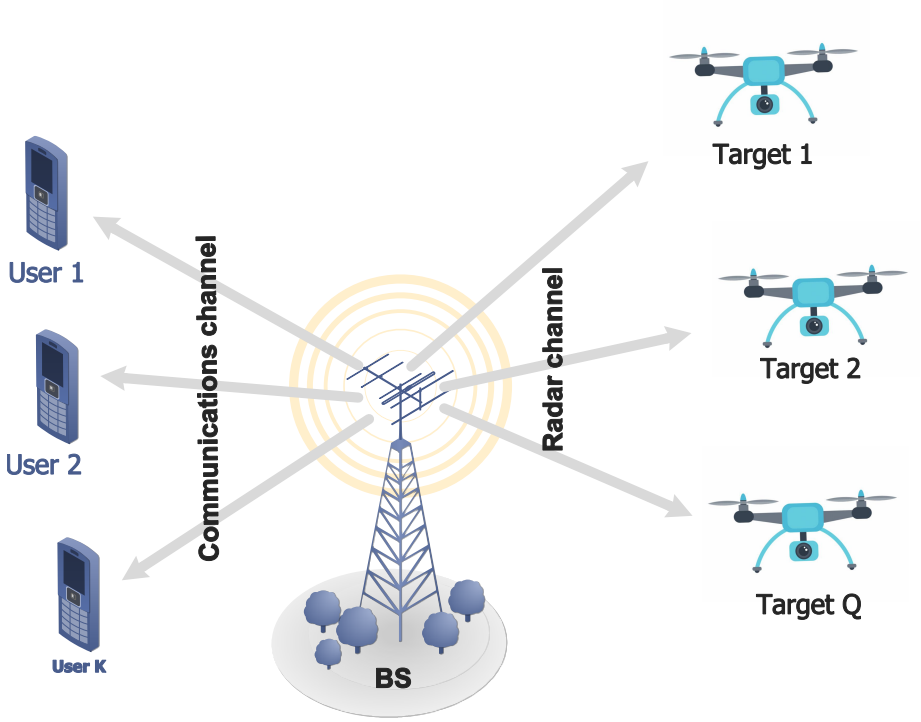

Fig. 2.2 Dual functional radar-communication (DFRC).

opportunities and challenges, indicating a need for continued research to fully reap the potential of these advanced systems in the landscape of RCC.

2.4.2 Dual Functional Radar-Communication (DFRC) system design

The evolution of DFRC systems marks a significant stride in Cooperative Radar and Spectrum Sharing (CRSS). At the heart of DFRC is the innovative integration of radar and communication functions into a unified hardware system at the transmitter, epitomizing spectral, energy, and hardware efficiency, leading to substantial cost reductions [6, 92–95]. This integration, as illustrated in Fig. 2.2, depicts the seamless amalgamation of sensing and communication operations within a single system.

A primary challenge in DFRC lies in crafting a waveform that adaptively handles both target detection and data transmission. This design process typically falls into three categories: radar-centric, communication-centric, and joint design approaches [6, 61, 96]. Radar-centric designs originate from radar probing signals, dating back to initial studies [97], where communication

data is integrated onto the radar pulses through pulse interval modulation (PIM). Examples of this approach include amalgamating amplitude shift keying (ASK), phase shift keying (PSK) and frequency shift keying (FSK) with linear frequency modulation (LFM) signals [6, 98, 99], and combining spread spectrum sequences for communication with binary- and poly-phase codes for radar [100].

Communication-centric designs, on the other hand, are based on pre-existing communication waveforms and protocols. A pioneering example [101] demonstrated the use of OFDM for target detection. In OFDM, the radar target processing for Doppler and delay is separated and performed using Fast Fourier Transform (FFT) techniques. Any unintended communication data effects on the radar echo can be mitigated by dividing the echo and reference OFDM signal matrices on an element-wise basis. Enhancements in sensing are achievable by substituting the sinusoidal carrier in OFDM with a linear frequency modulated (LFM) signal, which benefits from the efficiencies of the fractional Fourier transform (FrFT) [102]. The IEEE 802.11ad protocol, a WLAN standard in the millimeter-wave (mmWave) band, has also been adapted for simultaneous radar sensing and communication in vehicular networks [103]. Additionally, the waveform used for communication must be precisely designed to meet certain requirements for sensing, such as a low peak-to-average power ratio (PAPR), effective correlation characteristics, and the ability to handle clutter interference effectively [61].

Instead of utilizing established sensing and communication waveforms, initiating an ISAC waveform design from the beginning allows for a readily adjustable balance between performance aspects. This approach, known as joint design or collaborative design, positions sensing-focused and communication-focused designs as its outer limits. Typically, the process of designing a joint ISAC waveform is framed as an optimization problem in mathematics, with the goal being to improve metrics related to sensing or communication, subject to conditions that ensure the alternate functionality's effectiveness [61]. As demonstrated in [8, 26, 84, 96], this encompasses enhancing the probability of detection in sensing applications, adhering to SINR constraints for communication users, or prioritizing the SINR optimization while maintaining specific constraints on the probability of detection.

With the advent of 6G networks, DFRC systems have garnered increasing attention, revealing a rich tapestry of research brimming with advancements and challenges. Key contributions include Bazzi *et al*. [104], focusing on efficient beamforming strategies under imperfect CSI, alongside foundational works by Chiriyath *et al*. [73] and Barneto *et al*. [105], which explored the coexistence of radar and communication systems and the importance of efficient resource utilization. Further significant research by Hu *et al.* [106], focused on low-PAPR waveform

design in MIMO-OFDM DFRC systems, while Xu *et al.* [107], designed optimal transmit beampatterns. The intricacies of spectrum sharing, highlighted by Li *et al.* [70], underscore the complexity of resource allocation in shared environments. With mmWave frequencies becoming prominent in 6G networks, insights from Mishra *et al.* [108] on mmWave joint radar communications are particularly relevant. The need for secure and efficient waveform designs was emphasized by Liu *et al.* [94] and Su *et al.* [109], addressing pivotal aspects of waveform design and security. Zhang *et al.* [60] provided a comprehensive overview of signal processing techniques for joint communication and radar sensing.

The DFRC system proposed by Liu *et al.* [6] is an exemplar of innovation, building upon earlier work [96] to optimize both the radar beam patterns and the SINR for communication users. This model distinctively precoded communication symbols and individual radar waveforms, expanding the DoF in MIMO radar waveforms to match the number of antennas. The research outlined in [110] introduced an innovative ISAC strategy that enhances angle of arrival (AoA) estimation at BS through a hybrid fusion of radar data, integrating downlink and uplink information. Furthermore, the research introduced a system model that seamlessly integrates monostatic with bistatic radar modes, harnessing communication signals for sensing alongside communication.

In summary, the fusion of radar sensors with communication systems has sparked a surge of interest in DFRC systems [6, 93, 96, 111–113]. Employing a common spectrum and integrated signal processing techniques, these methodologies enable concurrent radar sensing and wireless communication [114]. The design of DFRC waveforms has evolved through various approaches, including radar-centric [97–99], communication-centric [101–103], and joint designs [6]. Recent advancements in multi-antenna arrays have opened new frontiers, as seen in Hassanien *et al.* [93, 111] and Ma *et al.* [95], which offered robust solutions in complex non-LoS (NLoS) communication channels.

Recent advancements in CF-mMIMO systems, particularly for ISAC, are making significant impacts on 5G and beyond network technologies. Studies such as those by Zeng *et al.* [115], Behdad *et al.* [24], Demirhan *et al.* [25], Mao *et al.* [116], and Elfiatoure *et al.* [26], demonstrated capabilities of CF-mMIMO systems are showcased through their superior network performance and service quality, addressing the constraints found in conventional single-cell ISAC configurations. These systems excel by enabling simultaneous multipoint transmission and reception, coupled with a notable reduction in inter-cell interference. This achievement stems from a sophisticated network architecture comprising distributed APs connected to a CPU, which collaboratively provide information services to users and engage in radar sensing

for target identification. Such a strategic approach results in enhanced SE, decreased latency, and improved accuracy in detecting targets within specific areas. Notably, Zeng *et al*. [115] have furthered this field with their work on power allocation techniques in CF-mMIMO ISAC systems, enhancing the balance between communication and sensing functionalities. In their study, Behdad *et al.* [24] explored the dynamics of a CF-mMIMO ISAC system, characterized by a designated array of transmitting and receiving APs. This setup ensures that users receive services through the transmitting APs, while simultaneously, these signals facilitate sensing operations to pinpoint the location of targets. Signals that bounce back from such targets are captured by the receiving APs and forwarded to the CPU for analysis. To optimize the system's efficiency in target detection, the researchers introduced a power distribution strategy aimed at enhancing the SNR while maintaining the SINR within acceptable limits for users. Building on similar themes, Demirhan *et al.* [25] delved into the challenges of beamforming design within CF-mMIMO ISAC systems. Their research proposed a joint beamforming strategy, meticulously designed to amplify the sensing SNR while concurrently adhering to the communication SINR requirements. This approach underscores the critical balance between ensuring high-quality target sensing and maintaining robust communication links within CF-mMIMO ISAC systems. Additionally, the works of Mao *et al*. [116] and Da *et al*. [117] have advanced the field by focusing on precoder design for CF-mMIMO ISAC systems. Significantly, Da *et al*. [117] explored beyond the efficient balance between communication and sensing functionalities to assess privacy risks associated with target location inference by internal adversaries in ISAC networks.

To succinctly showcase this thesis's novel contributions, we now present two tables for clarity and comparison. The first table (6.1), "Contrasting Our Contributions to the Literature Review," directly highlights how our findings push the boundaries of current research on spectrum sharing in wireless communications. Its main objective is to offer a straightforward comparison, underscoring the advancements we bring to the field. The second table (2.2), "Comparison of PhD Research Papers with Literature Review," a step further by benchmark each of our doctoral papers against the backdrop of existing studies, illustrating how our work both complements and advances the scholarly conversation. These tables aim to provide a clear framework for understanding the unique value of our research, facilitating its appreciation and application by fellow researchers.

Table 2.1 Contrasting our contributions to the literature

Ref.	mMIMO	MIMO Radar	Beamforming design	Power allocation	Imperfect CSI	Multi-target	AP operation mode selection	CF-mMIMO
[24, 25, 115–117]			✓	✓	✓			✓
[40, 65–71]		✓	✓		✓			
[83]	✓	✓	✓	✓	✓			
[85, 86]	✓		✓		✓			
[67, 72–74]		✓	✓					
[92–95, 118]		✓	✓					
[89]		✓	✓			✓		
[110]			✓			✓		
This thesis	✓	✓	✓	✓	✓	✓	✓	✓

Table 2.2 Comparison of PhD research papers with literature review

Research Aspect	Comparison
Coexistence Strategy, Precoding and Power Allocation	*Literature Review*: Focuses on the mutual interference management between MIMO communication systems and radar. Investigates NSP and techniques for interference management beamforming design in MIMO radar and cellular networks [66–68]. *My Papers*: Emphasizes the coexistence of massive MIMO and MIMO radar systems using novel interference mitigation techniques and advanced power allocation strategies.
System Performance Analysis	*Literature Review*: Addresses the integration of OFDM communications with MIMO radar and the use of transmit beamforming to reduce interference [40, 101]. *My Papers*: Provides analytical results for system performance, including radar detection probability and downlink, in mMIMO environments.
mMIMO Integration	*Literature Review*: Highlights the burgeoning interest in integrating mMIMO into RCC systems [83, 85, 86]. *My Papers*: Showcases the application of mMIMO technologies in RCC, providing novel insights and advancements in this emerging area.
CF-mMIMO ISAC	*Literature Review*: Mentions recent advancements in CF-mMIMO systems for ISAC, focusing on power allocation and precoder design [24, 25, 115–117]. *My Papers*: introduce an innovative approach to dynamic AP operation mode selection in CF-mMIMO ISAC networks. This strategy significantly enhances downlink user performance and the capabilities of target detection. Our contributions substantially advance both the theoretical and practical frameworks for CF-mMIMO ISAC systems. By enabling improved communication performance and more robust sensing across multi-zone environments, our work represents a significant step forward in wireless communication technologies

In conclusion, **Chapter 2** offers a comprehensive literature review, providing a holistic understanding of the subject matter. The subsequent chapters will further explore specialized areas of literature review, delving into specific themes and aspects relevant to the research topic.

Chapter 3

Coexistence Between Massive MIMO and Radar Communications: Performance Analysis

3.1 Introduction

The fifth generation (5G) of wireless communication is being rolled out globally. More importantly, both fixed and mobile wireless services are becoming increasingly important with the rapid growth of the wireless communication industry, whilst multiple antenna systems are essential components of 5G networks [10, 11]. The wireless communication sector is expanding at a fast rate and the staggering proliferation of connected devices and services is contributing to the growing congestion of the frequency spectrum. This has led to a phenomenon, coined as the *spectrum congestion problem.* Recently, sharing spectrum between communication systems and radar systems is considered as a promising option and for this reason, has attracted increasing interest in beyond-5G wireless communication systems as a potential solution to spectrum congestion. Thus, sharing spectrum through signal processing is becoming increasingly important as the number of wireless users increases continuously [2–4].

We now recall that the radar bands are an excellent choice to be shared with cellular communication systems due to the extensive spectrum available at radar frequencies for commercial and governmental uses. For instance, radars cover a wide range of frequencies, such as airborne navigation radars around the 3.4 GHz band, shipborne radars and vessel traffic service radars (VTS) at 5.6 GHz [5, 6].

In the last decade, multiple-input multiple-output (MIMO) radar systems have demonstrated superior performance compared with conventional phased-array radars, in terms of providing adaptive arrays for target detection, parameter (location, distance and speed of targets) identifiability, as well as enhanced flexibility for beam pattern design [119, 120, 30]. Unlike the phase-shifted counterparts of a benchmark waveform, each antenna in a MIMO radar transmits an individual waveform [121]. Due to this, phased array radars are less flexible and have a weaker sensing performance than those with an enlarged virtual aperture as in MIMO radar. We also note that the foundations of MIMO radar were built upon concepts, such as degrees-of-freedom (DoFs) and diversity, which were "borrowed" from the MIMO communication theory space [30].

Previous works on sharing spectrum between communication systems and radar, such as [72, 73], almost exclusively focused on a limited number of antennas at the base station (BS) and radar and considered only the interference from the BS to the receive radar which deteriorates its detection probability capabilities. In addition, the radar interference was examined from the perspective of a cellular system, where the BS attempts to estimate the radar-cellular interference by identifying whether or not the radar is in search or tracking mode via a hypothesis testing. Then, the BS estimates the channel parameters to obtain channel state information (CSI) [74]. Recently, a number of works have considered the coexistence between multiple-input multiple-output (MIMO) communication and MIMO radar and focused on developing mutual interference management techniques between MIMO communication and MIMO radar. By doing so, both systems can operate harmonically without interfering with each other while guaranteeing satisfactory performance. For example, in [32], a study has been conducted on the feasibility of combining Orthogonal Frequency Division Multiplexing (OFDM) communications and MIMO radar.

In the context of this work, transmit beamforming has been identified as a promising method for reducing mutual interference between radar and communications. To this end, [40] focused on robust beamforming for MIMO radar and maximized the probability of detection, while guaranteeing a satisfactory received signal-to-interference-plus-noise-ratio (SINR) for each downlink user. The approach used in this investigation is similar to that used by other researchers, such as in [75], who developed a Software-Defined Radio (SDR) based cognitive MIMO radar prototype using Universal Software Radio Peripheral (USRP) devices that coexist with LTE links. Moreover, [67] focused on the interference created by the operation of the radar to the BS by using a projection based technique, where the radar waveforms are projected on the null space of the channel interference matrix between communication and radar system,

but ignored interference to the users. The recent works of [81] and [82] introduced the concept of reconfigurable intelligent surfaces (RISs) to improve the coexistence of radar and communication systems and also to reduce the mutual interference between both systems. In the recent study of [85], only the uplink was considered for the coexistence of massive MIMO and MIMO radar, ignoring the downlink of massive MIMO and the detection probability of the MIMO radar. Furthermore, it examined the interference caused by the radar that affects the uplink of communication systems. We also recall [122], which proposed an opportunistic interference alignment approach for spectrum-shared radar and uplink cellular communications, both of which utilize multiple antennas. The study placed more emphasis on the uplink quality of the user equipment than on the downlink, which is considered as an interference source for radar and the sharing process, whereas the study in [123] investigated the impact of worst-case cellular interference on the radar performance. In order to characterize the impact of cellular uplink interference on the radar performance. It is notable that information sharing, such as CSI, and security issues in information exchange make it difficult to manage interference simultaneously at radars and communication systems [124]. When radar and communication systems are aware of each other, they can cooperate to exchange information that will help in designing their transmissions optimally under some security constraints. There have been some works on interference management in cognitive radio, but from a communication systems perspective only. Nevertheless, it becomes harder to maintain the coexistence between radar and communication, since interference signals stem not only from the communication side, but also from the radar side [125]. Therefore, this paper seeks to develop efficient methodologies to address this challenging issue.

In general, the above mentioned works, focusing on interference mitigation for the coexistence between MIMO radar and communications, have mainly considered the interference from one side; for example, from the BS to the radar or from the radar to BS. They have also exclusively focused on the probability of detection with a limited number of antennas at the radar and BS.

By availing of the recent advances in massive MIMO communications, we intend to investigate the potential benefits of having a very large number of antennas when massive MIMO coexists with MIMO radar to mitigate the mutual interference from communication and radar. The specific contributions of our paper can be summarized as follows:

- We analyze the system performance in the asymptotic regime, where the number of BS antennas (denoted by M) goes to infinity. We show that by deploying more antennas at the BS, we can improve the performance of the massive MIMO system, while keeping

the interference to the radar system unchanged. Moreover, if we use large M and at the same time reduce the transmit power M times, we can avoid the interference to the radar system, while maintaining a satisfactory quality of service at the massive MIMO system.

- We derive closed-form expressions for the average probability of detection of the radar system, and the downlink spectral efficiency of the massive MIMO system using the use-and-then-forget bounding technique. Our numerical results corroborate our theoretical analysis and provide interesting designs into the interplay between massive MIMO communications and radar operation.

- We propose a power allocation scheme which selects the transmit powers at the MIMO radar and the BS to maximize the probability of detection for MIMO radar, given a quality-of-service constraint at the communication systems. The optimal powers can be determined in closed-form. Considering the power budget at the radar and BS, our proposed power allocation achieves substantial improvement in the probability of detection over the case without optimal power allocation.

- As demonstrated by the numerical results, by increasing the number of antennas at both the BS and radar, the system improves in terms of target detection performance and spectral efficiency. This improvement is even more striking when the environmental conditions are harsh, for example in the case of low signal-to-noise ratio (SNR). In addition, the investigation of the trade-off between the performance of radar and communication is revealed.

3.2 System Model

We consider a time division duplex (TDD) downlink massive MIMO communication system coexisting with a MIMO radar system on the same time-frequency resources. A BS consisting of an array with M elements serves K single-antenna users $(M > K)$. The MIMO radar system consists of a uniform linear array (ULA) radar, equipped with N_t transmitting antennas and N_r receiving antennas, that is detecting targets located in the far field. For the sake of analytical tractability and without significant loss of generality, we henceforth assume that $N_t = N_r = N$. The basic structure of the system model is illustrated in Fig. 1, where:

- $z_k \in \mathbb{C}^{M\times 1}$ is the channel vector response between the BS and the k-th user. The channel z_k is modeled as follows:

$$z_k = \beta_k^{1/2} \boldsymbol{h}_k, \tag{3.1}$$

  where $\boldsymbol{h}_k$ represents the small-scale fading, assuming to include independent and identically distributed (i.i.d.) random variables, i.e., $\boldsymbol{h}_k \sim \mathscr{CN}(0, \boldsymbol{I}_M)$, while β_k represents the large-scale fading.

- $\boldsymbol{G} \in \mathbb{C}^{M\times N}$ represents the interference channel matrix from the BS to the radar receiver, whose elements are i.i.d. $\sim \mathscr{CN}(0, \beta_{br})$, where β_{br} is the corresponding large-scale fading coefficient.

- $\boldsymbol{f}_k \in \mathbb{C}^{N\times 1}$ is the interference channel from the radar transmitter to the k-th user. Denote by $\boldsymbol{F} = [\boldsymbol{f}_1 \ldots \boldsymbol{f}_K] \in \mathbb{C}^{N\times K}$ the corresponding channel matrix from the radar transmitter to all K users. We assume that $\boldsymbol{f}_k \sim \mathscr{CN}\left(0, \bar{\beta}_k \boldsymbol{I}_N\right)$, where $\bar{\beta}_k$ represents the large-scale fading.

For the downlink transmission, we assume that the BS has perfect channel state information[1] and employs maximum-ratio (MR) precoding to process the data symbols before broadcasting to the K users. We consider MR precoding at the BS because MR has low computational complexity for practical implementation and performs sufficiently well in the massive MIMO regime [126]. In addition, MR precoding is very suitable for distributed massive MIMO or cell-free massive MIMO systems, where the antennas are distributed in a large area, since it can be implemented locally at each antenna. The system performance can be improved with other linear processing techniques, such as zero-forcing (ZF). However, it requires high computational complexity (due to the matrix inversion), and cannot be implemented in a distributed manner. The transmitted signal from the BS to all K users is

$$\boldsymbol{x} = \sum_{k=1}^{K} \boldsymbol{t}_k d_k, \tag{3.2}$$

where ρ is the normalized transmit power at the BS, i.e. $\mathbb{E}\left\{\|\boldsymbol{x}\|^2\right\} = \rho$. where d_k is the symbol intended for the k-th user, with $\mathbb{E}\left\{|d_k|^2\right\} = 1$ and $\boldsymbol{t}_k \in \mathbb{C}^{M\times 1}$ is the MR precoding vector given

[1] We assume that the BS has perfect CSI knowledge from its users and of the large-scale fading (channel statistics) from the radar to the BS. Note that the channels from the BS to the users can be acquired easily by uplink pilots via time-division duplex operation [126]. The large-scale fading coefficients from the radar to the BS change very slowly with time (compared to the instantaneous CSI), and hence, can be estimated readily [127]. Although this is an idealistic assumption, it offers analytical tractability and also is very relevant for systems with small mobility with a relatively large coherence interval.

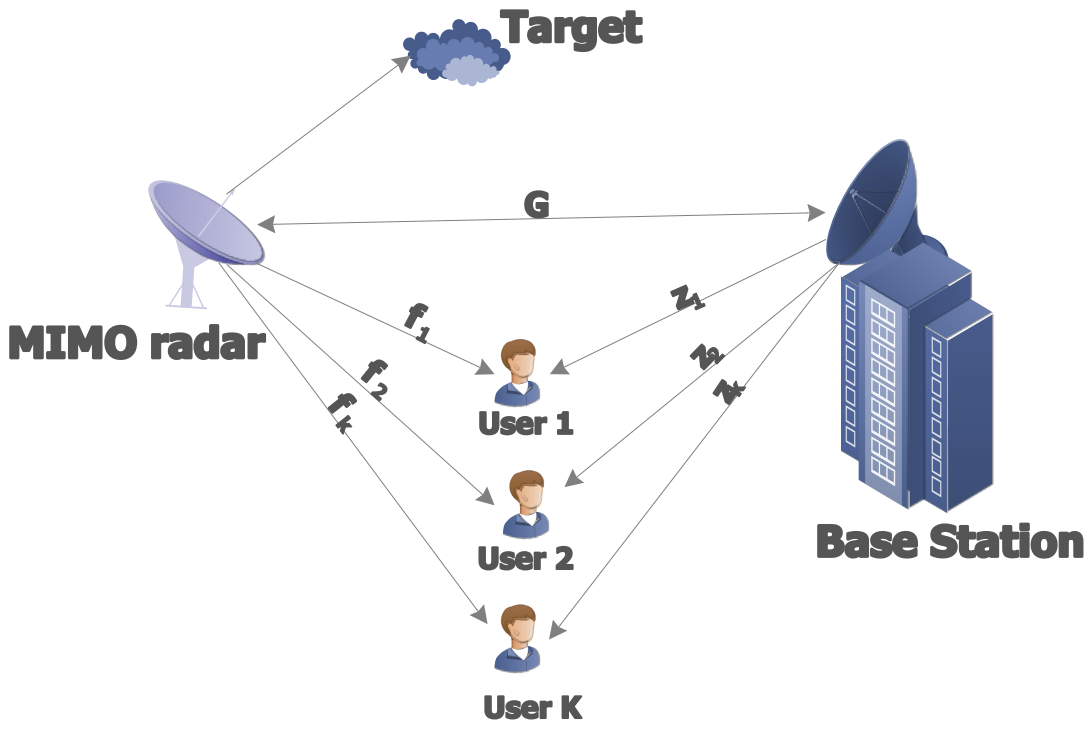

Fig. 3.1 The considered system setup where a mMIMO communication system coexists with a MIMO radar.

by

$$\boldsymbol{t}_k = \sqrt{\frac{\rho}{\beta_k KM}} \boldsymbol{z}_k{}^*. \tag{3.3}$$

At the same time, the radar transmitter sends probing signals to the target. Let $\boldsymbol{s} \in \mathbb{C}^{N\times 1}$, where $\mathbb{E}\left\{\boldsymbol{s}\boldsymbol{s}^H\right\} = \boldsymbol{I}_N$, be the radar transmit waveform. Then, the received signal at user k is

$$y_k = \boldsymbol{z}_k{}^T \boldsymbol{x} + \sqrt{P_R}\mathbf{f}_k^T \boldsymbol{s} + n_k, \tag{3.4}$$

where P_R and $n_k \sim \mathscr{CN}\left(0, \sigma_C^2\right)$ denote the transmitted power of the radar signal and the noise at user k, respectively.

For the radar link, we make the classical assumption that the channel from the MIMO radar to the target is line-of-sight (LoS) [119, 121] . Then, the received vector by the radar receiver, $\mathbf{y}^R$, contains the desired signal (echo from the target) and the interference from BS, described as follows:

$$\boldsymbol{y}^R = \underbrace{\alpha\sqrt{P_R}\boldsymbol{A}(\theta)\boldsymbol{s}}_{\text{desired signal}} + \underbrace{\boldsymbol{G}^T \sum_{k=1}^{K} \boldsymbol{T}_k d_k}_{\text{interference from BS}} + \boldsymbol{w}, \tag{3.5}$$

where $\boldsymbol{w} \sim \mathscr{CN}\left(0, \sigma_R^2 \boldsymbol{I}_N\right)$ is the noise at the radar receiver. In addition, α is the complex path loss of the radar-target-radar path, θ is the azimuth angle of the target, and $\boldsymbol{A}(\theta) = \boldsymbol{A}_R(\theta)$ $\boldsymbol{A}_T^T(\theta)$, where $\boldsymbol{A}_R(\theta)$ and $\boldsymbol{A}_T^T(\theta)$ represent the transmit and receive steering vectors of radar antenna array respectively, where [40]

$$\boldsymbol{A}_T(\theta) = \left[1, e^{-j\frac{2\pi d}{\lambda}\sin(\theta)}, \ldots, e^{-j\frac{2\pi d}{\lambda}(N-1)\sin(\theta)}\right]^T, \tag{3.6}$$

$$\boldsymbol{A}_R(\theta) = \boldsymbol{A}_T(\theta) = \boldsymbol{A}(\theta). \tag{3.7}$$

In the above, λ and d denote the signal wavelength and inter-antenna spacing, where $d = \lambda/2$.

3.3 Probability of Detection and Spectral Efficiency Analysis

3.3.1 Large-M Analysis

In this section, in order to see how massive MIMO supports the coexistence between radar and communication systems, we analyze the system performance when the number of BS antennas goes to infinity.

Scenario 1 ($M \to \infty$ and ρ is fixed):

For the radar communication link, by substituting (3.3) into (4.11), we obtain

$$\boldsymbol{y}^R = \alpha\sqrt{P_R}\boldsymbol{A}(\theta)\boldsymbol{s} + \boldsymbol{G}^T \sum_{k=1}^{K} \sqrt{\frac{\rho}{\beta_k K M}} z_k{}^* d_k + \boldsymbol{w}. \tag{3.8}$$

Applying the Lindeberg-Lévy central limit theorem, we obtain

$$\boldsymbol{y}^R \xrightarrow{d} \alpha\sqrt{P_R}\boldsymbol{A}(\theta)\boldsymbol{s} + \sum_{k=1}^{K}\sqrt{\frac{\rho}{K}}\mathbf{v}_k d_k + \boldsymbol{w}, \text{ as } M \to \infty, \tag{3.9}$$

where $\xrightarrow{d}$ denotes convergence in distribution, and $\mathbf{v}_k$ is Gaussian vector with i.i.d. $\mathscr{CN}(0,\beta_{br})$ elements. We can see that, when the number of BS antennas grows without bound, the interference from the BS is independent of M. This means that even when the number of BS antennas increases, the performance of the radar communications will remain unchanged.

For the massive MIMO system, the substitution of (3.2) into (3.4) gives the received signal at the k-th user, as follows

$$y_k = {z_k}^T \boldsymbol{T}_k d_k + \sum_{j=1, j\neq k}^{K} {z_k}^T \boldsymbol{T}_j d_j + \sqrt{P_R}{\boldsymbol{f}_k}^T \boldsymbol{s} + n_k. \tag{3.10}$$

By dividing the LHS and RHS of (3.10) by $\sqrt{M}$ and using the law of large numbers, we obtain

$$\frac{y_k}{\sqrt{M}} \xrightarrow{a.s.} \sqrt{\frac{\rho\beta_k}{K}} d_k, \text{ as } M \to \infty. \tag{3.11}$$

where $\xrightarrow{a.s.}$ denotes almost sure convergence. The above result implies that, as $M \to \infty$, the interuser interference, interference from radar, and noise disappear, and hence, the system performance of massive MIMO improves without bound. In other words, the use of more antennas at the BS can improve the massive MIMO system performance, while does not cause more interference to the radar.

Scenario 2 ($M \to \infty$ and $\rho = \rho_0/M$, where ρ_0 is fixed):

In this section, we consider the case where the number of BS antennas goes to infinity, and at the same time the transmit power is scaled down proportionally to $1/M$. For the radar communication link, with $\rho = \rho_0/M$, (3.8) becomes

$$\begin{aligned}\boldsymbol{y}^R &= \alpha\sqrt{P_R}\boldsymbol{A}(\theta)\boldsymbol{s} + \boldsymbol{G}^T \sum_{k=1}^{K}\sqrt{\frac{\rho}{\beta_k K M^2}}{z_k}^* d_k + \boldsymbol{w} \\ &\xrightarrow{a.s.} \alpha\sqrt{P_R}\boldsymbol{A}(\theta)\boldsymbol{s} + \boldsymbol{w},\end{aligned} \tag{3.12}$$

where we have used the law of large numbers to obtain the above convergence. For the massive MIMO system, by substituting (3.3) and $\rho = \rho_0/M$ into (3.10), and using again the law of large numbers, we obtain

$$\begin{aligned} y_k &= \sqrt{\frac{\rho_0}{\beta_k K M^2}} \|z_k\|^2 d_k + \sum_{j=1, j\neq k}^{K} {z_k}^T \sqrt{\frac{\rho_0}{\beta_j K M^2}} \mathbf{z}_j^* d_j \\ &\quad + \sqrt{P_R} {\boldsymbol{f}_k}^T \boldsymbol{s} + n_k \\ &\xrightarrow{a.s.} \sqrt{\frac{\rho_0 \beta_k}{K}} d_k + \sqrt{P_R} {\boldsymbol{f}_k}^T \boldsymbol{s} + n_k. \end{aligned} \tag{3.13}$$

The results obtained in (3.12) and (3.13) imply that by using a large number of antennas at the BS together with cutting down the BS transmit power proportionally to $1/M$, we can avoid the interference to the radar system, while maintaining a given quality of service at the massive MIMO system.

3.3.2 Probability of Detection

In this section, we derive a closed-form expression for the average probability of detection, under the Neyman-Pearson criterion. By using the generalized likelihood ratio test, the asymptotic probability of detection for radar, P_d, is [40]

$$P_d = 1 - \mathfrak{F}_{X_2^2(\mu)} \left(\mathfrak{F}_{X_2^2}^{-1} (1 - P_{FA}) \right), \tag{3.14}$$

where P_{FA}, $\mathfrak{F}_{X_2^2(\mu)}$, $\mathfrak{F}_{X_2^2}^{-1}$ represent the probability of false alarm, the non-central Chi-square Cumulative Distribution Function (CDF) with 2 Degrees of Freedom (DoF) and the inverse function of Chi-square CDF, respectively. The non-centrality parameter (μ) for X_2^2 is given by

$$\mu = |\alpha|^2 L P_R \mathrm{tr} \left(\boldsymbol{A}\boldsymbol{A}^H \left(\boldsymbol{G}^T \tilde{\boldsymbol{T}} \boldsymbol{G}^* + \sigma_R^2 \boldsymbol{I}_N \right)^{-1} \right), \tag{3.15}$$

where L is the length of the communication frame for the radar link, and

$$\tilde{\boldsymbol{T}} = \sum_{k=1}^{K} \boldsymbol{T}_k \boldsymbol{t}_k^H = \mathbf{T}\mathbf{T}^H = \frac{\rho}{KM} \left(\boldsymbol{H}^* \boldsymbol{H}^T \right), \tag{3.16}$$

where $\boldsymbol{H} = [\boldsymbol{h}_1 \ldots \boldsymbol{h}_K]$. By the definition of the generalized Marcum Q-function, P_d given by (3.14) can be rewritten as

$$P_d = Q_1(\sqrt{\mu}, \sqrt{C_{FA}}), \tag{3.17}$$

where $Q_1(.,.)$ is the Marcum Q-function of order 1 [128], and $C_{FA} = \mathfrak{F}^{-1}_{x_2^2}(1 - P_{FA})$. Thus, the average probability of detection is given by

$$\mathbb{E}\{P_d\} = \mathbb{E}\left\{Q_1(\sqrt{\mu}, \sqrt{C_{FA}})\right\}, \tag{3.18}$$

where the expectation is taken over μ.

It is difficult (if not impossible) to obtain a closed-form solution for the above average probability of detection due to the analytically intractable form of Marcum-Q function and μ given in (4.29). To render (3.18) more amenable to further analysis, we use a tight approximation for μ, which is obtained from the massive MIMO space. More precisely, by using the trace lemma, as $M \to \infty$, we obtain

$$\frac{1}{M}\boldsymbol{G}^T \tilde{\boldsymbol{T}} \boldsymbol{G}^* - \frac{\beta_{br}}{M}\mathrm{tr}(\tilde{\boldsymbol{T}})\boldsymbol{I}_N \overset{a.s.}{\to} \boldsymbol{0}. \tag{3.19}$$

This implies that at large M, $\frac{1}{M}\boldsymbol{G}^T \tilde{\boldsymbol{T}} \boldsymbol{G}^*$ is very close to $\frac{\beta_{br}}{M}\mathrm{tr}(\tilde{\boldsymbol{T}})\boldsymbol{I}_N$. As a result, the non-centrality parameter μ given by (4.29) can be approximated by

$$\begin{aligned}\mu &\approx |\alpha|^2 L P_R \mathrm{tr}\left(\boldsymbol{A}\boldsymbol{A}^H \left(\beta_{br}\mathrm{tr}(\tilde{\boldsymbol{T}})\boldsymbol{I}_N + \sigma_R^2 \boldsymbol{I}_N\right)^{-1}\right) \\ &= \frac{|\alpha|^2 L P_R \mathrm{tr}(\boldsymbol{A}\boldsymbol{A}^H)}{\beta_{br}\mathrm{tr}(\tilde{\boldsymbol{T}}) + \sigma_R^2} = \frac{|\alpha|^2 L P_R \mathrm{tr}(\boldsymbol{A}\boldsymbol{A}^H)}{\varepsilon + \sigma_R^2},\end{aligned} \tag{3.20}$$

where $\varepsilon = \beta_{br}\mathrm{tr}(\tilde{\boldsymbol{T}})$. From (6.24) and the law of large numbers together with the fact that, in massive MIMO, the number of BS is large, we can reasonably consider ε is close to $\beta_{br}\rho$ with high probability. Since ρ is the transmit power at the BS, which is normally chosen so that $\beta_{br}\rho$ is much larger than the noise power σ_R^2, we can remove σ_R^2 from the denominator of (3.20) to obtain

$$\mu \approx \frac{\left|\alpha|^2 L P_R \mathrm{tr}\left(\boldsymbol{A}\boldsymbol{A}^H\right)\right.}{\varepsilon}. \tag{3.21}$$

By using the approximation (3.21), we can obtain an approximating closed-form expression for the average probability of detection provided in the following proposition.

Proposition 1 *The average probability of detection can be approximated by*

$$\bar{\mathrm{P}}_d = 1 - \sum_{n\geq 0} \frac{1}{2^{MK}\Gamma(MK)} \left(\frac{c}{2}\right)^n d_n 2c^{\frac{MK-n}{2}} \times I_{(MK-n)}(\sqrt{c}), \tag{3.22}$$

where $I_{(MK-n)}(\sqrt{c})$ *denotes the modified Bessel function of the second kind and* $(MK-n)$ *order,* $c = 2MK|\alpha|^2 LP_R tr(\boldsymbol{A}\boldsymbol{A}^H)/(\beta_{br}\rho)$*, and*

$$d_n = \frac{\gamma\left(1+n, \frac{\mathfrak{F}^{-1}_{x_2^2}(1-P_{FA})}{2}\right)}{\Gamma(1+n)},$$

where $\Gamma(\cdot)$ *is the Gamma function, and* $\gamma(\cdot,\cdot)$ *is the lower incomplete Gamma function.*

Proof 1 *See Appendix A.*

3.3.3 Spectral Efficiency

In this section, we derive a closed-form expression for the spectral efficiency of the downlink transmission from the BS to the users. The signal received at the k-th user given in (3.10) can be further expressed as

$$y_k = \mathbb{E}\left\{\boldsymbol{z}_k{}^T \boldsymbol{t}_k\right\} d_k + \left(\boldsymbol{z}_k{}^T \boldsymbol{t}_k - \mathbb{E}\left\{\boldsymbol{z}_k{}^T \boldsymbol{t}_k\right\}\right) d_k + \sum_{j=1, j\neq k}^{K} \boldsymbol{z}_k{}^T \boldsymbol{t}_{kj} d_j + \sqrt{P_R}\boldsymbol{f}_k{}^T \boldsymbol{s} + n_k. \tag{3.23}$$

By using the use-and-then-forget bounding technique [126, Eq. (2.44)], we obtain the following spectral efficiency at the k-th user:

$$\mathrm{SE}_k = \log_2\left(1 + \mathrm{SINR}_k\right), \tag{3.24}$$

where

$$\mathrm{SINR}_k = \frac{|\mathbb{E}\left\{\boldsymbol{z}_k{}^T \boldsymbol{T}_k\right\}|^2}{\mathbb{E}\left\{|\boldsymbol{z}_k{}^T \boldsymbol{T}_k|^2\right\} - \left|\mathbb{E}\left\{\boldsymbol{z}_k{}^T \boldsymbol{T}_k\right\}\right|^2 + A_k}, \tag{3.25}$$

where A_k represents the interference from other users and radar, given by

$$A_k = \underbrace{\sum_{j=1, j\neq k}^{K} \mathbb{E}\left\{\left|\boldsymbol{z}_k{}^T \boldsymbol{T}_j\right|^2\right\}}_{\text{inter-user interference}} + \underbrace{P_R \mathbb{E}\left\{\left\|\boldsymbol{f}_k\right\|^2\right\}}_{\text{radar interference}} + \sigma_c^2. \tag{3.26}$$

Proposition 2 *The downlink spectral efficiency (in bit/s/Hz) for user k is*

$$\mathrm{SE}_k = \log_2\left(1 + \frac{\rho M \beta_k / K}{\rho \beta_k + P_R N \bar{\beta}_k + \sigma_c^2}\right). \tag{3.27}$$

Proof 2 *See Appendix A.*

Remark 1 *From (3.27), we can first represent ρ as a function of the spectral efficiency as follows:*

$$\rho = \frac{\left(2^{\mathrm{SE}_k} - 1\right)\left(P_R N \bar{\beta}_k + \sigma_c^2\right)}{M\beta_k / K - \left(2^{\mathrm{SE}_k} - 1\right)\beta_k}. \tag{3.28}$$

Then, by substituting (3.28) into (3.22), we can represent the average probability of detection as a function of the spectral efficiency which enables us to further investigate the performance tradeoff between the radar and massive communications.

3.4 Power Allocation

We aim at allocating the transmitted power at the radar P_R and transmit power at the BS ρ to maximize the probability of detection, under the constraints on per user spectral efficiency and transmit powers at the radar and the BS. More precisely, the optimization problem is mathematically described as:

$$(\mathbb{P}1): \quad \max_{P_R, \rho} \quad P_d \tag{3.29a}$$

$$\text{s.t.} \quad \mathrm{SE}_k \geq \mathrm{SE}_{\mathrm{th}}, \ \forall k, \tag{3.29b}$$

$$P_R \leq P_{R_{(max)}}, \tag{3.29c}$$

$$\rho \leq \rho_{(max)}, \tag{3.29d}$$

where $\rho_{(max)}$ denotes the maximum transmit power at the BS, $P_{R(max)}$ is the maximum transmit power at the MIMO radar, and $\mathrm{SE}_{\mathrm{th}}$ is the minimum spectral efficiency required by the k-th user.

By using (3.17) and (3.21), problem $(\mathbb{P}1)$ can be (approximately) equivalent to

$$(\mathbb{P}2): \quad \max_{P_R,\rho} \quad \bar{\mu} \triangleq \frac{\left|\alpha\right|^2 L P_R \mathrm{tr}\left(\boldsymbol{A}\boldsymbol{A}^H\right)}{\beta_{br}\rho} \tag{3.30a}$$

$$\text{s.t.} \quad \frac{\rho M \beta_k / K}{\rho\beta_k + P_R N \bar{\beta}_k + \sigma_c^2} \geq \gamma_{th}, \ \forall k, \tag{3.30b}$$

$$P_R \leq P_{R_{(max)}} \tag{3.30c}$$

$$\rho \leq \rho_{(max)}, \tag{3.30d}$$

where $\gamma_{th} = 2^{\mathrm{SE}_{\mathrm{th}}} - 1$. The constraint (30b) is equivalent to

$$\left(\frac{M\beta_k}{K} - \gamma_{th}\beta_k\right)\rho \geq \gamma_{th} P_R N \bar{\beta}_k + \gamma_{th}\sigma_c^2. \tag{3.31}$$

Note that, if $\left(\frac{M\beta_k}{K} - \gamma_{th}\beta_k\right) \leq 0$, then (3.31) is not satisfied, and hence, the optimization problem is infeasible. This means that we cannot find transmit powers at the radar and the BS to meet the constraints. We next consider the case where $\left(\frac{M\beta_k}{K} - \gamma_{th}\beta_k\right) > 0$. Under this condition, (3.31) results in

$$\rho \geq \underbrace{\frac{\gamma_{th} N \bar{\beta}_k}{\frac{M\beta_k}{K} - \gamma_{th}\beta_k}}_{C_{1,k}} P_R + \underbrace{\frac{\gamma_{th}\sigma_c^2}{\frac{M\beta_k}{K} - \gamma_{th}\beta_k}}_{C_{2,k}}, \ \forall k. \tag{3.32}$$

From (30d) and (32), the problem is feasible only if

$$\rho_{(max)} \geq C_{1,k} P_R + C_{2,k}, \ \forall k, \tag{3.33}$$

which is equivalent to

$$P_R \leq \frac{\rho_{(max)} - C_{2,k}}{C_{1,k}}, \ \forall k. \tag{3.34}$$

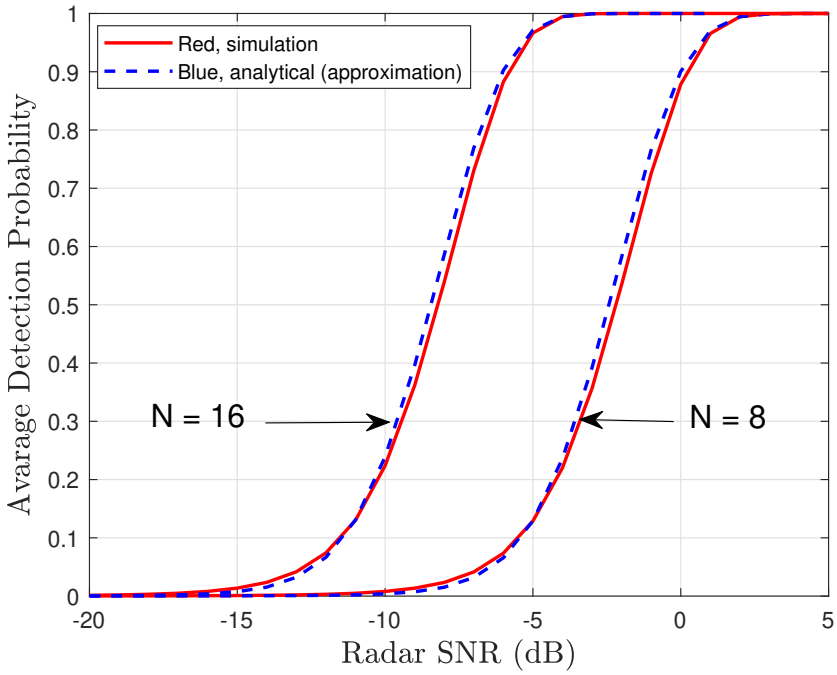

Fig. 3.2 Average detection probability versus the radar SNR with different N, with $P_{FA} = 10^{-5}$, $M = 35$, $K = 4$.

Thus, the optimization problem is feasible only if

$$P_R \leq \min\left(P_{R(max)}, \frac{\rho_{(max)} - C_{2,1}}{C_{1,1}}, \ldots, \frac{\rho_{(max)} - C_{2,K}}{C_{1,K}}\right) \triangleq \bar{P}_R. \tag{3.35}$$

From (30a) and (33), we have

$$\begin{aligned} \bar{\mu} &\leq \frac{\left|\alpha\right|^2 L P_R \mathrm{tr}\left(\boldsymbol{A}\boldsymbol{A}^H\right)}{\beta_{br} \max\limits_k \left(C_{1,k} P_R + C_{2,k}\right)} \\ &= \frac{\left|\alpha\right|^2 L \mathrm{tr}\left(\boldsymbol{A}\boldsymbol{A}^H\right)}{\beta_{br} \max\limits_k \left(C_{1,k} + C_{2,k}/P_R\right)} \\ &\leq \frac{\left|\alpha\right|^2 L \bar{P}_R \mathrm{tr}\left(\boldsymbol{A}\boldsymbol{A}^H\right)}{\beta_{br} \max\limits_k \left(C_{1,k} \bar{P}_R + C_{2,k}\right)}. \end{aligned} \tag{3.36}$$

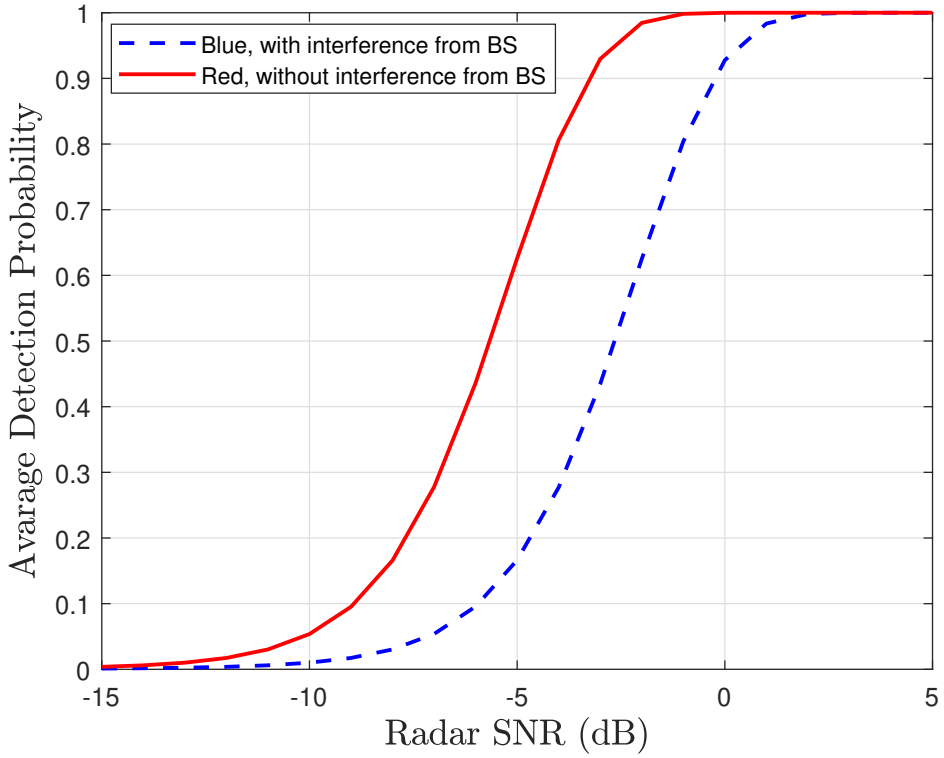

Fig. 3.3 Average detection probability versus the radar SNR, with and without interference from the BS.

Therefore, the optimal values of P_R and ρ are

$$\begin{cases} P_R^* = \bar{P}_R \\ \\ \rho^* = \max\limits_k (C_{1,k}\bar{P}_R + C_{2,k}), \end{cases} \tag{36}$$

which yield the optimum value of $\bar{\mu}$ as

$$\bar{\mu}^* = \frac{|\alpha|^2 L \bar{P}_R \mathrm{tr}\left(\boldsymbol{A}\boldsymbol{A}^H\right)}{\beta_{br} \max\limits_k (C_{1,k}\bar{P}_R + C_{2,k})}. \tag{3.37}$$

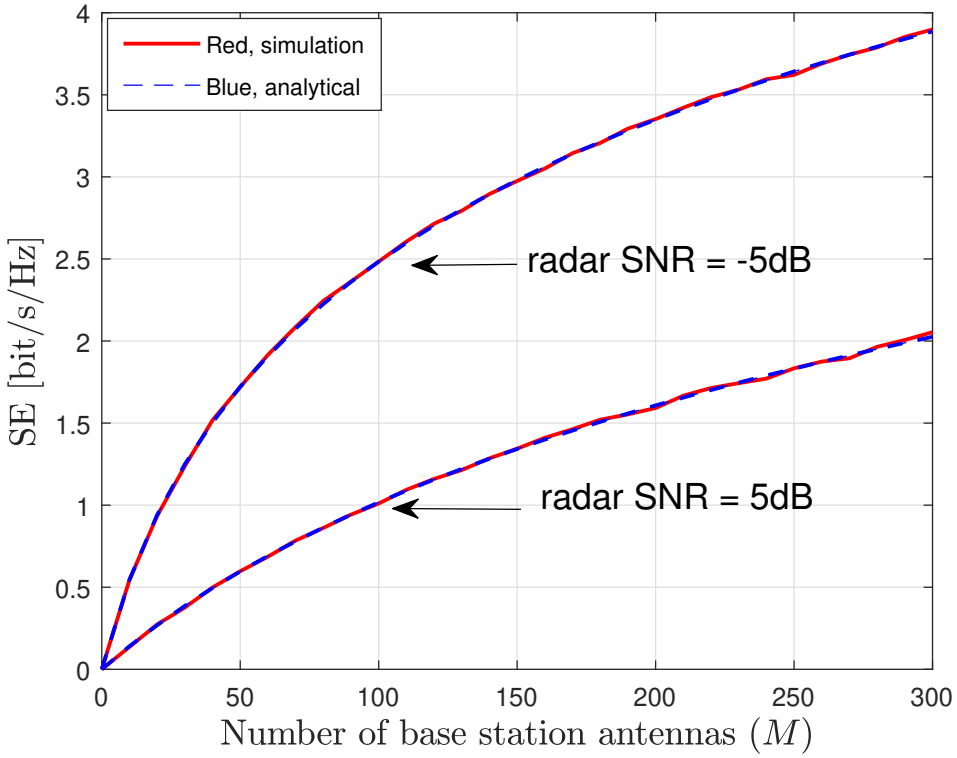

Fig. 3.4 The downlink spectral efficiency versus the number of base station antennas (M), for different radar SNR, $K = 10$.

3.5 Numerical Results

In this section, we provide numerical results to verify our analysis based on Monte-Carlo simulations with 50,000 iterations. For all examples, we choose $\sigma_R^2 = \sigma_C^2 = 1$, and $P_{FA} = 10^{-5}$. We start with a simple model where all large-scale fading coefficients are equal to 1, i.e, $\beta_k = \bar{\beta}_k = \beta_{br} = 1, \forall k$. We first evaluate the tightness of our closed-form expression for the probability of detection. Figure 3.2 shows the average probability of detection versus the radar SNR, for $M = 35$, $K = 4$, and $\rho = 0$ dB. As mentioned before, we assume that the MIMO radar system deploys a ULA. The inter-antenna spacing for MIMO radar is $d = \lambda/2$. The radar SNR is defined as $SNR_R = \frac{L|\alpha|^2 P_R}{\sigma_R^2}$ [40]. The target is set to be located at the direction of $\theta = 10^\circ$. In Fig. 3.2, the analytical curves are generated by using the closed-form expression given by (3.22), while the simulation curves are generated by using (3.18) together with Monte-Carlo experiments. We can see from the figure that the relative gap between our analytical results and the simulation results is very small which verifies the tightness of our approximating closed-

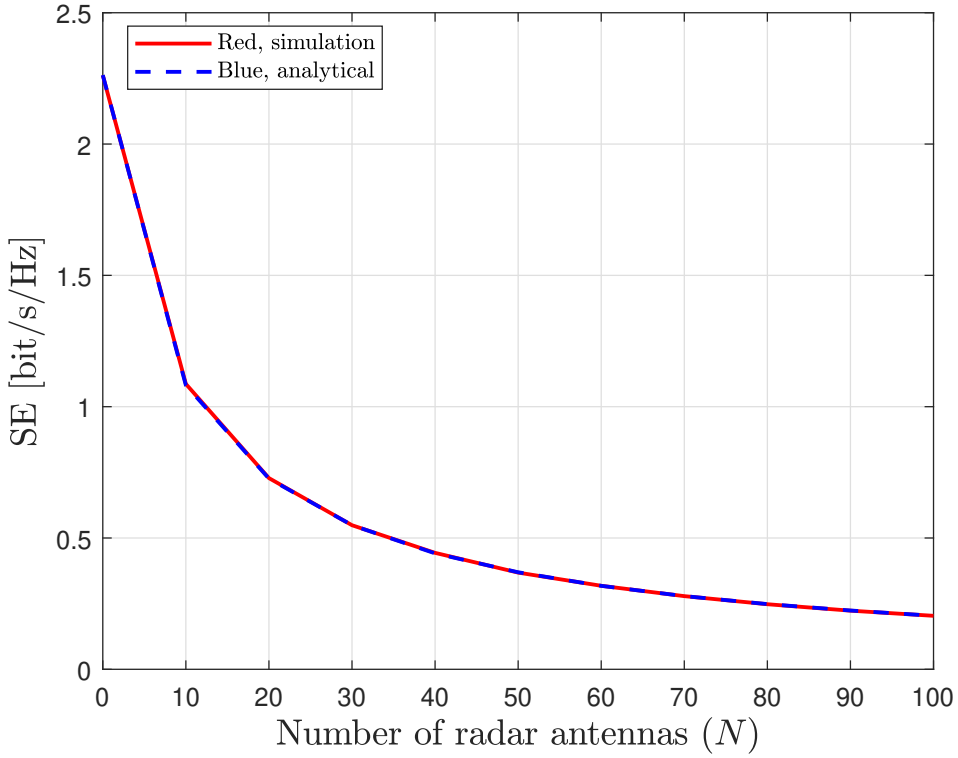

Fig. 3.5 The downlink spectral efficiency versus the number of the radar antennas (N), $K = 20$, $\rho = 5$ dB.

form expression. In addition, as expected, Fig. 3.2 shows that the probability of detection improves when the SNR increases or the number of antennas at the radar increases.

Next, we study the effect of interference from the BS on the performance of the radar link. Figure 3.3 shows the average probability of detection with and without interference from the BS. The case of without interference from the BS is equivalent to the scenario where there is no coexistence between massive MIMO and radar communications. For this case, we set $\rho = 0$. It can be seen from Fig. 3.3 that the interference from the BS significantly reduces the performance of the radar communications. For example, when the radar SNR is -2 dB, the average probability of detection is equal to 0.4 and 0.9 for the cases with and without interference from the BS, respectively.

Figure 3.4 shows the downlink spectral efficiency of massive MIMO systems versus the number of BS antennas M, for different radar SNRs. The analytical results perfectly match with the simulation results, which verifies the correctness of our analysis. As expected, when the number of BS antennas increases, the spectral efficiency increases as well. In addition,

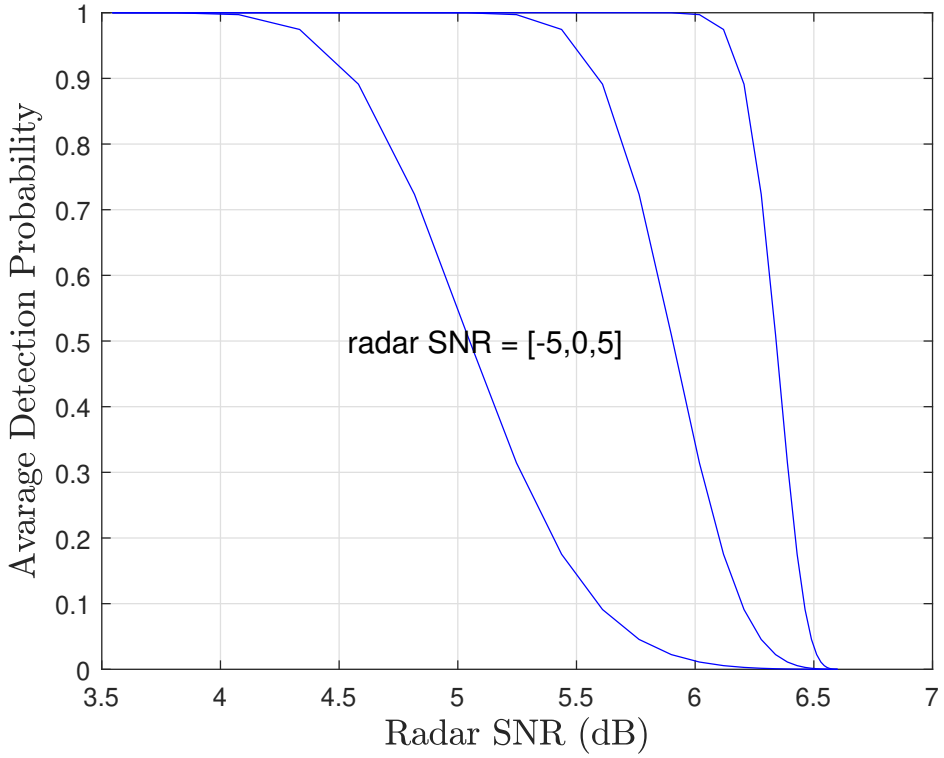

Fig. 3.6 Trade-off between the downlink spectral efficiency and the probability of detection with different radar SNR, $M = 500$.

the radar SNR has a strong effect on the spectral efficiency. The figure also shows that by using more antennas at the BS, we can reduce the effect of interference from the radar. For example, when the radar SNR increases from -5 dB to 5 dB, the spectral efficiency reduces about 2.5 times at $M = 100$, and about 2 times at $M = 200$. The strong effect of the radar interference on the massive MIMO systems is also shown in Fig. 3.5 where we plot the spectral efficiency as a function of the number of transmit/receive antennas at the radar. Note that the transmit signal vector at the radar is $\sqrt{P_R}\boldsymbol{s}$, where $\mathbb{E}\left\{\boldsymbol{s}\boldsymbol{s}^H\right\} = \boldsymbol{I}_N$. Thus, the total transmit power at the radar is NP_R. As a result, the more antennas are used at the radar, the more interference is caused on the massive MIMO system, and hence, the spectral efficiency reduces. Finally, Fig. 3.6 shows the important trade-off between the performance of massive MIMO and radar communication systems. For a given radar SNR, when the spectral efficiency increases, the probability of detection decreases and vice versa. Figure 3.7 shows the comparison of detection probability with and without optimal power allocation following the methodology in Section 3.4. Without power allocation means that we use the full powers at the BS and the radar, i.e., $\rho = \rho_{(max)}$ and $P_R = P_{R(max)}$. For fair comparison, in power allocation, we choose SE_{th}

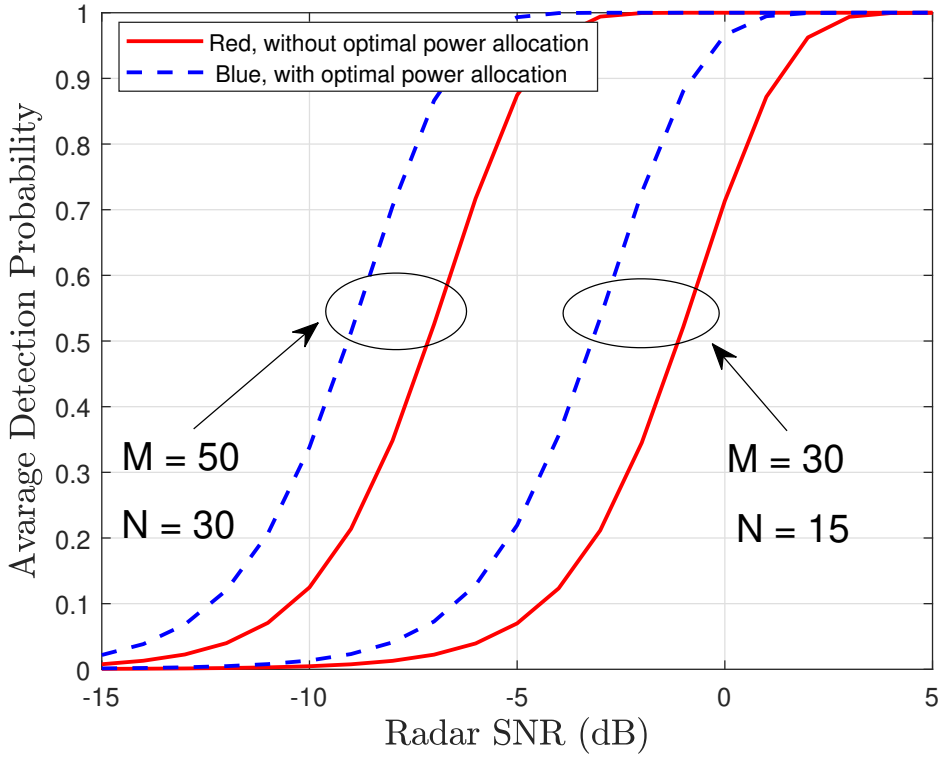

Fig. 3.7 Average probability of detection with and without power allocation for different number of antennas (M) and (N), where $P_{R(max)}$ = 0 dB, $\rho_{(max)}$ = 10 dB, $K = 4$.

based on the case of without power allocation. It is evident to see the substantial improvement in the probability of detection. For example, at ($M = 30,\ N = 15$), when the radar SNR is 0 dB, the average probability of detection is about 0.97 and 0.7 for the cases with and without optimal power allocation, respectively. In addition, as shown in the figure, the probability of detection improves when M and N increase. This implies that using more antennas at the BS will improve the massive MIMO system performance without affecting the radar performance.

We next consider a more practical scenario, where the large-scale fading is modeled by path loss, shadow fading, and random user locations. To generate the large-scale fading $\beta_k, \bar{\beta}_k$ and β_{br}, we follow the model described in [129]. More precisely, we consider a circular cell with a radius of 1 Km. In the centre of the cell, there is a BS with M antennas serving K users that are randomly located within this cell. The MIMO radar is located 2 Km from the BS. The large-scale fading coefficient β_k is modeled as

$$\beta_k = \mathrm{PL}_0 \left(\frac{d_k}{R_{\min}} \right)^{\upsilon} \times 10^{\frac{\sigma_{\mathrm{sh}} \cdot \mathcal{N}(0,1)}{10}}, \tag{3.38}$$

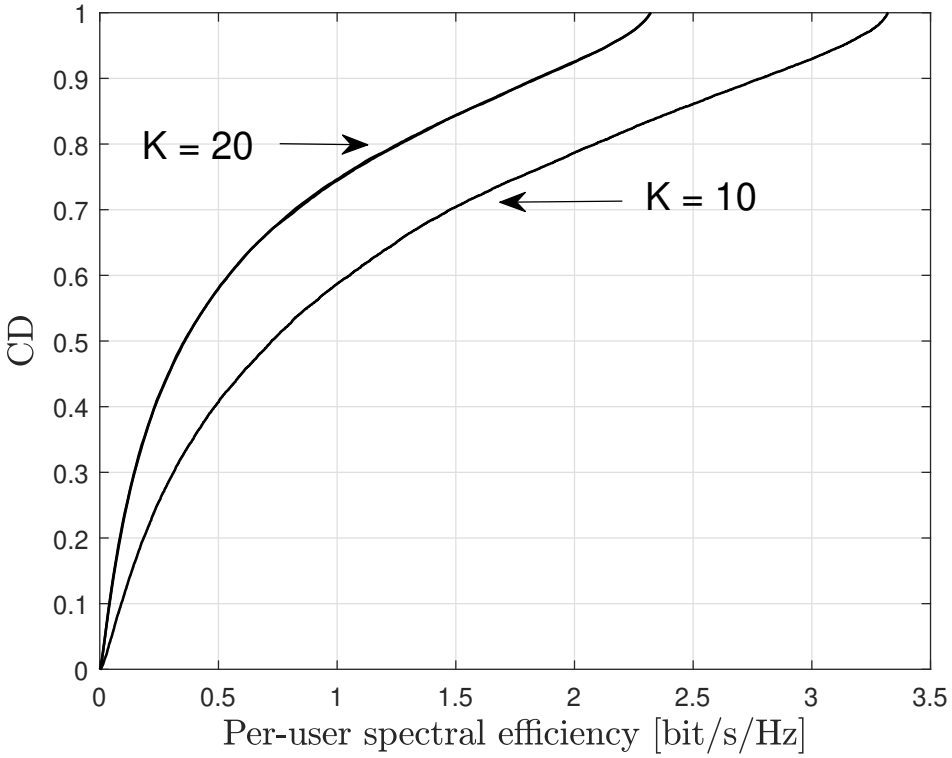

Fig. 3.8 CDF of the per-user spectral efficiency. Here, $M = 100$.

where d_k is the distance between user k and the MIMO radar, while $PL_0, \upsilon, \sigma_{\text{sh}}$ denote a reference path loss constant which is chosen to satisfy a given downlink cell-edge SNR, path loss exponent and the standard deviation of the shadow fading, respectively. The same model is applied for $\bar{\beta}_k$ and β_{br}. In our examples, we chose $\upsilon = 3.8$, $\sigma_{\text{sh}} = 8$dB, $R_{\min} = 100$ m. Figure 3.8 illustrates the cumulative distribution of the per-user spectral efficiency for different K, with $M = 100$ and $SNR_d = 20$dB. We can see that per-user rate in the case of $K = 10$ is higher than that in the case of $K = 20$. This comes from the fact that when the number of users is large, the system suffers more interuser interference. Finally, Fig. 3.9 shows the cumulative distribution of the probability of detection for different transmit power at the BS. As we can see, the transmit power of the BS has a significant effect on the performance of the radar link. In particular, when the transmit power ρ increases from 0 dB to 20 dB, the probability of detection reduces significantly.

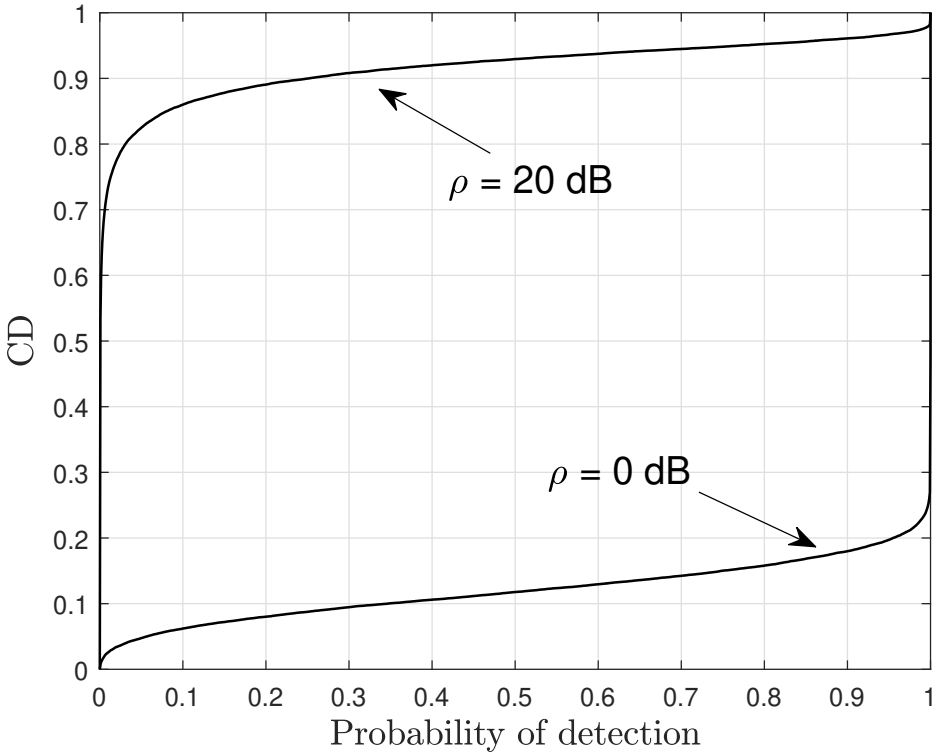

Fig. 3.9 CDF of the probability of detection. Here, $M = 100, K = 10$.

3.6 Conclusions

In this work, we have considered the coexistence between downlink massive MIMO communication and MIMO radar systems to enable the operation of these two systems with minimal mutual interference. In the massive MIMO system, we consider TDD operation with the MR precoding scheme. Our asymptotic analysis showed that the use of massive number of antennas at the BS can reduce the interference to the radar system, while guaranteeing a satisfactory quality of service at the massive MIMO system. This implies that by using massive MIMO architectures, we can make the coexistence between radar and communication systems feasible. To get more insights, and to facilitate the subsequent design of the considered system, we analytically derived the approximating probability of detection and exact downlink spectral efficiency in closed-forms. Based on the constraints on the transmit powers at the BS and the radar, and quality of service of communication systems, we formulated and solved a power allocation problem to maximize the probability of detection for MIMO radar. In comparison with the non-optimized scenario, our proposed power allocation improves the detection proba-

bility significantly. Our numerical results verified the tightness as well as the correctness of our closed-form expressions.

Chapter 4

Protecting Massive MIMO-Radar Coexistence: Precoding Design and Power Control

4.1 Introduction

Spectrum sharing between the radar and cellular communication systems, termed as *communication/radar co-existing systems*, has been envisioned as an enabling solution to address the explosive growth of wireless traffic demands and shortage of licensed spectra [3, 1, 6, 73]. Nevertheless, the inherent challenge of spectrum sharing, i.e., inter-system interference that compromises the performance of both systems, calls for an efficient cross interference management and spectrum assignment. To facilitate co-existence with overlaid communication systems, a variety of techniques, such as opportunistic spectrum sharing between cellular and rotating radar [130], interference mitigation [3, 131], precoding or spatial separation [3, 132], and waveform design for radar [3, 133, 134] have been proposed in the literature.

The widespread deployment of the massive multiple-input, multiple-output (MIMO) technology in cellular networks on one hand [10, 11], and the potential of MIMO radars on the other hand [30], has paved the way to the co-existence of MIMO structures. MIMO technology offers waveform diversity and higher detection capability for the radars, while at the same time, massive MIMO technology delivers the significant user coverage and spectral efficiency (SE) enhancement for the cellular systems. While the literature has focused more on conventional MIMO for both systems, the potential of massive MIMO technology to further boost the

system's performance has not been thoroughly studied yet. Massive MIMO is a key enabling technology for 5G and beyond networks, which relies on a large number of antennas at the BS to provide high spectral and energy efficiency using relatively simple processing [126]. More importantly, a BS with a large-antenna array can easily form a null to minimize interference to a coexistent radar. This motivates us to develop a massive MIMO communication system overlaid with a radar system.

4.1.1 Related Works

To manage the interference between the MIMO radar system and MIMO cellular networks, the null space projection method [76, 77] and optimum beamforming design [40, 78, 79, 135] have been widely discussed in the literature. More specifically, Mahal *et al.* [76] proposed a radar precoder design using subspace projection methods and based on zero-forcing (ZF) and minimum mean-square-error (MMSE) criteria. Biswas *et al.* [77] applied null-space based waveform projection to mitigate the interference from the radar system toward a full-duplex cellular system and proposed a joint transceiver design at the base station (BS) and users to maximize the detection probability of the MIMO radar system. The authors in [40] considered the transmit beamforming design for spectrum sharing between downlink multiuser MIMO communication and colocated MIMO radar to maximize the detection probability of the radar, while guaranteeing the transmit power budget of the BS and the received signal-to-interference-plus-noise-ratio (SINR) of each downlink user. The authors in [40] focused on the transmit beamforming design for spectrum sharing between downlink multiuser MIMO communication and colocated MIMO radar. Their aim was to maximize the radar's detection probability, while ensuring that the base station's transmit power budget and each downlink user's received signal-to-interference-plus-noise ratio (SINR) are maintained. Qian *et al.* [78] addressed the problem of joint design of the radar transmit code, radar receive filter, and the communication system codebook for the co-existence of MIMO radar and MIMO communication. Liu *et al.* [79] investigated power efficient transmission in the overlaid systems, where the BS beamforming is designed to minimize the transmit power at the BS, while guaranteeing the receive SINR at the users and the interference level from BS to radar. Pu *et al.* [135] extended the proposed design in [79] by taking the radar transmit waveform design into consideration and maximized the radar SINR, under the constraints of communication constructive interference, radar waveform similarity and constant modulus.

4.1.2 Research Gap and Main Contributions

The integration of the massive MIMO into communication/radar co-existing systems has been recently studied in [83, 8]. In [83], the rate region of a coexistence based joint radar and communications system, comprising a single cell massive MIMO communication system and a static MIMO radar has been characterized. In the presence of radar interference, the uplink and downlink achievable rates of the cellular system have been derived by applying MMSE combining and regularized ZF beamformer at the BS, respectively. In [8], closed-form expressions for the detection probability of the radar system and the downlink SE of the massive MIMO system with maximum ratio (MR) precoding were derived. Nonetheless, research on the coexistence of massive MIMO communications and radar systems is still in its infancy and how joint precoding design and power allocation affects its performance remains unclear.

Thanks to the promising features of the massive MIMO technology, in this paper, we investigate the potential benefits of massive MIMO coexisting with MIMO radar to alleviate the inter-system interference. We consider a joint radar communication system comprising a single-cell massive MIMO cellular communication system and a MIMO radar operating over the same frequency band. The specific contributions of our paper can be summarized as follows:

- We characterize the performance of the cellular and radar system in terms of downlink SE and detection probability, respectively, in the presence of imperfect channel state information (CSI). Analytical results for MR and ZF beamforming at the BS are derived. In order to manage the inter-system interference, we design protective ZF (PZF) precoding at the BS to ensure the radar's functionality is not significantly impaired by the interference caused by downlink transmission towards users. Accordingly, we characterize the performance of the cellular and radar system with the PZF scheme.

- We formulate a power allocation problem with the objective of maximizing the detection probability for MIMO radar, subject to a power budget constraint at the radar and minimum SE requirements at the cellular users. This problem is efficiently solved via the bisection method. Our proposed power allocation strategy provides a significant detection probability gain for all precoding designs compared to the case without power allocation.

- Our numerical results show that by increasing the number of BS antennas, the gap between the PZF and MR design reduces, while ZF constantly outperforms the MR. Nev-

ertheless, while increasing the number of antennas at the radar results in SE degradation, it can also significantly enhance the detection probability at the radar site. By implementing power control at both the BS and radar, the MR, ZF, and PZF schemes achieve detection probability improvements of up to 55%, 49%, and 38%, respectively, compared to their baseline values, while the detection probability approaches to 1. Finally, our findings demonstrate that the PZF scheme, when combined with optimal power control, can consistently achieve a probability of detection exceeding 0.8 with a high probability (greater than 0.6).

4.2 System Model

We consider a time division duplex (TDD) downlink massive MIMO communication system coexisting with a MIMO radar system on the same time-frequency resource. Radar is equipped with N transmit and N receive antennas, while the massive MIMO communication system includes an M-antenna BS serving K single-antenna users $(M > K)$. The basic structure of the model is illustrated in Fig. 4.1, where

- $\mathbf{g}_k \in \mathbb{C}^{M\times 1}$ is the channel vector response between the BS and the k-th user. The channel $\mathbf{g}_k$ is modeled as follows:
$$\mathbf{g}_k = \sqrt{\beta_k}\mathbf{z}_k, \tag{4.1}$$
where $\mathbf{z}_k$ represents the small-scale fading, assuming to include independent and identically distributed (i.i.d.) RVs, i.e., $\mathbf{z}_k \sim \mathscr{CN}(0, \mathbf{I}_M)$, while β_k represents the large-scale fading. Denote by $\mathbf{G} = [\mathbf{g}_1 \dots \mathbf{g}_K] \in \mathbb{C}^{M\times K}$ the corresponding channel matrix from the BS to all K users.

- $\mathbf{R} \in \mathbb{C}^{N\times M}$ represents the channel matrix from the BS to the radar receiver, whose elements are i.i.d. $\sim \mathscr{CN}(0, \beta_{br})$ RVs, where β_{br} is the corresponding large-scale fading coefficient.

- $\mathbf{f}_k \in \mathbb{C}^{N\times 1}$ is the channel from the radar transmitter to the k-th user. Denote by $\mathbf{F} = [\mathbf{f}_1 \dots \mathbf{f}_K] \in \mathbb{C}^{N\times K}$ the corresponding channel matrix from the radar transmitter to all K users. We assume that $\mathbf{f}_k \sim \mathscr{CN}\left(0, \bar{\beta}_k \mathbf{I}_N\right)$, where $\bar{\beta}_k$ represents the large-scale fading.

In the following subsections, we provide details on the architecture of the two systems.

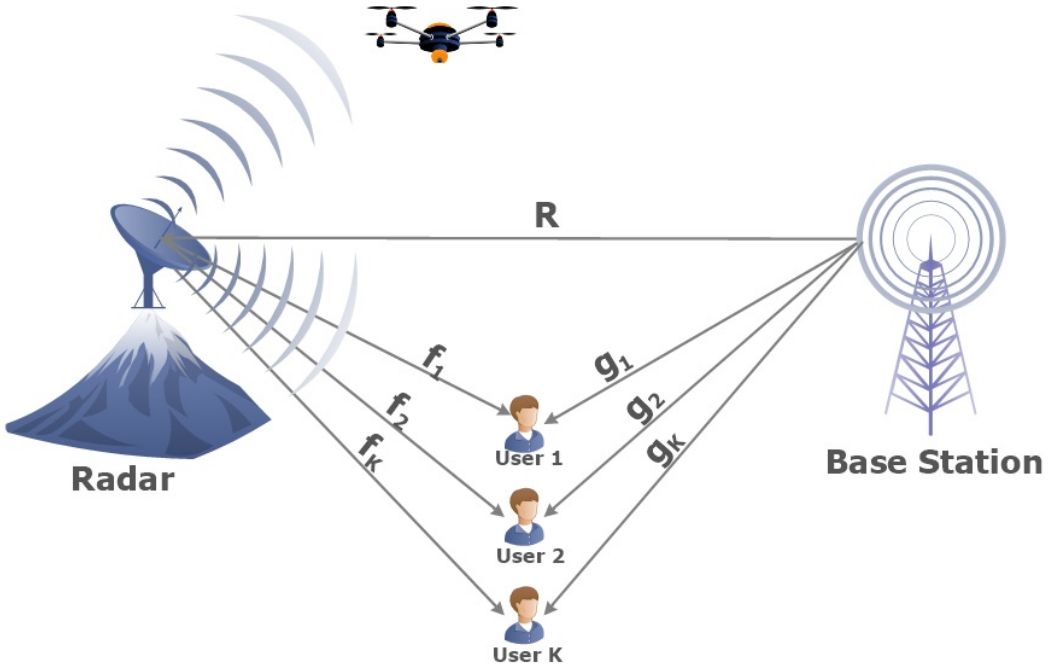

Fig. 4.1 Coexistence between mMIMO cellular systems and MIMO radar.

4.2.1 Massive MIMO Communication System

Our focus here is on data transmission over the downlink with TDD operation. Each transmission frame is divided to two phases: 1) uplink training phase and 2) downlink data transmission. Relying on the channel estimates obtained in the uplink training phase, different linear processing schemes are applied at the BS to transmit information towards all users.

Uplink Training

In this phase, the users and radar will first send the pilot sequences to the BS. Then, based on the received pilot signals, the BS will estimate the channels to users and radar. The CSI of the radar at the BS is required to design the PZF scheme and protect the radar against the interference from the BS. Let τ_{p} be the number of symbols per coherence interval used for uplink training phase. All users and radar simultaneously transmit pilot sequences of length τ_{p} symbols.

Let $\sqrt{\tau_{\mathrm{p}}}\boldsymbol{\Phi}_r \in \mathbb{C}^{\tau_{\mathrm{p}} \times N}$, and $\sqrt{\tau_{\mathrm{p}}}\boldsymbol{\Phi}_p \in \mathbb{C}^{\tau_{\mathrm{p}} \times K}$ be the pilot sequences sent by the radar and the K users, respectively. It is assumed that pilot sequences transmitted from all users and radar are pairwisely orthogonal, i.e., $\boldsymbol{\Phi}_r^H \boldsymbol{\Phi}_r = \boldsymbol{I}_N$, $\boldsymbol{\Phi}_p^H \boldsymbol{\Phi}_p = \boldsymbol{I}_K$, $\boldsymbol{\Phi}_r^H \boldsymbol{\Phi}_p = \mathbf{0}_{N \times K}$, and $\boldsymbol{\Phi}_p^H \boldsymbol{\Phi}_r = \mathbf{0}_{K \times N}$.

This requires $\tau_{\mathrm{p}} \geq N+K$. Then, the received pilot signal at the BS can be expressed as

$$\mathbf{Y}_{\mathrm{p}} = \sqrt{\tau_{\mathrm{p}} P_R}\mathbf{R}^H \mathbf{\Phi}_r^H + \sqrt{\tau_{\mathrm{p}}\rho_u}\mathbf{G}\mathbf{\Phi}_p^H + \mathbf{N}, \tag{4.2}$$

where $\mathbf{N} \in \mathbb{C}^{M\times\tau_{\mathrm{p}}}$ is the AWGN, whose elements have zero mean and variance σ_C^2.

Denote by $\hat{\mathbf{R}}$ and $\hat{\mathbf{g}}_k$ the MMSE estimates of $\mathbf{R}$ and $\mathbf{g}_k$, respectively. Then, they can be expressed as

$$\hat{\mathbf{R}} = \mathbf{R} + \tilde{\mathbf{R}}, \tag{4.3}$$

$$\hat{\mathbf{g}}_k = \mathbf{g}_k + \tilde{\mathbf{g}}_k, \tag{4.4}$$

where $\tilde{\mathbf{R}}$ and $\tilde{\mathbf{g}}_k$ represent the corresponding channel estimation errors. Following [136], the elements of $\hat{\mathbf{R}}$ and the elements of $\hat{\mathbf{g}}_k$ are independent and distributed as $\mathscr{CN}(0,\gamma_r)$ and $\mathscr{CN}(0,\gamma_k)$, respectively, with

$$\gamma_r = \frac{\tau_{\mathrm{p}} P_R \beta_{br}^2}{\tau_{\mathrm{p}} P_R \beta_{br} + \sigma_C^2}, \tag{4.5}$$

$$\gamma_k = \frac{\tau_{\mathrm{p}} \rho_u \beta_k^2}{\tau_{\mathrm{p}} \rho_u \beta_k + \sigma_C^2}, \tag{4.6}$$

where P_R and ρ_u are the transmit power of each pilot symbol at the radar and the user, respectively, and σ_C^2 is the noise power at the BS. From the MMSE estimation property, $\tilde{\mathbf{R}}$ is independent of $\hat{\mathbf{R}}$ and $\tilde{\mathbf{g}}_k$ is independent of $\hat{\mathbf{g}}_k$, and hence, $[\tilde{\mathbf{R}}]_{n,m} \sim \mathscr{CN}\Big(0,(\beta_{br}-\gamma_r)\Big)$ and $\tilde{\mathbf{g}}_k \sim \mathscr{CN}\Big(0,(\beta_k-\gamma_k)\mathbf{I}_M\Big)$. We can represent the overall channel estimation matrix between the BS and users as

$$\hat{\mathbf{G}} = \mathbf{H}\mathbf{D}_\gamma^{\frac{1}{2}}, \tag{4.7}$$

where $\hat{\mathbf{G}} = [\hat{\mathbf{g}}_1,\ldots,\hat{\mathbf{g}}_K] \in \mathbb{C}^{M\times K}$, $\mathbf{H} = [\mathbf{h}_1,\ldots,\mathbf{h}_K] \in \mathbb{C}^{M\times K}$ with $\mathbf{h}_k \sim \mathscr{CN}(0,\mathbf{I}_M)$, while $\mathbf{D}_\gamma = \mathrm{diag}\{\gamma_1,\ldots,\gamma_K\}$ is a diagonal matrix. We can further represent $\hat{\mathbf{g}}_k$ as

$$\hat{\mathbf{g}}_k = \sqrt{\gamma_k}\mathbf{h}_k. \tag{4.8}$$

Downlink Signal Transmission

By using the channel estimates obtained during the training phase, precoding matrix is designed at the BS for downlink data transmission phase. Suppose that the information symbols $\mathbf{d} = [d_1, \ldots, d_K]^T \in \mathbb{C}^{K\times 1}$ are independent with $\mathbb{E}\left\{\mathbf{d}\mathbf{d}^H\right\} = \mathbf{I}_K$, where d_k denotes the information symbol intended for the k-th user. Then, the signal transmitted from the BS can be expressed as

$$x = \mathbf{T}\mathbf{D}_\eta^{\frac{1}{2}}\mathbf{d} = \sum_{k=1}^{K} \sqrt{\eta_k}\mathbf{t}_k d_k, \tag{4.9}$$

where $\mathbf{T} = [\mathbf{t}_1 \ldots \mathbf{t}_K] \in \mathbb{C}^{M\times K}$ is the precoding matrix, which is a function of the channel estimate $\hat{\mathbf{G}}$ and $\mathbf{t}_k \in \mathbb{C}^{N\times 1}$, where $\mathbb{E}\left\{\|\mathbf{t}_k\|^2\right\} = 1$, is the precoding vector for user k, $\mathbf{D}_\eta = \text{diag}\{\eta_1, \ldots, \eta_K\}$ is a diagonal matrix whose k-th diagonal element, η_k, represents the power control coefficient for user k, chosen to satisfy the power constraint at the BS $\mathbb{E}\{\|\mathbf{x}\|^2\} \leq 1$, which implies $\sum_{k=1}^{K} \eta_k \leq 1$. The received signal vector at the users can be expressed as

$$y = \underbrace{\sqrt{\rho}\mathbf{G}^{\mathrm{T}}x}_{\text{desired signal}} + \underbrace{\sqrt{P_R}\mathbf{F}^T\mathbf{s},}_{\text{interference from radar}} + n, \tag{4.10}$$

where ρ denotes the BS transmit power, $\mathbf{s} \in \mathbb{C}^{N\times 1}$ is the transmitted probing signal from the radar, with $\mathbb{E}\left\{\mathbf{s}\mathbf{s}^H\right\} = \mathbf{I}_N$, to the target, while $n \sim C\mathcal{N}\left(0, \sigma_C^2\mathbf{I}_N\right)$ is the AWGN at the users.

4.2.2 MIMO Radar

We consider a MIMO radar system that detects targets located in the far field. Assuming the MIMO radar-to-target channel is line-of-sight (LoS), the reflected signal (echo from the target) from one point-like target to the radar receiver is interfered by the signal transmitted from the BS. Assuming that a uniform linear array (ULA) is used at the radar, at the l-th snapshot, the discrete signal vector $\mathbf{y}_R[l]$ received by the radar is given by [40, 137]

$$\mathbf{y}_R[l] = \alpha\sqrt{P_R}\mathbf{A}(\theta)\mathbf{s}[l] + \mathbf{R}\sum_{k=1}^{K} \sqrt{\eta_k}\mathbf{t}_k d_k[l], + \mathbf{w}[l], \tag{4.11}$$

where α denotes the complex path loss of the radar-target-radar path; P_R is the transmitted power from the MIMO radar; θ is the azimuth angle of the target; $\mathbf{w}[l] = \left[w_i[l], \ldots w_N[l]\right]^T \in \mathbb{C}^{N\times 1}$ is the received additive white Gaussian noise (AWGN) vector at the l-th snapshot with $w_m[l] \sim \mathscr{C}\mathcal{N}\left(0, \sigma_R^2\right)$, $\forall m$; $\mathbf{A}(\theta) = \mathbf{a}_R(\theta)\mathbf{a}_T^T(\theta)$, in which $\mathbf{a}_T(\theta) \in \mathbb{C}^{N\times 1}$ and $\mathbf{a}_R(\theta) \in \mathbb{C}^{N\times 1}$

are the transmit and receive steering vectors of the radar antenna array. Similar to [40, 137], and without significant loss of generality, we assume that $\mathbf{a}_R(\theta) = \mathbf{a}_T(\theta) = \mathbf{a}(\theta)$, where

$$\mathbf{a}(\theta) = \left[1, e^{-j2\pi d \sin(\theta)}, \ldots, e^{-j2\pi d(N-1)\sin(\theta)}\right]^T, \tag{4.12}$$

where d represents the inter-antenna spacing normalized by the carrier wavelength.

4.3 Performance Analysis

We evaluate the performance, in terms of downlink SE of the cellular communication systems and detection probability for the radar system, for different precoding schemes. Theoretically, the precoding matrix, $\mathbf{T}$, can be optimized to achieve the optimal performance of the system. However, the complexity of the optimum precoding grows dramatically with M and K. For the massive antenna regime with $M \gg K$, it is known that linear precoders, i.e., MR and ZF perform fairly well [13, 20, 138]. Therefore, we focus on the performance of those precoders in the following subsections. While these two precoders provide cellular users with satisfactory performance, the BS may create interference at the radar receiver. To address this issue, we propose to use PZF precoding at the BS, to guarantee full protection for the radar against signals intended for cellular users.

4.3.1 Spectral Efficiency

We assume that estimated CSI is not available at the user side and each user uses only the statistical CSI for signal detection. Therefore, users treat the mean effective channel gain as the channel knowledge for data detection. By invoking (4.10) and using the use-and-then-forget bounding technique in [126, Eq. (2.44)][9], known as hardening bound, we derive a lower bound on the downlink SE of user k. To this end, using (4.10) we first rewrite the received signal at user k as

$$y_k = \mathrm{DS}_k d_k + \mathrm{BU}_k d_k + \sum_{k' \neq k} \mathrm{IUI}_{kk'} d_{k'} + \sqrt{P_R}\mathbf{f}_k^T \mathbf{s} + n_k, \tag{4.13}$$

where

$$\mathrm{DS}_k = \sqrt{\rho\eta_k}\mathbb{E}\left\{\mathbf{g}_k^T\mathbf{t}_k\right\}, \tag{4.14}$$

$$\mathrm{BU}_k = \sqrt{\rho\eta_k}\left(\mathbf{g}_k^T\mathbf{t}_k - \mathbb{E}\left\{\mathbf{g}_k^T\mathbf{t}_k\right\}\right), \tag{4.15}$$

$$\mathrm{IUI}_{kk'} = \sqrt{\rho\eta_{k'}}\mathbf{g}_k^T\mathbf{t}_{k'}, \tag{4.16}$$

represent the strength of the desired signal (DS_k), the beamforming gain uncertainty (BU_k), and the interference caused by the k'-th user, respectively.

Accordingly, an achievable downlink SE at the k-th user can be expressed as

$$\mathrm{SE}_k = \left(1 - \frac{\tau_\mathrm{p}}{\tau}\right)\log_2(1+\mathrm{SINR}_k), \tag{4.17}$$

where the effective SINR is given by

$$\mathrm{SINR}_k = \frac{\left|\mathrm{DS}_k\right|^2}{\mathbb{E}\left\{\left|\mathrm{BU}_k\right|^2\right\} + \sum_{k'\neq k}\mathbb{E}\left\{\left|\mathrm{IUI}_{kk'}\right|^2\right\} + P_R\bar{\beta}_k N + \sigma_C^2}. \tag{4.18}$$

The achievable downlink SE in (4.17) is general and valid regardless of the precoding scheme used at the BS. We derive closed-form expressions for the MR, ZF, and PZF precoding schemes in the following subsection.

Maximum-Ratio Precoder

The MR precoder is employed at the BS, particularly due to its advantages including low computational complexity, ease of analysis, and reasonable performance, as shown in [13, 20, 138, 139]. With MR precoding design, the linear precoding vectors $\mathbf{t}_k = \mathbf{t}_k^{\mathrm{MR}}$ given by [20]

$$\mathbf{t}_k^{\mathrm{MR}} = \alpha_{\mathrm{MR}}\mathbf{h}_k^*, \tag{4.19}$$

where $\alpha_{\mathrm{MR}} = \frac{1}{\sqrt{M}}$ is the normalization factor.

Proposition 3 *The SE of the k-th user achieved by the* MR *precoding can be expressed by* (4.20)*, at the top of the next page.*

$$\mathrm{SE}_k^{\mathrm{MR}} = \left(1 - \frac{\tau_\mathrm{p}}{\tau}\right)\log_2\left(1 + \frac{M\rho\gamma_k\eta_k}{\rho\gamma_k\sum_{k'=1}^{K}\eta_{k'} + P_R\bar{\beta}_k N + \sigma_C^2}\right), \forall k. \tag{4.20}$$

Proof 3 *See Appendix B.*

Zero-Forcing Precoder

In order to mitigate the inter-user interference, we exploit the ZF principle for precoding design. With ZF, the precoding vector $\mathbf{t}_k$ can be expressed as

$$\mathbf{t}_k^{\mathrm{ZF}} = \alpha_{\mathrm{ZF}} \left[\mathbf{H}^* (\mathbf{H}^T \mathbf{H}^*)^{-1} \right]_{(:,k)}, \tag{4.21}$$

where $\alpha_{\mathrm{ZF}} = \sqrt{M-K}$ is the normalization factor [129].

Proposition 4 *The SE of the k-th user achieved by the* ZF *precoding can be expressed by* (4.22)*, at the top of the next page.*

$$\mathrm{SE}_k^{\mathrm{ZF}} = \left(1 - \frac{\tau_{\mathrm{p}}}{\tau}\right) \log_2 \left(1 + \frac{(M-K)\rho\gamma_k\eta_k}{\rho(\beta_k - \gamma_k)\sum_{k'=1}^{K}\eta_{k'} + P_R\bar{\beta}_k N + \sigma_C^2}\right), \forall k. \tag{4.22}$$

Proof 4 *See Appendix B.*

Protective Zero-Forcing Precoder

The MR and ZF precoders do not take the interference from the BS to radar into account. To protect the radar against the interference caused by the downlink transmission towards cellular users, we now elaborate on the PZF precoding scheme. The PZF scheme ensures that the radar is fully protected from BS interference if the BS has perfect CSI from the radar. To achieve this objective, some degrees-of-freedom at the BS are used to steer the BS beams into the radar's null-space. Therefore, from the perspective of the cellular communication network, we can see that PZF is inferior to ZF, while it performs better than the MR scheme. Importantly, it outperforms both ZF and MR in terms of the detection probability.

Let now $\mathbf{B}$ denote the projection matrix onto the orthogonal complement of $\hat{\mathbf{R}}$, which can be expressed as

$$\mathbf{B} = \mathbf{I}_M - \hat{\mathbf{R}}^H \left(\hat{\mathbf{R}}\hat{\mathbf{R}}^H\right)^{-1} \hat{\mathbf{R}}. \tag{4.23}$$

$$\mathrm{SE}_k^{\mathrm{PZF}} = \left(1-\frac{\tau_{\mathrm{p}}}{\tau}\right)\log_2\left(1+\frac{\frac{\rho}{M}(M-K)(M-N)\gamma_k\eta_k}{\frac{\rho}{M}(M-N)(M-K)(\beta_k-\gamma_k)\sum_{k'=1}^{K}\eta_{k'}+P_R\bar{\beta}_k N+\sigma_C^2}\right), \forall k. \tag{4.27}$$

Then, the PZF precoder is designed as

$$\mathbf{t}_k^{\mathrm{PZF}} = \alpha_{\mathrm{PZF}}\mathbf{B}\mathbf{w}_k^{\mathrm{ZF}}, \tag{4.24}$$

where $\mathbf{w}_k^{\mathrm{ZF}}$ and $\mathbf{t}_k^{\mathrm{PZF}}$ are k-th column of $\mathbf{W}^{\mathrm{ZF}}$ and $\mathbf{T}^{\mathrm{PZF}}$ matrices, respectively, where $\mathbf{W}^{\mathrm{ZF}} = \mathbf{H}^*(\mathbf{H}^T\mathbf{H}^*)^{-1}$ and $\mathbf{T}^{\mathrm{PZF}} = \alpha_{\mathrm{PZF}}\mathbf{B}\mathbf{W}^{\mathrm{ZF}}$. Moreover, the normalization factor is expressed as:

$$\alpha_{\mathrm{PZF}} = \frac{1}{\sqrt{\mathbb{E}\{\|\mathbf{B}\mathbf{w}_k^{\mathrm{ZF}}\|^2\}}} = \frac{1}{\sqrt{\mathbb{E}\{\mathrm{tr}(\mathbf{w}_k^{\mathrm{ZF}}(\mathbf{w}_k^{\mathrm{ZF}})^H\mathbf{B})\}}}, \tag{4.25}$$

where we have used $\mathbf{B}^H\mathbf{B} = \mathbf{B}$. By noticing that $\mathbf{B}$ is independent of $\mathbf{w}_k^{\mathrm{ZF}}$, we have

$$\begin{aligned}\alpha_{\mathrm{PZF}} &= \frac{1}{\sqrt{\mathrm{tr}\left(\mathbb{E}\left\{\mathbf{w}_k^{\mathrm{ZF}}(\mathbf{w}_k^{\mathrm{ZF}})^H\right\}\mathbb{E}\{\mathbf{B}\}\right)}} \\ &= \sqrt{\frac{M(M-K)}{(M-N)}},\end{aligned} \tag{4.26}$$

where we have applied Lemma 1 from Appendix B.0.1 and [140, Lemma 2.10] to derive the final result. Accordingly, the achievable SE by the k-th user using PZF precoding is given in the following proposition.

The idea of PZF is the same as interference nulling which has been introduced in the space of multi-cell cellular systems [141] to mitigate the inter-cell interference and next applied to the cell-free massive MIMO systems in [142] to suppress the interference caused by each access point to part of users.

Proposition 5 *The SE of the k-th user achieved by the* PZF *precoding can be expressed by* (4.27) *at the top of the next page.*

Proof 5 *See Appendix B.*

4.3.2 Detection Probability

In this subsection, we derive the detection probability for radar system, under the Neyman-Pearson criterion. By using the Generalized Likelihood Ratio Test, the asymptotic detection probability for radar P_d is given as [8]

$$P_d = 1 - \mathfrak{F}_{X_2^2(\mu)}\left(\mathfrak{F}_{X_2^2}^{-1}\left(1 - P_{FA}\right)\right), \tag{4.28}$$

where P_{FA} is the radar's probability of false alarm, $\mathfrak{F}_{X_2^2(\mu)}$ is the non-central chi-square cumulative distribution function (CDF) with two degrees-of-freedom (DoF), $\mathfrak{F}_{X_2^2}^{-1}$ is the inverse function of chi-square CDF, while the non-centrality parameter, μ, for X_2^2 is given by [8]

$$\mu = |\alpha|^2 L P_R \mathrm{tr}\left(\mathbf{A}\mathbf{A}^H\left(\mathbf{R}\tilde{\mathbf{T}}\mathbf{R}^H + \sigma_R^2\mathbf{I}_N\right)^{-1}\right), \tag{4.29}$$

where $\tilde{\mathbf{T}} = \mathbf{T}\mathbf{D}_\eta\mathbf{T}^H$.

By invoking the generalized Marcum Q-function, P_d can be written as

$$P_d = Q_1\left(\sqrt{\mu}, \sqrt{C_{FA}}\right), \tag{4.30}$$

where $C_{FA} = \mathfrak{F}_{x_2^2}^{-1}(1 - P_{FA})$ [8]. Hence, in order to derive P_d for different precoding schemes, we need to find μ.

By leveraging the massive MIMO concept, we are able to obtain a tight approximation to μ. Specifically, by using the trace lemma [143], as $M \to \infty$, for the considered linear precoding schemes, we get

$$\begin{cases} \frac{1}{M}\mathbf{R}\tilde{\mathbf{T}}^i\mathbf{R}^H - \frac{\beta_{br}}{M}\mathrm{tr}(\tilde{\mathbf{T}}^i)\mathbf{I}_N \xrightarrow{a.s.} 0 \quad i \in \{\mathrm{MR}, \mathrm{ZF}\} \\ \frac{1}{M}\mathbf{R}\tilde{\mathbf{T}}^{\mathrm{PZF}}\mathbf{R}^H - \frac{(\beta_{br}-\gamma_r)}{M}\mathrm{tr}(\tilde{\mathbf{T}}^{\mathrm{PZF}})\mathbf{I}_N \xrightarrow{a.s.} 0, \end{cases} \tag{4.31}$$

where $\xrightarrow{a.s.}$ denotes the almost sure convergence. Moreover, in the case of PZF scheme, we have used the fact that

$$\begin{aligned} \mathbf{R}\tilde{\mathbf{T}}^{\mathrm{PZF}}\mathbf{R}^H &= (\hat{\mathbf{R}} + \tilde{\mathbf{R}})\tilde{\mathbf{T}}^{\mathrm{PZF}}(\hat{\mathbf{R}} + \tilde{\mathbf{R}})^H \\ &= \tilde{\mathbf{R}}\tilde{\mathbf{T}}^{\mathrm{PZF}}\tilde{\mathbf{R}}^H. \end{aligned} \tag{4.32}$$

As a result, (4.29) can be tightly approximated as

$$\begin{aligned}\mu^i &\approx |\alpha|^2 LP_R \mathrm{tr}\left(\mathbf{A}\mathbf{A}^H\left(\zeta_i \mathrm{tr}(\tilde{\mathbf{T}}^i)\mathbf{I}_N + \sigma_R^2\mathbf{I}_N\right)^{-1}\right) \\ &= \frac{|\alpha|^2 LP_R \mathrm{tr}(\mathbf{A}\mathbf{A}^H)}{\zeta_i \mathrm{tr}\left(\tilde{\mathbf{T}}^i\right) + \sigma_R^2},\end{aligned} \tag{4.33}$$

where $\zeta_{\mathrm{MR}} = \zeta_{\mathrm{ZF}} = \beta_{br}$ and $\zeta_{\mathrm{PZF}} = (\beta_{br} - \gamma_r)$. We now derive closed-form expressions of μ for the MR, ZF, and PZF precoding schemes in the following subsections.

Maximum-Ratio Precoder:

From (4.19), $\tilde{\mathbf{T}}^{\mathrm{MR}}$ can be defined as

$$\begin{aligned}\tilde{\mathbf{T}}^{\mathrm{MR}} &= \sum_{k=1}^{K} \mathbf{t}_k^{\mathrm{MR}} \eta_k (\mathbf{t}_k^{\mathrm{MR}})^H = \mathbf{T}^{\mathrm{MR}} \mathbf{D}_\eta (\mathbf{T}^{\mathrm{MR}})^H \\ &= \frac{1}{M}(\mathbf{H}^* \mathbf{D}_\eta \mathbf{H}^T).\end{aligned} \tag{4.34}$$

Since $\frac{1}{M}\mathbf{H}^T\mathbf{H}^* \to \mathbf{I}_K$ for sufficiently large M [20], we have $\mathrm{tr}\left(\tilde{\mathbf{T}}^{\mathrm{MR}}\right) = \mathrm{tr}\left(\mathbf{D}_\eta \frac{\mathbf{H}^T\mathbf{H}^*}{M}\right) \approx \sum_{k=1}^{K} \eta_k$. As a result,

$$\mu^{\mathrm{MR}} \approx \frac{|\alpha|^2 LP_R \mathrm{tr}\left(\mathbf{A}\mathbf{A}^H\right)}{\beta_{br}\sum_{k=1}^{K}\eta_k + \sigma_R^2}. \tag{4.35}$$

Zero-Forcing Precoder:

Form (4.21), $\tilde{\mathbf{T}}^{\mathrm{ZF}}$ can be derived as

$$\begin{aligned}\tilde{\mathbf{T}}^{\mathrm{ZF}} &= \mathbf{T}^{\mathrm{ZF}} \mathbf{D}_\eta (\mathbf{T}^{\mathrm{ZF}})^H \\ &= (M-K)\mathbf{H}^*(\mathbf{H}^T\mathbf{H}^*)^{-1}\mathbf{D}_\eta(\mathbf{H}^T\mathbf{H}^*)^{-1}\mathbf{H}^T.\end{aligned} \tag{4.36}$$

To this end, by using (4.36), we get

$$\begin{aligned}\mathrm{tr}\left(\tilde{\mathbf{T}}^{ZF}\right) &= (M-K)\mathrm{tr}\left(\mathbf{D}_\eta(\mathbf{H}^T\mathbf{H}^*)^{-1}\right)\\ &\overset{(a)}{\approx} \frac{M-K}{M}\mathrm{tr}\left(\mathbf{D}_\eta\right)\\ &\overset{(b)}{=} \frac{M-K}{M}\sum_{k=1}^{K}\eta_k,\end{aligned} \tag{4.37}$$

where (a) follows from the fact that $(\mathbf{H}^T\mathbf{H}^*)^{-1} \approx \frac{1}{M}\mathbf{I}_K$ for sufficiently large values of M, and (b) holds since $\mathrm{tr}\left(\mathbf{D}_\eta\right) = \sum_{k=1}^{K}\eta_k$. Then, the non-centrality parameter μ^{ZF} can be approximated by

$$\mu^{\mathrm{ZF}} \approx \frac{|\alpha|^2 LP_R\mathrm{tr}\left(\mathbf{A}\mathbf{A}^H\right)}{\frac{M-K}{M}\beta_{br}\sum_{k=1}^{K}\eta_k + \sigma_R^2}. \tag{4.38}$$

Protective Zero-Forcing Precoder:

Proposition 6 *With PZF precoding, the non-centrality parameter, μ, can be derived as*

$$\mu^{\mathrm{PZF}} \approx \frac{|\alpha|^2 LP_R\mathrm{tr}\left(\mathbf{A}\mathbf{A}^H\right)}{\frac{M-K}{M}(\beta_{br}-\gamma_r)\sum_{k=1}^{K}\eta_k + \sigma_R^2}. \tag{4.39}$$

Proof 6 *See Appendix B.*

4.4 Power Optimization

To protect the radar system against the BS transmissions and at the same time to guarantee the performance requirements of the cellular users, power control at the BS and radar can be applied. In this regard, we aim at selecting the radar transmit power P_R and BS power control coefficients η_k to maximize the detection probability for MIMO radar, under the constraints on per-user SE and sum of power control coefficients η_k. More precisely, the optimization

problem is mathematically described as

$$(\mathbb{P}1): \quad \max_{P_R,\eta_k} \quad P_d \tag{4.40a}$$

$$\text{s.t.} \quad \text{SE}_k \geq \text{SE}_{k,\text{th}}, \ \forall k, \tag{4.40b}$$

$$0 \leq P_R \leq P_{R,max}, \tag{4.40c}$$

$$\sum_{k=1}^{K} \eta_k \leq 1, \tag{4.40d}$$

where $P_{R,max}$ is the maximum transmit power at the MIMO radar and $\text{SE}_{k,\text{th}}$ is the minimum SE requirement by the k-th user. The constraint (4.40d) represents the maximum transmit power constraint at the BS. By invoking (4.30), and since the Marcum Q-function is an increasing function of μ, we can further rewrite $(\mathbb{P}1)$ as the following optimization problem

$$(\mathbb{P}2): \quad \max_{P_R,\eta_k} \quad \mu \tag{4.41a}$$

$$\text{s.t.} \quad \text{SE}_k \geq \text{SE}_{k,\text{th}}, \ \forall k, \tag{4.41b}$$

$$0 \leq P_R \leq P_{R,max}, \tag{4.41c}$$

$$\sum_{k=1}^{K} \eta_k \leq 1. \tag{4.41d}$$

By invoking (4.35), (4.38), and (4.39), we can rewrite the optimization problem $(\mathbb{P}2)$ in the general form

$$(\mathbb{P}3): \quad \max_{P_R,\eta_k} \quad \frac{|\alpha|^2 L P_R \text{tr}\left(\mathbf{A}\mathbf{A}^H\right)}{a_i \sum_{k=1}^{K} \eta_k + \sigma_R^2} \tag{4.42a}$$

$$\text{s.t.} \quad \frac{b_i \rho \eta_k \gamma_k}{\rho c_{i,k} \sum_{k'=1}^{K} \eta_{k'} + \bar{\beta}_k P_R N + 1} \geq \gamma_{k,\text{th}}, \ \forall k, \tag{4.42b}$$

$$0 \leq P_R \leq P_{R,max}, \tag{4.42c}$$

$$\sum_{k=1}^{K} \eta_k \leq 1, \tag{4.42d}$$

where $\gamma_{k,\text{th}} = 2^{\text{SE}_{k,\text{th}}} - 1$, $i \in \{\text{MR}, \text{PZF}, \text{ZF}\}$ and $a_{\text{MR}} = \beta_{br}$, $a_{\text{ZF}} = \frac{(M-K)}{M}\beta_{br}$, $a_{\text{PZF}} = \frac{M-K}{M}(\beta_{br} - \gamma_r)$, $b_{\text{MR}} = M$; $b_{\text{PZF}} = \frac{1}{M}(M-K)(M-N)$, $b_{\text{ZF}} = (M-K)$; $c_{\text{MR},k} = \gamma_k$, $c_{\text{PZF},k} = b_{\text{PZF}}(\beta_k - \gamma_k)$, and $c_{\text{ZF},k} = \beta_k - \gamma_k$.

Algorithm 1 Bisection Algorithm for Solving $(\mathbb{P}4)$

1: Initialization: choose the initial values of $t_{\min}$ and $t_{\max}$, where $t_{\min}$ and $t_{\max}$ define a range of relevant values of the objective function, choose a tolerance $\varsigma \geq 0$.
2: While $t_{\min} - t_{\max} \leq \varsigma$.
3: Set $t = \frac{t_{\min}+t_{\max}}{2}$ and solve the feasibility problem.
4: If problem $(\mathbb{P}4)$ is feasible, then set $t_{\min} = t$, else set $t_{max} = t$.
5: Stop if $t_{\max} - t_{\min} \leq \varepsilon$. Otherwise, go to Step 2.

4.4.1 Bisection Search-Based Solution

Since expression (4.42a) is quasi-concave and constraints of the problem are linear functions of the optimization variables, the optimization problem $(\mathbb{P}3)$ is quasi-concave. Thus, it can be equivalently reformulated as

$$
\begin{aligned}
(\mathbb{P}4): \max_{P_R,\eta_k} \quad & t && \text{(4.43a)}\\
\text{s.t.} \quad & b_i \rho \eta_k \gamma_k \geq \\
& \gamma_{k,\text{th}} \left(\rho c_{i,k} \sum_{k'=1}^{K} \eta_{k'} + \bar{\beta}_k P_R N + 1 \right), \forall k, && \text{(4.43b)}\\
& \left| \alpha \right|^2 L P_R \text{tr}\left(\mathbf{A}\mathbf{A}^H \right) \geq t \left(a_i \sum_{k=1}^{K} \eta_k + \sigma_R^2 \right) && \text{(4.43c)}\\
& 0 \leq P_R \leq P_{R,max}, && \text{(4.43d)}\\
& \sum_{k=1}^{K} \eta_k \leq 1, && \text{(4.43e)}
\end{aligned}
$$

where

$$
t = \frac{\left| \alpha \right|^2 L P_R \text{tr}\left(\mathbf{A}\mathbf{A}^H \right)}{a_i \sum_{k=1}^{K} \eta_k + \sigma_R^2}, \tag{4.44}
$$

is an auxiliary variable.

Problems (4.43) can be solved efficiently by a bisection search[144], where in each step we solve a sequence of convex feasibility problems as detailed in **Algorithm 1**.

Convergence and Complexity Analysis

Let $p^\star$ denote the optimal value of the quasiconvex optimization problem ($\mathbb{P}3$). If the feasibility problem ($\mathbb{P}4$) is feasible, then we have $p^\star \leq t$. Conversely, if the problem ($\mathbb{P}4$) is infeasible, then we can conclude that $p^\star \geq t$. We can assess whether the optimal value, denoted as $p^\star$, for a quasiconvex optimization problem is less than or greater than a predefined value t by solving the convex feasibility problem ($\mathbb{P}4$). If the convex feasibility problem yields a feasible solution, we can conclude that $p^\star \leq t$. Conversely, if the convex feasibility problem is infeasible, it implies that $p^\star \geq t$. To implement a bisection algorithm, the interval $[t_{\min}, t_{\max}]$ is guaranteed to contain $p^\star$, i.e., we have $t_{\min} \leq p^\star \leq t_{\min}$ at each step. In each iteration, the interval is divided in two, i.e., bisected, so the length of the interval after k iterations is $\frac{(t_{\max}-t_{\min})}{2^k}$, where $(t_{\max}-t_{\min})$ is the length of the initial interval. It follows that exactly $\lceil \log 2((t_{\max}-t_{\min})/\varepsilon)\rceil$ iterations are required before the algorithm terminates. Each step involves solving the convex feasibility problem ($\mathbb{P}4$).

According to [145], the per-iteration cost to solve the feasibility problem ($\mathbb{P}4$) is $\mathscr{O}\Big((n_l+n_v)n_v^2 n_l^{0.5}\Big)$, where $n_l = K+3$ denotes the number of linear constraints and $n_v = K+1$ is the number of real valued scalar decision variables. Therefore, the overall complexity of the bisection algorithm is $\lceil \log 2((t_{\max}-t_{\min})/\varepsilon)\rceil \mathscr{O}\Big((n_l+n_v)n_v^2 n_l^{0.5}\Big)$.

4.4.2 Linear Programming Solution

The computational complexity of the bisection-based search algorithm can be reduced by noticing that ($\mathbb{P}1$) can be presented as a linear programming (LP) problem. The optimization problem in (4.42) is a non-concave problem due to non-concavity of the objective function. Before proceeding, we notice that both the objective function and first constraint (4.42a) are coupled together via the optimization variables P_R and η_k, for $k = 1,\ldots,K$. We now prove that the optimal value for P_R is $P_R^\star = P_{R,max}$. To this end, assume that $P_R^\star \geq P_{R,max}$. Now, we define the new variables $P_{R,\text{new}} = cP_R^\star$ and $\eta_{k,\text{new}} = c\eta_k^\star$, where $c \geq 1$. Then, the objective function (4.42a) can be obtained as

$$\begin{aligned} f(P_{R,\text{new}},\{\eta_{k,\text{new}}\}) &= \frac{|\alpha|^2 LcP_R^* \text{tr}\Big(\mathbf{A}\mathbf{A}^H\Big)}{a_i c\sum_{k=1}^K \eta_k^* + \sigma_R^2} \geq \frac{|\alpha|^2 LcP_R^\star \text{tr}\Big(\mathbf{A}\mathbf{A}^H\Big)}{a_i c\sum_{k=1}^K \eta_k^* + \sigma_R^2} \\ &= f(P_R^\star,\{\eta_k^\star\}). \end{aligned} \tag{4.45}$$

Moreover, at given $P_{R,\text{new}}$ and $\eta_{k,\text{new}}$, the first constraint is upper bounded as

$$\frac{b_i \rho c \eta_k^\star \gamma_k}{\rho c_{i,k} c \sum_{k'=1}^{K} \eta_{k'}^\star + \bar{\beta}_k c P_R^* N + 1} \geq \frac{b_i \rho \eta_k^\star \gamma_k}{\rho c_{i,k} \sum_{k'=1}^{K} \eta_{k'}^\star + \bar{\beta}_k P_R^* N + 1}, \ \forall k. \tag{4.46}$$

Therefore, by increasing P_R and η_k, respectively, beyond $P_{R,max}$ and $\eta_k^\star$, the objective function is increased, and the first constraint is still satisfied. This implies that at the optimal point we have $P_R^\star = P_{R,max}$.

Now, for the sake of notational simplicity, let $1_K = [1, \ldots, 1]^T$ be a vector of size $K \times 1$. Moreover, define $\eta = [\eta_1, \ldots, \eta_K]^T$. Then, the optimization problem ($\mathbb{P}3$) can be reduced to

$$(\mathbb{P}5): \max_{\eta} \ 1_K^T \eta + \frac{\sigma_R^2}{a_i} \tag{4.47a}$$

$$\text{s.t.} \ \mathbf{C}\eta \leq \mathbf{b}, \tag{4.47b}$$

where $\mathbf{b} = [\Lambda_1, \ldots, \Lambda_K, 1]$, with $\Lambda_k = -\gamma_{k,\text{th}}(\bar{\beta}_k P_{R,max} N + 1)$ and

$$\mathbf{C} = \begin{bmatrix} \Psi_1 & \Theta_1 & \Theta_1 & \ldots & \Theta_1 & \Theta_1 \\ \Theta_2 & \Psi_2 & \Theta_2 & \ldots & \Theta_2 & \Theta_2 \\ \vdots & \vdots & \vdots & \ddots & \vdots & \vdots \\ \Theta_K & \Theta_K & \Theta_K & \ldots & \Theta_K & \Psi_K \\ 1 & 1 & 1 & \ldots & 1 & 1 \end{bmatrix}, \tag{4.48}$$

with $\Theta_k = \rho c_{i,k} \gamma_{k,\text{th}}$ and $\Psi_k = \rho c_{i,k} \gamma_{k,\text{th}} - \rho b_i \gamma_k$. The problem ($\mathbb{P}5$) is an LP problem and can be efficiently solved via interior-point algorithms [144]. We use the *linprog* function in Matlab platform to solve Problem ($\mathbb{P}5$).

According to [145], the complexity of the optimization problem ($\mathbb{P}5$) is $\mathscr{O}\left((n_l + n_v) n_v^2 n_l^{0.5}\right)$, where $n_l = K + 1$ denotes the number of linear constraints while $n_v = K$ is the number of real valued scalar decision variables.

4.5 Extensions

4.5.1 Multi-target Scenarios

The considered spectrum sharing MIMO radar and communication system has interesting application scenarios. For instance, identifying abnormal or suspicious activities in a specific area and sending an alert is one potential scenario. Therefore, the coexistence of co-located MIMO radar for single-target detection and communication has been the subject of several research studies [40, 22]. On the other hand, multi-target detection can be achieved through the multibeam/beampattern design at the MIMO radar [146]. Accordingly, new performance metrics such as beampattern gain are used in the literature to study the performance of such designs.

The primary concept of beampattern design is to determine the covariance matrix of the radar probing signals through convex optimization problems. Let $\mathbf{R}_w = \frac{1}{L}\sum_{l=1}^{L}\mathbf{s}_l\mathbf{s}_l^H$ denote the covariance matrix of the probing signals, where $\mathbf{s}_l$ is the l-th snapshot across the radar antennas. Three different optimization problems have been proposed in the literature to determine $\mathbf{R}_w$. More specifically, the authors in [96] formulated a constrained least-squares problem to approach an ideal beampattern as

$$\min_{\alpha,\mathbf{R}_w} \sum_{m=1}^{M} \left|\alpha\tilde{P}_d(\theta_m) - \mathbf{a}^H(\theta_m)\mathbf{R}_w\mathbf{a}(\theta_m)\right|^2 \tag{4.49a}$$

$$s.t.\ \mathrm{diag}(\mathbf{R}_w) = \frac{P_0\mathbf{1}_N}{N}, \tag{4.49b}$$

$$\mathbf{R}_w \succeq \mathbf{0}, \mathbf{R}_w = \mathbf{R}_w{}^H, \tag{4.49c}$$

$$\alpha \geq 0 \tag{4.49d}$$

$$\mathrm{tr}(\mathbf{f}_i^*\mathbf{f}_i^T\mathbf{R}_w) = 0,\ \forall i, \tag{4.49e}$$

where $\{\theta_m\}_{m=1}^{M}$ is defined as a fine angular grid that covers the detection angle range of $[-\frac{\pi}{2}, \frac{\pi}{2}]$, $\mathbf{a}(\theta_m) = [1, e^{-j2\pi d\sin(\theta_m)}, \ldots, e^{-j2\pi d(N-1)\sin(\theta_m)}]^T \in \mathbb{C}^{N\times 1}$ is the steering vector of the transmit antenna array, $\tilde{P}_d(\theta_m)$ is the desired ideal beampattern gain at θ_m, P_0 is the power budget, α is a scaling factor, and $1_N \in \mathbb{R}^{N\times 1}$. We notice that via constraint (4.49e), we force the radar signals to fall into the nullspace of the channel between the radar antennas and downlink users.

Nevertheless, finding the detection probability of the radar is challenging. We leave the performance evaluation of the multi-target scenario for future investigation.

4.5.2 Correlated Fading

In this subsection, we extend our analysis to consider the spatially correlated Raleigh fading scenario. The correlated Rayleigh channel vector between the k-th user and the BS can be modeled as

$$\mathbf{g}_k \sim \mathscr{CN}(0, \Omega_k), \tag{4.50}$$

where $\Omega_k \in \mathbb{C}^{M\times M}$ is the transmit correlation matrix specific to terminal k.

Training phase: Based on the observable pilot matrix in (4.2), the BS correlates $\mathbf{Y}_{\mathrm{P}}$ with the pilot sequence $\boldsymbol{\varphi}_{p,k}$ of user k, leading to the processed pilot sequence

$$\check{\mathbf{y}}_{k,\mathrm{p}} = \mathbf{Y}_{\mathrm{p}}\boldsymbol{\varphi}_{p,k} = \sqrt{\tau_{\mathrm{p}}\rho_u}\mathbf{g}_k + \mathbf{N}\boldsymbol{\varphi}_{p,k}, \tag{4.51}$$

where $\boldsymbol{\varphi}_{p,k} \in \mathbb{C}^{\tau_{\mathrm{p}}\times 1}$ indicates the pilot signal assigned to the k-th user. Based on the observation $\check{\mathbf{y}}_{k,\mathrm{p}}$, the MMSE estimate of the channel $\mathbf{g}_k$ is given by

$$\hat{\mathbf{g}}_k = \sqrt{\tau_{\mathrm{p}}\rho_u}\Omega_k\Xi_k\check{\mathbf{y}}_{k,\mathrm{p}},$$

where

$$\Xi_k = \left(\tau_{\mathrm{p}}\rho_u\Omega_k + \mathbf{I}_M\right)^{-1}. \tag{4.52}$$

Therefore, the MMSE estimated channel $\hat{\mathbf{g}}_k$ and the corresponding estimation error $\tilde{\mathbf{g}}_k$ are complex Gaussian random vectors, distributed as follows

$$\hat{\mathbf{g}}_k \sim \mathscr{N}_{\mathbb{C}}(\mathbf{0},\ \mathbf{Q}_k),$$
$$\tilde{\mathbf{g}}_k \sim \mathscr{N}_{\mathbb{C}}(\mathbf{0}, \mathbf{C}_k),$$

where $\mathbf{Q}_k = \Omega_k - \mathbf{C}_k$ and $\mathbf{C}_k$ is expressed as

$$\mathbf{C}_k = \Omega_k - \tau_{\mathrm{p}}\rho_u\Omega_k\Xi_k\Omega_k. \tag{4.53}$$

The following Proposition provides the SE at the kth cellular user and detection probability at the radar over the spatially correlated fading environments and with MR precoding design at the BS.

We proceed to find closed-form expression for SINR_k with MR precoding.

Proposition 7 *For the considered spatially correlated Rayleigh channels, the SE of the k-th user achieved by the* MR *precoding is given by* (4.54) *at the top of the next page.*

$$\mathrm{SE}_k^{\mathrm{MR,Cor}} = \left(1 - \frac{\tau_{\mathrm{p}}}{\tau}\right) \log_2 \left(1 + \frac{\eta_k \rho \tau_{\mathrm{p}} \rho_u \mathrm{tr}(\Omega_k \Xi_k \Omega_k)}{\sum_{k'=1}^{K} \eta_{k'} \rho \frac{\mathrm{tr}(\Omega_{k'} \Xi_{k'} \Omega_{k'} \Omega_k)}{\mathrm{tr}(\Omega_{k'} \Xi_{k'} \Omega_{k'})} + P_R \bar{\beta}_k N + \sigma_C^2}\right), \tag{4.54}$$

Moreover, the detection probability at the radar is given by (4.28)*, where*

$$\mu^{\mathrm{MR,Cor}} \approx \frac{|\alpha|^2 L P_R \mathrm{tr}(\mathbf{A}\mathbf{A}^H)}{\zeta_{\mathrm{MR}} \sum_{k=1}^{K} \eta_k + \sigma_R^2}. \tag{4.55}$$

Proof 7 *See Appendix B.*

We notice that, in the case of uncorrelated fading channels $\mathrm{tr}(\Omega_k \Xi_k \Omega_k) = \frac{M\gamma_k}{\tau_{\mathrm{p}}\rho_u}$ and $\mathrm{tr}(\Omega_{k'} \Xi_{k'} \Omega_{k'} \Omega_k) = \frac{M\gamma_k\gamma_{k'}}{\tau_{\mathrm{p}}\rho_u}$. Therefore, $\mathrm{SE}_k^{\mathrm{MR,Cor}}$ reduces to $\mathrm{SE}_k^{\mathrm{MR}}$ in (4.20). Moreover, by comparing (4.55) and (4.35), we observe that when using MR precoding at the BS, the same detection probability is achieved over both correlated and uncorrelated Rayleigh fading channels.

Remark 1 *Finding closed-form expressions for the achievable SE and detection probability for* ZF *and* PZF *precoding designs seems intractable. However, the corresponding results can be obtained through numerical simulations.*

4.6 Numerical results

In this section, we provide numerical results to verify our analysis and evaluate the performance of the proposed power control design. We assume that the MIMO radar system deploys a uniform linear array with inter-antenna spacing $d = \lambda/2$. The radar SNR is defined as $\mathrm{SNR}_R = \frac{L|\alpha|^2 P_R}{\sigma_R^2}$ [40]. The target is set to be located at the direction of $\theta = 10^\circ$. In the communication system, we consider large-scale fading with path loss, shadow fading, and random user locations. To generate the large-scale fading coefficients, we adopt the model proposed in [129]. For the sake of understanding, let us visualize a circular cell with a radius of approximately 15 kilometres. At the center of the cell, the BS equipped with M antennas

serves K users randomly distributed within the cell. Furthermore, a MIMO radar is positioned 10 kilometres away from the BS. We model the large-scale fading coefficient β as [129]

$$\beta = \mathrm{PL}_0 \left(\frac{d}{R_{\min}} \right)^{\upsilon} \times 10^{\frac{\sigma_{\mathrm{sh}} z}{10}}, \tag{4.56}$$

where $\beta \in \{\beta_k, \bar{\beta}_k, \beta_{br}\}$, $d \in \{d_k, \bar{d}_k, d_{br}\}$ with d_k ($\bar{d}_k$) being the distance between the BS (radar) and user k, while d_{br} is the distance between the BS and radar; PL_0 denotes a reference path loss constant which is chosen to satisfy a given downlink cell-edge SNR; υ and σ_{sh} represent the path loss exponent and standard deviation of the shadow fading, respectively; and $z \sim \mathcal{N}(0,1)$. In our examples, we chose υ = 3.8, $\sigma_{\mathrm{sh}} = 8$ dB.

The (i,j) entry in the correlation matrix of terminal k is given by [147]

$$[\Omega_k]_{i,j} = \frac{1}{2\Delta} \int_{-\Delta+\phi_k}^{\Delta+\phi_k} e^{-j2\pi d(i-j)\sin(\theta_k)} d\theta_k, \tag{4.57}$$

where Δ denotes the azimuth angular spread, ϕ_k is the central azimuth angle from BS array to the terminal k, θ_k is the actual angle-of-departure and $d\,(i-j)$ captures the inter-element spacing normalized by the carrier wavelength between i-th and j-th antenna elements. Unless explicitly stated, we set $d(1) = 0.5$ and assume that ϕ_k drawn from a uniform distribution on 0, 2π, i.e., $\phi_k \sim \mathscr{U}[0, 2\pi]$. The instantaneous value of θ_k is also drawn from a uniform distribution on $-\frac{\Delta}{2}, \frac{\Delta}{2}$, i.e., $\theta_k \sim \mathscr{U}[-\frac{\Delta}{2}, \frac{\Delta}{2}]$. As such, Δ represents the tota angular spread, naturally bounded from 0 to 2π radians.

Figure 4.2 shows the downlink SE of different massive MIMO systems versus the number of BS antennas M, for different precoding schemes MR, ZF and PZF. Our analysis has been confirmed by the simulation results, demonstrating a precise alignment between the analytical and simulated outcomes. As anticipated, an increase in the number of BS antennas directly corresponds to SE enhancement. We observe that the performance gaps between the considered precoding schemes are decreased, when the number of BS antennas increases. For example, by increasing the number of BS antennas from $M = 200$ to $M = 400$, the gap between the ZF (PZF) scheme and MR is reduced from 85% (50%) to 72% (27%). This behavior can be explained as follows: By comparing (4.22) and (4.27), we observe that by increasing the number of BS antennas M, for a fixed number of receive antennas at the radar, N, we have $\frac{M-N}{N} \xrightarrow{M\to\infty} 1$. Therefore, the numerators of the SINRs inside the logarithmic functions are approximately the same for the ZF and PZF schemes. However, the first term in the denominator of $\mathrm{SINR}_k^{\mathrm{PZF}}$ scales as $(M-K)$, whereas the corresponding term in $\mathrm{SINR}_k^{\mathrm{ZF}}$ scales as 1. Therefore, by

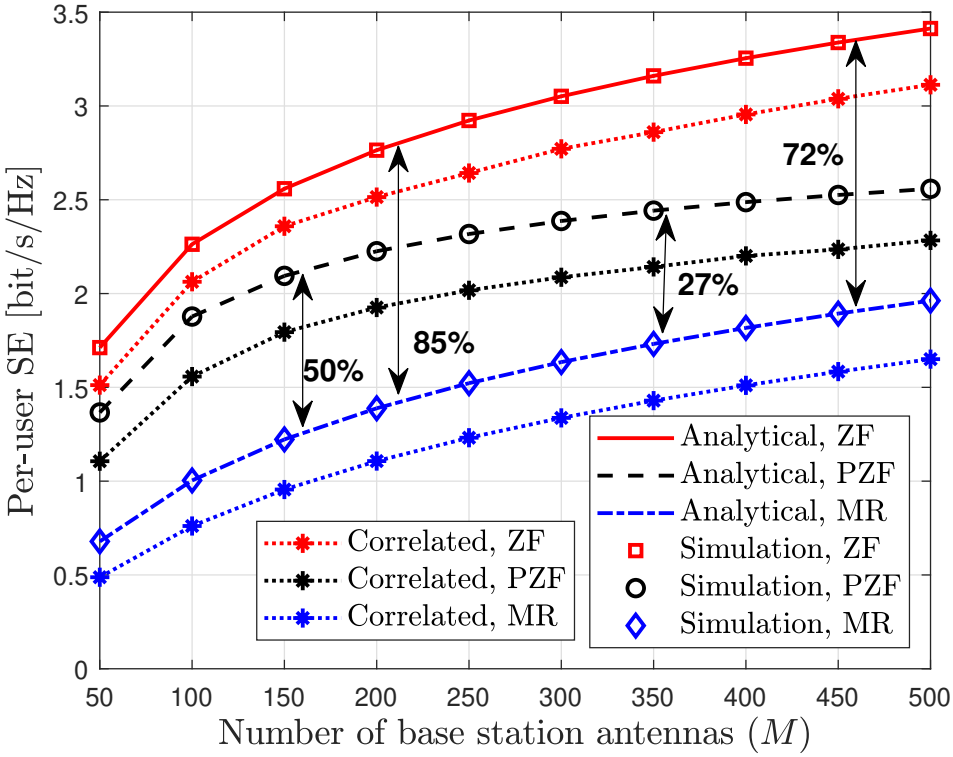

Fig. 4.2 Per-user SE versus the number of BS antennas, M, ($N = 20$, $\rho = 20$ dB, $K = 20$, $\Delta = 20^o$).

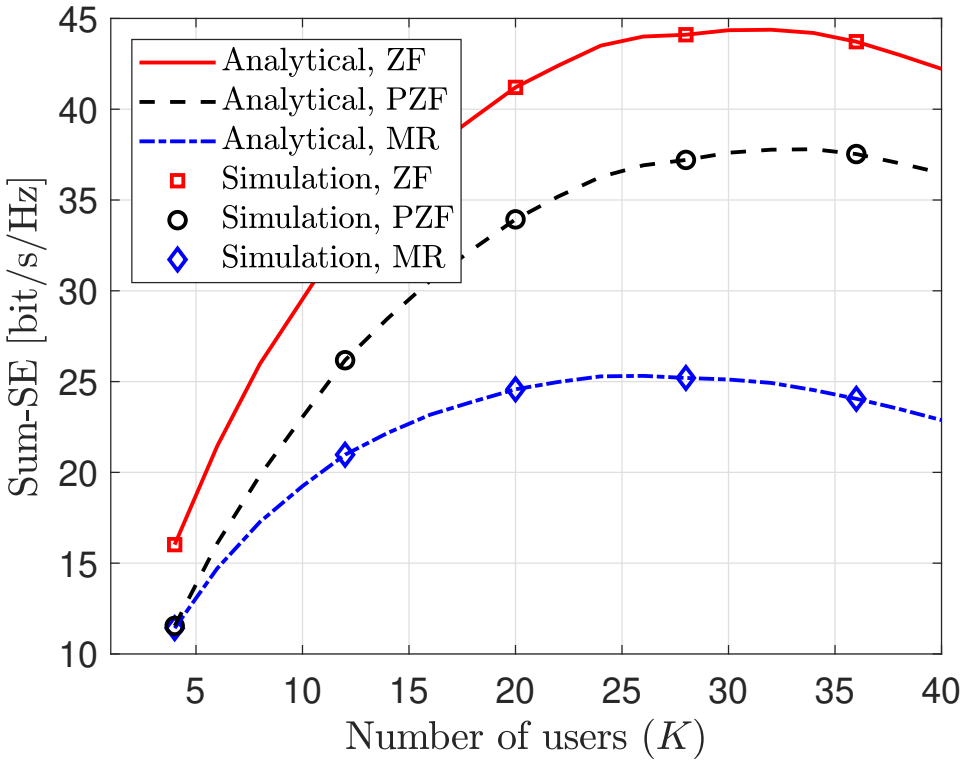

Fig. 4.3 Sum-SE versus the number of users, K, ($M = 200$, $\rho = 20$ dB, $N = 20$).

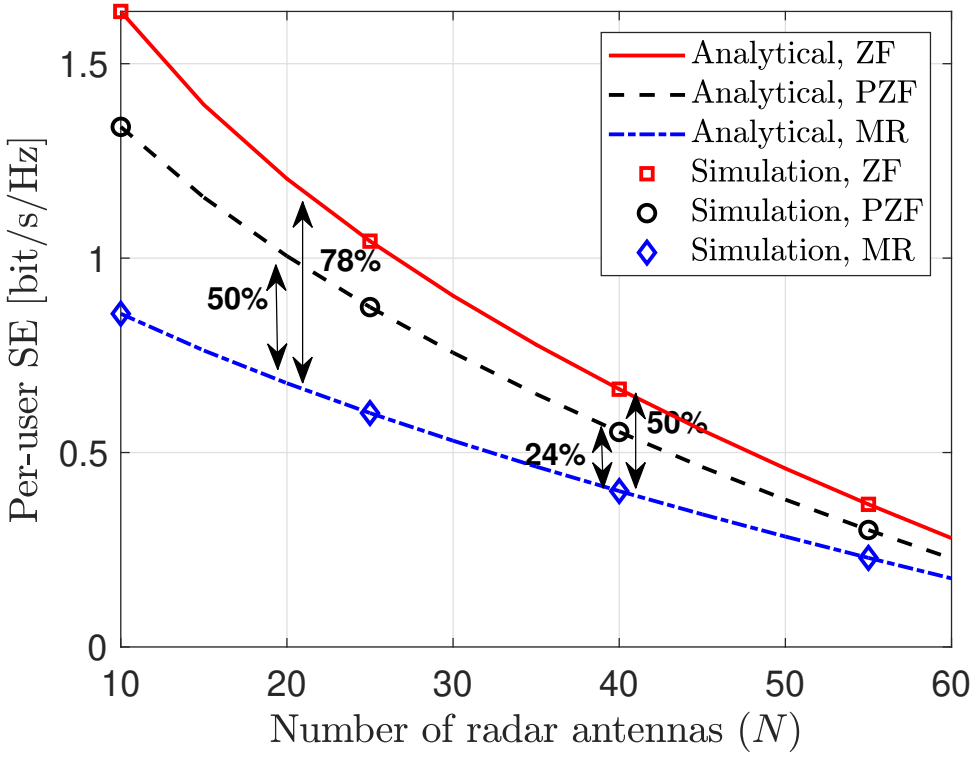

Fig. 4.4 Per-user SE versus the number of radar antennas, N, ($M = 200$, $\rho = 20$ dB, $K = 20$).

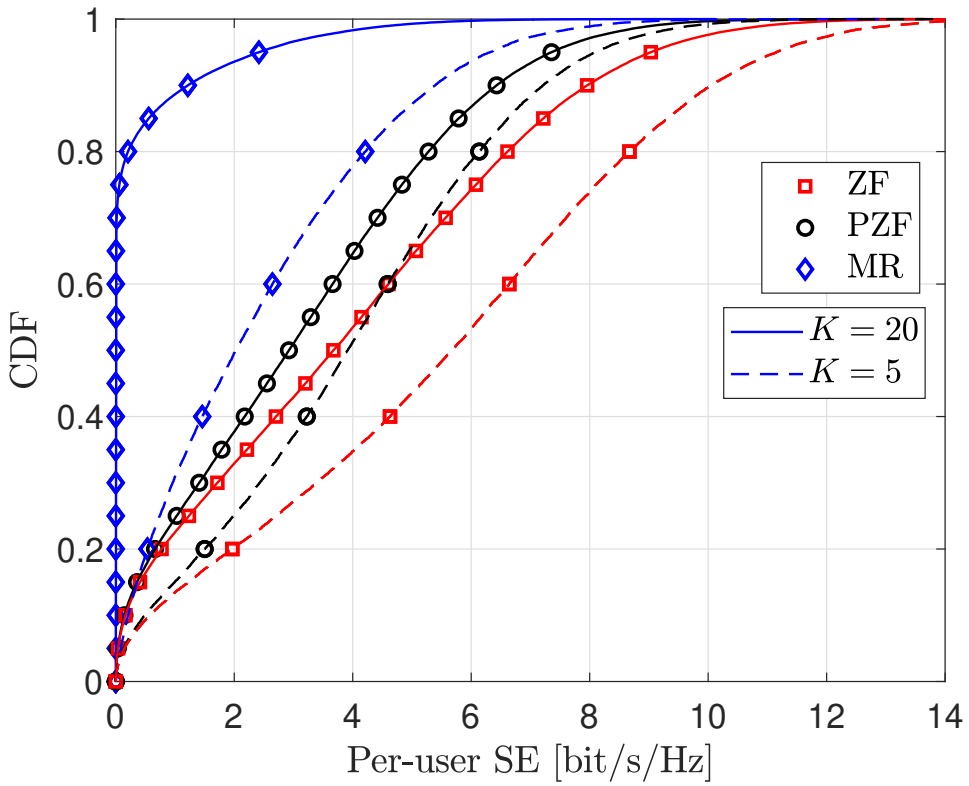

Fig. 4.5 CDF of the per-user SE for different number of users ($N = 20$, $M = 200$, $\rho = 20$ dB).

increasing M, the reduction in $\text{SINR}_k^{\text{PZF}}$ becomes greater compared to $\text{SINR}_k^{\text{ZF}}$. As a result, the gap between the SE achieved by ZF and PZF increases with higher values of M. Finally, when comparing the results between the correlated and uncorrelated channels, we find that the same insights apply to correlated environments.

Figure 4.3 shows the downlink sum-SE of massive MIMO system versus the number of users K, for different precoding schemes, i.,e MR, ZF and PZF. By increasing the number of users, sum-SE increases and tends to the maximum value and then starts to reduce due to increasing pilot overhead. Moreover, we observe that by increasing K, the gap between the ZF and MR increases, while the gap between the ZF and PZF remains constant, which is due to the severe increase of the inter-user interference in the case of MR processing. These results reveal the necessity of developing pilot reuse among different users and designing pilot assignment algorithms to manage the pilot contamination effects.

To demonstrate the impact of radar interference on massive MIMO systems, we examine the SE as a function of the number of transmit antennas at the radar in Figure 4.4. As the number of antennas at the radar increases, the interference towards the massive MIMO system

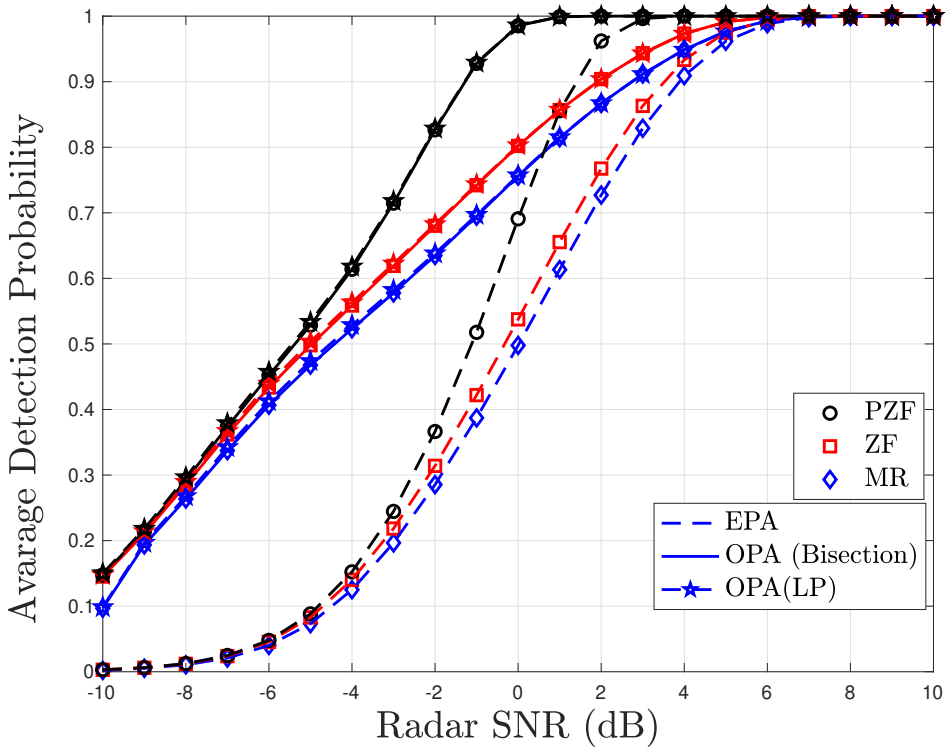

Fig. 4.6 Average detection probability versus the radar SNR ($M = 200$, $K = 20$, $N = 20$, $\mathtt{SNR}_R = 0$ dB).

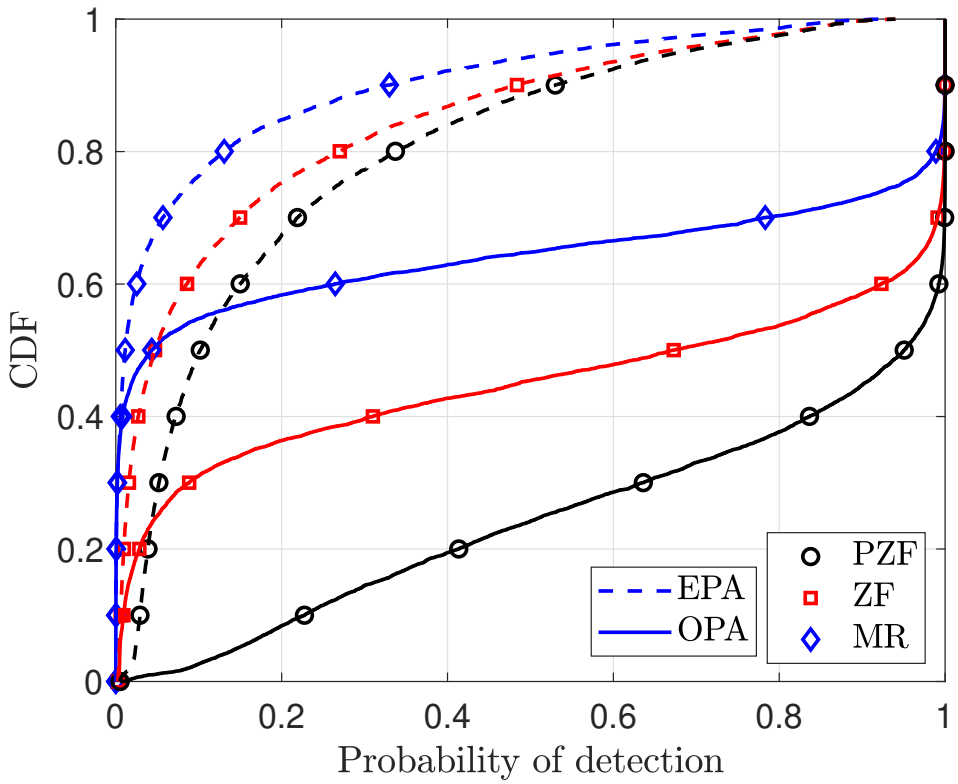

Fig. 4.7 CDF of detection probability ($M = 200$, $K = 20$, $N = 20$).

increases, leading to SE reduction. For different number of antennas at the radar, MR yields the worst performance, while ZF outperforms all schemes. Notably, ZF exhibits a remarkable improvement of 78% over MR, while PZF demonstrates a substantial enhancement of 50% compared to MR, when the number of radar antennas is $N = 20$. When the number of radar antennas is increased to $N = 80$, ZF achieves a significant improvement of up to 50% over MR, while PZF exhibits a substantial enhancement of 24% over MR. This further solidifies the superiority of ZF and PZF techniques over the MR scheme in the given context.

Figure 4.5 shows the cumulative distribution of the per-user SE for different values of $K = 5$ and $K = 20$, with $M = 200$ and $\rho = 20$ dB. We can observe that the per-user SE in the case of $K = 5$ is higher than that in the case of $K = 20$. This difference can be attributed to the fact that when there are more users, inter-user interference becomes more prevalent. Additionally, it is evident from the figure that MR suffers more from inter-user interference compared to ZF and PZF.

Figure 4.6 provides a comparative analysis of detection probabilities under two power allocation schemes: our proposed optimal power allocation (OPA) solutions and equal power

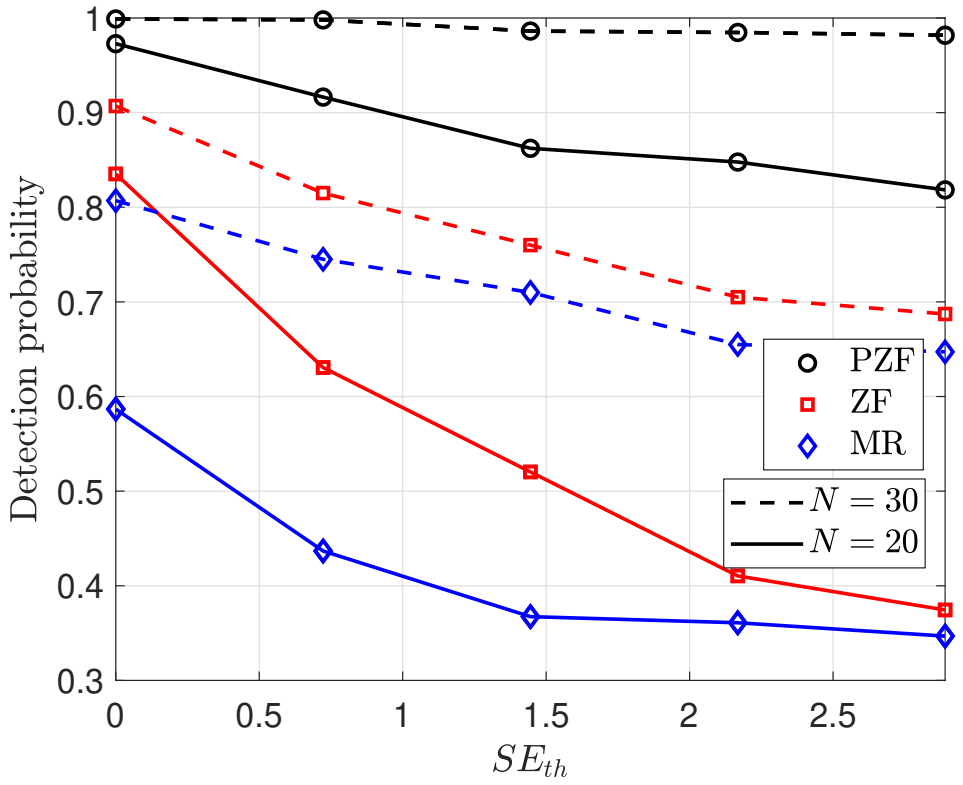

Fig. 4.8 Detection probability versus the SE threshold ($M = 200$, $K = 20$, $\mathtt{SNR}_R = 0$ dB).

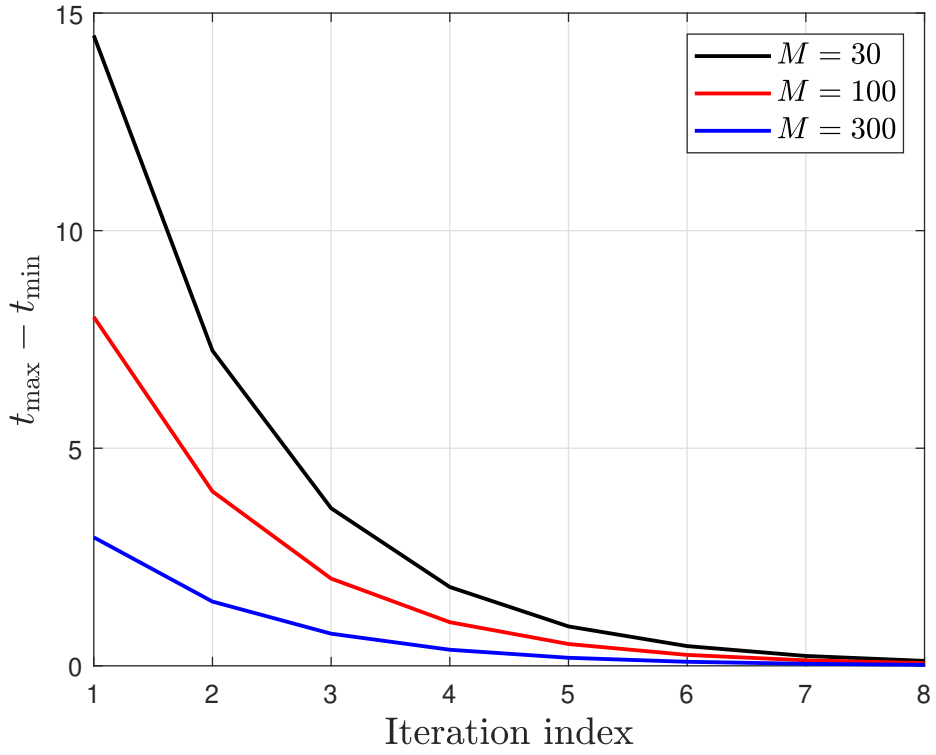

Fig. 4.9 Convergence behavior of the bisection algorithm to solve the problem $(\mathbb{P}4)$ for different number of BS antennas ($K = 20$, $N = 20$).

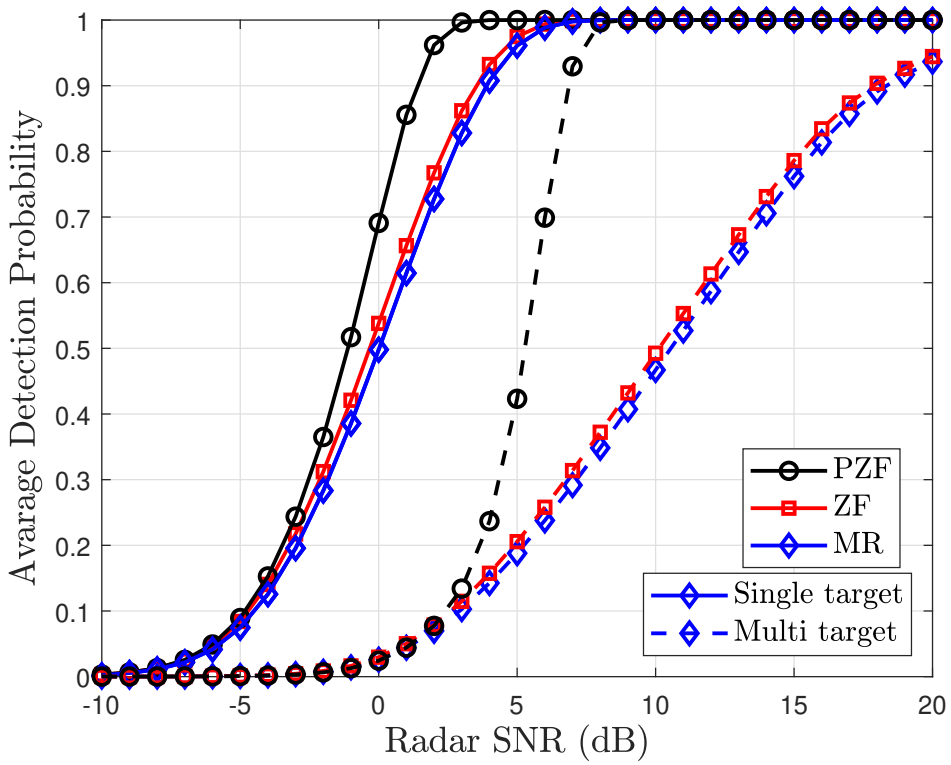

Fig. 4.10 Average detection probability versus the radar SNR for single and multiple target scenarios ($M = 200$, $K = 20$, $N = 20$, $\mathtt{SNR}_R = 0$ dB)

allocation (EPA). It can be observed that the results obtained using the OPA via the bisection algorithm closely match those obtained using LP. In the EPA scenario, the radar transmits with maximum power level, i.e, $P_R = P_{R,max}$ and power control coefficients at the BS are set as $\eta_k = \frac{1}{K}, \forall k = 1, \ldots, K$. To ensure a fair comparison, the selection of the SE threshold ($\mathrm{SE}_{\mathrm{th}}$) in the power allocation scheme is based on the EPA scenario. Among the considered schemes, our proposed PZF scheme yields the highest performance, followed by ZF and MR, respectively. Moreover, our proposed power allocation scheme yields a remarkable enhancement in the detection probability. For example, when the radar SNR is 2 dB and OPA is applied, the detection probability of PZF, ZF and MR precoding schemes improved from 0.5, 0.35, and 0.3 to 0.97, 0.72, and 0.68, respectively.

Figure 4.7 shows the CDF of the detection probability for PZF, ZF, and MR precoding designs and for OPA and EPA. It is evident that our proposed OPA strategy yields a substantial improvement in the detection probability performance and PZF design provides the best performance.

Figure 4.8 examines the trade-off between the detection probability and SE for PZF, ZF, and MR precoding designs and for two different radar antenna number. For a specific network realization, we first derive the maximum value for $\mathrm{SE}_{k,\mathrm{th}}$, termed as $\mathrm{SE}_{k,\mathrm{th}}^{\max}$, according to the EPA. Then, the optimization problem ($\mathbb{P}4$) is solved for different values of $\mathrm{SE}_{k,\mathrm{th}} = [0, \mathrm{SE}_{k,\mathrm{th}}^{\max}]$, and corresponding detection probability is derived. From Fig. 4.8, we can observe that for small values of $\mathrm{SE}_{k,\mathrm{th}}$, the radar can transmit with more power, yielding better detection probability performance. Moreover, by increasing the number of radar receive antennas the detection probability is improved, while it degrades the SE of the users in the communication system (cf Fig. 4.4).

Figure 4.9 shows value of $(t_{\max} - t_{\min})$ versus the number of iterations for one randomly generated set of channel realizations for different number of BS antennas. It can be observed that the algorithm with different number of BS antennas has a similar convergence speed and, as a matter of fact, converges to the optimal value after only a small number of iterations.

Figure 4.10 presents a comparison of average detection probabilities versus the radar SNR for both single and multiple target scenarios. In the multiple target scenario, three targets are located at specific angular directions. The comparison is conducted for three precoding techniques: MR, ZF, and PZF. A key observation from the figure is the enhanced detection probability in single target scenarios compared to multiple targets, which is likely due to the increased interference challenges in multi-target environments. Notably, the PZF scheme emerges as the most effective technique, achieving the highest detection probability across

various SNR levels. The superiority of PZF is particularly marked in multiple target scenarios, underlining its efficiency in interference mitigation.

Remark 2 *To improve the detection probability at the radar, the multiple-target detection problem can be modeled as a multi-hypothesis testing, followed by beampattern design at the radar [148, 44]. Exploring the development of a closed-form expression for the detection probability and subsequently applying joint power control and beamforming design at the BS represent interesting future research directions.*

4.7 Conclusion

We have studied the coexistence of massive MIMO communication and MIMO radar. PZF precoding design has been proposed to achieve favourable SE performance in the cellular system, while delivering substantial improvements to the radar system. Closed-form expressions for the SE of users and the detection probability at the radar have been derived for MR, ZF, and PZF precoding designs. Accordingly, power control at the BS and radar has been developed to manage the inter-system interference, subject to the SE requirements of the users. The optimization problem has been efficiently solved, showing substantial improvement in detection probability, when compared with the equal power allocation scenario.

Chapter 5

Cell-Free Massive MIMO for ISAC: Access Point Operation Mode Selection and Power Control

5.1 Introduction

ISAC has recently been envisioned as a key enabling technology for future wireless networks, aiming to efficiently utilize the congested resources for both communication and sensing [59, 146]. The radar bands set aside for sensing can be harnessed for wireless communication operation, enabling the implementation of high data-rate applications. To unify the radar and communication operations, two well-known designs, namely separated and co-located systems, were introduced in [40, 88, 8] and [73, 96], respectively. The former utilizes different devices, operating over the same frequency band, for communication and sensing, while in the latter a single device acts as radar and communication base station (BS) by simultaneously communicating with multiple downlink users and detecting radar targets.

The main driving force behind the transition from the separated design to a co-located design was to reduce the complexity induced by side-information exchange among the radar and communication devices [96]. However, co-located design with a MIMO BS often suffers from a fairness problem, since the cell-boundary users are subject to inter-cell interference and significant power decay over long distances. The key feature of massive MIMO technology, i.e., inter/intra-cell interference suppression, revitalizes the interest towards separated design with multiple communication and radar devices to implement distributed ISAC architectures. In

this context, cell-free massive MIMO with distributed MIMO APs can be exploited to support ISAC. In cell-free massive MIMO, all users are coherently served by all APs over the same time-frequency band. Each AP is connected to a central processing unit (CPU) via fronthaul links, and the CPU is responsible for coordination [10, 9].

The integration of ISAC into cell-free massive MIMO networks, has been recently investigated in [24, 25]. Specifically, Behdad *et al.* [24] studied a cell-free massive MIMO ISAC system, consisting of a fixed number of transmit and receive APs. Users are served by the transmit APs and, at the same time, the transmitted signals are used for sensing to detect the presence of a target in a certain location. The reflected signals are received at the receive APs and then processed at the CPU. The authors proposed a power allocation algorithm to maximize the sensing signal-to-noise ratio (SNR) under signal-to-interference-plus-noise ratio (SINR) constraints at the user. Demirhan *et al.* [25] studied the sensing and communication beamforming design problem in cell-free massive MIMO ISAC systems, where a joint beamforming design was proposed to maximize the sensing SNR, while satisfying the communication SINR constraints.

Different from the above-mentioned works [24, 25], where the AP operation modes are fixed, we consider a novel cell-free massive MIMO ISAC network with dynamic AP operation mode selection. The APs' operation mode is designed to maximize the minimum SE of the downlink users, while satisfying the sensing requirement to detect the presence of a single target in a certain location. Relying on the long-term channel state information (CSI), the APs are divided into communication APs (C-APs) and sensing APs (S-AP) to support downlink communication and sensing operations simultaneously. The main contributions of our paper can be summarized as follows:

- By leveraging the use-and-then-forget strategy, we derive closed-form expressions for the downlink SE and MRSR to evaluate the performance of the communication and sensing operation, respectively. Then, we formulate the problem of joint AP operation mode selection and power control, considering per-AP power constraints and a MASR constraint for target detection.
- We propose a greedy algorithm for AP operation mode selection. Accordingly, an alternating optimization (AO) algorithm is developed to handle the coupling between the C-AP and R-AP power control coefficients' design.
- Numerical results show that our proposed greedy AP operation mode selection with optimal power control (GAP-OPC) significantly improves the SE performance of the

downlink users for given MASR, compared to the greedy/random operation mode selection with no power control (GAP/RAP-NPC) benchmarks.

5.2 System Model

We consider a cell-free massive MIMO ISAC system under time division duplex operation, where M APs serve K_d users in the downlink, while radiating probing signals to a target direction for radar sensing. Each user is equipped with one single antenna, while each AP is equipped with N antennas. All APs and users operate as half-duplex devices. For notational simplicity, we define the sets $M \triangleq \{1,\ldots,M\}$ and $K \triangleq \{1,\ldots,K_d\}$ as the collections of indices of the APs and users, respectively. As shown in Fig. 6.1, downlink communication as well as target detection take place simultaneously and over the same frequency band. The AP operation mode selection approach is designed according to the network requirements, determining whether an AP is dedicated to information transmission or radar sensing. The users receive information from a group of the APs, termed as C-APs, while the remaining APs, termed as S-APs, are used for target detection.

5.2.1 Channel Model and Uplink Training

We assume a quasi-static channel model, with each channel coherence interval spanning a duration of τ symbols. The duration of the training is denoted as τ_t, while the duration of downlink information transfer and target detection is $(\tau - \tau_t)$.

For the sensing channel model, we assume there is a line-of-sight (LOS) path between the target location and each AP, which is a commonly adopted model in the literature [24, 25]. The LOS channel between AP m and target is given by

$$\mathbf{g}_m = \mathbf{a}_N(\phi^a_{m,t}, \phi^e_{m,t}),\ \forall m \in M, \tag{5.1}$$

where $\phi^a_{m,t}$, $\phi^e_{m,t}$ denote the azimuth and elevation angles of departure (AoD) from AP m towards the target. Moreover, the q-th entry of the array response vector $\mathbf{a}_N(\phi^a_{m,t}, \phi^e_{m,t}) \in \mathbb{C}^{N\times 1}$, is given by

$$[\mathbf{a}_N(\phi^a_{m,t}, \phi^e_{m,t})]_q = \frac{1}{\sqrt{N}} \exp\left(j2\pi \frac{d}{\lambda}(q-1)\sin\phi^e_{m,t}\sin\phi^a_{m,t}\right), \tag{5.2}$$

where d and λ denote the AP antenna spacing and carrier wavelength, respectively.

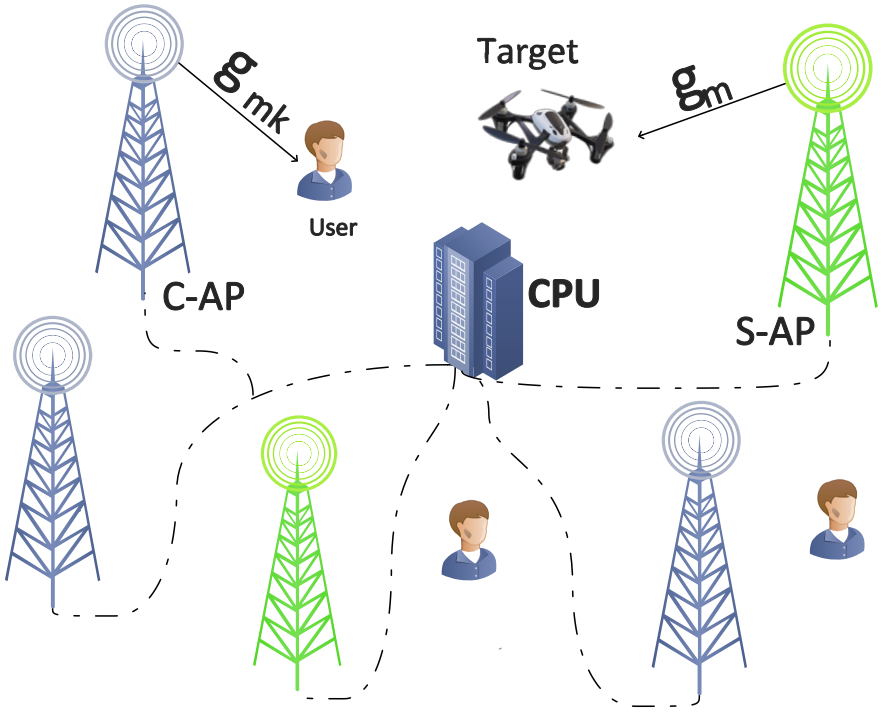

Fig. 5.1 Cell-free massive MIMO ISAC system.

The channel vector between the m-th AP and k-th user is modeled as $\mathbf{g}_{mk} = \sqrt{\beta_{mk}}\mathbf{h}_{mk}$, where β_{mk} is the large scale fading coefficients, and $\mathbf{h}_{mk} \in \mathbb{C}^{N\times 1}$ is the small-scale fading vector, whose elements are independent and identically distributed $\mathscr{CN}(0,1)$ random variables [9].

An uplink training process is implemented to acquire the local CSI between each AP and all users. In each coherence block of length τ, all users are assumed to transmit their pairwisely orthogonal pilot sequence of length τ_t to all APs, which requires $\tau_t \geq K_d$. At AP m, $\mathbf{g}_{mk}$ is estimated by using the received pilot signals and applying the minimum mean-square error (MMSE) estimation technique. By following [9], the MMSE estimate $\hat{\mathbf{g}}_{mk}$ of $\mathbf{g}_{mk}$ is obtained as $\hat{\mathbf{g}}_{mk} \sim \mathscr{CN}(0, \gamma_{mk}\mathbf{I}_N)$, where

$$\gamma_{mk} = \frac{\tau_t \rho_t \beta_{mk}^2}{\tau_t \rho_t \beta_{mk} + 1}, \tag{5.3}$$

while ρ_t represents the normalized transmit power of each pilot symbol.

5.2.2 Data and Probing Signal Transmission

AP operation mode selection is performed by considering large-scale fading effects and relying on the statistical CSI, obtained during the training phase. The binary variables used to indicate the operation mode for each AP m are defined as

$$a_m = \begin{cases} 1, & \text{if AP } m \text{ operates as C-AP} \\ 0, & \text{if AP } m \text{ operates as S-AP.} \end{cases} \tag{5.4}$$

The transmission phase comprises information transmission from C-APs to users and probing signal transmission from S-APs to the target. Let $\mathbf{x}_{c,m}$ and $\mathbf{x}_{r,m}$ denote the data and probing signals, respectively, where $\mathbb{E}\left\{|\mathbf{x}_{c,m}|^2\right\} = 1$ and $\mathbb{E}\left\{|\mathbf{x}_{r,m}|^2\right\} = 1$. The signal vector transmitted from AP m can be expressed as

$$\mathbf{x}_m = a_m \mathbf{x}_{c,m} + (1 - a_m)\mathbf{x}_{r,m}. \tag{5.5}$$

The power control coefficients at AP m are chosen to satisfy the power constraint at each S-AP and C-AP, respectively, i.e.,

$$a_m \mathbb{E}\{\|\mathbf{x}_{c,m}\|^2\} + (1 - a_m)\mathbb{E}\{\|\mathbf{x}_{r,m}\|^2\} \leq \rho, \tag{5.6}$$

where ρ denotes the maximum normalized downlink power.

The transmit signal for communication at the m-th C-AP can be expressed as $\mathbf{x}_{c,m} = \sum_{k \in K_d} \sqrt{\eta_{mk}\rho}\mathbf{t}_{mk}^{\text{Com}} x_{c,k}$, where η_{mk} represents the downlink power control coefficient at the m-th C-AP during communication, while $\mathbf{t}_{mk}^{\text{Com}} \in \mathbb{C}^{N\times 1}$ and $x_{c,k}$ denote the precoding vector and intended signal for user k, respectively.

Moreover, the probing signal transmitted by the m-th S-AP can be expressed as $\mathbf{x}_{r,m} = \sqrt{\eta_m \rho}\mathbf{t}_m^{\text{Sen}} x_r$, where η_m denotes the power control coefficient at S-AP m, while $\mathbf{t}_m^{\text{Sen}} \in \mathbb{C}^{N\times 1}$ denotes the beamforming vector for sensing and x_r is the sensing symbol.

We note that in the absence of communication users, conjugate sensing beamforming solution becomes optimal, as it directly maximizes the sensing SNR [24, 25]. Therefore, to detect the presence of a target in a certain location, we design the sensing beamforming vector

at S-AP m as

$$\mathbf{t}_m^{\text{Sen}} = \mathbf{a}_N(\phi_{m,t}^a, \phi_{m,t}^e). \tag{5.7}$$

Furthermore, the conjugate precoder is employed at the C-AP, particularly due to its advantages including low computational complexity, ease of analysis, and reasonable performance, as shown in [149, 139]. Hence, $\mathbf{t}_{mk}^{\text{Com}}$ is given by

$$\mathbf{t}_{mk}^{\text{Com}} = \hat{\mathbf{g}}_{mk}^*. \tag{5.8}$$

5.2.3 Sensing Operation and MASR

For a given channel realization, the average spatial power pattern for sensing is defined as

$$\begin{aligned} P^{\text{ave}}(\phi_{m,t}^a, \phi_{m,t}^e) &= \mathbb{E}\left\{ \sum_{m\in M} |\mathbf{a}_N^H(\phi_{m,t}^a, \phi_{m,t}^e)\mathbf{x}_m|^2 \right\} \\ &= \rho \sum_{m\in M} a_m \mathbb{E}\left\{ \left| \sum_{k\in K_d} \sqrt{\eta_{mk}} \mathbf{a}_N^H(\phi_{m,t}^a, \phi_{m,t}^e)\mathbf{t}_{mk}^{\text{Com}} \right|^2 \right\} \\ &\quad + \rho \sum_{m\in M} (1-a_m)\eta_m \mathbb{E}\left\{ \left| \mathbf{a}_N^H(\phi_{m,t}^a, \phi_{m,t}^e)\mathbf{t}_m^{\text{Sen}} \right|^2 \right\}, \end{aligned} \tag{5.9}$$

where the expectation is taken over the transmitted signals, assuming that the information signal and probing signals are independent zero-mean Gaussian distributed.

Proposition 8 *The average spatial power pattern for sensing is given by* $P^{\text{ave}}(\phi_{m,t}^a, \phi_{m,t}^e) = P_{\text{Com}}^{\text{ave}}(\phi_{m,t}^a, \phi_{m,t}^e) + P_{\text{Sen}}^{\text{ave}}(\phi_{m,t}^a, \phi_{m,t}^e)$*, where*

$$P_{\text{Com}}^{\text{ave}}(\phi_{m,t}^a, \phi_{m,t}^e) = \rho \sum_{m\in M} \sum_{k\in K_d} a_m \eta_{mk} \gamma_{mk}, \tag{5.10a}$$

$$P_{\text{Sen}}^{\text{ave}}(\phi_{m,t}^a, \phi_{m,t}^e) = \rho \sum_{m\in M} (1-a_m)\eta_m. \tag{5.10b}$$

Proof 8 *By invoking* (5.7) *and* (5.8)*, and then taking the expectation of* (5.9) *over* $\mathbf{t}_{mk}^{\text{Com}}$*, the desired result is obtained.*

We would like $P^{\text{ave}}\text{Com}(\phi m, t^a, \phi_{m,t}^e)$, $\forall \phi_{m,t}^a, \phi_{m,t}^e$, to be as small as possible to confine the pattern distortion. For illuminating a target angle $(\phi_{m,t}^a, \phi_{m,t}^e)$, it is desirable that the mainlobe

level $P_{\text{Sen}}^{\text{ave}}(\phi_{m,t}^{a},\phi_{m,t}^{e})$ is higher than $P_{\text{Com}}^{\text{ave}}(\phi_{m,t}^{a},\phi_{m,t}^{e})$ by a certain minimum sensing level κ, which is referred to as the MASR:

$$\begin{aligned}\text{MASR}(\mathbf{a},\eta^{\text{Com}},\eta^{\text{Sen}}) &= \frac{P_{\text{Sen}}^{\text{ave}}(\phi_{m,t}^{a},\phi_{m,t}^{e})}{P_{\text{Com}}^{\text{ave}}(\phi_{m,t}^{a},\phi_{m,t}^{e})} \\ &= \frac{\sum_{m\in M}(1-a_m)\eta_m}{\sum_{m\in M}\sum_{k\in K_d}a_m\eta_{mk}\gamma_{mk}} \geq \kappa,\end{aligned} \tag{5.11}$$

where $\mathbf{a}=\{a_1,\ldots,a_M\}$, $\eta^{\text{Com}}=\{\eta_{m1},\ldots,\eta_{mK_d}\}$, $\forall m\in M$, and $\eta^{\text{Sen}}=\{\eta_1,\ldots,\eta_M\}$.

5.2.4 Communication Operation and Downlink SE

The received signal at k-th user can be expressed as

$$\begin{aligned}y_k = &\sum_{m\in M}a_m\sqrt{\rho\,\eta_{mk}}\mathbf{g}_{mk}^{T}\mathbf{t}_{mk}^{\text{Com}}x_{c,k}+\sum_{m\in M}\sum_{k'\in K_d\setminus k}a_m\sqrt{\rho\,\eta_{mk'}}\mathbf{g}_{mk}^{T}\mathbf{t}_{mk'}^{\text{Com}}x_{c,k'} \\ &+\sum_{m\in M}(1-a_m)\sqrt{\rho\,\eta_m}\mathbf{g}_{mk}^{T}\mathbf{t}_{m}^{\text{Sen}}x_r+n_k,\end{aligned} \tag{5.12}$$

where the second term is the inter-user interference, the third term represents the interference from S-APs, and $n_k\sim\mathscr{CN}(0,\sigma_n^2)$ denotes the additive white Gaussian noise at the user k.

Proposition 9 *With conjugate precoding at the APs for downlink communication, the achievable downlink SE of user k, can be expressed as* $\text{SE}_k=\left(1-\frac{\tau_{\text{p}}}{\tau}\right)\log_2\left(1+\text{SINR}_k(\mathbf{a},\eta^{\text{Com}},\eta^{\text{Sen}})\right)$, *where* $\text{SINR}_k(\mathbf{a},\eta^{\text{Com}},\eta^{\text{Sen}})$ *is given by*

$$\text{SINR}_k(\mathbf{a},\eta^{\text{Com}},\eta^{\text{Sen}})=\frac{\rho N^2\left(\sum_{m\in M}a_m\eta_{mk}^{1/2}\gamma_{mk}\right)^2}{\rho N\sum_{m\in M}\sum_{k'\in K_d}a_m\eta_{mk'}\gamma_{mk'}\beta_{mk}+\rho\sum_{m\in M}(1-a_m)\eta_m\beta_{mk}+1}. \tag{5.13}$$

Proof 9 *See Appendix C.*

5.3 Proposed Design Problem and Solution

In this section, we formulate and solve the AP mode selection to maximize the minimum SE. More specifically, we aim to optimize the AP operation mode selection vector ($\mathbf{a}$) and

power control coefficients $(\eta^{\text{Com}}, \eta^{\text{Sen}})$ to maximize the minimum per-user SE subject to a prescribed MASR level for the target detection and transmit power constraints at the APs. The optimization problem is then formulated as

$$\textbf{(P1):} \max_{\mathbf{a},\eta^{\text{Com}},\eta^{\text{Sen}}} \min_{k\in K_d} \quad \text{SINR}_k(\mathbf{a},\eta^{\text{Com}},\eta^{\text{Sen}}) \tag{5.14a}$$

$$\text{s.t.} \quad \text{MASR}(\mathbf{a},\eta^{\text{Com}},\eta^{\text{Sen}}) \geq \kappa, \tag{5.14b}$$

$$a_m \sum_{k\in K_d} \eta_{mk}\gamma_{mk} \leq \frac{1}{N}, \ \forall m \in M, \tag{5.14c}$$

$$\eta_m \leq 1 - a_m, \ \forall m \in M, \tag{5.14d}$$

$$a_m \in \{0,1\}. \tag{5.14e}$$

Problem (**P1**) is a challenging combinatorial problem. Therefore, for AP operation mode selection, we only focus on a heuristic greedy method which simplifies the computation, while providing a significantly successful monitoring performance gain.

5.3.1 AP Operation Mode Selection with Fixed Power Control

Let A_{Sen} and A_{Com} denote the sets containing the indices of APs operating as radar, i.e., APs with $a_m = 0$, and APs operating in communication mode, i.e., APs with $a_m = 1$, respectively. In addition, $\text{MASR}(A_{\text{Sen}}, A_{\text{Com}})$ and $\text{SINR}_k(A_{\text{Sen}}, A_{\text{Com}})$ underline the dependence of the sensing MASR and received SINR of the k-th user on the different choices of AP mode selections. Our greedy algorithm of AP mode selection is shown in **Algorithm 6**. To guarantee the sensing MASR requirement, all APs are initially assigned for sensing operation, i.e., $A_{\text{Sen}} = M$ and $A_{\text{Com}} = \emptyset$. Then, in each iteration, one AP switches into communication operation mode for maximizing the minimum of SE (or equivalently SINR in (5.13)), while the minimum MARS required for target sensing is guaranteed. This process continues until there is no more improvement in the minimum SINR among all users.

Algorithm 2 Greedy AP Operation Mode Selection

Initialize: Set $A_{\text{Com}} = \emptyset$ and $A_{\text{Sen}} = M$. Set iteration index $i = 0$.
Calculate $\Pi^{\star}[i] = \min_{k \in K_d} \text{SE}_k(A_{\text{Sen}}, A_{\text{Com}})$
repeat
  for all $m \in A_{\text{Sen}}$ **do**
    Set $A_s = A_{\text{Sen}} \setminus m$.
    if $\text{MASR}(A_s, A_{\text{Com}} \bigcup m) \geq \kappa$ **then**
      Calculate $\Pi_m = \min_{k \in K_d} \text{SINR}_k(A_s, A_{\text{Com}} \bigcup m)$
    else
      Set $\Pi_m = 0$
    end if
  end for
  Set $\Pi^{\star}[i+1] = \max_{m \in A_{\text{Com}}} \Pi_m$
  $e = |\Pi^{\star}[i+1] - \Pi^{\star}[i]|$
  if $e \geq e_{\min}$ **then**
    Update $A_{\text{Com}} = \{A_{\text{Com}} \bigcup m^{\star}\}$ and $A_{\text{Sen}} = A_{\text{Sen}} \setminus m^{\star}$
  end if
  Set $i = i + 1$
until $e < e_{\min}$
return A_{Sen} and A_{Com}, i.e., the indices of APs operating in radar mode and communication mode, respectively.

5.3.2 Power Control

For a given AP mode selection, the optimization problem (5.14) reduces to the power control problem, given by

$$\textbf{(P2):} \max_{\eta^{\text{Com}}, \eta^{\text{Sen}}} \min_{k \in K_d} \text{SINR}_k(\eta^{\text{Com}}, \eta^{\text{Sen}}) \tag{5.15a}$$

$$\text{s.t.} \quad (5.14\text{b}) - (5.14\text{e}). \tag{5.15b}$$

Problem (**P2**) is a non-convex optimization problem due the to non-convex objective function and constraints. Since the variables η^{Com} and η^{Sen} are coupled in both the objective and MASR constraint, it is difficult to simultaneously optimize them. Therefore, we propose an AO algorithm to jointly optimize η^{Com} and η^{Sen} in two sub-problems.

Firstly, for a given η^{Sen}, we formulate the sub-problem for optimizing η^{Com} as

$$\textbf{(P2-1):} \max_{\eta^{\text{Com}}} \min_{k \in K_d} \text{SINR}_k(\eta^{\text{Com}}) \tag{5.16a}$$

$$\text{s.t.} \quad (5.14\text{b}), (5.14\text{c}). \tag{5.16b}$$

By introducing the slack variables $\theta_{mk} = \eta_{mk}^{\frac{1}{2}}$ and υ_m, we reformulate (**P2-1**) as

$$\textbf{(P2-2):} \max_{\eta^{\text{Com}},t} \quad t \tag{5.17a}$$

$$\text{s.t.} \quad \frac{\left(\sum_{m\in M} a_m \theta_{mk}\gamma_{mk}\right)^2}{\frac{1}{N}\sum_{m\in M} a_m \beta_{mk}\upsilon_m^2 + \varphi_k} \geq t, \ \forall k \in K_d \tag{5.17b}$$

$$\frac{\sum_{m\in M}(1-a_m)\eta_m}{\sum_{m\in M} a_m \upsilon_m^2} \geq \kappa, \tag{5.17c}$$

$$\sum_{k'\in K_d} a_m \theta_{mk'}^2 \leq \upsilon_m^2, \ \forall m \in M \tag{5.17d}$$

$$0 \leq a_m \upsilon_m^2 \leq \frac{1}{N}, \ \forall m \in M, \tag{5.17e}$$

$$\theta_{mk} \geq 0, \forall m \in M, \forall k \in K_d, \tag{5.17f}$$

where $\varphi_k \triangleq \frac{1}{N^2}\sum_{m\in M}(1-a_m)\eta_m\beta_{mk} + \frac{1}{\rho N^2}$ and and $\upsilon_m^2 \triangleq \sum_{k\in K_d} a_m \eta_{mk}$. The equivalence between (5.17) and (5.16) follows directly from the fact that the second constraint in (5.17) holds with equality at the optimum. Problem (**P2-2**) can be reformulated as a second-order cone program (SOCP). More precisely, for given t, we have

$$\textbf{(P2-3):} \max_{\eta^{\text{Com}}} \quad t \tag{5.18}$$

$$\text{s.t.} \quad \|\mathbf{v}_k\| \leq \frac{1}{\sqrt{t}} \sum_{m\in M} a_m \theta_{mk}\gamma_{mk}, \ \forall k \in K_d, \tag{5.19}$$

$$(5.23c) - (5.17f), \tag{5.20}$$

where $\mathbf{v}_k = [\mathbf{v}_{k1}^T, \sqrt{\varphi_k}]^T$, with $\mathbf{v}_{k1} = \left[\sqrt{\frac{\beta_{1k}}{N}}\upsilon_1, \ldots, \sqrt{\frac{\beta_{Mk}}{N}}\upsilon_M\right]^T$. The first constraint represents a second order cone and thus (**P2-3**) is a standard SOCP, which is a convex problem. The bisection search method is exploited to find the optimal solution, in each step solving a sequence of convex feasibility problem. This bisection based search method is summarized in **Algorithm 2**.

Secondly, when η^{Com} is fixed, the sub-problem for optimizing η^{Sen} can be expressed as

$$\textbf{(P2-4):} \max_{\eta^{\text{Sen}}} \quad \min_{k\in K_d} \quad \text{SINR}_k(\eta^{\text{Sen}}) \tag{5.22a}$$

$$\text{s.t.} \quad (5.14b), (5.23d). \tag{5.22b}$$

Algorithm 3 Bisection Method for Power Control

1: Initialization of $t_{\min}$ and $t_{\max}$, where $t_{\min}$ and $t_{\max}$ define a range of relevant values of the objective function in (5.16). Initial line-search accuracy ε.
2: **repeat**
3: Set $t := \frac{t_{\min}+t_{\max}}{2}$. Solve the following convex feasibility program

$$\begin{cases} \|\mathbf{v}_k\| \leq \frac{1}{\sqrt{t}}\left(\sum_{m\in M} a_m \theta_{mk}\gamma_{mk}\right), \ \forall k \in K_d. \\ \sum_{m\in M} a_m \upsilon_m^2 \leq \frac{1}{\kappa}\sum_{m\in M}(1-a_m)\eta_m, \\ \sum_{k'\in K_d} a_m \theta_{mk'}^2 \leq \upsilon_m^2, \ \forall m \in M \\ 0 \leq a_m \upsilon_m \leq \frac{1}{\sqrt{N}}, \ \forall m \in M, \\ \theta_{mk} \geq 0, \forall m \in M, \forall k \in K_d, \end{cases} \tag{5.21}$$

4: If problem (5.21) is feasible, then set $t_{\min} := t$, else set $t_{\max} := t$.
5: **until** $t_{\max} - t_{\min} < \varepsilon$.

By introducing a new slack variable ρ, we can reformulate the optimization problem as

$$\textbf{(P2-5):} \max_{\eta^{\text{Sen}},\rho} \quad \rho \tag{5.23a}$$

$$\text{s.t.} \quad \frac{\sum_{m\in M}(1-a_m)\eta_m\beta_{mk}+\phi_k}{\left(N\sum_{m\in M} a_m\theta_{mk}\gamma_{mk}\right)^2} \leq \frac{1}{\rho}, \ \forall k \in K_d \tag{5.23b}$$

$$\sum_{m\in M}(1-a_m)\eta_m \geq \kappa \sum_{m\in M} a_m \upsilon_m^2, \tag{5.23c}$$

$$\eta_m \leq 1-a_m, \ \forall m \in M, \tag{5.23d}$$

where $\phi_k \triangleq \frac{1}{N}\sum_{m\in M} a_m\beta_{mk}\upsilon_m^2 + \frac{1}{\rho N^2}$. Now, for a fixed ρ, all inequalities involved in (**P2-5**) are linear, hence the solution to the optimization problem can be obtained by harnessing a line-search over ρ to find the maximal feasible value. Therefore, we can apply the bisection method in **Algorithm 2** to solve (5.23), where $t_{\min}$, $t_{\max}$, and the feasibility problem (5.21) are replaced with $\rho_{\min}$, $\rho_{\max}$ and problem (5.23), respectively. We summarize the overall AO algorithm in **Algorithm 3**.

5.3.3 Complexity Analysis

Here, we provide the computational complexity of Algorithm 3, which involves a SOCP problem in (5.18) and a linear-search problem (5.23) at each iteration. In order to solve a SOCP, the iterative bisection search method requires $\mathcal{O}(n_{v_1}^2 n_c)$ arithmetic operations, where n_{v_1}

Algorithm 4 AO Algorithm for Problem **P2**

1: Initialize a feasible initial point, $(\eta^{\text{Sen}})^{(0)}$ and $(\eta^{\text{Sen}})^{(0)}$.
2: Set the iteration number $n = 1$.
3: **repeat**
4: Determine $(\eta^{\text{Com}})^{(n)}$ by using **Algorithm 2**.
5: Compute $(\eta^{\text{Sen}})^{(n)}$ by solving (5.23).
6: Set $n = n + 1$.
7: **until** some stopping criterion is satisfied.

is the number of optimization variables and n_c is the total number of SOC constraints [150]. Moreover, the total number of iterations required is $\log_2\left(\frac{t_{\max}-t_{\min}}{\varepsilon}\right)$. In (5.18), the total number of variables is $n_{v_1} = MK_d$ and there are $n_v = K_d$ SOC constraints. Therefore, the per-iteration computational complexity for solving (5.18) is $\log_2\left(\frac{t_{\max}-t_{\min}}{\varepsilon}\right)\mathcal{O}(MK_d^3)$. Problem (5.23) involves $n_{v_2} = M$ scalar-value variables and $n_{c_2} = M + K_d + 1$ linear constraints. According to [151], the per-iteration cost to solve (5.23) is $\mathcal{O}\left((n_{c_2} + n_{v_2})n_{v_2}^2 n_{c_2}^{0.5}\right)$.

5.4 Numerical Results

We assume that the M APs and K_d users are uniformly distributed at random within a square of size $D \times D$ km^2, whose edges are wrapped around to avoid the boundary effects. The large-scale fading coefficient β_{mk} models the path loss and shadow fading, according to $\beta_{mk} = \text{PL}_{mk} 10^{\frac{\sigma_{sh} z_{mk}}{10}}$, where PL_{mk} represents the path loss, and $10^{\frac{\sigma_{sh} z_{mk}}{10}}$ represents the shadow fading with the standard deviation σ_{sh}, and $z_{mk} \sim \mathcal{CN}(0,1)$. We use the three-slope model for the path-loss PL_{mk} (in dB) as

$$\text{PL}_{mk} = \begin{cases} -L - 35\log_{10}(d_{mk}) & d_{mk} > d_1, \\ -L - 15\log_{10}(d_1) - 20\log_{10}(d_{mk}) & d_0 < d_{mk} \leq d_1 \\ -L - 15\log_{10}(d_1) - 20\log_{10}(d_0) & d_{mk} \leq d_0. \end{cases}$$

where L is a constant depending on the carrier frequency, the user and AP heights, given in [9]. We further use the correlated shadowing model for $d_{mk} > d_1$ [9]. Here, we choose $\sigma_{sh} = 8$ dB, $D = 0.5$ km, $d_1 = 50$ m, and $d_0 = 10$ m. We further set the noise power $\sigma_n^2 = -108$ dBm. Let $\tilde{\rho} = 1$ W and $\tilde{\rho}_t = 0.25$ W be the maximum transmit power of the APs and uplink training pilots, respectively. The normalized maximum transmit powers ρ and ρ_t are calculated by dividing these powers by the noise power σ_n^2.

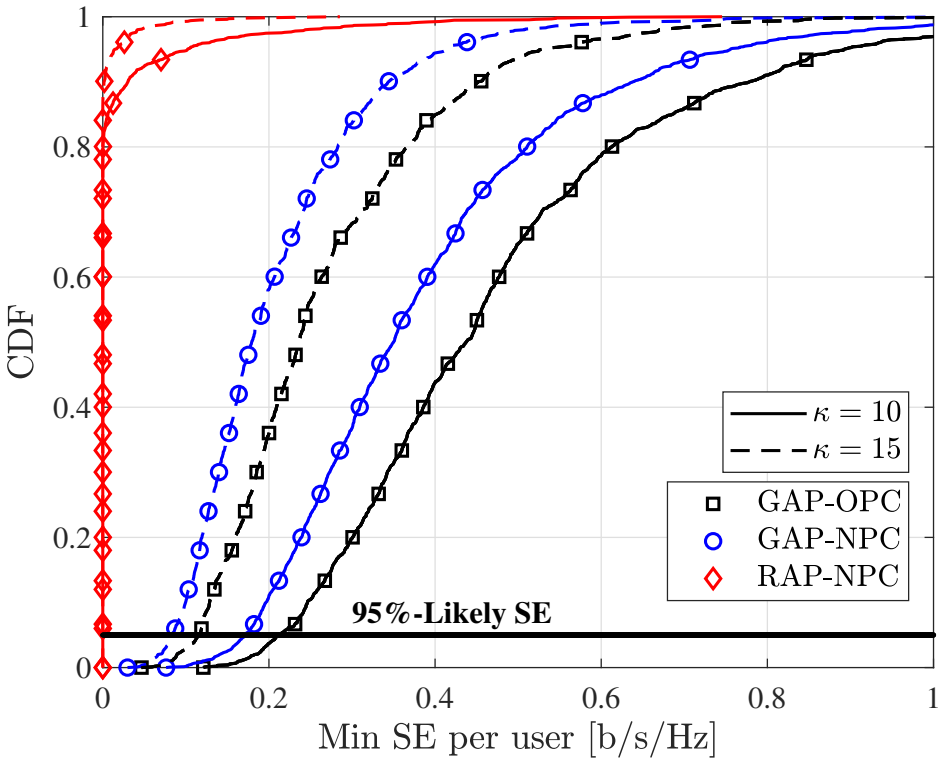

Fig. 5.2 The CDF of the minimum per user SE for different values of κ ($M = 80$, $N = 3$, $K_d = 5$).

In the absence of power control, termed as no power control (NPC) design, both C-APs and S-APs transmit at full power. With NPC, the power coefficients at the m-th C-AP are the same and $\eta_{mk} = \left(N \sum_{k \in K_d} \gamma_{mk}\right)^{-1}$, $\forall k \in K_d$. Moreover $\eta_m = 1$, $\forall m \in M$. For comparison, two benchmark system designs are studied: 1) Random AP mode selection with NPC (RAP-NPC), and 2) Greedy AP mode selection with NPC (GAP-NPC).

Figure 5.2 shows the cumulative distribution function (CDF) of the minimum per-user SE for two different values of κ. For a fair comparison, the achievable SE of the RAP-NPC is set to zero, when the MASR target value is not satisfied. It is noteworthy that the 95%-likely minimum per-user SE increases, when κ decreases from 15 to 10. This behavior can be explained by the fact that a great number of APs are assigned for downlink communication by reducing κ. Furthermore, by applying power control, the 95%-likely SE is improved by 50% (for $\kappa = 15$) and 35% (for $\kappa = 10$) compared to the GAP-NPC design.

Figure 5.3 shows the minimum SE of the downlink communication system versus the MASR requirement of the radar system, κ. In this figure, we assume that a fixed number of service antennas, i.e., $MN = 240$, is utilized to support both communication and sensing

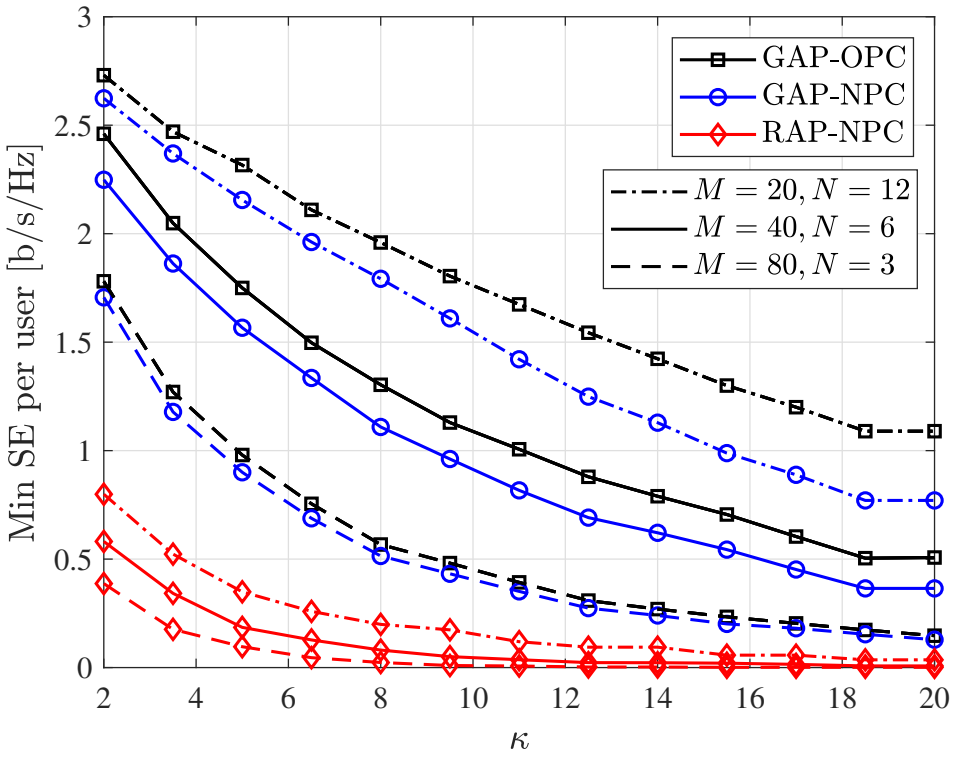

Fig. 5.3 Average minimum SE versus MASR level ($K_d = 5$, $NM = 240$).

applications. We observe that by increasing κ, the achievable downlink SE is decreased since the number of C-APs is decreased. Moreover, while RAP-NPC nearly fails to satisfy the MASR requirements, the GAP scheme with NPC and OPC not only meets the MASR requirements of the sensing operation, but also provides significant SE for the communication system, especially when the number of antennas per each AP is increased from $N = 3$ to $N = 12$.

5.5 Conclusion

In this chapter, we studied the problem of AP operation mode selection and power control design in a cell-free massive MIMO ISAC system, aiming to support multiuser downlink communication and single-target detection. After deriving closed-form expressions for the per-user effective SINR and sensing MASR, we formulated a max-min SE fairness problem. To deal with the complicated non-convex problem, a greedy algorithm, grounded on long-term statistics, was proposed for the AP operation mode design and an AO algorithm was developed for power control design at all APs. Our numerical results highlighted that our proposed

GAP-OPC design significantly enhances the downlink SE compared to the GAP-NPC and RAP-NPC benchmarks, while maintaining reliable sensing performance.

Chapter 6

Multiple-Target Detection in Cell-Free Massive MIMO-Assisted ISAC

6.1 Introduction

The advent of ISAC marks a significant leap forward for the sixth generation (6G) of wireless technology, introducing a pivotal shift in the use of limited spectral resources [59, 146, 63]. This innovative approach aims at enhancing both the radar sensing capabilities and communication efficiency, by assigning frequencies traditionally dedicated to sensing for wireless communication purposes as well. Such dual functionality supports high data-rate applications, contributing to the efficient utilization of spectral resources. ISAC's innovative framework has catalyzed the development of two distinct system architectures: the separated system and the co-located system. The separated system, also referred to as coexistence communication and radar, relies on distinct devices to perform radar sensing and communication within the same frequency band, generating sensing and communication beams independently. This method has been thoroughly investigated in our previous studies [84, 8] among others. In contrast, the co-located systems, or dual-functional radar-communication (DFRC), integrate these functionalities within a single device. This allows for the simultaneous detection of radar targets and communication with multiple users (UEs), facilitated by an ISAC base station (BS) that utilizes shared hardware components for concurrent beam generation [6]. Recognized for its efficiency and cost-effectiveness, the DFRC architecture is heralded as a significant breakthrough for the beyond 5G (B5G) era, poised to redefine the network performance and optimization [152, 153, 96].

Transitioning from separated to co-located systems reflects an intention to streamline operational efficiency and reduce the complexity inherent in managing the exchange of side-information between radar and communication technologies [153, 96]. This evolution is notably supported by the integration of massive multiple-input multiple-output (mMIMO) technology, which particularly within co-located architectures, can effectively minimize the inter-user interference across the same time-frequency resources. Leveraging the substantial spatial degrees of freedom and intrinsic sensing capabilities, the fusion of mMIMO technology with MIMO-ISAC is poised to deliver high-quality wireless communication, while ensuring high-resolution and robust sensing. Such advancements are instrumental in accelerating the development of various emerging applications, including, but not limited to, autonomous driving in intelligent transportation systems and unmanned aerial vehicle (UAV) networks in smart cities [154, 155].

Expanding on this groundwork, recent research endeavors, as highlighted in studies by [156] and [157], have delved into the intricacies of a dual-functional system that marries communication and radar functionalities within an mMIMO-orthogonal frequency division mutliplexing (OFDM) architecture. These studies comprehensively address both downlink and uplink scenarios, offering insightful analytical derivations of the achievable rate and detection efficiency under various conditions of channel side information (CSI), encompassing both perfect and imperfect scenarios. Moreover, the work in [158] sought to optimize this dual-functional system. The focus is on maximizing the sum-rate and energy efficiency, while ensuring compliance with essential operational parameters, including a baseline target detection probability and the satisfaction of individual UE rate demands.

A new architectural paradigm, cell-free mMIMO (CF-mMIMO), has gained attention for its potential to significantly improve the quality of service (QoS) at the network edges. Diverging from traditional cellular setups that centralize all antennas at the BS, CF-mMIMO distributes antennas across multiple access points (APs). These APs are then coordinated by a central processing unit (CPU), paving the way for a more distributed and flexible network architecture [10, 9]. A CF-mMIMO ISAC topology has several advantages over the single-cell ISAC, including larger monitoring areas, broader sensing coverage, and a wider range of sensing angles. Nevertheless, in such systems, proper resource allocation plays a key role to facilitate both communication and sensing functionalities.

Table 6.1 Contrasting our contributions to the mMIMO ISAC literature

Contributions	**This paper**	[115]	[24]	[25]	[116]
CF-mMIMO	✓	✓	✓	✓	✓
Power allocation	✓	✓	✓	✓	
Beamforming design	✓	✓	✓	✓	
AP operation mode selection	✓				
Multi-target	✓				✓
Asymptotic analysis	✓				

6.1.1 Related Works

Recent research efforts have focused on integrating ISAC capabilities within CF-mMIMO networks. These studies aim to harness the benefits of both ISAC and CF-mMIMO technologies to further the enhance network performance and service delivery, as evidenced by works such as those in [115, 24, 25, 116, 117].

Among these contributions, Zeng *et al.*[115] made notable advancements in power allocation techniques within CF-mMIMO ISAC systems, optimizing the balance between communication and sensing functionalities. Behdad *et al.*[24] further explored the operational dynamics of CF-mMIMO ISAC systems, demonstrating how transmitting APs not only provide service to UEs but also partake in sensing operations for target location identification. Their research introduced a power distribution strategy that enhances the sensing signal-to-noise ratio (SNR) while adhering to signal-to-interference-plus-noise ratio (SINR) constraints for UEs. Building on these themes, Demirhan *et al.* [25] tackled the challenges of beamforming design in CF-mMIMO ISAC systems. They proposed a joint beamforming approach designed to maximize sensing SNR without compromising the communication SINR, highlighting the critical balance required for effective sensing and communication within these networks. Additionally, the papers by Mao *et al.*[116] and Da *et al.*[117] have been instrumental in advancing precoder design for CF-mMIMO ISAC systems. These works also delved into the assessment of privacy risks associated with the inference of target locations by internal adversaries, marking a significant exploration beyond the technical aspects to include security and privacy considerations within ISAC networks.

6.1.2 Contributions

Contrary to the above studies, which assume static AP operation modes, our research introduces an innovative approach to CF-mMIMO ISAC networks by adopting dynamic AP operation mode selection. This novel strategy aims to optimize the spectral efficiency (SE) fairness among the UEs, while also ensuring the system's capability to detect multiple designated target. Utilizing long-term CSI, APs are categorized into communication APs (C-APs) and sensing APs (S-APs) to simultaneously support both downlink communication and sensing tasks. Compared to our recent work [26], where a single sensing zone area was considered and maximum ratio transmission (MRT) was performed at all APs, we consider a multiple sensing zone scenario and apply local partial zero-forcing (PZF) and maximum ratio transmit precoding at the C-APs and S-APs, respectively. The principle behind PZF design is that each AP only suppresses the inter-UE interference it causes to the strongest UEs, namely the UEs with the largest channel gain, while the inter-UE interference caused to the weakest UEs is tolerated [142]. The main contributions of our paper can be summarized as follows:

- We develop a framework for analyzing the performance of a CF-mMIMO ISAC system with multiple C-APs and S-APs employing PZF and MRT precodings, respectively, under channel estimation errors. By leveraging the use-and-then-forget strategy, we derive closed-form expressions for the downlink SE of the communication UEs and mainlobe-to-average sensing ratio (MASR) of the sensing zones. We further pursue an asymptotic SE analysis, which discloses that when the number of C-APs and S-APs, denoted by M_c and M_s respectively, are large, we can scale down the transmit powers at the C-APs and S-APs proportionally to $1/M_c^2$ and $1/M_s^2$, respectively.
- We formulate an interesting problem of joint AP operation mode selection and power control design, considering per-AP power constraints and a MASR constraint for target detection in a multi-target environment. A new algorithm is developed to solve the challenging formulated mixed-integer non-convex problem. In particular, we transform the formulated problem into more tractable problem with continuous variables only. Then, we solve the problem using successive convex approximation (SCA) techniques.
- To achieve a performance-complexity tradeoff, we propose a greedy algorithm for AP operation mode selection. This algorithm iteratively selects the optimal mode for each AP by considering the constraints for sensing operation, while maximizing fairness among UEs. Then, we propose a power control design algorithm for fixed AP operation mode design.

- Our numerical results show that the proposed optimum algorithm can provide perfect fairness among the UEs, while ensuring successful sensing performance for all sensing zones. The greedy algorithm achieves an acceptable level of success in the sensing rate.

A comparison of our contributions against the state of the art in the space of CF-mMIMO ISAC is tabulated in Table 6.1.

6.2 System Model

We consider a CF-mMIMO ISAC system operating under time division duplex, where M APs serve K downlink UEs, while concurrently emitting probing signals towards L specific sensing zones. Each UE is equipped with a single antenna, and each AP deploys an array of N antennas. All APs and UEs function in a half-duplex mode. For the ease of exposition, we introduce the sets $\mathscr{M} \triangleq \{1,\ldots,M\}$, $\mathscr{L} \triangleq \{1,\ldots,L\}$, and $\mathscr{K} \triangleq \{1,\ldots,K\}$ to represent the indices of the APs, sensing areas, and UEs, respectively. As depicted in Fig. 6.1, downlink communication and target detection are conducted concomitantly over the same frequency band. To accommodate the varying network demands, a dynamic AP operation mode selection strategy is implemented, determining the allocation of APs for downlink information transmission or radar sensing. A subset of APs, designated as communication-APs, termed as C-APs, is responsible for delivering information to the UEs. In contrast, the rest, labeled as S-APs, are employed for target detection. This categorization enables a specialized functionality of each AP group, where the C-APs aim to optimize the communication quality, while the S-APs enhance the radar sensing accuracy.

6.2.1 Channel Model and Uplink Training

We assume a quasi-static channel model, with each channel coherence interval spanning a duration of τ symbols. The duration of the training is denoted as τ_t, while the duration of downlink information transfer and target detection is $(\tau - \tau_t)$.

For the sensing channel model, we assume there is a line-of-sight (LoS) path between the sensing area and each AP, which is a commonly adopted model in the literature [24, 25]. The LoS channel between AP m and senssing area l is given by

$$\bar{\mathbf{g}}_{ml} = \mathbf{a}_N(\phi^a_{t,ml}, \phi^e_{t,ml}),\ \forall m \in \mathscr{M}, \tag{6.1}$$

where $\phi^a_{t,ml}$, $\phi^e_{t,ml}$ denote the azimuth and elevation angles of departure (AoD) from AP m towards the sensing area l. Moreover, the q-th entry of the array response vector $\mathbf{a}_N(\phi^a_{t,ml}, \phi^e_{t,ml}) \in \mathbb{C}^{N\times 1}$, is given by

$$[\mathbf{a}_N(\phi^a_{t,ml}, \phi^e_{t,ml})]_q = \exp\left(j\frac{2\pi d}{\lambda}(q-1)\sin(\phi^a_{t,ml})\cos(\phi^e_{t,ml})\right), \tag{6.2}$$

where d, and λ denote the AP antenna spacing and carrier wavelength, respectively.

The channel vector between the m-th AP and k-th UE is modeled as $\mathbf{g}_{mk} = \sqrt{\beta_{mk}}\mathbf{h}_{mk}$, where β_{mk} is the large scale fading coefficient, while $\mathbf{h}_{mk} \in \mathbb{C}^{N\times 1}$ is the small-scale fading vector, whose elements are independent and identically distributed $\mathscr{CN}(0,1)$ random variables (RVs).

An uplink training process is implemented to acquire the local CSI between each AP and all UEs. In each coherence block of length τ, all UEs are assumed to transmit their pairwisely orthogonal pilot sequence of length τ_t to all APs, which requires $\tau_t \geq K$. At AP m, $\mathbf{g}_{mk}$ is estimated by using the received pilot signals and applying the minimum mean-square error (MMSE) estimation technique. By following [9], the MMSE estimate $\hat{\mathbf{g}}_{mk}$ of $\mathbf{g}_{mk}$ is obtained as $\hat{\mathbf{g}}_{mk} \sim \mathscr{CN}(0, \gamma_{mk}\mathbf{I}_N)$, where

$$\gamma_{mk} = \frac{\tau_t \rho_t \beta^2_{mk}}{\tau_t \rho_t \beta_{mk} + 1}, \tag{6.3}$$

while ρ_t represents the normalized transmit power of each pilot symbol.

6.2.2 Data and Probing Signal Transmission

AP operation mode selection is performed by considering large-scale fading effects and relying on the statistical CSI, obtained during the training phase. The binary variables used to indicate the operation mode for each AP m are defined as

$$a_m = \begin{cases} 1, \text{ if AP } m \text{ operates as C-AP} \\ 0, \text{ if AP } m \text{ operates as S-AP.} \end{cases} \tag{6.4}$$

The transmission phase comprises information transmission from the C-APs to UEs and probing signal transmission from the S-APs to the target. Let $\mathbf{x}_{c,m}$ and $\mathbf{x}_{r,m}$ denote the data and probing signals, respectively. The signal vector transmitted from AP m can be expressed as

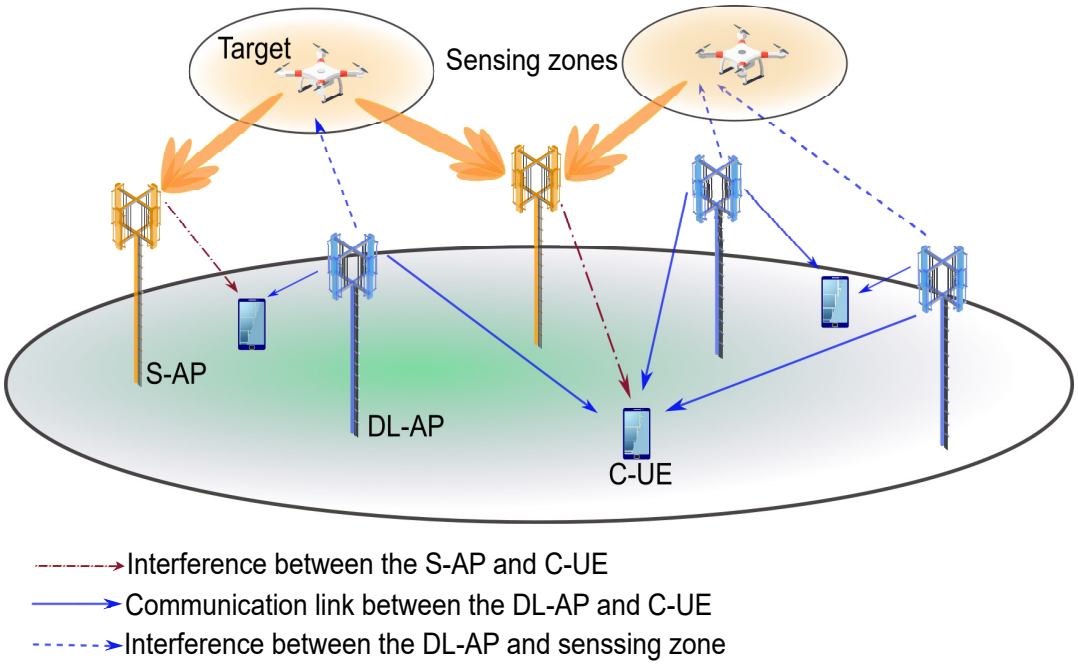

Fig. 6.1 Illustration of the CF-mMIMO ISAC system.

$$\mathbf{x}_m = \sqrt{a_m}\mathbf{x}_{c,m} + \sqrt{(1-a_m)}\mathbf{x}_{r,m}. \tag{6.5}$$

The probing signal transmitted by the m-th S-AP, targeting specific sensing zones, can be expanded as

$$\mathbf{x}_{r,m} = \sum_{l\in\mathscr{L}} \sqrt{\rho\,\eta_{ml}^{s}}\mathbf{t}_{ml}^{\text{Sen}} x_{r,ml}, \tag{6.6}$$

where ρ denotes the maximum normalized downlink power; η_{ml}^{s} is the power control coefficient at S-AP m related to sensing zone l; $\mathbf{t}_{ml}^{\text{Sen}} \in \mathbb{C}^{N\times 1}$ denotes the beamforming vector for sensing the lth sensing area, while $x_{r,ml}$, with $\mathbb{E}\{|x_{r,ml}|^2\} = 1$, is the radar sensing symbol from S-AP m for sensing the lth zone. This directional beamforming approach allows each S-AP to transmit a beam focused on a specific sector, facilitating spatially distributed sensing across the network. Therefore, to detect the presence of a target within its designated sector, each S-AP tailors its sensing beamforming vector to concentrate the radiated energy towards a specific direction. This is accomplished by configuring the beamforming vector to align with the azimuth and elevation angles that correspond to the sector of interest. Therefore, to detect the presence of a target in a certain location, we design the sensing beamforming vector at the mth S-AP as

$$\mathbf{t}_{ml}^{\text{Sen}} = \mathbf{a}_N(\phi_{t,ml}^a, \phi_{t,ml}^e). \tag{6.7}$$

This focused beamforming ensures that the radar echo from the target is sufficiently strong for reliable detection.

6.2.3 Downlink Communication and SE

In this section, we investigate the performance of partial zero forcing (PZF) precoding scheme. The conventional maximum ratio (MR) and ZF are special cases of PZF, and hence, their performances can be directly obtained from PZF.

PZF precoding emerges as an innovative method with the potential to combine the benefits of both ZF and MR approaches. The cornerstone of PZF lies in its ability to suppress interference caused to the strongest UEs, i.e., UEs with the highest channel gain, while tolerating the interference caused to the weakest UEs. In more detail, for any given AP (denoted as AP m), the set of active UEs is conceptually divided into two distinct subsets: (i) strong UEs, and (ii) weak UEs. The sets of indices for strong and weak UEs are represented as $S_m \subset \{1,\ldots,K\}$, and $W_m \subset \{1,\ldots,K\}$ respectively. It should be noted that $S_m \cap W_m = \phi$ and $|S_m| + |W_m| = K$. The grouping strategy can be determined using various criteria. For example, it may be based on the mean-square of the channel gain: a UE k is allocated to S_m if β_{mk} exceeds a predetermined threshold, otherwise, k is placed in W_m. PZF operates locally in the following manner: AP m transmits to all the UEs $k \in S_m$ using ZF, and to all the UEs $k \in W_m$ using MR.

The UE grouping can be based on different criteria. Inspired by [159, 142], the UE grouping strategy in PZF relies on the following rule

$$\sum_{k=1}^{|S_m|} \frac{\bar{\beta}_{mk}}{\sum_{t=1}^{K} \beta_{mt}} \geq \rho\%, \tag{6.8}$$

where AP m constructs its set S_m by selecting the UEs that contribute to, at least, $\rho\%$ of the overall channel gain. Note that in (6.8), $\{\bar{\beta}_{m1},\ldots,\bar{\beta}_{mK}\}$ indicates the set of the large-scale fading coefficients sorted in descending order.

Therefore, transmit signal from AP m can be expressed as

$$\mathbf{x}_{c,m} = \left(\sum_{k\in S_m} \sqrt{\rho\,\eta_{mk}^c}\,\mathbf{t}_{mk}^{\text{ZF-Com}} + \sum_{k\in W_m} \sqrt{\rho\,\eta_{mk}^c}\,\mathbf{t}_{mk}^{\text{MR-Com}} \right) x_{c,k}, \tag{6.9}$$

where η_{mk}^{c} denotes the power control coefficient between C-AP m and UE k, $k \in \mathscr{K}$; $x_{c,k}$ is the communication symbol satisfying $\mathbb{E}\{|x_{c,k}|^2\} = 1$; $\mathbf{t}_{mk}^{\mathrm{ZF-Com}}$ and $\mathbf{t}_{mk}^{\mathrm{MR-Com}}$ represent the ZF and MR precoding vectors, respectively, given by

$$\mathbf{t}_{mk}^{\mathrm{ZF-Com}} = \gamma_{mk}\hat{\mathbf{G}}_{S_m}\left(\hat{\mathbf{G}}_{S_m}^{H}\hat{\mathbf{G}}_{S_m}\right)^{-1}\mathbf{e}_k \tag{6.10}$$

$$\mathbf{t}_{mk}^{\mathrm{MR-Com}} = \hat{\mathbf{g}}_{mk}^{*}, \tag{6.11}$$

where $\mathbf{e}_k$ is the kth column of $\mathbf{I}_{|S_m|}$ and $\hat{\mathbf{G}}_{S_m} = [\hat{\mathbf{g}}_{mk}^{T} : k \in S_m]$. Therefore, for any pair of UEs k and k' belonging to the S_m, we have

$$\hat{\mathbf{g}}_{mk'}^{T}\mathbf{t}_{mk}^{\mathrm{ZF-Com}} = \begin{cases} \gamma_{mk} & \text{if } k = k', \\ 0 & \text{otherwise.} \end{cases} \tag{6.12}$$

The power control coefficients at AP m are chosen to satisfy the power constraint at each S-AP and C-AP, respectively, i.e.,

$$a_m\mathbb{E}\{\|\mathbf{x}_{c,m}\|^2\} + (1-a_m)\mathbb{E}\{\|\mathbf{x}_{r,m}\|^2\} \leq \rho. \tag{6.13}$$

For the sake of notation simplicity, we introduce Z_k and M_k as the set of indices of APs that transmit to UE k using $\mathbf{t}_{mk}^{\mathrm{ZF-Com}}$ and $\mathbf{t}_{mk}^{\mathrm{MR-Com}}$ respectively, given as

$$Z_k \triangleq \Big\{m : k \in S_m, m = 1,\ldots,M\Big\}, \tag{6.14a}$$

$$M_k \triangleq \Big\{m : k \in W_m, m = 1,\ldots,M\Big\}, \tag{6.14b}$$

with $Z_k \cap M_k = \phi$ and $Z_k \cup M_k = \mathscr{M}$. The PZF precoding approach provides a sophisticated balance between ZF and MR, catering to interference suppression for the strongest UEs and signal strength maximization for the weakest ones.

The received signal at the k-th UE can be represented as

$$\begin{aligned} y_k = &\left(\sum\nolimits_{m\in Z_k}\sqrt{a_m\rho\,\eta_{mk}^{c}}\,\mathbf{g}_{mk}^{T}\mathbf{t}_{mk}^{\mathrm{ZF-Com}} + \sum\nolimits_{m\in M_k}\sqrt{a_m\rho\,\eta_{mk}^{c}}\,\mathbf{g}_{mk}^{T}\mathbf{t}_{mk}^{\mathrm{MR-Com}}\right)x_{c,k} \\ &+\sum\nolimits_{k'\in\mathscr{K}\setminus k}\left(\sum\nolimits_{m\in Z_k}\sqrt{a_m\rho\,\eta_{mk'}^{c}}\,\mathbf{g}_{mk}^{T}\mathbf{t}_{mk'}^{\mathrm{ZF-Com}} + \sum\nolimits_{m\in M_k}\sqrt{a_m\rho\,\eta_{mk'}^{c}}\,\mathbf{g}_{mk}^{T}\mathbf{t}_{mk'}^{\mathrm{MR-Com}}\right)x_{c,k'} \\ &+\sum\nolimits_{m\in\mathscr{M}}\sum\nolimits_{l\in\mathscr{L}}\sqrt{(1-a_m)\,\rho\,\eta_{ml}^{s}}\,\mathbf{g}_{mk}^{T}\mathbf{t}_{ml}^{\mathrm{Sen}}x_{r,ml} + n_k, \end{aligned} \tag{6.15}$$

where the second term is the inter-user interference, the third term represents the interference from S-APs, and $n_k \sim \mathscr{CN}(0,1)$ denotes the additive white Gaussian noise at the UE k. In order to apply the use-then-forget technique to derive the downlink SE at UE k, we rewrite (6.15) as

$$y_k = \mathrm{DS}_k x_{c,k} + \mathrm{BU}_k x_{c,k} + \sum\nolimits_{k' \in \mathscr{K} \setminus k} \mathrm{IUI}_{kk'} x_{c,k'} + \mathrm{IR}_k + n_k, \tag{6.16}$$

where

$$\mathrm{DS}_k \triangleq \mathbb{E}\left\{ \sum\nolimits_{m \in Z_k} \sqrt{a_m \rho \eta_{mk}^c} \mathbf{g}_{mk}^T \mathbf{t}_{mk}^{\mathrm{ZF-Com}} + \sum\nolimits_{m \in M_k} \sqrt{a_m \rho \eta_{mk}^c} \mathbf{g}_{mk}^T \mathbf{t}_{mk}^{\mathrm{MR-Com}} \right\} \tag{6.17a}$$

$$\mathrm{BU}_k \triangleq \left(\sum\nolimits_{m \in Z_k} \sqrt{a_m \rho \eta_{mk'}^c} \mathbf{g}_{mk}^T \mathbf{t}_{mk'}^{\mathrm{ZF-Com}} + \sum\nolimits_{m \in M_k} \sqrt{a_m \rho \eta_{mk'}^c} \mathbf{g}_{mk}^T \mathbf{t}_{mk'}^{\mathrm{MR-Com}} \right) - \mathrm{DS}_k, \tag{6.17b}$$

$$\mathrm{IUI}_{kk'} \triangleq \sum\nolimits_{m \in Z_k} \sqrt{a_m \rho \eta_{mk'}^c} \mathbf{g}_{mk}^T \mathbf{t}_{mk'}^{\mathrm{ZF-Com}} + \sum\nolimits_{m \in M_k} \sqrt{a_m \rho \eta_{mk'}^c} \mathbf{g}_{mk}^T \mathbf{t}_{mk'}^{\mathrm{MR-Com}}, \tag{6.17c}$$

$$\mathrm{IR}_k \triangleq \sum\nolimits_{m \in M} \sum\nolimits_{l \in \mathscr{L}} \sqrt{(1-a_m) \rho \eta_{ml}^s} \mathbf{g}_{mk}^T \mathbf{t}_{ml}^{\mathrm{Sen}} x_{r,ml}, \tag{6.17d}$$

represent the strength of the desired signal (DS_k), the beamforming gain uncertainty (BU_k), the interference caused by the k'-th UE ($\mathrm{IUI}_{kk'}$) and the interference caused by S-APs (IR_k), respectively. By invoking (6.16), an achievable downlink SE at the k-th UE can be expressed as

$$\mathrm{SE}_k = \left(1 - \frac{\tau_t}{\tau}\right) \log_2\left(1 + \mathrm{SINR}_k\right), \tag{6.18}$$

where

$$\mathrm{SINR}_k = \frac{\left|\mathrm{DS}_k\right|^2}{\mathbb{E}\left\{\left|\mathrm{BU}_k\right|^2\right\} + \sum_{k' \in \mathscr{K} \setminus k} \mathbb{E}\left\{\left|\mathrm{IUI}_{kk'}\right|^2\right\} + \mathbb{E}\left\{\left|\mathrm{IR}_k\right|^2\right\} + 1}. \tag{6.19}$$

For the simplicity of notation, let us introduce a pair of binary variables to indicate the group assignment for each DL UE k and AP m in the PZF combining scheme as

$$\zeta_m^{Z_k} = \begin{cases} 1 & \text{if } m \in Z_k, \\ 0 & \text{otherwise.} \end{cases} \tag{6.20a}$$

$$\zeta_m^{M_k} = \begin{cases} 1 & \text{if } m \in M_k, \\ 0 & \text{otherwise.} \end{cases} \tag{6.20b}$$

Proposition 10 *The SE achieved by the PZF scheme is given by*

$$\text{SINR}_k(\mathbf{a}, \eta^c, \eta^s) = \frac{\rho \left(\sum_{m \in \mathscr{M}} \sqrt{a_m \eta_{mk}^c} \gamma_{mk} (\zeta_m^{Z_k} + N \zeta_m^{M_k}) \right)^2}{\rho \sum_{m \in \mathscr{M}} \sum_{k' \in \mathscr{K}} \left(a_m \eta_{mk'}^c \gamma_{mk'} \left(\zeta_m^{Z_k} \frac{\beta_{mk} - \gamma_{mk}}{N - |S_m|} + \zeta_m^{M_k} N \beta_{mk} \right) \right) + \rho \sum_{m \in \mathscr{M}} \sum_{l \in \mathscr{L}} \eta_{ml}^s N (1 - a_m) \beta_{mk} + 1}, \tag{6.21}$$

Proof 10 *See Appendix D.2.*

Remark 3 *Setting $\zeta_m^{M_k} = 1$ and $\zeta_m^{Z_k} = 0$, $\forall m \in \mathscr{M}$, results in the SINR given by (6.21) being reduced to that achieved by the MR precoding scheme. Similarly, if $\zeta_m^{M_k} = 0$ and $\zeta_m^{Z_k} = 1$, $\forall m \in \mathscr{M}$, the SINR in (6.21) reduces to that achieved by the ZF precoding scheme, provided that $N > K$.*

6.2.4 Sensing Operation and MASR

For a given angles $(\phi_{m \in M}^a, \phi_{m \in M}^e)$, the average spatial power pattern is

$$\begin{aligned} P^{\text{ave}}(\phi_{m \in M}^a, \phi_{m \in M}^e) &= \mathbb{E}\left\{ \left| \sum_{m \in M} \mathbf{a}_N^H(\phi_m^a, \phi_m^e) \mathbf{x}_m \right|^2 \right\} \\ &= \underbrace{\mathbb{E}\left\{ \left| \sum_{m \in M} \sqrt{a_m} \mathbf{a}_N^H(\phi_m^a, \phi_m^e) \mathbf{x}_{c,m} \right|^2 \right\}}_{\mathscr{T}_1} \\ &\quad + \underbrace{\mathbb{E}\left\{ \left| \sum_{m \in M} \sqrt{(1 - a_m)} \mathbf{a}_N^H(\phi_m^a, \phi_m^e) \mathbf{x}_{r,m} \right|^2 \right\}}_{\mathscr{T}_2}, \end{aligned} \tag{6.22}$$

where the expectation is taken over the transmitted signal $\mathbf{x}_m$ and the small-sale fading.

Now, we proceed to derive $\mathscr{T}_1$ and $\mathscr{T}_2$. By using (6.9), we can express $\mathscr{T}_1$ as

$$\begin{aligned}\mathscr{T}_1 &= \mathbb{E}\left\{\left|\sum_{k\in\mathscr{K}}\left(\sum_{m\in Z_k}\sqrt{a_m\rho\eta_{mk}^c}\mathbf{a}_N^H(\phi_m^a,\phi_m^e)\mathbf{t}_{mk}^{\mathrm{ZF-Com}}+\sum_{m\in M_k}\sqrt{a_m\rho\eta_{mk}^c}\mathbf{a}_N^H(\phi_m^a,\phi_m^e)\mathbf{t}_{mk}^{\mathrm{MR-Com}}\right)\right|^2\right\},\\ &= \sum_{k\in\mathscr{K}}\left(\sum_{m\in Z_k}a_m\rho\eta_{mk}^c\mathbb{E}\left\{\left|\mathbf{a}_N^H(\phi_m^a,\phi_m^e)\mathbf{t}_{mk}^{\mathrm{ZF-Com}}\right|^2\right\}+\sum_{m\in M_k}a_m\rho\eta_{mk}^c\mathbb{E}\left\{\left|\mathbf{a}_N^H(\phi_m^a,\phi_m^e)\mathbf{t}_{mk}^{\mathrm{MR-Com}}\right|^2\right\}\right).\end{aligned} \tag{6.23}$$

By invoking Lemma 2 in Appendix D.1, we have

$$\mathscr{T}_1 = \sum_{k\in\mathscr{K}}\left(\sum_{m\in Z_k}a_m\rho\eta_{mk}^c\frac{\gamma_{mk}}{N-|S_m|}+\sum_{m\in M_k}a_m\rho\eta_{mk}^cN\gamma_{mk}\right). \tag{6.24}$$

Moreover, $\mathscr{T}_2$ can be obtained as

$$\mathscr{T}_2 = \rho\sum_{m\in M}\sum_{l'\in\mathscr{L}}(1-a_m)\eta_{ml'}^s\left|\mathbf{a}_N^H(\phi_m^a,\phi_m^e)\mathbf{t}_{ml'}^{\mathrm{sen}}\right|^2. \tag{6.25}$$

For the simplicity of notation, let us introduce a pair of binary variables to indicate the group assignment for each AP m and DL UE k, as

$$\delta_k^{S_m} = \begin{cases}1 & \text{if } k\in S_m,\\ 0 & \text{otherwise.}\end{cases} \tag{6.26a}$$

$$\delta_k^{W_m} = \begin{cases}1 & \text{if } k\in W_m,\\ 0 & \text{otherwise.}\end{cases} \tag{6.26b}$$

By invoking (6.22), the average spatial power pattern for sensing is given by

$$P^{\mathrm{ave}}(\phi_m^a,\phi_m^e) = P_{\mathrm{Com}}^{\mathrm{ave}}(\phi_m^a,\phi_m^e)+P_{\mathrm{Sen}}^{\mathrm{ave}}(\phi_m^a,\phi_m^e), \tag{6.27}$$

where $P_{\mathrm{Sen}}^{\mathrm{ave}}(\phi_m^a,\phi_m^e)=\mathscr{T}_2$ represents power pattern related to L sensing zones, and $P_{\mathrm{Com}}^{\mathrm{ave}}(\phi_m^a,\phi_m^e)=\mathscr{T}_1$ represents the average sensing power distortion caused by simultaneous communication symbol transmissions in the network, given by

$$P_{\mathrm{Com}}^{\mathrm{ave}}(\phi_m^a,\phi_m^e) = \rho\sum_{m\in\mathscr{M}}\sum_{k\in\mathscr{K}}a_m\eta_{mk}^c\gamma_{mk}\left(\frac{\delta_k^{S_m}}{N-|S_m|}+N\delta_k^{W_m}\right), \tag{6.28}$$

which is independent of the angles.

Next, we consider the sensing performance associated with target l, i.e., at angle $(\phi^a_{t,ml}, \phi^e_{t,ml})$ for all $m \in M$. By using (6.25), $P^{\text{ave}}_{\text{Sen}}(\phi^a_{t,ml}, \phi^e_{t,ml})$ can be expressed as

$$P^{\text{ave}}_{\text{Sen}}(\phi^a_{t,ml}, \phi^e_{t,ml}) = \rho N^2 \sum_{m\in M}(1-a_m)\eta^s_{ml} + \rho \sum_{m\in M}\sum_{l'\in \mathscr{L}\setminus l}(1-a_m)\eta^s_{ml'}\left|\mathbf{a}^H_N(\phi^a_{t,ml}, \phi^e_{t,ml})\mathbf{t}^{\text{sen}}_{ml'}\right|^2, \tag{6.29}$$

where the first term denotes the desired power pattern for sensing at the angles related to target l and the second term is the average sensing power pattern distortion related to the other sensing zones.

It is desirable to have the average sensing power pattern distortion as well as $P^{\text{ave}}_{\text{Com}}(\phi^a_m, \phi^e_m)$, $\forall\ \phi^a_m$ and ϕ^e_m, as small as possible to confine the pattern distortion. Moreover, for illuminating a target angle $(\phi^a_{t,ml}, \phi^e_{t,ml})$, it is desirable that the mainlobe level of desired term in $P^{\text{ave}}_{\text{Sen}}(\phi^a_{t,ml}, \phi^e_{t,ml})$ is higher than the sum of sensing power pattern distortion and $P^{\text{ave}}_{\text{Com}}(\phi^a_m, \phi^e_m)$ by a certain minimum sensing level κ, $\forall\ \phi^a_m$ and ϕ^e_m, which is referred to as the MASR [160]. Accordingly, the MASR for the lth sensing zone is defined by (6.30) at the top of the next page. Note that, in general, in the MASR, we need to choose angles that maximize the average sensing power pattern distortion. However, this leads to an intractable MASR form. To alleviate such difficulty and make the MASR more amenable to further design, we choose $(\phi^a_{t,ml}, \phi^e_{t,ml})$ for computing the sensing power pattern distortion in MASR. This is reasonable since we assume that we know the sensing zone l, and thus, we only need to search some directions around the angles of target l.

$$\text{MASR}_l(\mathbf{a}, \eta^c, \eta^s) = \frac{\sum_{m\in M}(1-a_m)N^2\eta^s_{ml}}{\sum_{m\in M}\sum_{k\in\mathscr{K}} a_m\eta^c_{mk}\gamma_{mk}\left(\frac{\delta^{S_m}_k}{N-|S_m|}+N\delta^{W_m}_k\right)+\sum_{m\in M}\sum_{l'\in\mathscr{L}\setminus l}(1-a_m)\eta^s_{ml'}\left|\mathbf{a}^H_N(\phi^a_{t,ml}, \phi^e_{t,ml})\mathbf{t}^{\text{sen}}_{ml'}\right|^2}. \tag{6.30}$$

6.3 Asymptotic Analysis

The system comprises a total of M APs. The APs are divided into two categories: M_c APs designated for communication activities and M_s APs dedicated to sensing tasks, ensuring the total AP count remains as $M = M_c + M_s$. With the application of MR precoding across all

communication APs, we can pursue a detailed assessment of MR precoding's impact on the effectiveness of CF-mMIMO ISAC systems. In addition, we assume that equal power control is applied at the C-APs and S-APs, where

$$\eta_{mk}^{c} = \frac{1}{N\sum_{k'\in\mathscr{K}}\gamma_{mk'}}, \ \forall k, \tag{6.31a}$$

$$\eta_{ml}^{s} = \frac{1}{NL}. \tag{6.31b}$$

We analyze the performance of two case studies: *i)* M is large and N is fixed, and; *ii)* N is large and M is fixed.

6.3.1 Case I ($M_s, M_c \to \infty$ and N is fixed)

In this section, we explore a scenario where both the numbers of APs designated for M_s and M_c approach infinity. Importantly, during this expansion, we maintain a constant ratio between M_c and M_s, symbolized as $c = \frac{M_c}{M_s}$. This examination sheds light on the system's asymptotic performance characteristics, when both the sensing and communication resources are scaled infinitely but proportionally. A critical aspect of this scenario involves the transmit power scaling of each AP. As M_c becomes very large, the transmit power per AP is adjusted according to $\rho = \frac{E}{M_c^2}$, where E is fixed. By applying (6.31) into (6.15), we have

$$\begin{aligned} y_k = &\sum_{m\in\mathscr{M}}\sqrt{\frac{a_m E}{N\sum_{k\in K}\gamma_{mk}}}\frac{1}{M_c}\mathbf{g}_{mk}^{T}\mathbf{t}_{mk}^{\mathrm{MR-Com}}x_{c,k} \\ &+\sum_{k'\in\mathscr{K}\setminus k}\sum_{m\in\mathscr{M}}\sqrt{\frac{a_m E}{N\sum_{k\in K}\gamma_{mk}}}\frac{1}{M_c}\mathbf{g}_{mk}^{T}\mathbf{t}_{mk'}^{\mathrm{MR-Com}}x_{c,k'} \\ &+\sum_{m\in\mathscr{M}}\sum_{l\in\mathscr{L}}\sqrt{\frac{(1-a_m)E}{NL}}\frac{1}{cM_s}\mathbf{g}_{mk}^{T}\mathbf{t}_{ml}^{\mathrm{Sen}}x_r + n_k. \end{aligned} \tag{6.32}$$

Then, by applying Tchebyshev's theorem we have[1]

$$\sum_{m\in\mathscr{M}}\sqrt{\frac{a_m E}{N\sum_{k\in K}\gamma_{mk}}}\frac{1}{M_c}\mathbf{g}_{mk}^{T}\mathbf{t}_{mk}^{\mathrm{MR-Com}} - \sum_{m\in M}\sqrt{\frac{a_m NE}{\sum_{k\in K}\gamma_{mk}}}\frac{\gamma_{mk}}{M_c} \xrightarrow[M_c\to\infty]{P} 0. \tag{6.33}$$

[1]Let $X_1,\ldots,X_n$ be independent RVs, such that $\mathbb{E}\Big\{X_i\} = \bar{x}_i$ and $\mathrm{Var} \le c \le \infty$. Then, Tchebyshev's theorem states $\frac{1}{n}\sum_{n'=1}^{n}X_{n'} - \frac{1}{n}\sum_{n'}\bar{x}_{n'} \xrightarrow[n\to\infty]{P} 0$ [161].

Now, we turn our attention on the interference terms. For inter-user interference, by noting that the zero-mean channel vector $\mathbf{g}_{mk}$ is independent of $\mathbf{t}_{mk'}^{\mathrm{MR-Com}}$ for $k' \neq k$, we have

$$\sum_{m\in\mathscr{M}} \sqrt{\frac{a_m E}{N\sum_{k\in K}\gamma_{mk}}} \frac{1}{M_c} \mathbf{g}_{mk}^T \mathbf{t}_{mk'}^{\mathrm{MR-Com}} \xrightarrow[M_c\to\infty]{P} 0. \tag{6.34}$$

Moreover, for the deterministic $\mathbf{t}_{ml}^{\mathrm{Sen}}$, we have

$$\sum_{m\in\mathscr{M}} \sum_{l\in\mathscr{L}} \sqrt{\frac{(1-a_m)E}{NL}} \frac{1}{cM_s} \mathbf{g}_{mk}^T \mathbf{t}_{ml}^{\mathrm{Sen}} \xrightarrow[M_s\to\infty]{P} 0. \tag{6.35}$$

Accordingly, by using (6.33), (6.34), and (6.35), we have

$$y_k - \left(\sum_{m\in M} \sqrt{\frac{a_m NE}{\sum_{k\in K}\gamma_{mk}}} \frac{\gamma_{mk}}{M_c}\right) x_{c,k} - n_k \xrightarrow[M_c,M_s\to\infty]{P} 0. \tag{6.36}$$

The result in (6.36) indicates that when both M_c and M_s approach infinity, the received signal contains the desired signal plus noise. This indicates that inter-user interference and interference caused by S-APs fade, enhancing the signal quality. Most importantly, as M grows large, while the ratio of M_c and M_s is kept fixed, the transmit power at each AP can be made inversely proportional to the square of the number of APs with no degradation in performance.

6.3.2 Case II ($N \to \infty$ and M_c and M_s are fixed)

We explore the scenario where N approaches infinity, while M_c and M_s remain constant. The scaling of the transmit power for each AP is adjusted according to $\rho = \frac{E}{N}$, where E remains a fixed value.

By implementing the power scaling rule $\rho = \frac{E}{N}$, considering (6.15) and substituting $\mathbf{g}_{mk} = (\hat{\mathbf{g}}_{mk} + \tilde{\mathbf{g}}_{mk})$, the desired received signal at the UE can be characterized, as follows

$$\sum_{m\in\mathscr{M}} \sqrt{\frac{a_m E}{\sum_{k\in K}\gamma_{mk}}} \frac{1}{N} (\hat{\mathbf{g}}_{mk} + \tilde{\mathbf{g}}_{mk})^T \hat{\mathbf{g}}_{mk}^* \xrightarrow{a.s.} \sum_{m\in\mathscr{M}} \sqrt{\frac{a_m E}{\sum_{k\in K}\gamma_{mk}}} \gamma_{mk}, \tag{6.37}$$

where we have used the results on very long random vectors [162].

For the interference terms, noticing that $\mathbf{g}_{mk}^T$ and $\mathbf{t}_{mk'}^{\mathrm{MR-Com}}$ are independent zero-mean vectors, we have

$$\sum_{m\in\mathscr{M}} \sqrt{\frac{a_m E}{\sum_{k\in K}\gamma_{mk}}} \frac{1}{N} \mathbf{g}_{mk}^T \mathbf{t}_{mk'}^{\mathrm{MR-Com}} \xrightarrow{a.s.} 0 \tag{6.38a}$$

$$\sum_{m\in\mathscr{M}} \sum_{l\in\mathscr{L}} \sqrt{\frac{(1-a_m)E}{L}} \frac{1}{N} \mathbf{g}_{mk}^T \mathbf{t}_{ml}^{\mathrm{Sen}} \xrightarrow{a.s.} 0. \tag{6.38b}$$

Then, by using (6.37) and (6.38) we have

$$y_k - \sum_{m\in\mathscr{M}} \sqrt{\frac{a_m E}{\sum_{k\in K}\gamma_{mk}}} \gamma_{mk} x_{c,k} - n_k \xrightarrow{a.s.} 0, \text{ as } N \to \infty, \tag{6.39}$$

where $\xrightarrow{a.s.}$ denotes almost sure convergence. Akin to colocated mMIMO systems, the huge power gain (i.e. $\rho = \frac{E}{N}$) can be achieved, and the channels between the UEs and APs tend toward orthogonality as $N \to \infty$, elucidating the profound impact of deploying an extensive number of antennas in the CF-mMIMO ISAC space. This tendency towards channel orthogonality inherently mitigates the interference and enhances the signal quality, thereby reinforcing the premise that increasing the antenna count per AP not only avails of the advantages seen in traditional mMIMO architectures, but also significantly boosts the overall system performance and SE within the CF-mMIMO ISAC paradigm.

6.4 Proposed Design Problems and Solution

In this extended section, we formulate and solve the problem of joint AP mode selection and power allocation to provide fairness across the UEs, subject to quality of service (QoS) requirements of the sensing zone. More specifically, we aim to optimize the AP operation mode selection vector ($\mathbf{a}$) and power control coefficients (η_{mk}^c, η_{ml}^s) to maximize the minimum per-UE SE subject to a prescribed MASR level for the target detection and transmit power constraints at the APs.

In order to further simplify the optimization problem, we propose a greedy-based algorithm for AP mode selection and power control design. More specifically, the joint optimization problem is decomposed into two sub-problems: 1) AP mode selection, which is performed via a greedy algorithm and 2) Power control design for fixed AP modes.

Note that AP m is required to meet the average normalized power constraint, i.e., $\mathbb{E}\left\{\|\mathbf{x}_{c,m}\|^2\right\} \leq \rho$. By invoking (6.13), and noticing that $\mathbb{E}\left\{\left\|\mathbf{t}_{mk}^{\mathrm{ZF-Com}}\right\|^2\right\} = \frac{\gamma_{mk}}{N-|S_m|}$, we have the following per-AP power constraint

$$\sum_{k\in S_m} \eta_{mk}^c \frac{\gamma_{mk}}{N-|S_m|} + \sum_{k\in W_m} N\gamma_{mk}\eta_{mk}^c \leq a_m. \tag{6.40}$$

6.4.1 Joint AP Mode Selection and Power Allocation Design

In this subsection, we formulate and solve the problem of joint AP mode selection and power control design. Define $\mathbf{a} \triangleq \{a_1,\ldots,a_M\}$, $\eta^c \triangleq \{\eta_{m1}^c,\ldots,\eta_{mK}^c\}$ and $\eta^s \triangleq \{\eta_{m1}^s,\ldots,\eta_{mL}^s\}$ for all $m \in M$. The optimization problem is then formulated as

$$\begin{aligned}
\textbf{(P1):} \max_{\mathbf{a},\eta^c,\eta^s} \min_{k\in\mathscr{K}} \quad & \mathrm{SINR}_k(\mathbf{a},\eta^c,\eta^s) && \text{(6.41a)}\\
\text{s.t.} \quad & \mathrm{MASR}_l(\mathbf{a},\eta^c,\eta^s) \geq \kappa,\ \forall l \in \mathscr{L}, && \text{(6.41b)}\\
& \sum_{k\in S_m} \eta_{mk}^c \frac{\gamma_{mk}}{N-|S_m|} \\
& + \sum_{k\in W_m} N\gamma_{mk}\eta_{mk}^c \leq a_m, \forall m \in \mathscr{M}, && \text{(6.41c)}\\
& \sum_{l\in\mathscr{L}} \eta_{ml}^s \leq \frac{(1-a_m)}{N}, \forall m \in \mathscr{M}, && \text{(6.41d)}\\
& a_m \in \{0,1\}, && \text{(6.41e)}
\end{aligned}$$

where the first constraint (6.41b) is to explicitly control the level of the MASR for all sensing zones, while the second and third constraint control the transmit power at the C-APs and S-APs, respectively.

Before proceeding, we introduce an auxiliary variable $t = \min_{k\in\mathscr{K}} \mathrm{SINR}_k(\mathbf{a},\eta^c,\eta^s)$. We further relax the binary constraint (6.42f). Since at the optimal point $a_m \in \{0,1\}$, we replace a_m with a_m^2 in the second and third constraint to accelerate the convergence speed of the optimization problem. Accordingly, the optimization problem (6.41) is reformulated as follows:

$$\textbf{(P2):} \max_{\mathbf{a},\eta^c,\eta^s,t} \quad t-\lambda\sum_{m\in\mathscr{M}}a_m-a_m^{(n)}\left(2a_m-a_m^{(n)}\right) \tag{6.42a}$$

$$\text{s.t.} \quad \text{SINR}_k(\mathbf{a},\eta^c,\eta^s)\geq t,\ \forall k\in\mathscr{K} \tag{6.42b}$$

$$\text{MASR}_l(\mathbf{a},\eta^c,\eta^s)\geq \kappa,\ \forall l\in\mathscr{L}, \tag{6.42c}$$

$$\sum_{k\in S_m}\eta_{mk}^c\frac{\gamma_{mk}}{N-|S_m|}+\sum_{k\in W_m}N\gamma_{mk}\eta_{mk}^c \leq a_m^{(n)}\left(2a_m-a_m^{(n)}\right),\forall m\in\mathscr{M}, \tag{6.42d}$$

$$\sum_{l\in\mathscr{L}}\eta_{ml}^s\leq\frac{(1-a_m^2)}{N},\ \forall m\in\mathscr{M}, \tag{6.42e}$$

$$0\leq a_m\leq 1,\ \forall m\in\mathscr{M}. \tag{6.42f}$$

The non-convex nature of constraints (6.42b) and (6.42c) make the resulting problem non-convex. To address the non-convexity, we employ the method of SCA. To deal with the non-convexity of (6.42b), we first define

$$\rho_{mk}\triangleq\zeta_m^{Z_k}\frac{(\beta_{mk}-\gamma_{mk})}{N-|S_m|}+\zeta_m^{M_k}N\beta_{mk}, \tag{6.43a}$$

$$f_{mk}\triangleq\zeta_m^{Z_k}+N\zeta_m^{M_k}. \tag{6.43b}$$

Now, constraint (6.42b) can be expressed as

$$\frac{\left(\sum_{m\in\mathscr{M}}\sqrt{a_m\rho\eta_{mk}^c}\gamma_{mk}f_{mk}\right)^2}{t}\geq \rho\sum_{m\in\mathscr{M}}a_m\left(\sum_{k'\in\mathscr{K}}\eta_{mk'}^c\gamma_{mk'}\rho_{mk}-\sum_{l\in\mathscr{L}}\eta_{ml}^sN\beta_{mk}\right) +\rho\sum_{m\in M}\sum_{l\in\mathscr{L}}\eta_{ml}^sN\beta_{mk}+1. \tag{6.44}$$

For ease of description, let us denote

$$\mu_{mk}\triangleq\sum_{k'\in\mathscr{K}}\eta_{mk'}^c\gamma_{mk'}\rho_{mk}-\sum_{l\in\mathscr{L}}\eta_{ml}^sN\beta_{mk}. \tag{6.45}$$

To this end, (6.44) is equivalent to

$$\frac{\left(2\sum_{m\in\mathscr{M}}\sqrt{a_m\eta^c_{mk}}\gamma_{mk}f_{mk}\right)^2}{t}+\sum_{m\in\mathscr{M}}(a_m-\mu_{mk})^2$$
$$\geq\sum_{m\in\mathscr{M}}(a_m+\mu_{mk})^2+4\sum_{m\in M}\sum_{l\in\mathscr{L}}\eta^s_{ml}N\beta_{mk}+4/\rho. \tag{6.46}$$

It is clear that we need to find a concave lower bound of the left-hand side of the above inequality. To this end, we note that the function x^2/y is convex for $y>0$, and thus, the following inequality holds

$$\frac{x^2}{y}\geq\frac{x_0}{y_0}\left(2x-\frac{x_0}{y_0}y\right), \tag{6.47}$$

which is obtained by linearizing x^2/y around x_0 and y_0. Let us now define

$$q^{(n)}_k\triangleq\frac{2\sum_{m\in\mathscr{M}}\sqrt{a^{(n)}_m(\eta^c_{mk})^{(n)}}\gamma_{mk}f_{mk}}{t^{(n)}}. \tag{6.48}$$

From the inequality (6.47), we can recast (6.46) as

$$q^{(n)}_k\left(4\sum_{m\in\mathscr{M}}\sqrt{a_m\eta^c_{mk}}\gamma_{mk}f_{mk}-q^{(n)}_k t\right)$$
$$+\sum_{m\in\mathscr{M}}\left(a^{(n)}_m-\mu^{(n)}_{mk}\right)\left(2\left(a_m-\mu_{mk}\right)-\left(a^{(n)}_m-\mu^{(n)}_{mk}\right)\right)$$
$$\geq\sum_{m\in\mathscr{M}}(a_m+\mu_{mk})^2+4\sum_{m\in M}\sum_{l\in\mathscr{L}}\eta^s_{ml}N\beta_{mk}+4/\rho, \tag{6.49}$$

where we have used the following inequality

$$x^2\geq x_0(2x-x_0), \tag{6.50}$$

and replaced x and x_0 by $a_m-\mu_{mk}$ and $a^{(n)}_m-\mu^{(n)}_{mk}$, respectively.

Now, we focus on (6.42c), which can be expressed as

$$\sum_{m\in M}(1-a_m)N^2\eta^s_{ml}$$
$$\geq\kappa\sum_{m\in M}\sum_{l'\in\mathscr{L}\setminus l}(1-a_m)\eta^s_{ml'}\left|\mathbf{a}^H_N(\phi^a_{t,ml},\phi^e_{t,ml})\mathbf{t}^{\text{sen}}_{ml'}\right|^2$$
$$+\kappa\sum_{m\in M}\sum_{k\in\mathscr{K}}a_m\eta^c_{mk}\gamma_{mk}\theta_{mk}, \tag{6.51}$$

where $\theta_{mk} \triangleq \frac{\delta_k^{S_m}}{N-|S_m|} + N\delta_k^{W_m}$. Now, we can recast (6.51) as

$$\begin{aligned}
&\textstyle\sum_{m\in M} N^2\eta_{ml}^s \geq \\
&\textstyle\sum_{m\in M} a_m \Bigg(N^2\eta_{ml}^s + \kappa \sum_{k\in\mathscr{K}} \eta_{mk}^c \gamma_{mk}\theta_{mk} \\
&\textstyle -\kappa \sum_{l'\in\mathscr{L}\setminus l} \eta_{ml'}^s \left|\mathbf{a}_N^H(\phi_{t,ml}^a, \phi_{t,ml}^e)\mathbf{t}_{ml'}^{\text{sen}}\right|^2 \Bigg) \\
&\textstyle +\kappa \sum_{m\in M}\sum_{l'\in\mathscr{L}\setminus l} \eta_{ml'}^s \left|\mathbf{a}_N^H(\phi_{t,ml}^a, \phi_{t,ml}^e)\mathbf{t}_{ml'}^{\text{sen}}\right|^2.
\end{aligned} \tag{6.52}$$

For ease of description let us denote

$$\begin{aligned}
\nu_{ml} \triangleq \Bigg(& N^2\eta_{ml}^s + \kappa \textstyle\sum_{k\in\mathscr{K}} \eta_{mk}^c \gamma_{mk}\theta_{mk} \\
& -\kappa \textstyle\sum_{l'\in\mathscr{L}\setminus l} \eta_{ml'}^s \left|\mathbf{a}_N^H(\phi_{t,ml}^a, \phi_{t,ml}^e)\mathbf{t}_{ml'}^{\text{sen}}\right|^2 \Bigg).
\end{aligned} \tag{6.53}$$

Accordingly, (6.52) can be written as

$$\begin{aligned}
&4\textstyle\sum_{m\in M} N^2\eta_{ml}^s + \sum_{m\in M}(a_m - \nu_{ml})^2 \geq \sum_{m\in M}(a_m + \nu_{ml})^2 \\
&+4\kappa \textstyle\sum_{m\in M}\sum_{l'\in\mathscr{L}\setminus l} \eta_{ml'}^s \left|\mathbf{a}_N^H(\phi_{t,ml}^a, \phi_{t,ml}^e)\mathbf{t}_{ml'}^{\text{sen}}\right|^2.
\end{aligned} \tag{6.54}$$

To this end, by using (6.50), we obtain the concave lower bound of the left-hand side of the above inequality. Then, we get

$$\begin{aligned}
&4\textstyle\sum_{m\in M} N^2\eta_{ml}^s + \sum_{m\in M}\left(a_m^{(n)} - \nu_{ml}^{(n)}\right) \\
&\times \left(2(a_m - \nu_{ml}) - (a_m^{(n)} - \nu_{ml}^{(n)})\right) \geq \textstyle\sum_{m\in M}(a_m + \nu_{ml})^2 \\
&+4\kappa \textstyle\sum_{m\in M}\sum_{l'\in\mathscr{L}\setminus l} \eta_{ml'}^s \left|\mathbf{a}_N^H(\phi_{t,ml}^a, \phi_{t,ml}^e)\mathbf{t}_{ml'}^{\text{sen}}\right|^2.
\end{aligned} \tag{6.55}$$

Now, the convex optimization problem is given as (6.56), at the top of the next page. Problem (**P3**) is a convex optimization problem and can be efficiently solved using CVX [163]. In **Algorithm 5**, we outline main steps to solve problem (**P3**), where $\widetilde{\mathbf{x}} \triangleq \{\mathbf{a}, \eta^c, \eta^s\}$ and $\widehat{\mathscr{F}} \triangleq \{(6.56b), (6.56c), (6.56d), (6.56e), (6.56f)\}$ is a convex feasible set. Starting from a random point $\widetilde{\mathbf{x}} \in \widehat{\mathscr{F}}$, we solve (6.56) to obtain its optimal solution $\widetilde{\mathbf{x}}^*$, and use $\widetilde{\mathbf{x}}^*$ as an initial point in the next iteration. The proof of this convergence property uses similar steps as the proof of [164, Proposition 2], and hence, is omitted herein due to lack of space.

Algorithm 5 Proposed algorithm for joint AP mode selection and power allocation design (JAP-PA)

1: **Initialize**: $n=0$, $\lambda > 1$, a random initial poin $\widetilde{\mathbf{x}}^{(0)} \in \widehat{\mathscr{F}}$.
2: **repeat**
3: Update $n = n+1$
4: Solve (6.56) to obtain its optimal solution $\widetilde{\mathbf{x}}^*$
5: Update $\widetilde{\mathbf{x}}^{(n)} = \widetilde{\mathbf{x}}^*$
6: **until** convergence

Complexity of Algorithm 5: **Algorithm 5** requires solving a series of convex problems (6.56). For ease of presentation, if we let $K = L$, problem (6.56) can be transformed to an equivalent problem that involves $A_v \triangleq (M+2MK+1)$ real-valued scalar variables, $A_l \triangleq 3M$ linear constraints, $A_q \triangleq 2K$ quadratic constraints. Therefore, the algorithm for solving problem (6.56) requires a complexity of $\mathscr{O}(\sqrt{A_l+A_q}(A_v+A_l+A_q)A_v^2)$ in each iteration [**?** **?**]. In Section 6.5, we will show that this algorithm converges to the optimal solution after a few iterations.

$$\textbf{(P3):} \max_{\mathbf{a},\eta^c,\eta^s,t} \quad t-\lambda\sum_{m\in\mathscr{M}} a_m - a_m^{(n)}\left(2a_m - a_m^{(n)}\right) \tag{6.56a}$$

$$\text{s.t.} \quad q_k^{(n)}\left(4\sum_{m\in\mathscr{M}}\sqrt{a_m\eta_{mk}^c}\gamma_{mk}f_{mk} - q_k^{(n)}t\right) + \sum_{m\in\mathscr{M}}\left(a_m^{(n)}-\mu_{mk}^{(n)}\right)\left(2\left(a_m-\mu_{mk}\right) - \left(a_m^{(n)}-\mu_{mk}^{(n)}\right)\right) \geq \sum_{m\in\mathscr{M}}(a_m+\mu_{mk})^2 + 4\sum_{m\in M}\sum_{l\in\mathscr{L}}\eta_{ml}^s N\beta_{mk} + 4/\rho, \tag{6.56b}$$

$$4\sum_{m\in M}N^2\eta_{ml}^s + \sum_{m\in M}\left(a_m^{(n)}-\nu_{ml}^{(n)}\right)\left(2(a_m-\nu_{ml}) - (a_m^{(n)}-\nu_{ml}^{(n)})\right) \geq \sum_{m\in M}(a_m+\nu_{ml})^2 + 4\kappa\sum_{m\in M}\sum_{l'\in\mathscr{L}\setminus l}\eta_{ml'}^s\left|\mathbf{a}_N^H(\phi_{t,ml}^a,\phi_{t,ml}^e)\mathbf{t}_{ml'}^{\text{sen}}\right|^2, \tag{6.56c}$$

$$\sum_{k\in S_m}\eta_{mk}^c\frac{\gamma_{mk}}{N-|S_m|} + \sum_{k\in W_m}N\gamma_{mk}\eta_{mk}^c \leq a_m^{(n)}\left(2a_m - a_m^{(n)}\right), \forall m\in\mathscr{M}, \tag{6.56d}$$

$$\sum_{l\in\mathscr{L}}\eta_{ml}^s \leq \frac{(1-a_m^2)}{N}, \forall m\in\mathscr{M}, \tag{6.56e}$$

$$0 \leq a_m \leq 1. \tag{6.56f}$$

6.4.2 Greedy AP Mode Selection and Optimized Power Allocation

In this subsection, to reduce the complexity of the joint optimization problem, while maintaining an acceptable system performance, we propose a greedy algorithm to determine the operation modes of the APs. Then, given the operation modes for the APs, we jointly optimize the power control coefficients at the C-APs and S-APs.

Greedy AP Mode Selection

Let $\mathscr{A}_{\text{Sen}}$ and $\mathscr{A}_{\text{Com}}$ denote the sets containing the indices of APs operating as radar, i.e., APs with $a_m = 0$, and of APs operating in communication mode, i.e., APs with $a_m = 1$, respectively. In addition, $\text{MASR}_l(\mathscr{A}_{\text{Sen}}, \mathscr{A}_{\text{Com}})$ and $\text{SINR}_k(\mathscr{A}_{\text{Sen}}, \mathscr{A}_{\text{Com}})$ underline the dependence of the sensing MASR (of the l-th zone) and received SINR (of the k-th UE) on the different choices of AP mode selection. Our greedy algorithm of AP mode selection is shown in **Algorithm 6**. To guarantee the sensing MASR requirement, all APs are initially assigned for sensing operation, i.e., $\mathscr{A}_{\text{Sen}} = \mathscr{M}$ and $\mathscr{A}_{\text{Com}} = \emptyset$. Then, in each iteration, one AP switches into communication operation mode for maximizing the minimum SE (or equivalently SINR), while the minimum MARSs, required for target sensing, in all sensing zones are guaranteed. This process continues until there is no more improvement in the minimum SINR across all UEs.

Power Allocation

For a given operation mode selection vector (**a**), we optimize the power control coefficients $(\eta^c_{mk}, \eta^s_{ml})$ to achieve maximum fairness among the EUs. Therefore, the optimization problem (6.41) is reduced to

$$
\begin{aligned}
\textbf{(P4):} \max_{\eta^c, \eta^s} \quad & t && \text{(6.57a)}\\
\text{s.t.} \quad & \text{SINR}_k(\eta^c, \eta^s) \geq t, && \text{(6.57b)}\\
& \text{MASR}_l(\eta^c, \eta^s) \geq \kappa, \ \forall l \in \mathscr{L}, && \text{(6.57c)}\\
& \textstyle\sum_{k \in S_m} \eta^c_{mk} \dfrac{\gamma_{mk}}{N - |S_m|} && \\
& + \textstyle\sum_{k \in W_m} N \gamma_{mk} \eta^c_{mk} \leq a_m, \forall m \in \mathscr{M}, && \text{(6.57d)}\\
& \textstyle\sum_{l \in \mathscr{L}} \eta^s_{ml} \leq \dfrac{(1 - a_m)}{N}, \forall m \in \mathscr{M}. && \text{(6.57e)}
\end{aligned}
$$

We note that constraints (6.57b) and (6.57c) are non-convex. To deal with this non-convexity, we first introduce the auxiliary variables $\xi_{mk}^2 = \eta_{mk}^c$, which yields the optimization problem (6.58), at the middle of the next page.

$$\textbf{(P5):} \max_{\xi,\eta^s,t} \quad t \tag{6.58a}$$

$$\text{s.t.} \quad \frac{\left(\sum_{m\in\mathscr{M}} \sqrt{\rho a_m}\xi_{mk}\gamma_{mk}f_{mk}\right)^2}{\rho\sum_{m\in\mathscr{M}} a_m\rho_{mk}\sum_{k'\in\mathscr{K}} \xi_{mk'}^2\gamma_{mk'}+\rho\sum_{m\in M} N(1-a_m)\beta_{mk}\sum_{l\in\mathscr{L}}\eta_{ml}^s+1} \geq t, \tag{6.58b}$$

$$\frac{\sum_{m\in M}(1-a_m)N^2\eta_{ml}^s}{\sum_{m\in M} a_m\sum_{k\in\mathscr{K}}\xi_{mk}^2\gamma_{mk}\theta_{mk}+\sum_{m\in M}(1-a_m)\sum_{l'\in\mathscr{L}\setminus l}\eta_{ml'}^s\left|\mathbf{a}_N^H(\phi_{t,ml}^a,\phi_{t,ml}^e)\mathbf{t}_{ml'}^{\text{sen}}\right|^2} \geq \kappa,\ \forall l\in\mathscr{L}, \tag{6.58c}$$

$$\sum_{k\in\mathscr{K}}\xi_{mk}^2\gamma_{mk}\theta_{mk} \leq a_m, \forall m\in\mathscr{M}, \tag{6.58d}$$

$$\sum_{l\in\mathscr{L}}\eta_{ml}^s \leq \frac{(1-a_m)}{N}, \forall m\in\mathscr{M}, \tag{6.58e}$$

At the next step, we replace the convex function in the numerator of (6.58b) with its concave lower bound, which results in the following constraint

$$\frac{z_k^{(n)}\left(2\sum_{m\in\mathscr{M}}\sqrt{a_m}\xi_{mk}\gamma_{mk}f_{mk}-z_k^{(n)}\right)}{\Delta(\xi,\eta^s)} \geq t, \tag{6.59}$$

where $\Delta(\xi,\eta^s) \triangleq \rho\sum_{m\in\mathscr{M}} a_m\rho_{mk}\sum_{k'\in\mathscr{K}}\xi_{mk'}^2\gamma_{mk'}+\rho\sum_{m\in M}N(1-a_m)\beta_{mk}\sum_{l\in\mathscr{L}}\eta_{ml}^s+1$ and $z_k^{(n)} \triangleq \sum_{m\in\mathscr{M}}\sqrt{a_m}\xi_{mk}^{(n)}\gamma_{mk}f_{mk}$. Therefore, the power control design problem for fixed AP mode operation is given by

$$\textbf{(P6):} \max_{\xi,\eta^s,t} \quad t \tag{6.60a}$$

$$\text{s.t.} \quad (6.59),\ (6.58c)-(6.58e), \tag{6.60b}$$

The optimization problem in (6.60) is again convex, which we can solve directly using the bisection technique and solving linear feasibility problems, as shown in **Algorithm 7.**

Algorithm 6 Greedy AP Mode Selection

Initialize: Set $\mathscr{A}_{\text{Com}} = \emptyset$ and $\mathscr{A}_{\text{Sen}} = \mathscr{M}$. Set iteration index $i = 0$.
Calculate $\Pi^{\star}[i] = \min_{k \in \mathscr{K}} \text{SE}_k(A_{\text{Sen}}, \mathscr{A}_{\text{Com}})$
repeat
  for all $m \in \mathscr{A}_{\text{Sen}}$ **do**
    Set $\mathscr{A}_s = \mathscr{A}_{\text{Sen}} \setminus m$.
    if $\text{MASR}_l(\mathscr{A}_s, \mathscr{A}_{\text{Com}} \bigcup m) \geq \kappa, \forall l \in \mathscr{L}$ **then**
      Calculate $\Pi_m = \min_{k \in \mathscr{K}} \text{SINR}_k(\mathscr{A}_s, \mathscr{A}_{\text{Com}} \bigcup m)$
    else
      Set $\Pi_m = 0$
    end if
  end for
  Set $\Pi^{\star}[i+1] = \max\limits_{m \in \mathscr{A}_{\text{Com}}} \Pi_m$
  $e = |\Pi^{\star}[i+1] - \Pi^{\star}[i]|$
  if $e \geq e_{\min}$ **then**
    Update $\mathscr{A}_{\text{Com}} = \{\mathscr{A}_{\text{Com}} \bigcup m^{\star}\}$ and $\mathscr{A}_{\text{Sen}} = \mathscr{A}_{\text{Sen}} \setminus m^{\star}$
  end if
  Set $i = i + 1$
until $e < e_{\min}$
return $\mathscr{A}_{\text{Sen}}$ and $\mathscr{A}_{\text{Com}}$, i.e., the indices of APs operating in radar mode and communication mode, respectively.

Remark 4 *It is important to note that, for a given network realization, it is likely that the greedy and/or random AP selection schemes cannot guarantee the sensing requirement in the network design. Hence, we introduce a new metric known as the* ***success sensing rate****, defined as the ratio of the number of network realizations with successful sensing for all sensing zones to the total number of channel realizations. For a fair comparison, in each channel realization, if the MASR requirements are not met or the optimization problem of a scheme is infeasible, we set the SE of that scheme to zero.*

6.5 Numerical Examples

In this section, we verify the correctness of our analytical results and the performance of the proposed algorithms.

Algorithm 7 Bisection algorithm for solving (6.60)

(1) *Initialization*: Choose the initial values of $t_{\max}$ and $t_{\min}$, where $t_{\max}$ and $t_{\min}$ define a range of objective function values. Set tolerance $\varepsilon > 0$.

(2) Set $t := \frac{t_{\max}+t_{\min}}{2}$ and solve the convex feasibility problem (6.60).

(3) If the problem in Step 2 is feasible, set $t_{\min} := t$; else set $t_{\max} := t$.

(5) Stop if $t_{\max} - t_{\min} < \varepsilon$. Otherwise, go to Step 2.

6.5.1 Large-scale Fading Model and System Parameters

We assume that the M APs and K UEs are uniformly distributed in a square of 0.5×0.5 km^2, whose edges are wrapped around to avoid the boundary effects. The large-scale fading coefficients β_{mk} are modeled as [165]

$$\beta_{mk}[\text{dB}] = -30.5 - 36.7 \log_{10}\left(\frac{d_{mk}}{1\,\text{m}}\right) + F_{mk}, \tag{6.61}$$

where d_{mk} is the distance between UE k and AP m (computed as the minimum over different wrap-around cases) and $F_{mk} \sim \mathcal{CN}(0, 4^2)$ is the shadow fading. The shadowing terms from an AP to different UEs are correlated, as

$$\mathbb{E}\{F_{mk}F_{jk'}\} \triangleq \begin{cases} 4^2 2^{-\delta_{kk'}/9\,\text{m}}, & \text{if } j = m, \\ 0, & \text{otherwise}, \end{cases} \tag{6.62}$$

where $\delta_{kk'}$ is the physical distance between UEs k and k'.

The values of the network parameters are $\tau = 200$, and $\tau_t = K + L$. We further set the bandwidth $B = 50$ MHz and noise figure $F = 9$ dB. Thus, the noise power $\sigma_n^2 = k_B T_0 B F$, where $k_B = 1.381 \times 10^{-23}$ Joules/^{o}K is the Boltzmann constant, while $T_0 = 290^o$K is the noise temperature. Let $\tilde{\rho} = 1$ W, and $\tilde{\rho}_t = 0.25$ W be the maximum transmit power of the APs and uplink training pilot sequences, respectively. The normalized maximum transmit powers ρ and ρ_t are calculated by dividing these powers by the noise power. To evaluate the performance of proposed AP mode selection schemes, we consider random AP selection with optimized power allocation (**RAP-OPA**). In the numerical results, **JAP-OPA** denotes our proposed design in Algorithm 5, i.e., joint AP mode selection and power allocation design. Moreover, greedy AP selection and optimized power allocation design is indicated by **GAP-OPA**.

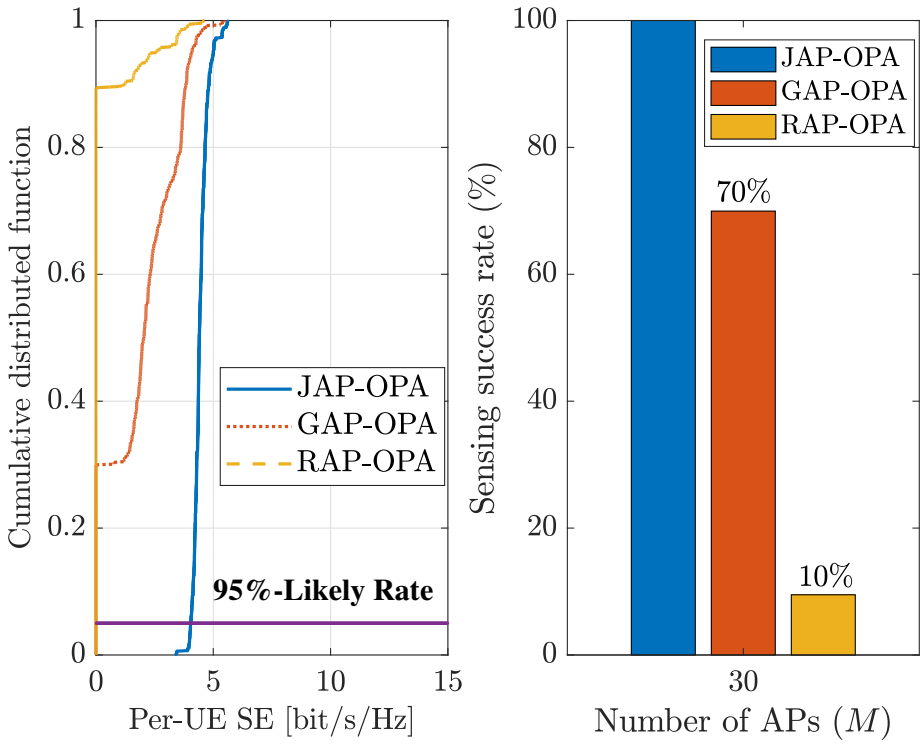

Fig. 6.2 CDF of the per-UE SE and sensing success rate ($\kappa = 8$ dB, $M = 30$, $N = 16$, $K = 4$, and $L = 2$).

6.5.2 Results and Discussions

The empirical cumulative distributed functions (CDFs) of the per-UE SE for all scenarios with $\kappa = 8$ dB, $MN = 480$, $K = 4$ and $L = 2$ are plotted in Fig. 6.2. The bar chart corresponds to the sensing success rate of different schemes. It can be observed that while **JAP-OPA** guarantees the sensing requirement for all network realizations, **RAP-OPA** fails to meet this requirement, with a success rate of 10%. In other words, the power allocation problem becomes infeasible in 90% of cases. On the other hand, **GAP-OPA** yields comparable results, achieving a success rate of approximately 70%, which confirms the effectiveness of the proposed greedy algorithm. For the infeasible cases, according to our discussion in Remark 4, we set the SE of the UEs to zero. By comparing the CDFs of the per-UE SE across all schemes, we observe that **JAP-OPA** provides a satisfactory fairness among the UEs. Moreover, the SE achieved by **JAP-OPA** is much higher than that of the **GAP-OPA** and **RAP-OPA**.

Figure 6.3 shows the worst SE (minimum SE) across the UEs for given realizations of the large-scale fading coefficients and for two different number of sensing zones: $L = 3$ (dashed lines) and $L = 2$ (solid lines). The proposed **JAP-OPA** scheme significantly improves the worst

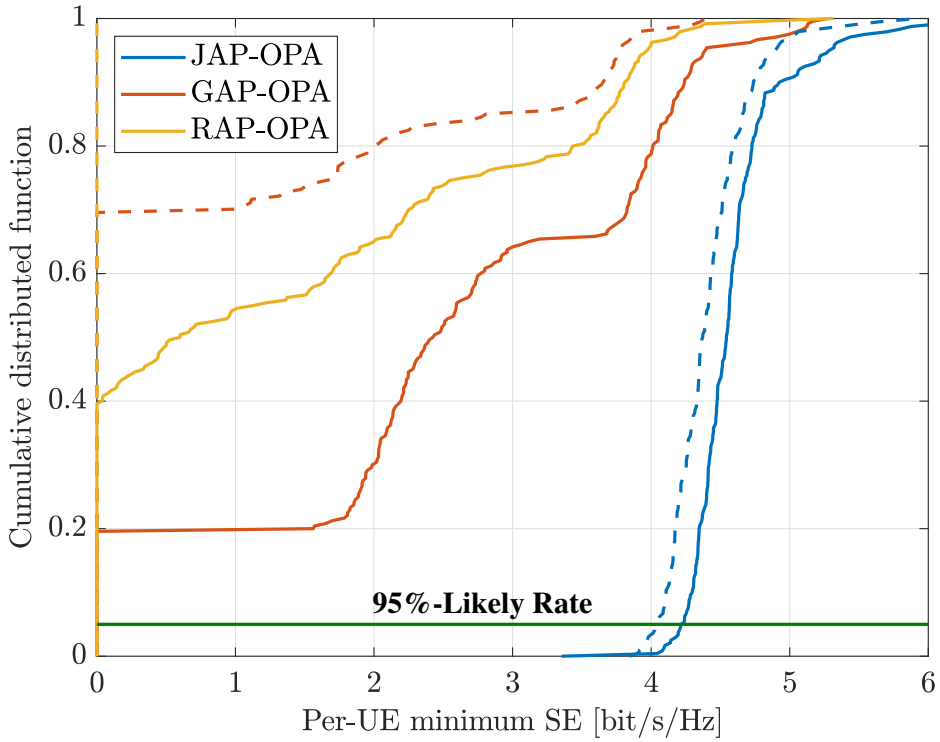

Fig. 6.3 CDF of the per-UE minimum SE for different schemes and for different number of sensing zones. The dashed lines depict results for $L = 3$ while the solid lines show results for $L = 2$ ($\kappa = 6$ dB, $M = 30$, $N = 16$, $K = 4$).

SE over the benchmarks and provides 100% sensing success rate for both scenarios. Moreover, we observe that joint optimization can guarantee nearly the same minimum SE per UE across all different channel realizations, while random and greedy AP selection provides varying levels of per-UE SE. For example, when $L = 2$, in 60% of channel realizations, the minimum SE obtained via **GAP-OPA** is less than 3 bit/s/Hz, while **JAP-OPA** consistently provides a minimum SE greater than 4 bit/s/Hz. Moreover, by increasing the number of sensing zones from 2 to 3, the sensing performance of both the **GAP-OPA** and **RAP-OPA** severely degraded, resulting in success rates of 27% and 1% for **GAP-OPA** and **RAP-OPA**, respectively. These findings confirm the importance of joint AP mode selection and power allocation for both communication and sensing operations. Figure 6.4 shows the average of the minimum SE per-UE with a fixed number of antenna units in the network versus the number of APs. By increasing the number of APs, the proposed **JAP-OPA** outperforms all other schemes, while **RAP-OPA** yields the worst performance in terms of SE. Moreover, the sensing success rate of **GAP-OPA** and **RAP-OPA** decreases as the number of APs increases. It is most likely for **RAP-OPA** to fail when $M > 30$. This behavior is due to the fact that the MASR heavily depends on N, (it is proportional to N^2 according to (6.30)). Therefore, the MASR decreases

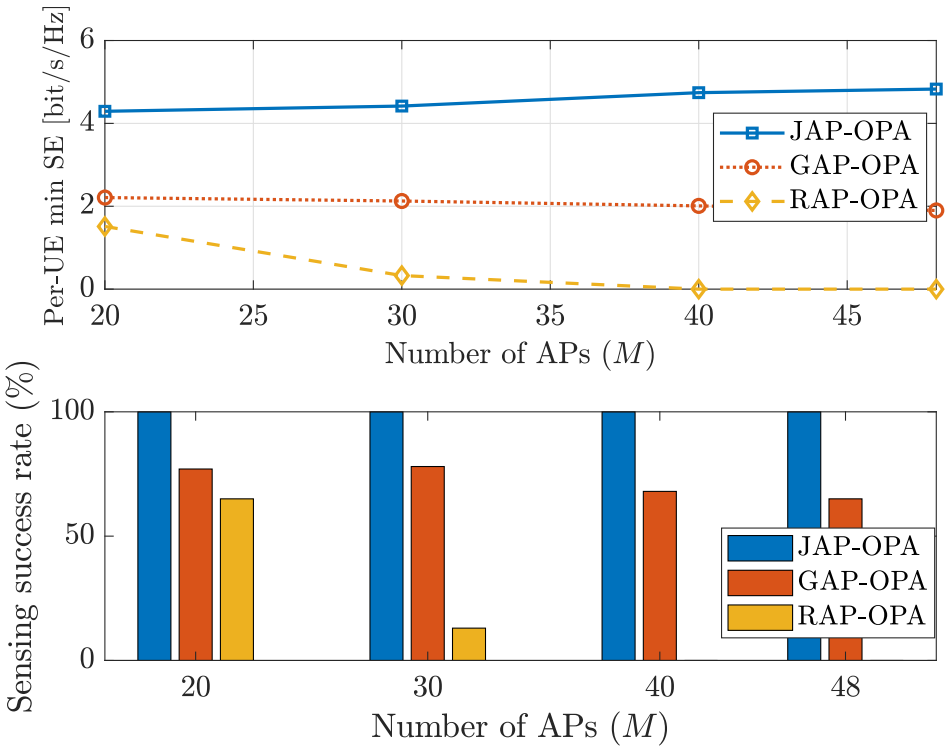

Fig. 6.4 Average of the per-UE minimum SE and sensing success rate versus the number of APs ($\kappa = 8$ dB, $MN = 480$, $K = 4$, and $L = 2$).

significantly as M increases, and both **RAP-OPA** and **GAP-OPA** schemes cannot guarantee to meet the sensing requirement under this condition. Conversely, the proposed **JAP-OPA** scheme ensures successful sensing for all network realizations, while delivering much higher per-UE minimum SE compared to the **RAP-OPA** and **GAP-OPA** schemes. Interestingly, the SE performance of the the proposed **JAP-OPA** scheme is improved by increasing the number of APs. These results reveal the importance of joint AP mode selection and power control design in dense CF-mMIMO networks.

Figure 6.5 illustrates the average of the minimum SE per-UE versus κ, along with the sensing success rate of different schemes as a function of κ. As the sensing requirements increase, the sensing success rate of the **RAP-OPA** and **GAP-OPA** schemes decreases, particularly when $\kappa > 8$ dB. Additionally, the minimum SE per-UE sharply decreases for these two schemes. However, the proposed **JAP-OPA** scheme continues to meet the MASR requirements and delivers high values for the minimum per-UE . Figure 6.5 illustrates the average of the minimum SE per-UE versus κ, along with the sensing success rate of different schemes as a function of κ. As the sensing requirements increase, the sensing success rate of the **RAP-OPA** and **GAP-OPA** schemes decreases, particularly when $\kappa > 8$ dB. Additionally, the minimum SE

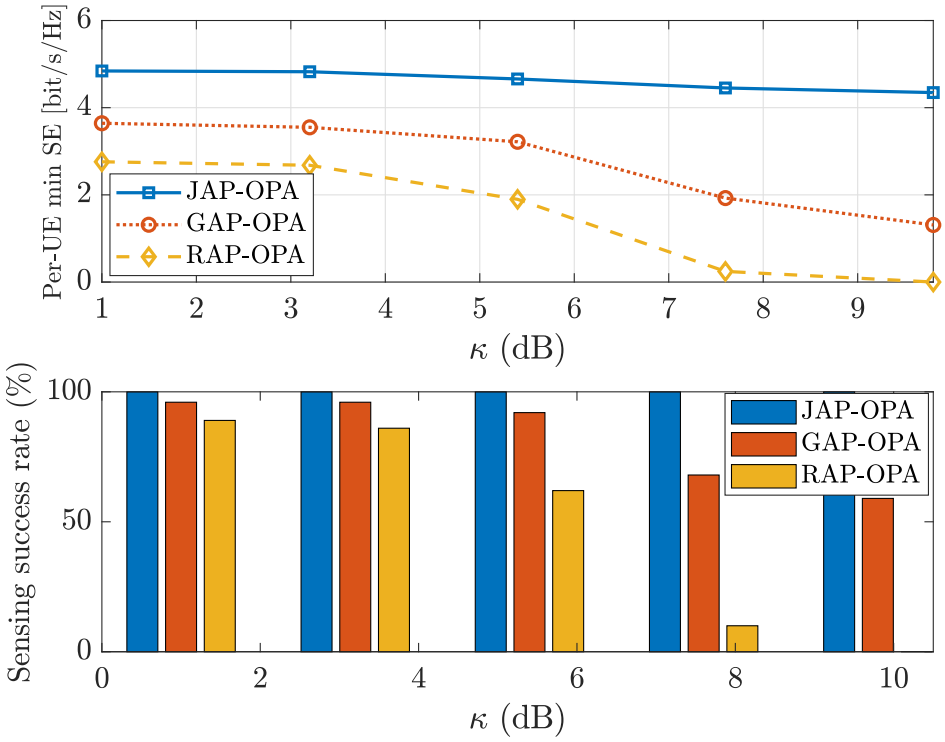

Fig. 6.5 Average of the per-UE minimum SE and sensing success rate versus κ ($MN = 480$, $M = 30$, $K = 4$, and $L = 2$).

per-UE sharply decreases for these two schemes. However, the proposed **JAP-OPA** continues to meet the MASR requirements and delivers high values for the minimum per-UE SE.

In Fig. 6.6, we compare the convergence rate of **Algorithm 5** for different number of APs in the network. To solve (6.56), we use the convex conic solver MOSEK and set $\lambda = 10$. We can see that with a small number of iterations (less than 60 iterations), **Algorithm 5** returns the optimized solution. The transient behavior stems from the penalty term $\lambda \sum_{m \in \mathcal{M}} a_m - a_m^{(n)} \left(2a_m - a_m^{(n)}\right)$ in the optimization problem. Furthermore, it is worth mentioning that the resulting values of the parameters a_m converge to 1 and 0 with high accuracy.

6.6 Conclusion

In this paper, we proposed a distributed ISAC implementation underpinned by a CF-mMIMO architecture. We analyzed both the exact and asymptotic SE performance of the downlink communication system and provided exact results for the MASR metric of the sensing zones. The operation mode of the distributed APs and their transmit power coefficients were jointly

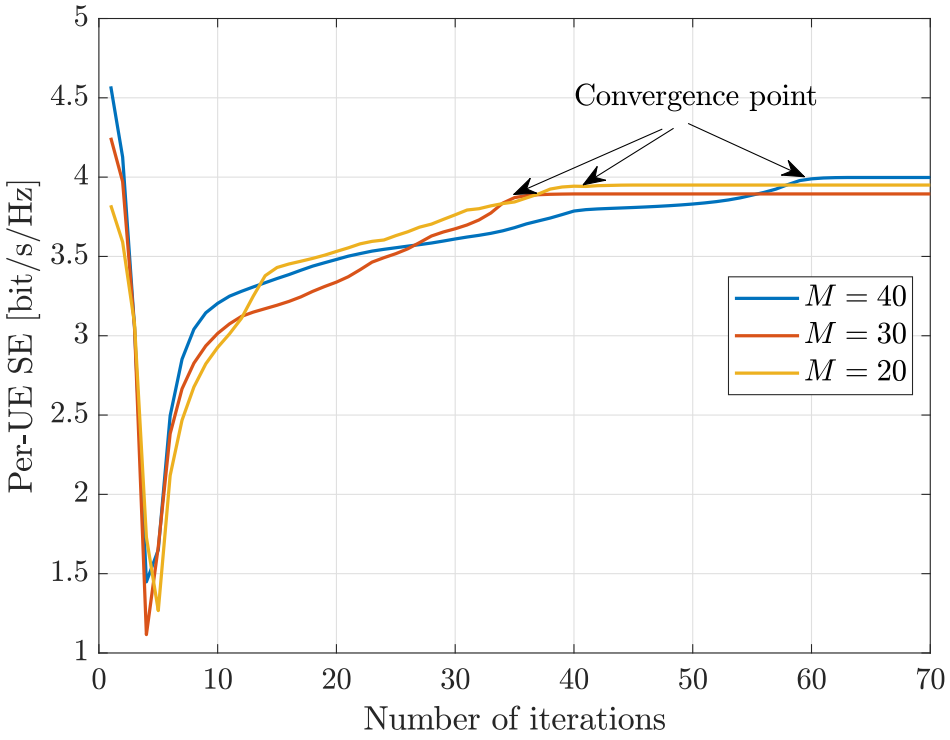

Fig. 6.6 Convergence behavior of **Algorithm 5** ($MN = 480$, $K = 4$, $L = 2$, $\lambda = 10$).

optimized to maximize fairness among communication UEs, while ensuring a specific level of MASR for different sensing zones in the network. To reduce the computational complexity of the proposed optimal scheme, a low-complexity design was also developed, wherein the operation mode of the APs was determined through a greedy algorithm and then the transmit power of the APs was optimized via a bisection algorithm. The proposed AP mode selection and power control design has shown to provide significant performance over the benchmark systems with random/greedy AP mode selection for both communication and sensing operations.

Chapter 7

Conclusions and Future Work

7.1 Summary of the Thesis

7.1.1 Conclusions

This thesis has journeyed through the dynamic and evolving field of wireless communication, with a particular focus on the pivotal role of mMIMO technologies and their coexistence with MIMO radar within the framework of ISAC. The research presented in this thesis spans forth comprehensive studies, each shedding light on different aspects of this challenging yet crucial domain, setting a path for the advancement of 5G and upcoming 6G networks.

In **Chapter 3**, the thesis laid the groundwork by exploring the coexistence of a multiuser mMIMO downlink system and MIMO radar. The chapter's significant contributions, such as deriving closed-form expressions for radar detection probability and mMIMO SE, and introducing an innovative power allocation scheme, set a strong foundation. These contributions are crucial in enhancing the mMIMO performance while carefully balancing the radar system interference.

Chapter 4 built upon these foundational insights to tackle more nuanced challenges in mMIMO and radar system coexistence, particularly under conditions of imperfect CSI. This chapter made significant strides in characterizing the performance with advanced precoding designs such as MR, ZF, and especially PZF, which is a key highlight, designed to mitigate interference and protect the radar functionality. In addition, this chapter developed power control strategies, providing practical solutions to optimize system performance in realistic scenarios. The chapter's in-depth analysis, including multiple target scenarios and correlated

fading environments, marked a substantial advancement in understanding and managing the complex interplay between mMIMO communication systems and MIMO radar.

Chapter 5 expanded the scope further into CF-mMIMO systems within ISAC frameworks, addressing innovative approaches for AP operation mode selection. The methodologies developed in this chapter for dynamic mode selection and algorithmic power control solutions significantly improved the communication performance while meeting stringent sensing requirements. These advancements are not only pivotal for the current network performance but also pave the way for future wireless networks where integrated communication and precise sensing are paramount.

Finally, **Chapter 6** extended the analysis from **Chapter 5** into the complex field of CF-mMIMO within the ISAC framework, with a special focus on multi-zone sensing and the evaluation of precoding strategies. It identified PZF as a key strategy for its efficient interference management, since it can optimize the network efficiency and improve the user experience by prioritizing users based on channel gains. In essence, **Chapter 6** contributed significantly to advancing CF-mMIMO ISAC systems, highlighting improvements in communication performance and sensing capabilities across various zones, and marking notable progress in wireless communication technologies.

Collectively, the studies presented in this thesis contribute profoundly to the field of ISAC, offering a comprehensive consideration of theoretical analysis, algorithmic solutions, and practical insights. They pave the way for more efficient spectrum sharing in future wireless networks, ensuring a harmonious coexistence of mMIMO communication systems and MIMO radar. The findings and methodologies established here are not merely academic achievements; they are beacons guiding the future development of advanced ISAC systems, promising a more connected and technologically advanced world. As the wireless communication landscape continues to evolve, the insights and innovations presented in this thesis will undoubtedly play a crucial role in shaping the future of ISAC, leading to more sophisticated, efficient, and integrated wireless networks in the era of 5G and beyond.

7.2 Future Work

This thesis has explored the coexistence of mMIMO systems and MIMO radar, presenting novel insights into spectrum sharing, precoding design, power control, and operational mode selection in CF-mMIMO systems. While the contributions significantly advance the understanding and

practical implementation of these technologies, several avenues for future research have been identified to further enhance the security and efficiency of ISAC systems, such as:

- **Enhancing Security Protocols in ISAC Systems**:

  Future research should focus on advancing the security protocols for ISAC environments, particularly in developing secure radar-communication systems to counteract malicious threats. For instance, the study on [59, 109, 166] served as a foundational reference, highlighting the need for integrated defense mechanisms against sophisticated cyber and physical threats.

- **Incorporation of Extremely Large-Scale mMIMO (XL-MIMO) Technologies**:

  As a pioneering approach for the forthcoming 6G networks, XL-MIMO promises substantial enhancements in wireless communication [167, 168]. Future research should explore how XL-MIMO technologies can be seamlessly integrated into ISAC frameworks, focusing on beamforming optimization to improve the SE while minimizing the cross-system interference. Furthermore, the adaptability and scalability of XL-MIMO in diverse environments, from urban landscapes to rural expanses, merit thorough examination to evaluate their performance resilience.

- **Applying Machine Learning for Dynamic ISAC Systems**:

  The application of machine learning in ISAC systems presents an extensive area for exploration, aimed at boosting the system flexibility and efficiency [169, 59]. Developing predictive models for dynamic spectrum management, interference control, and resource distribution, along with exploring the use of reinforcement learning for instantaneous decision-making in CF-mMIMO contexts, could significantly enhance the symbiosis between communication and sensing capabilities.

- **Hardware Implementation and Real-World Testing**:

  Translating theoretical and simulation insights into practical, real-world applications involves designing and building hardware prototypes of the proposed mMIMO and radar coexistence systems. This phase includes testing these systems in controlled environments before deploying them in real-world scenarios to assess their performance, identify unforeseen issues, and refine the system based on empirical data [95]. Challenges include ensuring the fidelity of the hardware implementation to the theoretical models, managing the complexities of real-world signal interference and propagation, and adapting the system to various operational environments [94].

Pursuing these directions will significantly contribute to the evolution and fortification of ISAC systems, ensuring they are primed for the future landscape of wireless communications.

References

[1] A. R. Chiriyath, B. Paul, G. M. Jacyna, and D. W. Bliss, "Inner bounds on performance of radar and communications co-existence," *IEEE Trans. Signal Process.*, vol. 64, no. 2, pp. 464–474, Jan. 2016.

[2] Y. Li, L. Zheng, M. Lops, and X. Wang, "Interference removal for radar/communication co-existence: The random scattering case," *IEEE Trans. Wireless Commun.*, vol. 18, no. 10, pp. 4831–4845, Jul. 2019.

[3] L. Zheng, M. Lops, Y. C. Eldar, and X. Wang, "Radar and communication coexistence: An overview: A review of recent methods," *IEEE Signal Process. Mag.*, vol. 36, no. 5, pp. 85–99, Sept. 2019.

[4] K. Singh, S. Biswas, O. Taghizadeh, and T. Ratnarajah, "Beamforming design for coexistence of full-duplex multi-cell MU-MIMO cellular network and MIMO radar," in *Proc. IEEE ICASSP.*, May 2019, pp. 7775–7779.

[5] H. Griffiths, L. Cohen, S. Watts, E. Mokole, C. Baker, M. Wicks, and S. Blunt, "Radar spectrum engineering and management: Technical and regulatory issues," *Proc. IEEE*, vol. 103, no. 1, pp. 85–102, Jan. 2014.

[6] F. Liu, C. Masouros, A. Petropulu, H. Griffiths, and L. Hanzo, "Joint radar and communication design: Applications, state-of-the-art, and the road ahead," *IEEE Trans. Commun.*, vol. 68, no. 6, pp. 3834–3862, Jun. 2020.

[7] L. Lu, G. Y. Li, A. L. Swindlehurst, A. Ashikhmin, and R. Zhang, "An overview of massive MIMO: Benefits and challenges," *IEEE J. Sel. Areas Commun*, vol. 8, no. 5, pp. 742–758, 2014.

[8] M. Elfiatoure, H. Q. Ngo, and M. Matthaiou, "Coexistence between massive MIMO and radar communications: Performance analysis," *J. Commun. Inf. Networks*, vol. 8, no. 1, pp. 37–47, Mar. 2023.

[9] H. Q. Ngo, A. Ashikhmin, H. Yang, E. G. Larsson, and T. L. Marzetta, "Cell-free massive MIMO versus small cells," *IEEE Trans. Wireless Commun.*, vol. 16, no. 3, pp. 1834–1850, Mar. 2017.

[10] M. Matthaiou, O. Yurduseven, H. Q. Ngo, D. Morales-Jimenez, S. L. Cotton, and V. F. Fusco, "The road to 6G: Ten physical layer challenges for communications engineers," *IEEE Commun. Mag.*, vol. 59, no. 1, pp. 64–69, Jan. 2021.

[11] J. Zhang, E. Björnson, M. Matthaiou, D. W. K. Ng, H. Yang, and D. J. Love, "Prospective multiple antenna technologies for beyond 5G," *IEEE J. Sel. Areas Commun.*, vol. 38, no. 8, pp. 1637–1660, Aug. 2020.

[12] M. Mohammadi, Z. Mobini, H. Q. Ngo, and M. Matthaiou, "Next generation multiple access with cell-free massive MIMO," *Authorea Preprints*, 2023. [Online]. Available: https://www.techrxiv.org/doi/full/10.36227/techrxiv.24545965.v1

[13] T. L. Marzetta, "Noncooperative cellular wireless with unlimited numbers of base station antennas," *IEEE Trans. Wireless Commun.*, vol. 9, no. 11, pp. 3590–3600, Nov. 2010.

[14] E. G. Larsson, O. Edfors, F. Tufvesson, and T. L. Marzetta, "Massive MIMO for next generation wireless systems," *IEEE Commun. Mag.*, vol. 52, no. 2, pp. 186–195, Feb. 2014.

[15] L. Wang, K.-K. Wong, H. Wang, and Y. Qin, "MIMO radar adaptive waveform design for extended target recognition," *Int. J. Distrib. Sensor Netw.*, vol. 11, no. 6, p. 154931, 2015.

[16] E. Björnson, M. Matthaiou, and M. Debbah, "Massive MIMO with non-ideal arbitrary arrays: Hardware scaling laws and circuit-aware design," *IEEE Trans. Wireless Commun.*, vol. 14, no. 8, pp. 4353–4368, Aug. 2015.

[17] T. Ahmed, X. Zhang, and W. U. Hassan, "A higher-order propagator method for 2D-DOA estimation in massive MIMO systems," *IEEE Commun. Lett.*, vol. 24, no. 3, pp. 543–547, Dec. 2019.

[18] D. He, X. Chen, L. Pei, F. Zhu, L. Jiang, and W. Yu, "Multi-BS spatial spectrum fusion for 2D DOA estimation and localization by using UCA in massive MIMO system," *IEEE Trans Instrum. Meas.*, vol. 70, pp. 1–13, Oct. 2021.

[19] M. Agiwal, A. Roy, and N. Saxena, "Next generation 5G wireless networks: A comprehensive survey," *IEEE Commun. Surveys Tuts.*, vol. 18, no. 3, pp. 1617–1655, 3rd Quart. 2016.

[20] H. Q. Ngo, E. G. Larsson, and T. L. Marzetta, "Energy and spectral efficiency of very large multiuser MIMO systems," *IEEE Trans. Commun.*, vol. 61, no. 4, pp. 1436–1449, Apr. 2013.

[21] C. Xiong, G. Y. Li, S. Zhang, Y. Chen, and S. Xu, "Energy-and spectral-efficiency tradeoff in downlink OFDMA networks," *IEEE Trans. Wireless Commun.*, vol. 10, no. 11, pp. 3874–3886, Nov. 2011.

[22] S. Fortunati, L. Sanguinetti, F. Gini, M. S. Greco, and B. Himed, "Massive MIMO radar for target detection," *IEEE Trans. Signal Process.*, vol. 68, pp. 859–871, Jan. 2020.

[23] L. Du, L. Li, H. Q. Ngo, T. C. Mai, and M. Matthaiou, "Cell-free massive MIMO: Joint maximum-ratio and zero-forcing precoder with power control," *IEEE Trans. Commun.*, vol. 69, no. 6, pp. 3741–3756, Jun. 2021.

[24] Z. Behdad, O. T. Demir, K. W. Sung, E. Björnson, and C. Cavdar, "Power allocation for joint communication and sensing in cell-free massive MIMO," in *Proc. IEEE GLOBECOM*, Dec. 2022, pp. 4081–4086.

[25] U. Demirhan and A. Alkhateeb, "Cell-free ISAC MIMO systems: Joint sensing and communication beamforming," *arXiv preprint arXiv:2301.11328*, 2023.

[26] M. Elfiatoure, M. Mohammadi, H. Q. Ngo, and M. Matthaiou, "Cell-free massive MIMO for ISAC: Access point operation mode selection and power control," in *Proc. IEEE GLOBECOM*, Dec. 2023.

[27] M. Mohammadi, T. T. Vu, H. Q. Ngo, and M. Matthaiou, "Network-assisted full-duplex cell-free massive MIMO: Spectral and energy efficiencies," *IEEE J. Sel. Areas Commun.*, vol. 41, no. 9, pp. 2833–2851, Sep. 2023.

[28] V. S. Chernyak, *Fundamentals of Multisite Radar Systems: Multistatic Radars and Multistatic Radar Systems*. CRC press, 1998.

[29] M. Skolnik, "An introduction and overview of radar," *Radar Handbook*, vol. 3, pp. 1–1, 2008.

[30] J. Li and P. Stoica, "MIMO radar with colocated antennas," *IEEE Signal Process. Mag.*, vol. 24, no. 5, pp. 106–114, Sept. 2007.

[31] M. A. Richards, *Fundamentals of Radar Signal Processing*. Tata McGraw-Hill Education, 2005.

[32] B. Donnet and I. Longstaff, "MIMO radar, techniques and opportunities," in *Proc. Eur. Radar Conf.*, 2006, pp. 112–115.

[33] A. Aubry, A. De Maio, and Y. Huang, "MIMO radar beampattern design via PSL/ISL optimization," *IEEE Trans. Signal Process.*, vol. 64, no. 15, pp. 3955–3967, Aug. 2016.

[34] F. Daum and J. Huang, "MIMO radar: Snake oil or good idea?" *IEEE Aerosp. Electron. Syst. Mag.*, vol. 24, no. 5, pp. 8–12, May 2009.

[35] A. Hassanien and S. A. Vorobyov, "Phased-MIMO radar: A tradeoff between phased-array and MIMO radars," *IEEE Trans. Signal Process.*, vol. 58, no. 6, pp. 3137–3151, Jun. 2010.

[36] I. Bekkerman and J. Tabrikian, "Target detection and localization using MIMO radars and sonars," *IEEE Trans. Signal Process.*, vol. 54, no. 10, pp. 3873–3883, Oct. 2006.

[37] A. M. Haimovich, R. S. Blum, and L. J. Cimini, "MIMO radar with widely separated antennas," *IEEE Signal Process. Mag.*, vol. 25, no. 1, pp. 116–129, Dec. 2007.

[38] H. Jiang, Y. Lu, and S. Yao, "Random matrix based method for joint DOD and DOA estimation for large scale MIMO radar in non-Gaussian noise," in *Proc. IEEE ICASSP.*, Mar. 2016, pp. 3031–3035.

[39] P. Chen, L. Zheng, X. Wang, H. Li, and L. Wu, "Moving target detection using colocated MIMO radar on multiple distributed moving platforms," *IEEE Trans. Signal Process.*, vol. 65, no. 17, pp. 4670–4683, Sep. 2017.

[40] F. Liu, C. Masouros, A. Li, and T. Ratnarajah, "Robust MIMO beamforming for cellular and radar coexistence," *IEEE Wireless Commun. Lett.*, vol. 6, no. 3, pp. 374–377, Apr. 2017.

[41] E. Fishler, A. Haimovich, R. S. Blum, L. J. Cimini, D. Chizhik, and R. A. Valenzuela, "Spatial diversity in radars—models and detection performance," *IEEE Trans. Signal Process.*, vol. 54, no. 3, pp. 823–838, Mar. 2006.

[42] H. Godrich, A. P. Petropulu, and H. V. Poor, "Sensor selection in distributed multiple-radar architectures for localization: A knapsack problem formulation," *IEEE Trans. Signal Process.*, vol. 60, no. 1, pp. 247–260, Jan. 2011.

[43] ——, "Power allocation strategies for target localization in distributed multiple-radar architectures," *IEEE Trans. Signal Process.*, vol. 59, no. 7, pp. 3226–3240, Jul. 2011.

[44] W. Yi, T. Zhou, Y. Ai, and R. S. Blum, "Suboptimal low complexity joint multi-target detection and localization for non-coherent MIMO radar with widely separated antennas," *IEEE Trans. Signal Process.*, vol. 68, pp. 901–916, 2020.

[45] L. Xu, J. Li, and P. Stoica, "Target detection and parameter estimation for MIMO radar systems," *IEEE Trans. Aerosp. Electron. Syst.*, vol. 44, no. 3, pp. 927–939, Jul. 2008.

[46] S. Haykin, "Cognitive radar: A way of the future," *IEEE Signal Process. Mag.*, vol. 23, no. 1, pp. 30–40, Jan. 2006.

[47] P. Lang, X. Fu, M. Martorella, J. Dong, R. Qin, X. Meng, and M. Xie, "A comprehensive survey of machine learning applied to radar signal processing," *arXiv preprint arXiv:2009.13702*, 2020.

[48] A. Morris, "German spectrum auction raises more than€ 5b," 2015.

[49] S. Riaz, "Us completes first 5G auction," 2019.

[50] M. B. Alabd, L. G. de Oliveira, B. Nuss, W. Wiesbeck, and T. Zwick, "Time-frequency shift modulation for chirp sequence based radar communications," in *IEEE MTT-S Int. Microw. Symp. Dig.*, Dec. 2020, pp. 1–4.

[51] A. Hassanien, M. G. Amin, Y. D. Zhang, and F. Ahmad, "Signaling strategies for dual-function radar communications: An overview," *IEEE Trans. Aerosp. Electron. Syst. Mag.*, vol. 31, no. 10, pp. 36–45, Oct. 2016.

[52] A. Alselwi, A. U. Khan, I. M. Qureshi, W. Khan, and A. Basit, "Throughput enhancement for the joint radar-communication systems based on cognitive closed-loop design," *IEEE Access*, vol. 9, pp. 64 785–64 807, 2021.

[53] F. Hessar and S. Roy, "Spectrum sharing between a surveillance radar and secondary Wi-Fi networks," *IEEE Trans. Aerosp. Electron. Syst*, vol. 52, no. 3, pp. 1434–1448, Jun. 2016.

[54] D. Mcqueen, "The momentum behind LTE adoption," *IEEE Commun. Mag*, vol. 47, no. 2, pp. 44–45, Feb. 2009.

[55] H. Wang, J. T. Johnson, and C. J. Baker, "Spectrum sharing between communications and ATC radar systems," *IET Radar Sonar Nav.*, vol. 11, no. 6, pp. 994–1001, Mar. 2017.

[56] W. Balani, M. Sarvagya, T. Ali, M. P. MM, J. Anguera, A. Andujar, and S. Das, "Design techniques of super-wideband antenna–existing and future prospective," *IEEE Access*, vol. 7, pp. 141 241–141 257, 2019.

[57] F. Qamar, M. N. Hindia, K. Dimyati, K. A. Noordin, M. B. Majed, T. Abd Rahman, and I. S. Amiri, "Investigation of future 5G-IoT millimeter-wave network performance at 38 GHz for urban microcell outdoor environment," *Electronics*, vol. 8, no. 5, p. 495, 2019.

[58] S. Lu *et al.*, "Integrated sensing and communications: Recent advances and ten open challenges," *arXiv preprint arXiv:2305.00179*, 2023.

[59] F. Liu, Y. Cui, C. Masouros, J. Xu, T. X. Han, Y. C. Eldar, and S. Buzzi, "Integrated sensing and communications: Toward dual-functional wireless networks for 6G and beyond," *IEEE J. Sel. Areas Commun.*, vol. 40, no. 6, pp. 1728–1767, Jun. 2022.

[60] J. A. Zhang, F. Liu, C. Masouros, R. W. Heath Jr., Z. Feng, L. Zheng, and A. Petropulu, "An overview of signal processing techniques for joint communication and radar sensing," *IEEE J. Sel. Topics Signal Process.*, vol. 15, no. 6, pp. 1295–1315, Nov. 2021.

[61] Y. Cui, F. Liu, X. Jing, and J. Mu, "Integrating sensing and communications for ubiquitous IoT: Applications, trends, and challenges," *IEEE Netw.*, vol. 35, no. 5, pp. 158–167, Oct. 2021.

[62] K. Chen, C. Qi, O. A. Dobre, and G. Y. Li, "Simultaneous beam training and target sensing in ISAC systems with RIS," *IEEE Trans. Wireless Commun.*, Aug. 2023.

[63] Z. Zhou, X. Li, J. He, X. Bi, Y. Chen, G. Wang, and P. Zhu, "6G integrated sensing and communication-sensing assisted environmental reconstruction and communication," in *Proc.IEEE ICASSP.*, Jun. 2023, pp. 1–5.

[64] Y. Chen, H. Hua, J. Xu, and D. W. K. Ng, "ISAC meets SWIPT: Multi-functional wireless systems integrating sensing, communication, and powering," *IEEE Trans. Wireless Commun.*, 2024.

[65] B. Donnet and I. Longstaff, "Combining MIMO radar with OFDM communications," in *Proc. IEEE EuRAD.*, Sep. 2006, pp. 37–40.

[66] S. Sodagari, A. Khawar, T. C. Clancy, and R. McGwier, "A projection based approach for radar and telecommunication systems coexistence," in *Proc. IEEE GLOBECOM*, Dec. 2012, pp. 5010–5014.

[67] A. Khawar, A. Abdelhadi, and C. Clancy, "Target detection performance of spectrum sharing MIMO radars," *IEEE Sensors J.*, vol. 15, no. 9, pp. 4928–4940, Sep. 2015.

[68] J. A. Mahal, A. Khawar, A. Abdelhadi, and T. C. Clancy, "Spectral coexistence of MIMO radar and MIMO cellular system," *IEEE Trans. Aerosp. Electron. Syst.*, vol. 53, no. 2, pp. 655–668, Jan 2017.

[69] B. Li and A. Petropulu, "MIMO radar and communication spectrum sharing with clutter mitigation," in *Proc. IEEE RadarConf*, May 2016, pp. 1–6.

[70] B. Li, A. P. Petropulu, and W. Trappe, "Optimum co-design for spectrum sharing between matrix completion based MIMO radars and a MIMO communication system," *IEEE Trans. Signal Process.*, vol. 64, no. 17, pp. 4562–4575, Sep. 2016.

[71] A. Abdelhadi and T. C. Clancy, "Network MIMO with partial cooperation between radar and cellular systems," in *Proc. Int. Conf. Comput. Netw. Commun*, Feb. 2016, pp. 1–5.

[72] J. Qian, M. Lops, L. Zheng, X. Wang, and Z. He, "Joint system design for coexistence of MIMO radar and MIMO communication," *IEEE Trans. Signal Process.*, vol. 66, no. 13, pp. 3504–3519, Apr. 2018.

[73] A. R. Chiriyath, B. Paul, and D. W. Bliss, "Radar-communications convergence: Coexistence, cooperation, and co-design," *IEEE Trans. Cogn. Commun. Netw.*, vol. 3, no. 1, pp. 1–12, Mar. 2017.

[74] F. Liu, A. Garcia-Rodriguez, C. Masouros, and G. Geraci, "Interfering channel estimation in radar-cellular coexistence: How much information do we need?" *IEEE Trans. Wireless Commun.*, vol. 18, no. 9, pp. 4238–4253, Sep. 2019.

[75] M. Alaee-Kerahroodi, E. Raei, S. Kumar, and B. S. M. R. Rao, "Coexistence of communications and cognitive MIMO radar: Waveform design and prototype," [Online]. Available https://arxiv.org/abs/2103.11890, 2021.

[76] J. A. Mahal, A. Khawar, A. Abdelhadi, and T. C. Clancy, "Spectral coexistence of MIMO radar and MIMO cellular system," *IEEE Trans. Aerosp. Electron. Syst.*, vol. 53, no. 2, pp. 655–668, Apr. 2017.

[77] S. Biswas, K. Singh, O. Taghizadeh, and T. Ratnarajah, "Coexistence of MIMO radar and FD MIMO cellular systems with QoS considerations," *IEEE Trans. Wireless Commun.*, vol. 17, no. 11, pp. 7281–7294, Nov. 2018.

[78] J. Qian, M. Lops, L. Zheng, X. Wang, and Z. He, "Joint system design for coexistence of MIMO radar and MIMO communication," *IEEE Trans. Signal Process.*, vol. 66, no. 13, pp. 3504–3519, Jul. 2018.

[79] F. Liu, C. Masouros, A. Li, T. Ratnarajah, and J. Zhou, "MIMO radar and cellular coexistence: A power-efficient approach enabled by interference exploitation," *IEEE Trans. Signal Process.*, vol. 66, no. 14, pp. 3681–3695, Jul. 2018.

[80] E. Grossi, M. Lops, and L. Venturino, "Joint design of surveillance radar and MIMO communication in cluttered environments," *IEEE Trans. Signal Process.*, vol. 68, pp. 1544–1557, Feb. 2020.

[81] H. Hua, J. Xu, and T. X. Han, "Optimal transmit beamforming for integrated sensing and communication," *IEEE Trans. Veh. Technol.*, vol. 72, no. 8, pp. 10 588 – 10 603, Aug. 2023.

[82] Y. He, Y. Cai, H. Mao, and G. Yu, "RIS-assisted communication radar coexistence: Joint beamforming design and analysis," *IEEE J. Sel. Areas Commun.*, vol. 40, no. 7, pp. 2131–2145, Jul. 2022.

[83] A. Mishra and R. Chopra, "MIMO radars and massive MIMO communication systems can coexist," *arXiv preprint arXiv:2304.00890*, 2023.

[84] M. Elfiatoure, M. Mohammadi, H. Q. Ngo, P. J. Smith, and M. Matthaiou, "Protecting massive MIMO-radar coexistence: Precoding design and power control," *IEEE Open J. commun. Society*, vol. 5, pp. 276–293, Jan. 2024.

[85] C. D'Andrea, S. Buzzi, and M. Lops, "Communications and radar coexistence in the massive MIMO regime: Uplink analysis," *IEEE Trans. Wireless Commun.*, vol. 19, no. 1, pp. 19–33, Jan. 2020.

[86] S. Buzzi, M. Lops, C. D'Andrea, and C. D'Elia, "Co-existence between a radar system and a massive MIMO wireless cellular system," in *Proc. IEEE SPAWC*, Jun. 2018, pp. 1–5.

[87] A. Babaei, W. H. Tranter, and T. Bose, "A nullspace-based precoder with subspace expansion for radar/communications coexistence," in *Proc. IEEE GLOBECOM*, Dec. 2013, pp. 3487–3492.

[88] B. Li and A. P. Petropulu, "Joint transmit designs for coexistence of MIMO wireless communications and sparse sensing radars in clutter," *IEEE Trans. Aerosp. Electron. Syst.*, vol. 53, no. 6, pp. 2846–2864, Dec. 2017.

[89] Y. Cui, V. Koivunen, and X. Jing, "Interference alignment based spectrum sharing for MIMO radar and communication systems," in *Proc. IEEE SPAWC*, Jun. 2018, pp. 1–5.

[90] J. Qian, L. Venturino, M. Lops, and X. Wang, "Radar and communication spectral coexistence in range-dependent interference," *IEEE Trans. Signal Process.*, vol. 69, pp. 5891–5906, Oct. 2021.

[91] Z. Cheng, B. Liao, S. Shi, Z. He, and J. Li, "Co-design for overlaid MIMO radar and downlink MISO communication systems via Cramér–Rao bound minimization," *IEEE Trans. Signal Process.*, vol. 67, no. 24, pp. 6227–6240, Dec. 2019.

[92] F. Liu, Y.-F. Liu, A. Li, C. Masouros, and Y. C. Eldar, "Cramér-Rao bound optimization for joint radar-communication beamforming," *IEEE Trans. Signal Process.*, vol. 70, pp. 240–253, Dec. 2021.

[93] A. Hassanien, M. G. Amin, Y. D. Zhang, and F. Ahmad, "Dual-function radar-communications: Information embedding using sidelobe control and waveform diversity," *IEEE Trans. Signal Process.*, vol. 64, no. 8, pp. 2168–2181, Apr. 2016.

[94] F. Liu, L. Zhou, C. Masouros, A. Li, W. Luo, and A. Petropulu, "Toward dual-functional radar-communication systems: Optimal waveform design," *IEEE Trans. Signal Process.*, vol. 66, no. 16, pp. 4264–4279, Aug. 2018.

[95] D. Ma, N. Shlezinger, T. Huang, Y. Shavit, M. Namer, Y. Liu, and Y. C. Eldar, "Spatial modulation for joint radar-communications systems: Design, analysis, and hardware prototype," *IEEE Trans. Veh. Technol.*, vol. 70, no. 3, pp. 2283–2298, Mar. 2021.

[96] F. Liu, C. Masouros, A. Li, H. Sun, and L. Hanzo, "MU-MIMO communications with MIMO radar: From co-existence to joint transmission," *IEEE Trans. Wireless Commun.*, vol. 17, no. 4, pp. 2755–2770, Apr. 2018.

[97] R. M. Mealey, "A method for calculating error probabilities in a radar communication system," *IEEE Trans. Space Electron. Telemetry*, vol. 9, no. 2, pp. 37–42, 1963.

[98] M. Roberton and E. Brown, "Integrated radar and communications based on chirped spread-spectrum techniques," in *IEEE MTT-S Int. Microw. Symp. Dig.*, vol. 1, Aug. 2003, pp. 611–614.

[99] G. N. Saddik, R. S. Singh, and E. R. Brown, "Ultra-wideband multifunctional communications/radar system," *IEEE Trans. Microw. Theory Techn.*, vol. 55, no. 7, pp. 1431–1437, Jul. 2007.

[100] M. Jamil, H.-J. Zepernick, and M. I. Pettersson, "On integrated radar and communication systems using Oppermann sequences," in *Proc. IEEE MILCOM.*, Nov. 2008, pp. 1–6.

[101] C. Sturm and W. Wiesbeck, "Waveform design and signal processing aspects for fusion of wireless communications and radar sensing," *Proc. IEEE*, vol. 99, no. 7, pp. 1236–1259, Jul. 2011.

[102] D. Gaglione, C. Clemente, C. V. Ilioudis, A. R. Persico, I. K. Proudler, and J. J. Soraghan, "Fractional Fourier based waveform for a joint radar-communication system," in *Proc. IEEE RadarConf*, May 2016, pp. 1–6.

[103] P. Kumari, J. Choi, N. González-Prelcic, and R. W. Heath Jr., "IEEE 802.11 ad-based radar: An approach to joint vehicular communication-radar system," *IEEE Trans. Veh. Technol.*, vol. 67, no. 4, pp. 3012–3027, Apr. 2017.

[104] A. Bazzi and M. Chafii, "On outage-based beamforming design for dual-functional radar-communication 6G systems," *IEEE Trans. Wireless Commun.*, vol. 22, pp. 5598–5612, Aug. 2023.

[105] C. B. Barneto, S. D. Liyanaarachchi, M. Heino, T. Riihonen, and M. Valkama, "Full duplex radio/radar technology: The enabler for advanced joint communication and sensing," *IEEE Wireless Commun.*, vol. 28, no. 1, pp. 82–88, Feb. 2021.

[106] X. Hu, C. Masouros, F. Liu, and R. Nissel, "MIMO-OFDM dual-functional radar-communication systems: Low-PAPR waveform design," *arXiv preprint arXiv:2109.13148*, 2021.

[107] H. Xu, R. S. Blum, J. Wang, and J. Yuan, "Colocated MIMO radar waveform design for transmit beampattern formation," *IEEE Trans. Aerosp. Electron. Syst*, vol. 51, no. 2, pp. 1558–1568, Apr. 2015.

[108] K. V. Mishra, M. B. Shankar, V. Koivunen, B. Ottersten, and S. A. Vorobyov, "Toward millimeter-wave joint radar communications: A signal processing perspective," *IEEE Signal Process. Mag.*, vol. 36, no. 5, pp. 100–114, Sep. 2019.

[109] N. Su, F. Liu, and C. Masouros, "Secure radar-communication systems with malicious targets: Integrating radar, communications and jamming functionalities," *IEEE Trans. Wireless Commun.*, vol. 20, no. 1, pp. 83–95, Jan. 2020.

[110] A. Chowdary, A. Bazzi, and M. Chafii, "On hybrid radar fusion for integrated sensing and communication," *IEEE Trans. Wireless Commun.*, Jan. 2024.

[111] A. Hassanien, M. G. Amin, Y. D. Zhang, F. Ahmad, and B. Himed, "Non-coherent PSK-based dual-function radar-communication systems," in *Proc.IEEE RadarConf*, May 2016, pp. 1–6.

[112] T. Huang, N. Shlezinger, X. Xu, Y. Liu, and Y. C. Eldar, "Majorcom: A dual-function radar communication system using index modulation," *IEEE Trans. Signal Process.*, vol. 68, pp. 3423–3438, May 2020.

[113] E. BouDaher, A. Hassanien, E. Aboutanios, and M. G. Amin, "Towards a dual-function MIMO radar-communication system," in *Proc. IEEE RadarConf*, May 2016, pp. 1–6.

[114] D. Ma, N. Shlezinger, T. Huang, Y. Liu, and Y. C. Eldar, "Joint radar-communication strategies for autonomous vehicles: Combining two key automotive technologies," *IEEE Signal Process. Mag.*, vol. 37, no. 4, pp. 85–97, Jul. 2020.

[115] F. Zeng, J. Yu, J. Li, F. Liu, D. Wang, and X. You, "Integrated sensing and communication for network-assisted full-duplex cell-free distributed massive MIMO systems," *arXiv preprint arXiv:2311.05101*, 2023.

[116] W. Mao *et al.*, "Beamforming design in cell-free massive MIMO integrated sensing and communication systems," in *Proc. IEEE GLOBECOM*, Dec. 2023, pp. 546–551.

[117] I. W. da Silva, D. P. Osorio, and M. Juntti, "Multi-static ISAC in cell-free massive MIMO: Precoder design and privacy assessment," *arXiv preprint arXiv:2309.13368*, 2023.

[118] X. Liu, T. Huang, N. Shlezinger, Y. Liu, J. Zhou, and Y. C. Eldar, "Joint transmit beamforming for multiuser MIMO communications and MIMO radar," *IEEE Trans. Signal Process.*, vol. 68, pp. 3929–3944, Jul. 2020.

[119] E. Fishler, A. Haimovich, R. Blum, D. Chizhik, L. Cimini, and R. Valenzuela, "MIMO radar: An idea whose time has come," in *Proc. IEEE Radar Conf.*, Apr. 2004, pp. 71–78.

[120] X. Yu, G. Cui, T. Zhang, and L. Kong, "Constrained transmit beampattern design for colocated MIMO radar," *Signal Process*, vol. 144, pp. 145–154, Mar. 2018.

[121] D. Cohen, D. Cohen, and Y. C. Eldar, "High resolution FDMA MIMO radar," *IEEE Trans. Aerosp. Electron. Syst*, vol. 56, no. 4, pp. 2806–2822, Aug. 2020.

[122] D.-H. Kim, J. Youn, and B. C. Jung, "Opportunistic interference alignment for spectrum sharing between radar and communication systems," *Sensors*, vol. 20, no. 17, p. 4868, 2020.

[123] R. M. Rao, H. S. Dhillon, V. Marojevic, and J. H. Reed, "Underlay radar-massive MIMO spectrum sharing: Modeling fundamentals and performance analysis," *IEEE Trans. Wireless Commun.*, vol. 20, no. 11, pp. 7213–7229, Nov. 2021.

[124] K. Singh, S. Biswas, T. Ratnarajah, and F. A. Khan, "Transceiver design and power allocation for full-duplex MIMO communication systems with spectrum sharing radar," *IEEE Trans. Cognit. Commun. Netw.*, vol. 4, no. 3, pp. 556–566, Sep. 2018.

[125] M. Rihan and L. Huang, "Optimum co-design of spectrum sharing between MIMO radar and MIMO communication systems: An interference alignment approach," *IEEE Trans. Veh. Technol.*, vol. 67, no. 12, pp. 11 667–11 680, Dec. 2018.

[126] T. L. Marzetta, E. G. Larsson, and H. Yang, *Fundamentals of Massive MIMO*. Cambridge University Press, 2016.

[127] A. Ashikhmin, L. Li, and T. L. Marzetta, "Interference reduction in multi-cell massive MIMO systems with large-scale fading precoding," *IEEE Trans. Inf. Theory.*, vol. 64, no. 9, pp. 6340–6361, Spe. 2018.

[128] A. Nuttall, "Some integrals involving the Q_M function (corresp.)," *IEEE Trans. Inf. Theory*, vol. 21, no. 1, pp. 95–96, Jan. 1975.

[129] H. Q. Ngo and E. G. Larsson, "No downlink pilots are needed in TDD massive MIMO," *IEEE Trans. Wireless Commun.*, vol. 16, no. 5, pp. 2921–2935, May 2017.

[130] R. Saruthirathanaworakun, J. M. Peha, and L. M. Correia, "Opportunistic sharing between rotating radar and cellular," *IEEE J. Sel. Areas Commun.*, vol. 30, no. 10, pp. 1900–1910, Nov. 2012.

[131] H. Deng and B. Himed, "Interference mitigation processing for spectrum-sharing between radar and wireless communications systems," *IEEE Trans. Aerosp. Electron. Syst.*, vol. 49, no. 3, pp. 1911–1919, Jul. 2013.

[132] A. Khawar, A. Abdel-Hadi, and T. C. Clancy, "Spectrum sharing between S-band radar and LTE cellular system: A spatial approach," in *Proc. IEEE DYSPAN.*, Apr. 2014, pp. 7–14.

[133] A. Aubry, A. De Maio, M. Piezzo, and A. Farina, "Radar waveform design in a spectrally crowded environment via nonconvex quadratic optimization," *IEEE Trans. Aerosp. Electron. Syst.*, vol. 50, no. 2, pp. 1138–1152, Apr. 2014.

[134] L. Zheng, M. Lops, X. Wang, and E. Grossi, "Joint design of overlaid communication systems and pulsed radars," *IEEE Trans. Signal Process.*, vol. 66, no. 1, pp. 139–154, Jan. 2017.

[135] Z. Pu, W. Wang, and F. Dong, "Beamforming and waveform designing for spectrum coexistence system based on constructive interference," *IEEE Commun. Lett.*, vol. 26, no. 11, pp. 2695–2699, Nov. 2022.

[136] S. M. Kay, *Fundamentals of Statistical Signal Processing: Estimation Theory*. Upper Saddle River, NJ, USA: Prentice-Hall, Inc., 1993.

[137] A. M. Ahmed, A. A. Ahmad, S. Fortunati, A. Sezgin, M. S. Greco, and F. Gini, "A reinforcement learning based approach for multitarget detection in massive MIMO radar," *IEEE Trans. Aerosp. Electron. Syst*, vol. 57, no. 5, pp. 2622–2636, Oct. 2021.

[138] A. Khansefid and H. Minn, "Achievable downlink rates of MRC and ZF precoders in massive MIMO with uplink and downlink pilot contamination," *IEEE Trans. Commun.*, vol. 63, no. 12, pp. 4849–4864, Dec. 2015.

[139] J. A. Sutton, H. Q. Ngo, and M. Matthaiou, "Hardening the channels by precoder design in massive MIMO with multiple-antenna users," *IEEE Trans. Veh. Technol.*, vol. 70, no. 5, pp. 4541–4556, May 2021.

[140] A. M. Tulino and Verdú, "*Random matrix theory and wireless communications*," *Foundations Trends Commun. Inf. Theory*, vol. 1, no. 1, pp. 1–182, Jun. 2004.

[141] J. Tang and S. Lambotharan, "Interference alignment techniques for MIMO multi-cell interfering broadcast channels," *IEEE Trans. Commun.*, vol. 61, no. 1, pp. 164–175, Jan. 2013.

[142] G. Interdonato, M. Karlsson, E. Björnson, and E. G. Larsson, "Local partial zero-forcing precoding for cell-free massive MIMO," *IEEE Trans. Wireless Commun.*, vol. 19, no. 7, pp. 4758–4774, Jul. 2020.

[143] S. Wagner, R. Couillet, M. Debbah, and D. T. M. Slock, "Large system analysis of linear precoding in correlated MISO broadcast channels under limited feedback," *IEEE Trans. Inf. Theory*, vol. 58, no. 7, pp. 4509–4537, Jul. 2012.

[144] S. Boyd, S. P. Boyd, and L. Vandenberghe, *Convex Optimization*. Cambridge Univ. Press, 2004.

[145] H. H. M. Tam, H. D. Tuan, D. T. Ngo, T. Q. Duong, and H. V. Poor, "Joint load balancing and interference management for small-cell heterogeneous networks with limited backhaul capacity," *IEEE Trans. Wireless Commun.*, vol. 16, no. 2, pp. 872–884, Feb. 2017.

[146] A. L. et al., "A survey on fundamental limits of integrated sensing and communication," *IEEE Commun. Surveys Tuts.*, vol. 24, no. 2, pp. 994–1034, Secondquarter 2022.

[147] H. Tataria, P. J. Smith, L. J. Greenstein, P. A. Dmochowski, and M. Matthaiou, "Impact of line-of-sight and unequal spatial correlation on uplink MU-MIMO systems," *IEEE Wireless Commun. Lett.*, vol. 6, no. 5, pp. 634–637, Oct. 2017.

[148] L. Wang, W. Zhu, Y. Zhang, Q. Liao, and J. Tang, "Multi-target detection and adaptive waveform design for cognitive MIMO radar," *IEEE Sensors J.*, vol. 18, no. 24, pp. 9962–9970, Dec. 2018.

[149] T. L. Marzetta, "Noncooperative cellular wireless with unlimited numbers of base station antennas," *IEEE Trans. Wireless Commun.*, vol. 9, no. 11, pp. 3590–3600, Nov. 2010.

[150] S. Boyd and L. Vandenberghe, *Convex Optimization*. New York, NY: Cambridge University Press, 2004.

[151] H. H. M. Tam, H. D. Tuan, D. T. Ngo, T. Q. Duong, and H. V. Poor, "Joint load balancing and interference management for small-cell heterogeneous networks with limited backhaul capacity," *IEEE Trans. Wireless Commun.*, vol. 16, no. 2, pp. 872–884, Feb. 2017.

[152] F. Liu, L. Zhou, C. Masouros, A. Lit, W. Luo, and A. Petropulu, "Dual-functional cellular and radar transmission: Beyond coexistence," in *2018 IEEE 19th International*

Workshop on Signal Processing Advances in Wireless Communications (SPAWC). IEEE, 2018, pp. 1–5.

[153] F. Liu, L. Zheng, Y. Cui, C. Masouros, A. P. Petropulu, H. Griffiths, and Y. C. Eldar, "Seventy years of radar and communications: The road from separation to integration," *IEEE Signal Process. Mag.*, 2023.

[154] A. Ali, N. Gonzalez-Prelcic, R. W. Heath, and A. Ghosh, "Leveraging sensing at the infrastructure for mmWave communication," *IEEE Communications Magazine*, vol. 58, no. 7, pp. 84–89, 2020.

[155] A. Zhang, M. L. Rahman, X. Huang, Y. J. Guo, S. Chen, and R. W. Heath, "Perceptive mobile networks: Cellular networks with radio vision via joint communication and radar sensing," *IEEE Veh. Technol. Mag.*, vol. 16, no. 2, pp. 20–30, Jun. 2020.

[156] M. Temiz, E. Alsusa, and M. W. Baidas, "A dual-functional massive MIMO OFDM communication and radar transmitter architecture," *IEEE Trans. Veh. Technol.*, vol. 69, no. 12, pp. 14 974–14 988, Dec. 2020.

[157] ——, "Optimized precoders for massive MIMO OFDM dual radar-communication systems," *IEEE Trans. Commun.*, vol. 69, no. 7, pp. 4781–4794, Jul. 2021.

[158] ——, "A dual-function massive MIMO uplink OFDM communication and radar architecture," *IEEE Trans. Cognit. Commun. Netw.*, vol. 8, no. 2, pp. 750–762, Jun. 2021.

[159] H. Q. Ngo, L.-N. Tran, T. Q. Duong, M. Matthaiou, and E. G. Larsson, "On the total energy efficiency of cell-free massive MIMO," *IEEE Trans. Green Commun. and Networking*, vol. 2, no. 1, pp. 25–39, Mar. 2018.

[160] B. Liao, H. Q. Ngo, M. Matthaiou, and P. J. Smith, "Low-complexity transmit beamforming design for massive MIMO-ISAC systems," in *Proc. GLOBECOM*, 2023, pp. 540–545.

[161] H. Cramér, *Random Variables and Probability Distributions*. U.K:Cambridge Univ. Press, 2004, no. 36.

[162] H. Q. Ngo, E. G. Larsson, and T. L. Marzetta, "Energy and spectral efficiency of very large multiuser MIMO systems," *IEEE Trans. Commun.*, vol. 61, no. 4, pp. 1436–1449, Apr. 2013.

[163] M. Grant and S. Boyd, "CVX: Matlab software for disciplined convex programming, version 2.1, [online]. available:http: //cvxr.com/cvx, 2014." 2014.

[164] T. T. Vu, D. T. Ngo, M. N. Dao, S. Durrani, and R. H. Middleton, "Spectral and energy efficiency maximization for content-centric C-RANs with edge caching," *IEEE Trans. Commun.*, vol. 66, no. 12, pp. 6628–6642, Dec. 2018.

[165] E. Björnson and L. Sanguinetti, "Making cell-free massive MIMO competitive with MMSE processing and centralized implementation," *IEEE Trans. Wireless Commun.*, vol. 19, no. 1, pp. 77–90, Jan. 2020.

[166] A. Bazzi and M. Chafii, "Secure full duplex integrated sensing and communications," *IEEE Trans. Inf. Forensics Secur.*, vol. 19, pp. 2082–2097, Dec. 2023.

[167] W. Yang, M. Li, and Q. Liu, "A practical channel estimation strategy for XL-MIMO communication systems," *IEEE Commun. Lett.*, vol. 27, Jun. 2023.

[168] M. Cui and L. Dai, "Channel estimation for extremely large-scale MIMO: Far-field or near-field?" *IEEE Trans. Commun.*, vol. 70, no. 4, pp. 2663–2677, Jan. 2022.

[169] U. Demirhan and A. Alkhateeb, "Integrated sensing and communication for 6g: Ten key machine learning roles," *IEEE Commun. Mag.*, vol. 61, no. 5, pp. 113–119, 2023.

[170] S. András, A. Baricz, and Y. Sun, "The generalized Marcum $Q-$ function: An orthogonal polynomial approach," *arXiv preprint arXiv:1010.3348*, 2010.

[171] I. S. Gradshteyn and I. M. Ryzhik, *Table of Integrals, Series, and Products*. Elsevier, 2007.

[172] P. Z. Peebles Jr, *Probability, Random Variables, and Random Signal Principles*. McGraw-Hill, 2001.

Appendix A

Proofs of Chapter 3

A.1 Proof of Proposition 1

From (3.18) and (3.21), the average probability of detection can be approximated by

$$\mathbb{E}\{P_d\} \approx \bar{P}_d = \mathbb{E}\left\{ Q_1\left(\sqrt{\frac{|\alpha|^2 L P_R \mathrm{tr}\left(\boldsymbol{A}\boldsymbol{A}^H\right)}{\varepsilon}}, \sqrt{C_{FA}}\right)\right\}. \tag{A.1}$$

From (3.16), we have

$$\varepsilon = \beta_{br}\mathrm{tr}(\tilde{\boldsymbol{T}}) = \frac{\beta_{br}\rho}{MK}\sum_{k=1}^{K}\|\boldsymbol{h}_k\|^2 = \frac{\beta_{br}\rho}{2MK}\bar{x}, \tag{A.2}$$

where $\bar{x}$ is a chi-square random distributed variable with $2MK$ degrees of freedom. Thus, the probability density function (PDF) of $\bar{x}$ is given by:

$$p(\bar{x}) = \frac{1}{2^{MK}\Gamma(MK)}\bar{x}^{MK-1}e^{-\bar{x}/2}. \tag{A.3}$$

The substitution of (A.2) into (A.1) gives

$$\bar{\mathrm{P}}_d = \int_0^{\infty} Q_1\left(\sqrt{\frac{c}{\bar{x}}}, \sqrt{C_{FA}}\right) p(\bar{x})d\bar{x}, \tag{A.4}$$

where c is defined in Proposition 1, i.e.,

$$c = 2MK|\alpha|^2 LP_R \mathrm{tr}(\boldsymbol{A}\boldsymbol{A}^H)/(\beta_{br}\rho). \tag{A.5}$$

By using the series representation of the Marcum Q-function [170]:

$$Q_v(a,b)_v = 1 - \sum_{n\geq 0} e^{-\frac{a^2}{2}} \left(\frac{a^2}{2}\right)^n \frac{\gamma\left(v+n, \frac{b^2}{2}\right)}{\Gamma(v+n)}, \tag{A.6}$$

we obtain

$$\bar{\mathrm{P}}_d = \int_0^\infty \left(1 - \sum_{n\geq 0} e^{-\frac{a^2}{2}} \left(\frac{a^2}{2}\right)^n \times d_n\right) p(\bar{x}) d\bar{x}, \tag{A.7}$$

where $a = \sqrt{\frac{c}{\bar{x}}}$, $b = \sqrt{C_{FA}}$ and $d_n = \frac{\gamma\left(1+n, \frac{b^2}{2}\right)}{\Gamma(1+n)}$.

As a next step, (A.7) is simplified as (A.8)

$$\bar{\mathrm{P}}_d = \left(\int_0^\infty \frac{1}{2^{MK/2}\Gamma(MK)} e^{\frac{-\bar{x}}{2}} \bar{x}^{MK-1} - \sum_{n\geq 0} \frac{1}{2^{MK}\Gamma(MK)} \int_0^\infty e^{-\frac{c}{2\bar{x}}} \left(\frac{c}{2\bar{x}}\right)^n d_n e^{\frac{-\bar{x}}{2}} \bar{x}^{MK-1} d\bar{x}\right). \tag{A.8}$$

By using the fact that

$$\int_0^\infty \frac{1}{2^{MK}\Gamma(MK)} e^{\frac{-\bar{x}}{2}} \bar{x}^{MK-1} d\bar{x} = 1, \tag{A.9}$$

we can obtain

$$\bar{\mathrm{P}}_d = 1 - \sum_{n\geq 0} \frac{1}{2^{MK}\Gamma(MK)} \int_0^\infty e^{-\frac{c}{2\bar{x}}} \left(\frac{c}{2\bar{x}}\right)^n d_n e^{\frac{-\bar{x}}{2}} \bar{x}^{MK-1} d\bar{x}. \tag{A.10}$$

The integral in the above expression can be further derived by using [171, Eq. (9)]. Then, we can obtain the closed-form expression for $\bar{\mathrm{P}}_d$ as given in Proposition 3.22.

A.1.1 Proof of Proposition 2

To derive the closed-form solution for the spectral efficiency given in (3.24), we need to compute 3 terms: $\mathbb{E}\left\{\boldsymbol{z}_k^T \boldsymbol{T}_k\right\}$, $\mathbb{E}\left\{|\boldsymbol{z}_k^T \boldsymbol{T}_k|^2\right\}$, and A_k. The first term represents the desired signal given by

$$\begin{aligned}\mathbb{E}\left\{\boldsymbol{z}_k^T \boldsymbol{T}_k\right\} &= \sqrt{\frac{\rho}{\beta_k KM}}\mathbb{E}\left\{\|\boldsymbol{z}_k\|^2\right\} \\ &= \sqrt{\frac{\rho\beta_k M}{K}}.\end{aligned} \tag{A.11}$$

The second term can be simplified as

$$\begin{aligned}\mathbb{E}\left\{|\boldsymbol{z}_k^T \boldsymbol{T}_k|^2\right\} &= \frac{\rho}{\beta_k KM}\mathbb{E}\left\{\|\boldsymbol{z}_k\|^4\right\} \\ &= \frac{\rho\beta_k}{K}(M+1).\end{aligned} \tag{A.12}$$

The third term represents the inter-user interference plus interference from radar, given by

$$\begin{aligned}A_k &= \sum_{j=1, j\neq k}^{K} \mathbb{E}\left\{\left|\boldsymbol{z}_k^T \boldsymbol{T}_j\right|^2\right\} + P_R\mathbb{E}\left\{\left\|\boldsymbol{f}_k\right\|^2\right\} + \sigma_c^2 \\ &= \sum_{j=1, j\neq k}^{K} \frac{\rho}{\beta_j KM}\mathbb{E}\left\{\left|\boldsymbol{z}_k^T \mathbf{z}_j^*\right|^2\right\} + P_R N\bar{\beta}_k + \sigma_c^2 \\ &= \frac{\rho\beta_k}{K}(K-1) + P_R N\bar{\beta}_k + \sigma_c^2.\end{aligned} \tag{A.13}$$

By substituting (A.11), (A.12), and (A.13) into (3.25), we arrive at the desired result in Proposition 2.

Appendix B

Proofs of Chapter 4

B.0.1 Useful Result

lemma 1 *For the projection matrix* $\mathbf{B} = \mathbf{I}_M - \hat{\mathbf{R}}^{\mathbf{H}} \left(\hat{\mathbf{R}} \hat{\mathbf{R}}^H \right)^{-1} \hat{\mathbf{R}}$, *we have*

$$\mathbb{E}\{\mathbf{B}\} = \frac{M-N}{M} \mathbf{I}_M, \quad M > N. \tag{B.1}$$

We denote $\mathbf{S} = \hat{\mathbf{R}}^H (\hat{\mathbf{R}} \hat{\mathbf{R}}^H)^{-1} \hat{\mathbf{R}}$ with $\hat{\mathbf{R}} \in \mathbb{C}^{N \times M}$. Assuming that $N < M$, by using the SVD technique, $\mathbf{R}$ can be expressed as

$$\hat{\mathbf{R}} = \mathbf{U} \mathbf{D} \mathbf{V}^H, \tag{B.2}$$

where $\mathbf{U} \in \mathbb{C}^{N \times N}$ and $\mathbf{V} \in \mathbb{C}^{M \times M}$ are unitary matrices and $\mathbf{D} = [\mathbf{D}_1, 0] \in \mathbb{C}^{N \times M}$ with $\mathbf{D}_1$ is $N \times N$ nonnegative diagonal matrix. Therefore, by using (B.2), we can express $\mathbf{S}$ as

$$\begin{aligned}\mathbf{S} &= \mathbf{V}\mathbf{D}^H\mathbf{U}^H(\mathbf{U}\mathbf{D}\mathbf{V}^H\mathbf{V}\mathbf{D}^H\mathbf{U}^H)^{-1}\mathbf{U}\mathbf{D}\mathbf{V}^H \\ &\overset{(a)}{=} \mathbf{V}\mathbf{D}^H\mathbf{U}^H(\mathbf{U}\mathbf{D}_1^2\mathbf{U}^H)^{-1}\mathbf{U}\mathbf{D}\mathbf{V}^H \\ &\overset{(b)}{=} \mathbf{V}\mathbf{D}^H\mathbf{D}_1^{-2}\mathbf{D}\mathbf{V}^H \\ &= \mathbf{V}\begin{bmatrix}\mathbf{I}_N & 0\\ 0 & 0\end{bmatrix}\mathbf{V}^H, \end{aligned} \tag{B.3}$$

where (a) follows from the fact that $\mathbf{V}^H\mathbf{V} = \mathbf{I}_M$ and (b) holds since $\mathbf{U}^H\mathbf{U} = \mathbf{I}_N$. Now assuming that $\mathbf{V} \triangleq [\mathbf{V}_1, \mathbf{V}_2]$ with $\mathbf{V}_1 = [\mathbf{v}_{1,1}, \ldots, \mathbf{v}_{1,N}] \in \mathbb{C}^{M\times N}$ and $\mathbf{V}_2 \in \mathbb{C}^{M\times(M-N)}$, we can further simplify (B.3) as

$$\mathbf{S} = \sum_{r=1}^{N} \mathbf{v}_{1,r}\mathbf{v}_{1,r}^H. \tag{B.4}$$

By using (B.4), the expectation of $\mathbf{S}$ can be expressed as

$$\mathbb{E}\Big\{\mathbf{S}\Big\} = \sum_{r=1}^{K} \mathbb{E}\Big\{\mathbf{v}_{1,r}.\mathbf{v}_{1,r}^H\Big\}. \tag{B.5}$$

Noticing that the distribution of $\mathbf{v}_{1,r}$ is the same as $\frac{\mathbf{z}}{\|\mathbf{z}\|}$, with $\mathbf{z} \sim \mathscr{CN}(0, \mathbf{I}_M)$, (B.5) can be further simplified as

$$\mathbb{E}\Big\{\mathbf{S}\Big\} = N\mathbb{E}\left\{\frac{\mathbf{z}\mathbf{z}^H}{\mathbf{z}^H\mathbf{z}}\right\}. \tag{B.6}$$

The diagonal elements of the expectation matrix in (B.6) can be obtained as

$$\begin{aligned}\Big[\mathbb{E}\Big\{\mathbf{S}\Big\}\Big]_{(r,r)} &= N\mathbb{E}\{t\} \\ &= \frac{N}{M}, \end{aligned} \tag{B.7}$$

where $t = \frac{|z_r|^2}{\sum_{s=1}^{M}|z_s|^2}$ is Beta distributed random variables with parameter $(1, M-1)$ and $\mathbb{E}\{t\} = \frac{1}{M}$ [172].

To find the off-diagonal elements of $\mathbb{E}\Big\{\mathbf{S}\Big\}$, we have [172]

$$\left[\mathbb{E}\Big\{\mathbf{S}\Big\}\right]_{(r,s)} = K\mathbb{E}\left\{\frac{z_r z_s^*}{\sum_{t=1}^{M}|z_t|^2}\right\} = 0, \forall r \neq s. \tag{B.8}$$

To this end, we can conclude that

$$\mathbb{E}\Big\{\mathbf{B}\Big\} = \mathbf{I}_M - \mathbb{E}\Big\{\mathbf{S}\Big\} = \frac{M-N}{M}\mathbf{I}_M. \tag{B.9}$$

B.0.2 Proof of Proposition 3

To derive the closed-form expression for the $\text{SINR}_k^{\text{MR}}$, we need to compute DS_k, $|\text{BU}_k|^2$ and $|\text{IUI}_{kk'}|^2$. By substituting (4.19) into the desired signal in (4.14), we obtain firstly DS_k as

$$\begin{aligned}\text{DS}_k &= \sqrt{\rho\eta_k}\mathbb{E}\Big\{(\hat{\mathbf{g}}_k^T - \tilde{\mathbf{g}}_k^T)\mathbf{t}_k^{\text{MR}}\Big\} \\ &= \sqrt{\frac{\rho\eta_k}{M}}\mathbb{E}\Big\{\hat{\mathbf{g}}_k^T\mathbf{h}_k^*\Big\} \\ &= \sqrt{\frac{\rho\eta_k\gamma_k}{M}}\mathbb{E}\{\Big\|\mathbf{h}_k\Big\|^2\} = \sqrt{M\rho\gamma_k\eta_k}.\end{aligned} \tag{B.10}$$

In order to compute $|\text{BU}_k|^2$, we have

$$\begin{aligned}\mathbb{E}\Big\{|\text{BU}_k|^2\Big\} &= \rho\eta_k\mathbb{E}\Big\{|\mathbf{g}_k^T\mathbf{t}_k^{\text{MR}}|^2\Big\} - |\text{DS}_k|^2 \\ &= \rho\gamma_k\eta_k(M+1) - M\rho\gamma_k\eta_k \\ &= \rho\gamma_k\eta_k.\end{aligned} \tag{B.11}$$

We now turn our attention to derive $|\text{IUI}_{kk'}|^2$, which is given by

$$\begin{aligned}\mathbb{E}\Big\{\Big|\text{IUI}_{kk'}\Big|^2\Big\} &= \rho\eta_{k'}\mathbb{E}\Big\{\Big|\mathbf{g}_k^T\mathbf{t}_{k'}^{\text{MR}}\Big|^2\Big\} \\ &= \rho\eta_{k'}\mathbb{E}\Big\{\mathbf{g}_k^T\mathbb{E}\Big\{\mathbf{t}_{k'}^{\text{MR}}(\mathbf{t}_{k'}^{\text{MR}})^H\Big\}\mathbf{g}_k^*\Big\} \\ &= \rho\eta_{k'}\gamma_k.\end{aligned} \tag{B.12}$$

Plugging (B.10), (B.11), and (B.12) into (4.18), we obtain the desired result in (4.20).

B.0.3 Proof of Proposition 4

By using $\mathbf{t}_k^{\mathrm{ZF}}$, i.e., the k-th column of $\mathbf{T}^{\mathrm{ZF}}$ in (4.21), the desired signal in (4.14), can be obtained as

$$\begin{aligned}\mathrm{DS}_k &= \sqrt{\rho\eta_k}\mathbb{E}\left\{(\hat{\mathbf{g}}_k^T - \tilde{\mathbf{g}}_k^T)\mathbf{t}_k^{\mathrm{ZF}}\right\} \\ &= \sqrt{\rho\eta_k}\mathbb{E}\left\{\hat{\mathbf{g}}_k^T\mathbf{t}_k^{\mathrm{ZF}}\right\} \\ &= \sqrt{\rho\eta_k\gamma_k}\mathbb{E}\left\{\mathbf{h}_k^T\mathbf{t}_k^{\mathrm{ZF}}\right\} \\ &= \sqrt{(M-K)\rho\eta_k\gamma_k}. \end{aligned} \tag{B.13}$$

In order to derive $\mathbb{E}\{|\mathrm{BU}_k|^2\}$, which can be further expressed by

$$\mathbb{E}\left\{|\mathrm{BU}_k|^2\right\} = \rho\eta_k\mathbb{E}\left\{|\mathbf{g}_k^T\mathbf{t}_k^{\mathrm{PZF}}|^2\right\} - |\mathrm{DS}_k|^2, \tag{B.14}$$

we need to obtain the first term in (B.17), which can be written as

$$\mathbb{E}\left\{|\mathbf{g}_k^T\mathbf{t}_k^{\mathrm{PZF}}|^2\right\} = \mathbb{E}\left\{\mathbf{g}_k^T\mathbf{t}_k^{\mathrm{ZF}}(\mathbf{t}_k^{\mathrm{ZF}})^H\mathbf{g}_k^*\right\}. \tag{B.15}$$

Denote $\mathbf{V}_k^{\mathrm{ZF}} = \mathbf{t}_k^{\mathrm{ZF}}(\mathbf{t}_k^{\mathrm{ZF}})^H$, we can express (B.15) as

$$\begin{aligned}\mathbb{E}\left\{|\mathbf{g}_k^T\mathbf{t}_k^{\mathrm{ZF}}|^2\right\} &= \mathbb{E}\left\{(\hat{\mathbf{g}}_k^T - \tilde{\mathbf{g}}_k^T)\mathbf{V}_k^{\mathrm{ZF}}(\hat{\mathbf{g}}_k^* - \tilde{\mathbf{g}}_k^*)\right\} \\ &= \mathbb{E}\left\{(\hat{\mathbf{g}}_k^T\mathbf{V}_k^{\mathrm{ZF}}\hat{\mathbf{g}}_k^* + \tilde{\mathbf{g}}_k^T\mathbf{V}_k^{\mathrm{ZF}}\tilde{\mathbf{g}}_k^*)\right\} \\ &= \mathbb{E}\left\{\hat{\mathbf{g}}_k^T\mathbf{V}_k^{\mathrm{ZF}}\hat{\mathbf{g}}_k^*\right\} + \mathbb{E}\left\{\tilde{\mathbf{g}}_k^T\mathbf{V}_k^{\mathrm{ZF}}\tilde{\mathbf{g}}_k^*\right\} \\ &= (M-K)\rho\eta_k\gamma_k + (\beta_k - \gamma_k). \end{aligned} \tag{B.16}$$

To this end, by substituting (B.16) into (B.17), we have

$$\begin{aligned}\mathbb{E}\left\{|\mathrm{BU}_k|^2\right\} &= \mathbb{E}\left\{|\mathbf{g}_k^T\mathbf{t}_k^{\mathrm{ZF}}|^2\right\} - |\mathrm{DS}_k|^2 \\ &= \rho\eta_k(\beta_k - \gamma_k). \end{aligned} \tag{B.17}$$

Then, we obtain the inter-user interference term as

$$\begin{aligned}\mathbb{E}\left\{\left|\mathrm{IUI}_{kk'}\right|^2\right\} &= \rho\eta_{k'}\mathbb{E}\left\{\left|\mathbf{g}_k^T\mathbf{t}_{k'}^{\mathrm{ZF}}\right|^2\right\}\\ &= \rho\eta_{k'}\mathbb{E}\left\{\tilde{\mathbf{g}}_k^T\mathbb{E}\left\{\mathbf{t}_{k'}^{\mathrm{ZF}}(\mathbf{t}_{k'}^{\mathrm{ZF}})^H\right\}\tilde{\mathbf{g}}_k^*\right\}\\ &= \rho\eta_{k'}(\beta_k-\gamma_k).\end{aligned} \tag{B.18}$$

Finally, (4.22) is obtained by plugging (B.13), (B.15), and (B.18) into (4.18).

B.0.4 Proof of Proposition 5

By using $\mathbf{t}^{\mathrm{PZF}}$ in (4.26), the desired signal in (4.14), can be obtained as

$$\begin{aligned}\mathrm{DS}_k &= \sqrt{\rho\eta_k}\mathbb{E}\left\{(\hat{\mathbf{g}}_k^T-\tilde{\mathbf{g}}_k^T)\mathbf{t}_k^{\mathrm{PZF}}\right\}\\ &= \alpha_{\mathrm{PZF}}\sqrt{\rho\eta_k\gamma_k}\mathbb{E}\left\{\mathbf{h}_k^T\mathbb{E}\{\mathbf{B}\}\mathbf{w}_k^{\mathrm{ZF}}\right\}\\ &\overset{(a)}{=} \alpha_{\mathrm{PZF}}\sqrt{\rho\eta_k\gamma_k}\left(\frac{M-N}{M}\right)\mathbb{E}\left\{\mathbf{h}_k^T\mathbf{w}_k^{\mathrm{ZF}}\right\}\\ &\overset{(b)}{=} \sqrt{\frac{\rho\eta_k\gamma_k(M-K)(M-N)}{M}},\end{aligned} \tag{B.19}$$

where we exploited, in (a) Lemma 1 and in (b) $\mathbb{E}\left\{\mathbf{h}_k^T\mathbf{w}_k^{\mathrm{ZF}}\right\}=1$.

In order to derive $\mathbb{E}\{|\mathrm{BU}_k|^2\}$, which can be expressed as

$$\mathbb{E}\left\{\left|\mathrm{BU}_k\right|^2\right\} = \rho\eta_k\mathbb{E}\left\{\left|\mathbf{g}_k^T\mathbf{t}_k^{\mathrm{PZF}}\right|^2\right\} - |\mathrm{DS}_k|^2, \tag{B.20}$$

we need to obtain the first term in (B.20), given by

$$\mathbb{E}\left\{\left|\mathbf{g}_k^T\mathbf{t}_k^{\mathrm{PZF}}\right|^2\right\} = \mathbb{E}\left\{\mathbf{g}_k^T\mathbf{B}\mathbf{w}_k^{\mathrm{ZF}}(\mathbf{w}_k^{\mathrm{ZF}})^H\mathbf{B}^H\mathbf{g}_k^*\right\}. \tag{B.21}$$

Denoting $\mathbf{V}_k = \mathbf{w}_k^{\mathrm{ZF}}(\mathbf{w}_k^{\mathrm{ZF}})^H$, we can express (B.21) as

$$\begin{aligned}\mathbb{E}\left\{\left|\mathbf{g}_k^T\mathbf{t}_k^{\mathrm{PZF}}\right|^2\right\} &= \mathbb{E}\left\{\mathbf{g}_k^T\mathbf{B}\mathbf{V}_k\mathbf{B}^H\mathbf{g}_k^*\right\}\\ &= \mathbb{E}\left\{\mathbf{g}_k^T\left(\mathbf{I}_M-\hat{\mathbf{R}}^H(\hat{\mathbf{R}}\hat{\mathbf{R}}^H)^{-1}\hat{\mathbf{R}}\right)\mathbf{V}_k\left(\mathbf{I}_M-\hat{\mathbf{R}}^H(\hat{\mathbf{R}}\hat{\mathbf{R}}^H)^{-1}\hat{\mathbf{R}}\right)\mathbf{g}_k^*\right\}\\ &= \mathbb{E}\left\{\mathbf{g}_k^T\mathbf{V}_k\mathbf{g}_k^*-2\mathbf{g}_k^T\mathbf{V}_k\hat{\mathbf{R}}^H(\hat{\mathbf{R}}\hat{\mathbf{R}}^H)^{-1}\hat{\mathbf{R}}\mathbf{g}_k^*+\mathbf{g}_k^T\hat{\mathbf{R}}^H(\hat{\mathbf{R}}\hat{\mathbf{R}}^H)^{-1}\hat{\mathbf{R}}\mathbf{V}_k(\hat{\mathbf{R}}^H(\hat{\mathbf{R}}\hat{\mathbf{R}}^H)^{-1}\hat{\mathbf{R}}\mathbf{g}_k^*\right\}.\end{aligned} \tag{B.22}$$

Now, by using the fact that $\hat{\mathbf{R}}$ is independent of $\mathbf{g}_k$ and $\mathbf{V}_k$, we can derive (B.22) as

$$\begin{aligned}&\mathbb{E}\left\{\left|\mathbf{g}_k^T\mathbf{t}_k^{\mathrm{PZF}}\right|^2\right\} = \mathbb{E}\left\{\mathbf{g}_k^T\mathbf{V}_k\mathbf{g}_k^*\right\}-2\mathbb{E}\left\{\mathbf{g}_k^T\mathbf{V}_k\mathbb{E}\left\{\hat{\mathbf{R}}^H(\hat{\mathbf{R}}\hat{\mathbf{R}}^H)^{-1}\hat{\mathbf{R}}\right\}\mathbf{g}_k^*\right\}\\ &+\mathbb{E}\left\{\mathbf{g}_k^T\mathbb{E}\left\{\hat{\mathbf{R}}^H(\hat{\mathbf{R}}\hat{\mathbf{R}}^H)^{-1}\hat{\mathbf{R}}\mathbf{V}_k(\hat{\mathbf{R}}^H(\hat{\mathbf{R}}\hat{\mathbf{R}}^H)^{-1}\hat{\mathbf{R}}\right\}\mathbf{g}_k^*\right\}\\ &\overset{(a)}{=}\mathbb{E}\left\{\mathbf{g}_k^T\mathbf{V}_k\mathbf{g}_k^*\right\}-2\frac{N}{M}\mathbb{E}\left\{\mathbf{g}_k^T\mathbf{V}_k\mathbf{g}_k^*\right\}+\left(\frac{N}{M}\right)^2\mathbb{E}\left\{\mathbf{g}_k^T\mathbf{V}_k\mathbf{g}_k^*\right\}\\ &=\left(1-\frac{N}{M}\right)^2\mathbb{E}\left\{\mathbf{g}_k^T\mathbf{V}_k\mathbf{g}_k^*\right\},\end{aligned} \tag{B.23}$$

where (a) holds since according to Lemma 1 we have $\mathbb{E}\left\{\hat{\mathbf{R}}^H(\hat{\mathbf{R}}\hat{\mathbf{R}}^H)^{-1}\hat{\mathbf{R}}\right\} = \frac{N}{M}\mathbf{I}_M$, while the final result follows from the fact that $\mathbb{E}\left\{\mathbf{g}_k^T\mathbf{V}_k\mathbf{g}_k^*\right\} = 1$.

Then, we need to derive $\mathbb{E}\left\{\mathbf{g}_k^T\mathbf{V}_k\mathbf{g}_k^*\right\}$, which after vanishing the cross-expectations can be obtained as

$$\begin{aligned}\mathbb{E}\left\{\mathbf{g}_k^T\mathbf{V}_k\mathbf{g}_k^*\right\} &= \mathbb{E}\left\{(\hat{\mathbf{g}}_k^T-\tilde{\mathbf{g}}_k^T)\mathbf{V}_k(\hat{\mathbf{g}}_k^*-\tilde{\mathbf{g}}_k^*)\right\}\\ &= \mathbb{E}\left\{\hat{\mathbf{g}}_k^T\mathbf{V}_k\hat{\mathbf{g}}_k^*\right\}+\mathbb{E}\left\{\tilde{\mathbf{g}}_k^T\mathbf{V}_k\tilde{\mathbf{g}}_k^*\right\}\\ &= 1+(\beta_k-\gamma_k).\end{aligned} \tag{B.24}$$

To this end, by substituting (B.24) into (B.23) and then plugging the result into (B.20), we get

$$\begin{aligned}\mathbb{E}\left\{\left|\mathrm{BU}_k\right|^2\right\} &= \mathbb{E}\left\{\left|\mathbf{g}_k^T\mathbf{t}_k^{\mathrm{PZF}}\right|^2\right\} - |\mathrm{DS}_k|^2 \\ &= \rho\eta_k\alpha_{\mathrm{PZF}}^2\left(1-\frac{N}{M}\right)^2(\beta_k-\gamma_k).\end{aligned} \tag{B.25}$$

In order to derive IUI in (4.16), by using similar steps as in (B.22), we have

$$\begin{aligned}\mathbb{E}\left\{\left|\mathrm{IUI}_{kk'}\right|^2\right\} &= \rho\eta_{k'}\mathbb{E}\left\{\left|\mathbf{g}_k^T\mathbf{B}\mathbf{w}_{k'}^{\mathrm{ZF}}\right|^2\right\} \\ &= \rho\eta_{k'}\left(\mathbb{E}\left\{\mathbf{g}_k^T\mathbf{V}_{k'}\mathbf{g}_k^*\right\} - 2\frac{N}{M}\mathbb{E}\left\{\mathbf{g}_k^T\mathbf{V}_{k'}\mathbf{g}_k^*\right\}\right. \\ &\quad \left. + \left(\frac{N}{M}\right)^2\mathbb{E}\left\{\mathbf{g}_k^T\mathbf{V}_{k'}\mathbf{g}_k^*\right\}\right) \\ &= \rho\eta_{k'}\left(1-\frac{N}{M}\right)^2\mathbb{E}\left\{\mathbf{g}_k^T\mathbf{V}_{k'}\mathbf{g}_k^*\right\}.\end{aligned} \tag{B.26}$$

Therefore, we need to derive $\mathbb{E}\left\{\mathbf{g}_k^T\mathbf{V}_{k'}\mathbf{g}_k^*\right\}$, which, after averaging out the cross-expectations, it becomes

$$\begin{aligned}\mathbb{E}\left\{\mathbf{g}_k^T\mathbf{V}_{k'}\mathbf{g}_k^*\right\} &= \mathbb{E}\left\{(\hat{\mathbf{g}}_k^T-\tilde{\mathbf{g}}_k^T)\mathbf{V}_{k'}(\hat{\mathbf{g}}_k^*-\tilde{\mathbf{g}}_k^*)\right\} \\ &= \mathbb{E}\left\{(\hat{\mathbf{g}}_k^T\mathbf{V}_{k'}\hat{\mathbf{g}}_k^*+\tilde{\mathbf{g}}_k^T\mathbf{V}_{k'}\tilde{\mathbf{g}}_k^*)\right\} \\ &= \mathbb{E}\left\{\hat{\mathbf{g}}_k^T\mathbf{V}_{k'}\hat{\mathbf{g}}_k^*\right\}+\mathbb{E}\left\{\tilde{\mathbf{g}}_k^T\mathbf{V}_{k'}\tilde{\mathbf{g}}_k^*\right\} \\ &= (\beta_k-\gamma_k).\end{aligned} \tag{B.27}$$

Therefore, the IUI in (B.26), can be derived as

$$\mathbb{E}\left\{\left|\mathrm{IUI}_{kk'}\right|^2\right\} = \rho\eta_{k'}\left(1-\frac{N}{M}\right)^2(\beta_k-\gamma_k). \tag{B.28}$$

Finally, by substituting (B.19), (B.25), and (B.28), into (4.18), the desired result in (4.27) is obtained.

B.0.5 Proof of Proposition 6

From (4.24), $\tilde{\mathbf{T}}^{\mathrm{PZF}}$ can be expressed as

$$\begin{aligned}\tilde{\mathbf{T}}^{\mathrm{PZF}} &= \mathbf{T}^{\mathrm{PZF}}\mathbf{D}_{\eta}(\mathbf{T}^{\mathrm{PZF}})^{H} \\ &= \frac{M(M-K)}{(M-N)}\mathbf{B}\mathbf{W}^{\mathrm{ZF}}\mathbf{D}_{\eta}(\mathbf{W}^{\mathrm{ZF}})^{H}\mathbf{B}^{H}.\end{aligned} \tag{B.29}$$

Therefore, $\mathrm{tr}(\tilde{\mathbf{T}}^{\mathrm{PZF}})$ can be obtained as

$$\begin{aligned}\mathrm{tr}(\tilde{\mathbf{T}}^{\mathrm{PZF}}) &\overset{(a)}{=} \frac{M(M-K)}{(M-N)}\mathrm{tr}(\mathbf{W}^{\mathrm{ZF}}\mathbf{D}_{\eta}(\mathbf{W}^{\mathrm{ZF}})^{H}\mathbf{B}^{H}\mathbf{B}) \\ &\overset{(b)}{=} \frac{M(M-K)}{(M-N)}\mathrm{tr}(\mathbf{H}^{*}(\mathbf{H}^{T}\mathbf{H}^{*})^{-1}\mathbf{D}_{\eta}(\mathbf{H}^{T}\mathbf{H}^{*})^{-1}\mathbf{H}^{T}\mathbf{B}),\end{aligned} \tag{B.30}$$

where we have exploited: in (a) $\mathrm{tr}(\mathbf{XY}) = \mathrm{tr}(\mathbf{YX})$, in (b) $\mathbf{B}^{H}\mathbf{B} = \mathbf{B}$. To derive $\mathrm{tr}(\tilde{\mathbf{T}}^{\mathrm{PZF}})$, let us denote $\mathbf{C}$ as

$$\mathbf{C} = \mathbf{H}^{*}(\mathbf{H}^{T}\mathbf{H}^{*})^{-1}\mathbf{D}_{\eta}(\mathbf{H}^{T}\mathbf{H}^{*})^{-1}\mathbf{H}^{T}. \tag{B.31}$$

Then, by substituting (4.23) into (B.30), we get

$$\mathrm{tr}(\tilde{\mathbf{T}}^{\mathrm{PZF}}) = \frac{M(M-K)}{(M-N)}\left(\underbrace{\mathrm{tr}(\mathbf{C})}_{\mathrm{T}_1} - \underbrace{\mathrm{tr}(\mathbf{C}\hat{\mathbf{R}}^{\mathbf{H}}\left(\hat{\mathbf{R}}\hat{\mathbf{R}}^{H}\right)^{-1}\hat{\mathbf{R}})}_{\mathrm{T}_2}\right). \tag{B.32}$$

The first term T_1 can be calculated as

$$\begin{aligned}T_1 &= \mathrm{tr}(\mathbf{H}^{*}(\mathbf{H}^{T}\mathbf{H}^{*})^{-1}\mathbf{D}_{\eta}(\mathbf{H}^{T}\mathbf{H}^{*})^{-1}\mathbf{H}^{T}) \\ &\overset{(a)}{=} \mathrm{tr}(\mathbf{D}_{\eta}(\mathbf{H}^{T}\mathbf{H}^{*})^{-1}) \\ &\overset{(b)}{\approx} \frac{1}{M}\mathrm{tr}(\mathbf{D}_{\eta}\mathbf{I}_{K}) \\ &= \frac{1}{M}\sum_{k=1}^{K}\eta_{k},\end{aligned} \tag{B.33}$$

where we have exploited: in (a) $\mathrm{tr}(\mathbf{XY}) = \mathrm{tr}(\mathbf{YX})$, in (b) $(\mathbf{H}^{T}\mathbf{H}^{*})^{-1} \approx \frac{1}{M}\mathbf{I}_{K}$.

Before proceeding to derive T_2, we notice that

$$\begin{aligned}\mathbf{C} &= \mathbf{H}^*(\mathbf{H}^T\mathbf{H}^*)^{-1}\mathbf{D}_\eta(\mathbf{H}^T\mathbf{H}^*)^{-1}\mathbf{H}^T \\ &\approx \mathbf{H}^*(M\mathbf{I}_K)^{-1}\mathbf{D}_\eta(M\mathbf{I}_K)^{-1}\mathbf{H}^T \\ &= \frac{1}{M^2}\mathbf{H}^*\mathbf{D}_\eta\mathbf{H}^T. \end{aligned} \tag{B.34}$$

Therefore, we have

$$\begin{aligned}T_2 &= \mathrm{tr}\left(\mathbf{C}\hat{\mathbf{R}}^H\left(\hat{\mathbf{R}}\hat{\mathbf{R}}^{\mathbf{H}}\right)^{-1}\hat{\mathbf{R}}\right) \\ &\approx \frac{1}{M^2}\mathrm{tr}(\mathbf{D}_\eta\mathbf{H}^T\hat{\mathbf{R}}^H\left(\hat{\mathbf{R}}\hat{\mathbf{R}}^{\mathbf{H}}\right)^{-1}\hat{\mathbf{R}}\mathbf{H}^*). \end{aligned} \tag{B.35}$$

Accordingly, by using the law of large number when $M \to \infty$, we get

$$\frac{\mathbf{H}^T\hat{\mathbf{R}}^H\left(\hat{\mathbf{R}}\hat{\mathbf{R}}^{\mathbf{H}}\right)^{-1}\hat{\mathbf{R}}\mathbf{H}^*}{M} - \underbrace{\frac{\mathrm{tr}(\hat{\mathbf{R}}^H\left(\hat{\mathbf{R}}\hat{\mathbf{R}}^{\mathbf{H}}\right)^{-1}\hat{\mathbf{R}})}{M}}_{=N/M}\mathbf{I}_K \overset{M\to\infty}{\to} 0. \tag{B.36}$$

Finally, by substituting (B.36) into (B.35), T_2 can be approximated as

$$\begin{aligned}T_2 &\approx \frac{N}{M^2}\mathrm{tr}(\mathbf{D}_\eta) \\ &= \frac{N}{M^2}\sum_{k=1}^{K}\eta_k. \end{aligned} \tag{B.37}$$

To this end, by substituting (B.33) and (B.37) into (B.32) and then plugging the results into (4.33), the desired result in (4.39) is obtained.

B.0.6 Proof of Proposition 7

An achievable downlink SE at the k-th user can be obtained using (4.17) where the effective SINR is given by

$$\mathrm{SINR}_k = \frac{\rho\eta_k\left|\mathbb{E}\left\{\mathbf{g}_k^T\mathbf{t}_k\right\}\right|^2}{\sum_{k'=1}^{K}\rho\eta_{k'}\mathbb{E}\left\{\left|\mathbf{g}_k^T\mathbf{t}_{k'}\right|^2\right\} - \rho\eta_k\left|\mathbb{E}\left\{\mathbf{g}_k^T\mathbf{t}_k\right\}\right|^2 + P_R\bar{\beta}_k N + \sigma_C^2}. \tag{B.38}$$

Noticing that the MR precoding is given $\mathbf{t}_k^{\mathrm{MR}} = \frac{\hat{\mathbf{g}}_k^*}{\sqrt{\mathbb{E}\{\|\hat{\mathbf{g}}_k\|^2\}}}$, where $\mathbb{E}\{\|\hat{\mathbf{g}}_k\|^2\} = \mathrm{tr}(\mathbf{Q}_k)$, we have

$$\begin{aligned}\mathbb{E}\left\{\mathbf{g}_k^T\mathbf{t}_k^{\mathrm{MR}}\right\} &= \mathbb{E}\left\{(\hat{\mathbf{g}}_k^T + \tilde{\mathbf{g}}_k^T)\mathbf{t}_k^{\mathrm{MR}}\right\} \\ &= \frac{1}{\sqrt{\mathrm{tr}(\mathbf{Q}_k)}}\mathbb{E}\left\{\|\hat{\mathbf{g}}_k\|^2\right\} \\ &= \sqrt{\mathrm{tr}(\mathbf{Q}_k)} = \sqrt{\tau_{\mathrm{p}}\rho_u \mathrm{tr}(\Omega_k \Xi_k \Omega_k)}. \end{aligned} \tag{B.39}$$

To derive $\mathbb{E}\left\{\left|\mathbf{g}_k^T\mathbf{t}_{k'}^{\mathrm{MR}}\right|^2\right\}$, we consider two different cases as follows

- When $k' \neq k$:

$$\begin{aligned}\mathbb{E}\left\{|\mathbf{g}_k^T\hat{\mathbf{g}}_{k'}^*|^2\right\} &= \mathbb{E}\{\mathbf{g}_k^T\hat{\mathbf{g}}_{k'}^*\hat{\mathbf{g}}_{k'}^T\mathbf{g}_k^*\} \\ &= \mathrm{tr}\Big(\mathbb{E}\{\hat{\mathbf{g}}_{k'}^*\hat{\mathbf{g}}_{k'}^T\mathbf{g}_k^*\mathbf{g}_k^T\}\Big) \\ &= \mathrm{tr}\Big(\mathbb{E}\{\hat{\mathbf{g}}_{k'}^*\hat{\mathbf{g}}_{k'}^T\}\mathbb{E}\{\mathbf{g}_k^*\mathbf{g}_k^T\}\Big) \\ &= \tau_{\mathrm{p}}\rho_u \mathrm{tr}(\Omega_{k'}\Xi_{k'}\Omega_{k'}\Omega_k). \end{aligned} \tag{B.40}$$

- When $k' = k$: We notice that according to (4.51) and (4.52), we have $\check{\mathbf{y}}_{k,\mathrm{p}} = \check{\mathbf{y}}_{k',\mathrm{p}}$ and $\Xi_k = \Xi_{k'}$, respectively. We first rewrite $\mathbb{E}\left\{\left|\mathbf{g}_k^T\mathbf{t}_{k'}^{\mathrm{MR}}\right|^2\right\}$ as

$$\begin{aligned}\mathbb{E}\left\{\left|\mathbf{g}_k^T\mathbf{t}_{k'}^{\mathrm{MR}}\right|^2\right\} &= \frac{1}{\mathrm{tr}(\mathbf{Q}_{k'})}\mathbb{E}\left\{|\mathbf{g}_k^T\hat{\mathbf{g}}_{k'}^*|^2\right\} \\ &= \frac{1}{\mathrm{tr}(\mathbf{Q}_{k'})}\mathbb{E}\left\{(\hat{\mathbf{g}}_k^T\hat{\mathbf{g}}_{k'}^*\hat{\mathbf{g}}_{k'}^T\hat{\mathbf{g}}_k^* + \tilde{\mathbf{g}}_k^T\hat{\mathbf{g}}_{k'}^*\hat{\mathbf{g}}_{k'}^T\tilde{\mathbf{g}}_k^*)\right\}, \end{aligned} \tag{B.41}$$

  where the cross-expectations are vanished as the channel estimation error is zero-mean vector. Now, we derive the first term in (B.41), which can be expressed as

$$\mathbb{E}\left\{\hat{\mathbf{g}}_k^T\hat{\mathbf{g}}_{k'}^*\hat{\mathbf{g}}_{k'}^T\hat{\mathbf{g}}_k^*\right\} = \tau_{\mathrm{p}}^2\rho_{\mathrm{p}}^2\mathbb{E}\left\{\left|\check{\mathbf{y}}_{k,\mathrm{p}}^T\Xi_k\Omega_{k'}\Omega_k\Xi_k\check{\mathbf{y}}_{k,\mathrm{p}}^*\right|^2\right\}. \tag{B.42}$$

  Before proceeding, we present the following results [16]

$$\mathbb{E}\left\{\left|\mathbf{u}^H\mathbf{B}\mathbf{u}\right|^2\right\} = |\mathrm{tr}(\mathbf{B}\Psi)|^2 + \mathrm{tr}\left(\mathbf{B}\Psi\mathbf{B}^H\Psi\right), \tag{B.43}$$

$$\mathbb{E}\left\{\left|\mathbf{g}_k^T\mathbf{t}_{k'}^{\mathrm{MR}}\right|^2\right\}=\begin{cases}\frac{\tau_{\mathrm{p}}\rho_u}{\mathrm{tr}(\mathbf{Q}_{k'})}\left(\tau_{\mathrm{p}}\rho_{\mathrm{p}}\left|\mathrm{tr}\left(\Omega_{k'}\Omega_k\Xi_k\right)\right|^2+\mathrm{tr}\left(\Omega_{k'}\Omega_k\Xi_k\Omega_k\right)\right) & k'=k\\ \frac{\tau_{\mathrm{p}}\rho_u}{\mathrm{tr}(\mathbf{Q}_{k'})}\mathrm{tr}(\Omega_{k'}\Xi_{k'}\Omega_{k'}\Omega_k) & k'\neq k\end{cases} \tag{103}$$

where $\mathbf{u}\sim\mathscr{CN}(0,\Psi)$ with covariance matrix $\Psi\in\mathbb{C}^{M\times M}$ and any diagonalizable matrix $\mathbf{B}\in\mathbb{C}^{M\times M}$.

By exploiting (B.43) and noticing that $\check{\mathbf{y}}_{k,\mathrm{p}}\sim\mathscr{CN}(0,(\Xi_k)^{-1})$, we can derive (B.42) as

$$\begin{aligned}\mathbb{E}\left\{\hat{\mathbf{g}}_k^T\hat{\mathbf{g}}_{k'}^*\hat{\mathbf{g}}_{k'}^T\hat{\mathbf{g}}_k^*\right\}&=\tau_{\mathrm{p}}^2\rho_{\mathrm{p}}^2\Bigg(\left|\mathrm{tr}\left(\Xi_k\Omega_{k'}\Omega_k\Xi_k(\Xi_k)^{-1}\right)\right|^2\\&\quad+\mathrm{tr}\left(\Xi_k\Omega_{k'}\Omega_k\Xi_k(\Xi_k)^{-1}\Xi_k\Omega_k\Omega_{k'}\Xi_k(\Xi_k)^{-1}\right)\Bigg)\\&=\tau_{\mathrm{p}}^2\rho_{\mathrm{p}}^2\left|\mathrm{tr}\left(\Xi_k\Omega_{k'}\Omega_k\right)\right|^2\tau_{\mathrm{p}}\rho_{\mathrm{p}}\mathrm{tr}\left((\Omega_{k'}-\mathbf{C}_{k'})\Omega_k\Xi_k\Omega_k\right),\end{aligned} \tag{B.44}$$

where in the last step we used the fact that $\mathrm{tr}(\mathbf{AB})=\mathrm{tr}(\mathbf{BA})$ and applied (4.53). We now turn our attention to the second term in (B.41), which can be expressed as

$$\begin{aligned}\mathbb{E}\left\{\tilde{\mathbf{g}}_k^T\hat{\mathbf{g}}_{k'}^*\hat{\mathbf{g}}_{k'}^T\tilde{\mathbf{g}}_k^*\right\}&=\mathrm{tr}\left(\mathbb{E}\left\{\tilde{\mathbf{g}}_k^*\tilde{\mathbf{g}}_k^T\right\}\mathbb{E}\{\hat{\mathbf{g}}_{k'}^*\hat{\mathbf{g}}_{k'}^T\}\right)\\&=\tau_{\mathrm{p}}\rho_{\mathrm{p}}\mathrm{tr}(\mathbf{C}_{k'}\Omega_k\Xi_k\Omega_k).\end{aligned} \tag{B.45}$$

To this end, by substituting (B.44) and (B.45) into (B.41), we obtain $\mathbb{E}\left\{\left|\mathbf{g}_k^T\mathbf{t}_{k'}^{\mathrm{MR}}\right|^2\right\}$ as (103) at the top of the page. Finally, by substituting (B.39) and (103) into (B.38) and then plugging the result into (4.17), the desired result in (4.54) is obtained.

To derive the detection probability over spatially correlated fading channels, according to (4.32), we need to obtain $\mathrm{tr}(\tilde{\mathbf{T}}^{\mathrm{MR}})$, which can be expressed as

$$\begin{aligned}\mathrm{tr}(\tilde{\mathbf{T}}^{\mathrm{MR}})&=\sum_{k=1}^{K}\frac{\eta_k}{\mathrm{tr}(\mathbf{Q}_k)}\mathrm{tr}(\hat{\mathbf{g}}_k^*\hat{\mathbf{g}}_k^T)\\&=\sum_{k=1}^{K}\frac{\eta_k}{\mathrm{tr}(\mathbf{Q}_k)}\|\hat{\mathbf{g}}_k\|^2.\end{aligned} \tag{104}$$

We notice that $\hat{\mathbf{g}}_k\sim\mathscr{CN}(\mathbf{0},\mathbf{Q}_k)$ can be represented as

$$\hat{\mathbf{g}}_k=\mathbf{Q}_k^{\frac{1}{2}}\mathbf{z}_k, \tag{105}$$

where $\mathbf{z}_k \sim \mathscr{CN}(\mathbf{0}, \mathbf{I}_M)$. Therefore, $\|\hat{\mathbf{g}}_k\|^2$ in (104) can be expressed as

$$\|\hat{\mathbf{g}}_k\|^2 = \mathbf{z}_k^H \mathbf{Q}_k \mathbf{z}_k. \tag{106}$$

By substituting (106) into (104) and then applying the trace lemma, i.e., $\mathbf{z}_k^H \mathbf{Q}_k \mathbf{z}_k \approx \mathrm{tr}(\mathbf{Q}_k)$ as M is large, we get

$$\mathrm{tr}(\tilde{\mathbf{T}}^{\mathrm{MR}}) \approx \sum_{k=1}^{K} \eta_k. \tag{107}$$

To this end, by substituting (107) to (4.32), the non-centrality parameter for MR processing and over spatially correlated fading channels is obtained as (4.55).

Appendix C

Proofs of Chapter 5

C.1 Proof of Proposition 9

In order to apply the use-then-forget technique to derive the downlink SE at user k, we rewrite (5.12) as

$$y_k = \mathrm{DS}_k x_{c,k} + \mathrm{BU}_k x_{c,k} + \sum_{k' \in K_d \setminus k} \mathrm{IUI}_{kk'} x_{c,k'} + \mathrm{IR}_k x_r + n_k, \tag{C.1}$$

where

$$\mathrm{DS}_k \triangleq \sum_{m \in M} a_m \sqrt{\rho \eta_{mk}} \mathbb{E}\left\{ \mathbf{g}_{mk}^T \mathbf{t}_{mk}^{\mathrm{Com}} \right\} \tag{C.2a}$$

$$\mathrm{BU}_k \triangleq \sum_{m \in M} a_m \sqrt{\rho \eta_{mk}} \left(\mathbf{g}_{mk}^T \mathbf{t}_k - \mathbb{E}\left\{ \mathbf{g}_{mk}^T \mathbf{t}_k \right\} \right), \tag{C.2b}$$

$$\mathrm{IUI}_{kk'} \triangleq \sum_{m \in M} \sum_{k' \in K_d \setminus k} a_m \sqrt{\rho \eta_{mk'}} \mathbf{g}_{mk}^T \mathbf{t}_{mk'}^{\mathrm{Com}}, \tag{C.2c}$$

$$\mathrm{IR}_k \triangleq \sum_{m \in M} (1 - a_m) \sqrt{\eta_m \rho} \mathbf{g}_{mk}^T \mathbf{t}_m^{\mathrm{Sen}}, \tag{C.2d}$$

respectively represent the strength of the desired signal (DS_k), the beamforming gain uncertainty (BU_k), interference caused by the k'-th user ($\mathrm{IUI}_{kk'}$) and the interference caused by S-APs (IR_k), respectively. By invoking (C.1), the achievable downlink SE at the k-th user can be expressed

as $\mathrm{SE}_k = \left(1-\frac{\tau_\mathrm{p}}{\tau}\right)\log_2\left(1+\mathrm{SINR}_k\right)$, where

$$\mathrm{SINR}_k = \frac{\left|\mathrm{DS}_k\right|^2}{\mathbb{E}\left\{\left|\mathrm{BU}_k\right|^2\right\}+\sum_{k'\in K_d\setminus k}\mathbb{E}\left\{\left|\mathrm{IUI}_{kk'}\right|^2\right\}+\mathbb{E}\left\{\left|\mathrm{IR}_k\right|^2\right\}+1}. \tag{C.3}$$

Now, we proceed to the desired signal term as

$$\begin{aligned}\mathrm{DS}_k &= \sqrt{\rho}\,\mathbb{E}\left\{\sum_{m\in M} a_m \eta_{mk}^{1/2}(\hat{\mathbf{g}}_{mk}+\tilde{\mathbf{g}}_{mk})^T\hat{\mathbf{g}}_{mk}^*\right\}\\ &= \sqrt{\rho}\sum_{m\in M} a_m N \eta_{mk}^{1/2}\gamma_{mk},\end{aligned} \tag{C.4}$$

where we have used the fact that $\hat{\mathbf{g}}_{mk}$ and $\tilde{\mathbf{g}}_{mk}$ are zero mean and independent.

Noticing that the variance of a sum of independent RVs is equal to the sum of the variances, we can derive $\mathbb{E}\left\{\left|\mathrm{BU}_k\right|^2\right\}$ as

$$\begin{aligned}\mathbb{E}\left\{\left|\mathrm{BU}_k\right|^2\right\} &= \rho\sum_{m\in M} a_m\eta_{mk}\mathbb{E}\left\{\left|\mathbf{g}_{mk}^T\hat{\mathbf{g}}_{mk}^* - \mathbb{E}\left\{\mathbf{g}_{mk}^T\hat{\mathbf{g}}_{mk}^*\right\}\right|^2\right\}\\ &= \rho\sum_{m\in M} a_m\eta_{mk}\left(\mathbb{E}\left\{\left|\mathbf{g}_{mk}^T\hat{\mathbf{g}}_{mk}^*\right|^2\right\} - \left|\mathbb{E}\left\{\mathbf{g}_{mk}^T\hat{\mathbf{g}}_{mk}^*\right\}\right|^2\right)\\ &= \rho\sum_{m\in M} a_m\eta_{mk}\left(\mathbb{E}\left\{\left|\tilde{\mathbf{g}}_{mk}^T\hat{\mathbf{g}}_{mk}^*\right|^2\right\}+\mathbb{E}\left\{||\hat{\mathbf{g}}_{mk}||^4\right\}-N^2\gamma_{mk}^2\right).\end{aligned}$$

By using the fact that $\mathbb{E}\left\{\left|\tilde{\mathbf{g}}_{mk}^T\hat{\mathbf{g}}_{mk}^*\right|^2\right\} = \mathbb{E}\left\{\tilde{\mathbf{g}}_{mk}^T\mathbb{E}\left\{\hat{\mathbf{g}}_{mk}^*\hat{\mathbf{g}}_{mk}^T\right\}\tilde{\mathbf{g}}_{mk}^*\right\} = N\gamma_{mk}(\beta_{mk}-\gamma_{mk})$ and $\mathbb{E}\left\{||\hat{\mathbf{g}}_{mk}||^4\right\} = N(N+1)(\gamma_{mk})^2$, we get

$$\mathbb{E}\left\{\left|\mathrm{BU}_k\right|^2\right\} = \rho N\sum_{m\in M} a_m\eta_{mk}\gamma_{mk}\beta_{mk}. \tag{C.5}$$

By following the same steps, we can obtain

$$\mathbb{E}\left\{\left|\mathrm{IUI}_{kk'}\right|^2\right\} = \rho N\sum_{m\in M} a_m\eta_{mk'}\gamma_{mk'}\beta_{mk}. \tag{C.6}$$

Moreover, by substituting (5.7) into (C.2d) and noticing that $\mathbf{t}_m^{\text{Sen}}(\mathbf{t}_m^{\text{Sen}})^H = \frac{1}{N}\mathbf{I}_N$, we get

$$\begin{aligned}\mathbb{E}\left\{\left|\text{IR}_k\right|^2\right\} &= \sum_{m\in M}(1-a_m)\mathbb{E}\left\{\left|\mathbf{g}_{mk}^T\mathbf{t}_m^{\text{Sen}}\right|^2\right\} \\ &= \rho\sum_{m\in M}\eta_m(1-a_m)\beta_{mk}. \end{aligned} \tag{C.7}$$

To this end, by substituting (C.4), (C.5), (C.6), and (C.7) into (C.3), the desired result in (5.13) is obtained.

Appendix D

Proofs of Chapter 6

D.1 Useful Lemma

lemma 2 *For ZF beamforming vector* $\mathbf{t}_{mk}^{\mathrm{ZF-Com}}$*, defined in* (6.10)*, we have*

$$\mathbb{E}\left\{\mathbf{t}_{mk}^{\mathrm{ZF-Com}}(\mathbf{t}_{mk}^{\mathrm{ZF-Com}})^H\right\} = \frac{\gamma_{mk}}{N(N-|S_m|)}\mathbf{I}_N. \tag{D.1}$$

We first define $\mathbf{Q} \triangleq \hat{\mathbf{G}}_{S_m}\left(\hat{\mathbf{G}}_{S_m}^H\hat{\mathbf{G}}_{S_m}\right)^{-1}$ and $\mathbf{q}_k = \mathbf{Q}\mathbf{e}_k$ which is the kth column of $\mathbf{Q} \in \mathbb{C}^{N\times|S_m|}$. Then, we have

$$\gamma_{mk}^2\mathbb{E}\left\{\mathbf{q}_k\mathbf{q}_k^H\right\} = \frac{\gamma_{mk}^2}{|S_m|}\sum_{k'=1}^{|S_m|}\mathbb{E}\left\{\mathbf{q}_{k'}\mathbf{q}_{k'}^H\right\}. \tag{D.2}$$

Accordingly, we have

$$\begin{aligned}\mathbb{E}\left\{\mathbf{t}_{mk}^{\mathrm{ZF-Com}}(\mathbf{t}_{mk}^{\mathrm{ZF-Com}})^H\right\} &= \frac{\gamma_{mk}^2}{|S_m|}\mathbb{E}\left\{\mathbf{Q}\mathbf{Q}^H\right\}\\ &= \frac{\gamma_{mk}^2}{|S_m|}\mathbb{E}\left\{\hat{\mathbf{G}}_{S_m}\left(\hat{\mathbf{G}}_{S_m}^H\hat{\mathbf{G}}_{S_m}\right)^{-1}\left(\hat{\mathbf{G}}_{S_m}^H\hat{\mathbf{G}}_{S_m}\right)^{-1}\hat{\mathbf{G}}_{S_m}^H\right\}.\end{aligned} \tag{D.3}$$

Let $\mathbf{B} = \mathbb{E}\left\{\hat{\mathbf{G}}_{S_m}\left(\hat{\mathbf{G}}_{S_m}^H\hat{\mathbf{G}}_{S_m}\right)^{-1}\left(\hat{\mathbf{G}}_{S_m}^H\hat{\mathbf{G}}_{S_m}\right)^{-1}\hat{\mathbf{G}}_{S_m}^H\right\}$, For any $N\times N$ unitary matrix Ω, we have

$$\Omega\mathbf{B}\Omega^H = \mathbb{E}\left\{\Omega\hat{\mathbf{G}}_{S_m}\left(\hat{\mathbf{G}}_{S_m}^H\hat{\mathbf{G}}_{S_m}\right)^{-1}\left(\hat{\mathbf{G}}_{S_m}^H\hat{\mathbf{G}}_{S_m}\right)^{-1}\hat{\mathbf{G}}_{S_m}^H\Omega^H\right\}. \tag{D.4}$$

Now, denote by $\bar{\mathbf{G}}_{S_m} = \Omega\hat{\mathbf{G}}_{S_m}$. Thus, using (D.4), we have

$$\Omega\mathbf{B}\Omega^H = \mathbb{E}\left\{\bar{\mathbf{G}}_{S_m}\left(\bar{\mathbf{G}}_{S_m}^H\bar{\mathbf{G}}_{S_m}\right)^{-1}\left(\bar{\mathbf{G}}_{S_m}^H\bar{\mathbf{G}}_{S_m}\right)^{-1}\bar{\mathbf{G}}_{S_m}^H\right\}, \tag{D.5}$$

where we have used

$$\bar{\mathbf{G}}_{S_m}^H\bar{\mathbf{G}}_{S_m} = \hat{\mathbf{G}}_{S_m}^H\Omega^H\Omega\hat{\mathbf{G}}_{S_m} = \hat{\mathbf{G}}_{S_m}^H\hat{\mathbf{G}}_{S_m}. \tag{D.6}$$

Since $\bar{\mathbf{G}}_{S_m} = \Omega\hat{\mathbf{G}}_{S_m}$ is statistically identical to $\hat{\mathbf{G}}_{S_m}$, we have $\Omega\mathbf{B}\Omega^H = \mathbf{B}$, for any unitary matrix Ω. By using the eigenvalue decomposition, $\mathbf{B}$ can be expressed as $\mathbf{B} = \mathbf{W}\mathbf{D}_\lambda\mathbf{W}^H$, where $\mathbf{W}$ is a unitary matrix and $\mathbf{D}_\lambda$ is a diagonal matrix. Then, $\Omega\mathbf{B}\Omega^H = \mathbf{B}$ is equivalent to

$$\Omega\mathbf{W}\mathbf{D}_\lambda\Omega^H\mathbf{W}^H = \mathbf{U}\mathbf{D}_\lambda\mathbf{U}^H = \mathbf{B}. \tag{D.7}$$

Since (D.7) is true for any unitary $\mathbf{U}$, $\mathbf{B}$ must be a scaled identity matrix. This implies that $\mathbf{B} = c_1\mathbf{I}_N$, where c_1 is a constant, given by

$$\begin{aligned} c_1 &= \frac{1}{N}\mathbb{E}\left\{\mathrm{tr}\left(\hat{\mathbf{G}}_{S_m}\left(\hat{\mathbf{G}}_{S_m}^H\hat{\mathbf{G}}_{S_m}\right)^{-1}\left(\hat{\mathbf{G}}_{S_m}^H\hat{\mathbf{G}}_{S_m}\right)^{-1}\hat{\mathbf{G}}_{S_m}^H\right)\right\} \\ &= \frac{1}{N}\mathbb{E}\left\{\mathrm{tr}(\hat{\mathbf{G}}_{S_m}^H\hat{\mathbf{G}}_{S_m})^{-1}\right\} \\ &= \frac{\gamma_{mk}}{N(N-|S_m|)}. \end{aligned} \tag{D.8}$$

D.2 Proof of Proposition 10

Now, we proceed to the desired signal term as

$$\begin{aligned} \mathrm{DS}_k &= \mathbb{E}\Big\{\textstyle\sum_{m\in Z_k} a_m\sqrt{\rho\,\eta_{mk}^c}(\hat{\mathbf{g}}_{mk}+\tilde{\mathbf{g}}_{mk})^T\mathbf{t}_{mk}^{\mathrm{ZF-Com}} \\ &\quad + \textstyle\sum_{m\in M_k} a_m\sqrt{\rho\,\eta_{mk}^c}(\hat{\mathbf{g}}_{mk}+\tilde{\mathbf{g}}_{mk})^T\mathbf{t}_{mk}^{\mathrm{MR-Com}}\Big\} \\ &= \sqrt{\rho}\left(\textstyle\sum_{m\in Z_k} a_m\sqrt{\eta_{mk}^c}\gamma_{mk} + N\sum_{m\in M_k} a_m\sqrt{\eta_{mk}^c}\gamma_{mk}\right), \end{aligned} \tag{D.9}$$

where we have used the fact that $\mathbf{t}_{mk}^{\mathrm{ZF-Com}}$, $\mathbf{t}_{mk}^{\mathrm{MR-Com}}$ and $\tilde{\mathbf{g}}_{mk}$ are zero mean and independent. In addition, the variance of the sum of independent RVs is equal to the sum of the variances.

We can now proceed with the following derivation

$$\mathbb{E}\left\{\left|\mathrm{BU}_k\right|^2\right\} = \mathbb{E}\left\{\left|\sum_{m\in Z_k} a_m\sqrt{\rho\,\eta^c_{mk'}}\mathbf{g}^T_{mk}\mathbf{t}^{\mathrm{ZF-Com}}_{mk'} + \sum_{m\in M_k} a_m\sqrt{\rho\,\eta^c_{mk'}}\mathbf{g}^T_{mk}\mathbf{t}^{\mathrm{MR-Com}}_{mk'}\right|^2\right\} - \mathrm{DS}_k. \tag{D.10}$$

We notice that

$$\begin{aligned}\vartheta &= \mathbb{E}\left\{\left|\sum_{m\in Z_k} a_m\sqrt{\rho\,\eta^c_{mk'}}\mathbf{g}^T_{mk}\mathbf{t}^{\mathrm{ZF-Com}}_{mk} + \sum_{m\in \mathscr{M}_\kappa} a_m\sqrt{\rho\,\eta^c_{mk}}\mathbf{g}^T_{mk}\mathbf{t}^{\mathrm{MR-Com}}_{mk}\right|^2\right\} \\ &= \vartheta_Z + \vartheta_M + 2\left(\sum_{m\in Z_k} a_m\sqrt{\rho\,\eta^c_{mk}}\gamma_{mk}\right)\left(N\sum_{m\in\kappa^{\mathscr{M}}} a_m\sqrt{\rho\,\eta^c_{mk}}\gamma_{mk}\right),\end{aligned} \tag{D.11}$$

where

$$\begin{aligned}\vartheta_Z &= \mathbb{E}\left\{\left|\sum_{m\in Z_k} a_m\sqrt{\rho\,\eta^c_{mk'}}\mathbf{g}^T_{mk}\mathbf{t}^{\mathrm{ZF-Com}}_{mk'}\right|^2\right\} \\ \vartheta_M &= \mathbb{E}\left\{\left|\sum_{m\in M_k} a_m\sqrt{\rho\,\eta^c_{mk'}}\mathbf{g}^T_{mk}\mathbf{t}^{\mathrm{MR-Com}}_{mk'}\right|^2\right\}.\end{aligned} \tag{D.12}$$

We first focus on ϑ_Z, which can be obtained as

$$\begin{aligned}\vartheta_Z &= \mathbb{E}\left\{\left|\sum_{m\in Z_k} a_m\sqrt{\rho\,\eta^c_{mk'}}(\hat{\mathbf{g}}_{mk}+\tilde{\mathbf{g}}_{mk})^T\mathbf{t}^{\mathrm{ZF-Com}}_{mk'}\right|^2\right\} \\ &= \sum_{m\in Z_k} a_m\rho\,\eta^c_{mk}\mathbb{E}\left\{(\mathbf{t}^{\mathrm{ZF-Com}}_{mk'})^H\mathbb{E}\left\{\tilde{\mathbf{g}}^T_{mk}(\tilde{\mathbf{g}}^T_{mk})^H\right\}\mathbf{t}^{\mathrm{ZF-Com}}_{mk}\right\} \\ &= \sum_{m\in Z_k} a_m\rho\,\eta^c_{mk}(\beta_{mk}-\gamma_{mk})\gamma^2_{mk}\mathbb{E}\left\{\left[(\mathbf{G}^H_{S_m}\mathbf{G}_{S_m})^{-1}\right]_{kk}\right\} \\ &= \sum_{m\in Z_k} a_m\rho\,\eta^c_{mk}(\beta_{mk}-\gamma_{mk})\frac{\gamma_{mk}}{N-|S_m|}.\end{aligned} \tag{D.13}$$

Then, the second term of (D.11), ϑ_M, can be derived as

$$\begin{aligned}
\vartheta_M &= \sum_{m\in M_k} a_m \eta_{mk}^c \mathrm{var}\left((\|\hat{\mathbf{g}}_{mk}\|^2 + \tilde{\mathbf{g}}_{mk}^T \hat{\mathbf{g}}_{mk}) \right) \\
&+ \left| \mathbb{E}\left\{ \sum_{m\in M_k} a_m \sqrt{\eta_{mk}^c} (\hat{\mathbf{g}}_{mk} + \tilde{\mathbf{g}}_{mk})^T \mathbf{t}_{mk}^{\mathrm{MR-Com}} \right\} \right|^2 \\
&= \sum_{m\in M_k} a_m \eta_{mk}^c \left(\mathbb{E}\left\{ \left| \|\hat{\mathbf{g}}_{mk}\|^2 + \tilde{\mathbf{g}}_{mk}^T \hat{\mathbf{g}}_{mk} \right|^2 \right\} \right. \\
&\left. - \left| \mathbb{E}\left\{ \|\hat{\mathbf{g}}_{mk}\|^2 + \tilde{\mathbf{g}}_{mk}^T \hat{\mathbf{g}}_{mk} \right\} \right|^2 \right) + N^2 \left(\sum_{m\in M_k} a_m \sqrt{\eta_{mk}^c} \right)^2 \\
&= \sum_{m\in M_k} a_m \eta_{mk}^c \left(\mathbb{E}\left\{ \left\| \hat{\mathbf{g}}_{mk} \right\|^4 \right\} + \mathbb{E}\left\{ \left| (\tilde{\mathbf{g}}_{mk})^T \hat{\mathbf{g}}_{mk} \right|^2 \right\} - (N\gamma_{mk})^2 \right) + \left(N \sum_{m\in M_k} a_m \sqrt{\eta_{mk}^c} \right)^2 \\
&= \sum_{m\in M_k} a_m \eta_{mk}^c N \gamma_{mk} \beta_{mk} + \left(N \sum_{m\in M_k} a_m \sqrt{\eta_{mk}^c} \right)^2 . \qquad \text{(D.14)}
\end{aligned}$$

As a result, plugging (D.13) and (D.14) into (D.15), we have

$$\mathbb{E}\left\{ \left| \mathrm{BU}_k \right|^2 \right\} = \sum_{m\in Z_k} a_m \eta_{mk}^c (\beta_{mk} - \gamma_{mk}) \frac{\gamma_{mh}}{N - |S_m|} + \sum_{m\in M_k} N a_m \eta_{mk}^c \gamma_{mk} \beta_{mk}. \qquad \text{(D.15)}$$

The same steps can be followed to compute $\mathrm{IUI}_{kk'}$

$$\mathrm{IUI}_{kk'} = \sum_{m\in Z_k} a_m \eta_{mk'}^c (\beta_{mk} - \gamma_{mk}) \frac{\gamma_{mk'}}{N - |S_m|} + N \sum_{m\in M_k} a_m \eta_{mk'}^c \gamma_{mk} \beta_{mk'}. \qquad \text{(D.16)}$$

Moreover, by substituting (6.7) into (6.17d), we get

$$\begin{aligned}
\mathbb{E}\left\{ \left| \mathrm{IR}_k \right|^2 \right\} &= \sum_{m\in M} (1 - a_m) \mathbb{E}\left\{ |\mathbf{g}_{mk}^T \mathbf{t}_{ml}^{\mathrm{Sen}}|^2 \right\} \\
&= \sum_{m\in M} \sum_{l\in\mathscr{L}} \rho \eta_{ml}^s (1 - a_m) \mathbb{E}\left\{ |\mathbf{g}_{mk}^T \mathbf{a}_N(\phi_{t,ml}^a, \phi_{t,ml}^e)|^2 \right\}. \qquad \text{(D.17)}
\end{aligned}$$

We now define $\mathbf{A} = \mathbf{a}_N(\phi_{t,ml}^a, \phi_{t,ml}^e)(\mathbf{a}_N^H(\phi_{t,ml}^a, \phi_{t,ml}^e))$. Then, we have

$$\begin{aligned}
\mathbb{E}\left\{ \left| \mathrm{IR}_k \right|^2 \right\} &= \rho \sum_{m\in M} \sum_{l\in\mathscr{L}} \eta_{ml}^s (1 - a_m) \mathbb{E}\left\{ |\mathbf{g}_{mk}^T \mathbf{A}|^2 \right\} \\
&= \rho \sum_{m\in M} \sum_{l\in\mathscr{L}} \eta_{ml}^s (1 - a_m) \mathbb{E}\left\{ \mathbf{g}_{mk}^T \mathbf{A} \mathbf{g}_{mk}^* \right\} \\
&= \rho \sum_{m\in M} \sum_{l\in\mathscr{L}} \eta_{ml}^s (1 - a_m) \beta_{mk} \mathrm{tr}(\mathbf{A}), \qquad \text{(D.18)}
\end{aligned}$$

where $\text{tr}(\mathbf{A}) = N$. To this end, by substituting (D.9), (D.15), (D.16), and (D.18) into (6.19), the desired result in (6.21) is obtained.